

UNIVERSITÉ CATHOLIQUE DE LOUVAIN
FACULTÉ DES SCIENCES APPLIQUÉES
UNITÉ DE MÉCANIQUE APPLIQUÉE



**Mesoscopic modelling of the geometry of
dislocations and point-defect dynamics
in single crystals**

Nicolas Van Goethem

*Thèse présentée en vue de l'obtention du grade de
Docteur en Sciences Appliquées*

Advisor :

Prof. F. Dupret (MEMA, UCL)

Members of the Jury :

Prof. E. van der Giessen (University of Groningen)

Prof. J.P. Issi (PCPM, UCL)

Prof. I. Doghri (MEMA, UCL)

Dr. N. Van den Bogaert (FEMAGSoft)

Dr. V. Regnier (FEMAGSoft)

Prof. J.-C. Samin (PRM, UCL)

January 2007

Avant-propos et remerciements

Le texte que vous avez sous les yeux est sans doute le plus important de tout cet ouvrage, tant ce travail de thèse aurait été impossible sans le soutien de nombreux proches et amis, sans d'importantes rencontres et fructueuses amitiés approfondies ou renouvelées.

Ce travail fut au départ un cheminement individuel avec à son origine une intuition, un désir de prendre une certaine orientation dans un domaine dont j'ignorais tout. Aucune certitude, mais la conviction de vouloir suivre une voie personnelle au risque de l'impasse. Au fur et à mesure des questions soulevées, les problèmes rencontrés se firent plus précis et plus incisifs. Pendant six ans, je rencontrais à chaque étape du raisonnement et de l'élaboration de cette théorie une nouvelle difficulté, toujours inattendue, et requérant à chaque fois plusieurs mois de travail pour la surmonter. C'est dans ces moments que la nécessité du compagnonnage avec mon promoteur François Dupret se fit sentir: les plus beaux moments de cette recherche furent alors ces réflexions à deux, ces débats souvent à une heure avancée de la soirée, des calculs, beaucoup de calculs chacun son tour sur le grand tableau blanc. Été, hiver, jour et nuit, week-end parfois: six cycles de saisons complets se déroulèrent ainsi. En fait, une grande ressource d'énergie et d'enthousiasme provenait de notre décalage presque systématique à propos des découragements de l'un ou de l'autre.

En écrivant cete thèse, presque pour chaque calcul, formule, trace d'une piste explorée ou ébauche d'un calcul, j'ai souvent pu reconnaître un moment précis de ma vie qui elle aussi, comme cette recherche, absorbait corps et âme en laissant ses marques. De longues périodes furent improductives et je tiens ici à remercier François Dupret pour toute l'amitié et la compréhension manifestées dans ces moments. Temps, désir et amitié se révèlent être des ingrédients indispensables pour arriver au bout d'un tel travail.

C'est pourquoi j'y retrouve tous ceux que j'aime et tout ce que j'ai aimé. Les équations, entres elles ont leur propre langage, mais isolément ce sont des objets du monde sensible car produites par des êtres de chair et de coeur. Etonnamment, une formule mathématique peut toucher la sensibilité artistique. D'ailleurs l'exposé d'une théorie à un public "profane" peut susciter bien des commentaires pertinents et fructueux. Je tiens ici à me remémorer l'ADEM (atelier d'écriture musicale) lancé par le compositeur Pierre Bartholomé convaincu de la nécessité de faire entrer en "résonnances"

compositions musicales et sciences universitaires. Ces ateliers, que j'ai pu suivre pour ensuite tenter pendant des années de les maintenir jusqu'à ce jour, ont été d'une importance cruciale dans le développement de ma sensibilité et de mes connaissances musicales bien sûr, mais ont aussi constitué un apport certain dans mes recherches. En effet, la rigueur du musicien et son exigence sont très proches de celles requises par un chercheur. Cet apprentissage a été poursuivi avec le compositeur Peter Swinnen, très curieux de nos recherches et très pertinent dans ses remarques. Je tiens aussi à remercier Thierry De Smedt, Jean-Pierre Peuvion, Guy Danel, Marie-Dominique, Tanguy, et bien entendu Bruno, mon meilleur ami, pour cette aventure et cet apprentissage collectifs. L'extension de l'ADEM vers le LABO# est une aventure en cours: l'idéal poursuivi est celui d'une démarche de création collective permettant d'affiner les choix et les sensibilités individuelles autour de projets de composition mêlant jeunes professionnels et amateurs de tous bords.

Je ne saurais trop insister sur l'importance que j'accorde à l'apprentissage auprès de "maîtres", du compagnonnage, de la recherche en équipe. J'ai pu expérimenter cela dans mes recherches dès mon mémoire de fin d'étude qui me conduisit en Allemagne pour un séjour de recherches expérimentales, puis à Pise, au département de mathématiques auprès de Giuseppe Buttazzo à qui je dois énormément. Sans me connaître au préalable, il répondit positivement à mon souhait de travailler dans son équipe de recherches sur des problèmes d'optimisation de forme. Durant ce séjour je réalisais comment des sujets de recherche fascinants à vocation appliquée, étaient traités dans des cadres mathématiques rigoureux. Mon orientation de chercheur fut vraiment déterminée par toute la série de séminaires suivis durant cette première année de recherche. A partir de ce séjour, ce fut une réelle vocation de se lancer dans ce que l'on appelle aujourd'hui la "mathématique des matériaux". Ceci eut un impact direct sur ma recherche qui débutait alors.

Fin 2003, j'eus la belle occasion de travailler trois mois avec David Preiss à la University College de Londres. Une recherche en Analyse Réelle sous forme de séminaires le mardi après-midi où nous ne sortions pas de son petit bureau avant d'avoir avancé sur le thème proposé. Autrement dit, nous y avons passé des heures...de temps en temps il sortait de sa poche une petite boulette de pain ou de papier et la mâchait, alors que nous restions affamés devant un début d'ébauche de solution esquissée sur le petit tableau noir. Après quelques semaines, il nous fut proposé de constituer entre nous des groupes de recherches, un Allemand, un Hongrois, deux Russes et moi avec l'opportun conseil de d'abord "match your different versions of English"...

Grâce à tout cela, de retour en Belgique, "les affaires" reprirent de plus belle. L'année 2004 fut très riche et commença par la plus belle rencontre d'entre toutes puisque je rencontrais Sabine qui avait rejoint mes amis de la ferme du Biéreau. Depuis ce jour c'est à Sabine et aux amis de "la Ferme": Christophe, Manu et Caroline, Pierre, Devi, Benjamin, ..., que je dois l'essentiel des belles heures de ces trois dernières années. L'organisation collective d'événements festifs, comme les fêtes saisonnières, le lancement d'un cycle de concerts de musique contemporaine, la résistance et la solidarité pour tenter de conserver un art de vivre lié à l'habitat et une

programmation indépendante représentent aujourd'hui les souvenirs les plus enthousiasmants de mon engagement extra-professionnel. Comment oublier la "Grande fête du Renon Constant" où nous rechaulâmes les murs de la Ferme contre forces de l'ordre communales et huissiers de tous ordres venus signifier l'ennième "renom" (sic) de notre bail. Comment oublier la "Conférence Mobile en Forme de Rose" que je conçus avec Bruno et la complicité de certains professeurs des départements de Lettres, Communication et Musicologie. Le 23 novembre 2004, l'auditoire SC10 fut réorganisé pour accueillir 4 pétales d'une rose imaginaire: les pétales "des Cantates", du "Théâtre Musical", "du docteur Faust" et "de l'Utopie". Une centaine de personnes avaient répondu présent et avaient pris place dans le pétale de leur choix. Il leur était demandé de chanter un fragment du "Temps des Surprises" en sachant que cette intervention collective au sein du pétale provoquait une convergence vers une seule note qui déclenchait alors, via un ingénieux procédé, l'évènement à suivre: des enfants avec leur instrument, une classe du secondaire, une classe de l'IAD, un comédien et plusieurs musiciens, ainsi que le public, intervenaient alors autour du travail commun du compositeur Henri Pousseur et du poète Michel Butor, tous deux présents au sein de la "Rose Butor-Bousseur" qui prenait forme sous nos yeux: en réagissant aux interventions, ils nous donnèrent à voir et à entendre une conférence d'un genre tout à fait nouveau.

Si je raconte cela c'est aussi pour affirmer l'extraordinaire lieu d'expérimentation que représente l'Université, si l'on en exploite ses ressources primordiales comme la curiosité et l'exigence. Bien autre chose, à mon avis, que l'"usine à cerveaux de demain"...pour servir le monde de hier?

Je tiens à présent remercier Françoise Paron, qui a été mon professeur de chinois à l'ILV pendant 5 ans. Ce furent aussi parmi les heures les plus insolites et passionnantes de mes 6 années sur ce campus. Je fut bien vite fasciné par l'écriture chinoise, par les idéogrammes surtout, sous leurs différentes formes, et entrepris de les introduire dans mes processus de composition musicale car je leur trouvais un sens musical profond. Ce travail continue de m'accompagner aujourd'hui, et je l'espère pourra rester un compagnon de route à l'avenir.

Tout cela a été possible durant cette importante période de ma vie, venant ponctuer une recherche dans mon domaine de thèse qui se précisait toujours davantage, alors que les immenses efforts consentis étaient peu à peu récompensés par une clarification progressive de notre théorie. J'ai dû beaucoup me documenter, lire des articles parfois anciens car cette théorie est née dans les années 50 des efforts de plusieurs mathématiciens et physiciens, pour disparaître vers la moitié des années 80 (sans doute par l'absence d'outils pour s'y engager d'avantage, ce à quoi ce travail est supposé contribuer) pour réémerger aujourd'hui très sporadiquement.

Cette théorie exige en effet une compréhension de domaines des mathématiques assez ardues, tels la géométrie non-riemannienne, par exemple. En simplifiant énormément, on peut donner une première vue de l'étude géométrique des dislocations dans les mono-cristaux en la comparant à la théorie de la Gravitation telle que décrite par Albert Einstein: des corps en mouvement qui déforment par leur masse l'espace-

temps, visualisé comme une toile d'araignée courbée aux endroits où ces corps massifs poursuivent leurs trajectoires. Les dislocations dans les cristaux sont des défauts concentrés sur des lignes consistant en des imperfections d'une structure cristalline considérée comme parfaite, c'est-à-dire sans défauts, lorsque les atomes qui la composent sont alignés de manière régulière, périodique. Ces structures atomiques caractérisent les cristaux, qui sont des solides déformables, mais si on observe les atomes de près, l'essentiel de la matière solide est en réalité constituée du vide. Le fait d'observer et d'analyser la matière à un niveau plus ou moins proche du niveau des atomes est le sens du mot "analyse multi-échelle" (en particulier l'échelle dite "mésoscopique" est intermédiaire entre les échelles atomiques et macroscopiques). A notre échelle (dite "macroscopique"), les dislocations impriment une trace visible de leur présence dans la matière, qui n'est pas nécessairement néfaste, bien au contraire. D'après notre théorie, les dislocations sont comprises comme des défauts provoquant courbure et torsion intrinsèques, non pas de l'espace-temps, mais du cristal tel qu'observé par un observateur interne lié à la structure cristalline: c'est le sens du terme "non-riemannien". Les singularités causées par leur présence sont cependant plus fortes que dans le cas de la Gravitation, c'est pourquoi nous utilisons une approche dite "distributionnelle".

Au sein de l'Unité, je voudrais remercier pour leur amitié et leur soutien Adrien, Brieux, François Bi(d)oul avec qui la cohabitation fut un vrai plaisir, Roman, Wu, Nathalie et Vincent, Michèle bien sûr avec qui j'ai beaucoup ri (notre "cantate" est toujours un work in progress...), Edmond, et tous ceux qui participèrent à son bon fonctionnement. En particulier Fabrice, qui fut un véritable compagnon de route tant nous avons suivi les parcours de vie de l'un et l'autre depuis 10 ans, avec beaucoup de discrétion et compréhension. De temps à autre, je retrouvais sur mon bureau un livre qu'il m'offrait, dont nous allions causer aux Halles sur le temps de midi. Si je repense aux temps de midi, j'ai été heureux de pouvoir compter sur Christophe, ma soeur Valérie et Mario ces trois dernières années pour m'échapper, un temps, hors de ce monde...D'autres belles rencontres durant ces années parmi les personnes rencontrées à la Ferme: Mathieu Dupont, Françoise et Charles, David et Joanna, entre autres, mais aussi certains étudiants rencontrés durant mes 6 années de TP en MMC.

Les deux dernières années de travail furent terriblement chargées: nous avons en réalité tout développé en deux ans, que ce soit la théorie des dislocations décrite dans la première partie de cette thèse (les trois premiers chapitres) ou le travail plus appliqué sur les défauts ponctuels décrit dans la seconde partie (le dernier chapitre). Pour cette partie, je tiens à remercier Nathalie et Vincent, Mathias et Arnaud de la société *Femagsoft* pour la collaboration fructueuse: je crois que nous avons bien développé ce module, qui est quasi-complet à présent. Pour toutes les recherches produites durant cette dernière période, je tiens tout particulièrement à remercier François Dupret pour son soutien indispensable à la compréhension et au développement des outils, de la physique et la mathématique en jeu, pour la rédaction du texte enfin, qu'il a eu la générosité de relire attentivement. J'ai appris énormément avec lui, cela va sans dire, et bien au delà des domaines scientifiques, sur le plan humain également. Je remercie également les autres membres du jury, Issam Doghri, Jean-Paul Issi et Erik van der

Giessen, qui ont bien voulu critiquer et apporter des commentaires sur mon texte, dont j'ai tenté de tenir compte. Je n'y suis certainement pas parvenu, et je m'en excuse: je leur ai donné beaucoup de mal avec un premier chapitre que j'avais imaginé comme "une boîte à outils" permettant la lecture et la compréhension des deux chapitres suivants, mais qui fut un flop, dans un premier temps, il faut bien le dire, pour cause d'une difficulté de ma part à conduire le lecteur de manière cohérente dans les méandres d'une théorie ardue. J'espère que les amendements apportés à cette partie corrigeront un tant soit peu le mauvais tir de départ.

Avant de terminer cette section, je tiens tout particulièrement à remercier mes parents et mes deux soeurs, Valérie et Laurence, qui m'ont beaucoup soutenu pendant ces années. Je ne pourrai jamais assez remercier Sabine pour sa compréhension et son soutien lorsque je rentrais à la maison après ces dures journées de travail, surtout vers fin. Ces marques furent indispensables à la réalisation de ce travail. Je leur dois beaucoup.

J'ai envie de dédier cette thèse à Mamy et Bon-Papa, mes grands-parents, en les remerciant de pouvoir partager tant de choses avec eux, hier comme aujourd'hui, et à Papy, qui n'est plus là mais avec qui je maintiens de très chers souvenirs.

Main contributions

This work has led to several contributions, with the principal ones listed here below :

- **Accepted paper:**

- Van Goethem, A. de Potter, N. Van den Bogaert, F. Dupret, “Dynamic Prediction of Point Defects in Czochralski Silicon Growth. An Attempt to Reconcile Experimental Defect Diffusion Coefficients with the V/G criterion”, Journal of Physics and Chemistry of Solids.

- **Submitted paper:**

- N. Van Goethem and F. Dupret, “A distributional approach to the geometry of 2D dislocations at the mesoscale”, submitted to the Journal of the Mechanics and Physics of Solids.

- **Conference abstracts :**

- N. van Goethem, F. Dupret, “A distributional approach to dislocations”, Second international conference of applied mathematics, 12-18 August 2005, Plovdiv, Bulgaria, p. 84.

- **Posters:**

- N. Van Goethem, “Dynamic prediction of defect formation in Czochralski silicon growth”, ISPN 2, Kaoshiung, Taiwan, October 2005.
- N. Van Goethem, N. Van den Bogaer, A. de Potter, F. Dupret, "Dynamic prediction of defect formation in Czochralski silicon growth. Analysis of the discrepancy between experimental defect diffusion coefficients and the V/G criterion", 5th International Workshop on Modeling in Crystal Growth, Bamberg, Germany, September 2006.

- **Conferences and proceedings:**

- R. Rolinsky, L. Wu, N. Van Goethem, B. Delsaute, F. Bioul, N. Van den Bogaert, V. Regnier, F. Dupret, "Dynamic Simulation of Bulk Crystal

Growth", Proc. 9th Scientific and Business Conference on Silicon Technology, Photovoltaic and Infrared Optics (SILICON 2004), Roznov pod Radhostem, Czech Republic, November 2004, K. Vojtechovsky editor, pp. 231-234.

- L. Wu, B. Delsaute, F. Bioul, R. Rolinsky, N. Van Goethem, V. Regnier, N. Van den Bogaert, F. Dupret, "Investigation of Short and Long Term Flow Transients in the Czochralski Silicon Growth Process", Proc. 14th Int. Conf. on Crystal Growth (ICCG-14), Grenoble, France, August 2004, paper 1223, p. 653.
- F. Dupret, N. Van den Bogaert, V. Regnier, R. Rolinsky, L. Wu, N. Van Goethem, B. Delsaute, F. Bioul, "Time-Dependent Modeling of the Entire Crystal Growth Process", Proc. Advanced Crystal Growth Conference and 2003 International Symposium on Substrate Engineering / Nano SOI Technology for Advanced Semiconductor Devices (ACGT & SNS), Seoul, Korea, November 2003, P.C. Kim editor, p. A03.
- F. Dupret, N. Van den Bogaert, V. Regnier, R. Rolinsky, L. Wu, N. Van Goethem, B. Delsaute, F. Bioul, "Time-Dependent Modeling of the Entire Crystal Growth Process", Proc. 4th International Workshop on Modeling in Crystal Growth, Fukuoka, Japan, November 2003, N. Imaishi, K. Kakimoto, Ch.-W. Lan editors, pp. 18-19.

- **Academic contributions (management of course exercises and applications):**

- MECA2901 : Mécanique des Milieux Continus, Prof. F. Dupret (edition of an exercise textbook, 2004).

Contents

Avant-propos et remerciements	iii
Main contributions	ix
I General introduction	1
II Mesoscopic modelling of the geometry of dislocations	11
Nomenclature	13
1 Ingredients for a multiscale analysis of the geometry of dislocations	17
1.1 Introduction	17
1.2 Dislocations and disclinations	19
1.2.1 Atomic formation of dislocations	19
1.2.2 Interaction of dislocations with point-defects	20
1.2.3 Five families of line-defects	22
1.2.4 A selection of dislocations and disclinations	23
1.3 The multiscale problem	23
1.3.1 The 3 scales of matter description	25
1.3.2 Burgers and Frank vectors and tensors	26
1.3.3 Atomic scale analysis: crystalline lattice	29
1.3.4 Meso-scale analysis: dislocated continuous medium	30
1.3.5 Macro-scale analysis: continuous medium	31
1.3.6 Defect densities.	32
1.4 Mesoscopic field multivaluedness	34
1.4.1 Basic properties of multivalued functions	34
1.4.2 The space of defect multifunctions	37
1.4.3 Single-valued strain and multivalued rotation and displacement fields	38
1.4.4 Weingarten's theorems and strain multivalued decomposition	39

1.4.5	Geometry of the dislocation lines	41
1.5	Expression of the Burgers vector in terms of the elastic strain only . .	42
1.6	Computation of 2D rectilinear dislocations	45
1.6.1	First group of solutions: planar displacement field	46
1.6.2	Second group of solutions: vertical displacement field	47
1.6.3	Three 2D examples of rectilinear defects	47
1.6.4	Screw and edge dislocations, and wedge disclination	49
1.7	Geometry of the dislocated crystal	50
1.7.1	Metric tensors, and the elastic strain	51
1.7.2	Space connexion and the internal observer	53
1.7.3	Non-Riemannian geometry of dislocated crystals	57
1.8	Classical and new approaches to the geometry of dislocations	58
1.8.1	Kleinert's approach	59
1.8.2	Kröner's approach	62
1.8.3	Proposal for a multiscale programme	65
1.9	Non-Riemannian objects in the dislocated crystal	69
1.9.1	Bravais distortion decomposition	70
1.9.2	Non-existence of the Bravais displacement field	71
1.10	Elementary notions of distribution and geometric measure theories . .	71
1.10.1	Distribution theory and Hadamard finite parts	72
1.10.2	Line integration and Hausdorff measures	76
2	A distributional approach to the geometry of 2D dislocations at meso-scale	81
2.1	Introduction	81
2.2	Multiple-valued fields and line invariants; distributions as a modelling tool at meso-scale	84
2.2.1	Distributional analysis of the multiple-valued fields	85
2.2.2	Rotation and displacement vectors	86
2.3	Distributional analysis of incompatibility for a single rectilinear dislocation	89
2.3.1	The 2D model for rectilinear dislocations	89
2.3.2	Mesosopic incompatibility for a single defect line	91
2.3.3	Applications of the main result	95
2.4	Distributional analysis of incompatibility for a set of isolated dislocations	96
2.4.1	Governing assumptions for the strain and Frank tensors	97
2.4.2	Mesosopic incompatibility for a set of isolated defect lines . .	101
2.4.3	Mesosopic defect densities in 2D incompatible elasticity . .	102
2.5	Macroscopic analysis	105
2.5.1	A first approach to homogenisation from meso- to macro-scale	105
2.5.2	The non-Riemannian macroscopic body	106
2.6	Concluding remarks	110

3	Extension of the distributional approach to 3D dislocations	113
3.1	Introduction	113
3.2	Geometrical analysis of the defect line L	114
3.2.1	Existence of a regular tube	115
3.2.2	Geometrical properties of the defect line L	118
3.3	3D elasticity of the dislocated crystal	122
3.3.1	Defect invariants and density tensors	122
3.3.2	3D strain compatibility	124
3.4	Governing assumptions for the strain and Frank tensors	128
3.5	Mesoscopic incompatibility for an isolated 3D defect line	135
3.5.1	The 3D expression of Kröner's formulas at the mesoscale.	138
3.6	Incompatibility of a discrete family of 3D dislocations	142
3.6.1	The case of an infinity of isolated dislocations	143
3.6.2	Analysis of the 0D clustering	143
3.6.3	Generalized Gauss-Green theorems and fractal clusters	144
3.6.4	Incompatibility of a 0D cluster	146
3.7	Conclusive remarks	148
III	Point-defect dynamics in single crystals	149
4	Dynamic prediction of point-defect formation in silicon crystals	151
	Dynamic prediction of point-defect formation in silicon crystals	151
4.1	Point-defects and grown-in defect modeling	152
4.1.1	Interstitial and vacancy equilibrium concentrations	152
4.1.2	Transport of interstitials and vacancies	154
4.1.3	Recombination of interstitials and vacancies	155
4.1.4	Diffusion of interstitials and vacancies	155
4.2	The mechanisms of diffusion	156
4.2.1	Atomic analysis of diffusion	157
4.2.2	General expression for the flux and the diffusion equation	158
4.2.3	Basic features of bulk diffusion in silicon crystals	159
4.2.4	The physics of thermo-diffusion	163
4.3	Model equations and asymptotic analysis	166
4.3.1	Thermal and point-defect models	166
4.3.2	Matched asymptotic analysis	168
4.3.3	Non dimensional equations	171
4.3.4	Alternative temperature gradient assumptions.	173
4.3.5	Outer solution	175
4.3.6	Inner solution	176
4.3.7	Far-field solution	178
4.4	A compilation of material data from the literature	183

4.5	Comparison of time-dependent and quasi-steady predictions	186
4.6	OSF-ring equilibrium of point-defects	187
4.6.1	The Sinno-Dornberger model	188
4.6.2	The Voronkov and Sinno simplified models	190
4.6.3	Computation of the V/G criterion	191
4.7	The influence of thermo-diffusion	193
4.7.1	Discussion and modification of the S-D model	193
4.7.2	An attempt to reconcile experimental defect diffusion coefficients with the V/G criterion	194
4.8	Conclusive remarks	195
IV	Conclusions	201

List of Figures

1	Crystal defects: a) impurity interstitial, b) dislocation, c) self-interstitial, d) cluster of impurity atoms, e) extrinsic dislocation loop, f) small substitutional impurity, g) vacancy, h) intrinsic dislocation loop, i) large substitutional impurity; from Föll and Kolbesen (1976).	4
1.1	Example of a dislocation loop (“edge dislocation”). In general the dislocation is a loop or an open curve ending at the crystal rim; from (Kleinert, 1989).	20
1.2	Multiple definition of the atomic dislocation location and displacement field multivaluedness; from (Kleinert, 1989).	21
1.3	Screw dislocation; from Kleinert(1989).	22
1.4	(a) Wedge disclination;(b) Splay (top) and twist (bottom) disclinations; from Kleinert (1989).	23
1.5	Dislocations in nickel observed by TEM. “The Transmission Electron Microscope is a powerful tool for materials science. A high energy beam of electrons is shone through a very thin sample, and the interactions between the electrons and the atoms can be used to observe features such as the crystal structure and features in the structure like dislocations and grain boundaries.”	
	24	
1.6	IBIC images of dislocations in relaxed silicon-germanium layers: “Ion Beam Induced Charge analysis of devices provides a unique method of studying fully functioning circuits beneath their thick surface layers without the need to remove any surface layers prior to analysis. This is due to the high penetrating power and low lateral scattering of the focused MeV ion beam used for analysis” (cf Dr. M. Breese, Univ. of Surrey).	

1.7	As precipitates decorating dislocations in a GaAs sample (from SEMI-LAB).	24
1.8	Dislocations in aluminum.	24
1.9	Atomic reference (left) and dislocated (right) crystal configurations for an edge dislocation. The Burgers circuit and vector are defined by atomic step counting; from Kleinert(1989).	26
1.10	Atomic scale observation of a crystal with a wedge disclination; from Kleinert (1989).	27
1.11	Example of multivalued function, with two branches.	36
1.12	Cubic root function on the complex plane. (a): Real part; (b): Imaginary part; from MIT OpenCourseWare	36
1.13	Scheme of a tube around L.	40
1.14	Rotation of 180° of a vector parallelly transported along path B (black path), while it keeps its south-east orientation along path A (white path) (a); Parallel transport along geodesics on a sphere (b).	54
1.15	Here the length of the curve is well-estimated by the sum of the diameters of the tiny balls, but grossly under-estimated by the diameter of the huge ball; from Ambrosio et al. (2000).	77
3.1	The sections of the tube do not intersect.	117
3.2	Curvature of the tube wrapped around L.	121
3.3	Example of a 2 dimensional (space-filling) Peano curve.	145
3.4	The snowflake as a sum of (oriented) simplexes (triangles) whose overlapping region has been cancelled (dotted lines).	146
3.5	(a) Simulation of defect-line clustering (snapshot of dislocation network evolution using the Paradis code; from Science & Technology review, November 2005; (b) Growing dislocations in sapphire exhibit very complex geometric structures.	147
4.1	(a) Elementary cell of crystalline silicon, where $a=0.543$ [nm] is the lattice constant; (b) Two-dimensional schematic representation of a neutral single vacancy; Two dimensional representation of a free silicon self-interstitial (c)-left, and a dumbbell configuration (c)-right; from Dornberger (1998).	153
4.2	Scheme of the principal diffusion mechanisms: 1) direct exchange, 2) ring mechanism, 3) vacancy mechanism, 4) interstitial mechanism, 5) interstitialcy mechanism, 6) crowdion; from Philibert (1988).	157
4.3	Successive jumps for the vacancy (a) and kick-out mechanisms (b). In the case of a tagged (tracer) atom (dashed point) these jumps are correlated; from Philibert, 1988.	160
4.4	Local lattice distortion and activation volumes for vacancy-atom interchanges; from Glicksman (2000).	161
4.5	Temperature field in the crystal at several growth stages.	167

4.6	Predicted interstitial distribution with quasi-steady (a) and time-dependent (b) defect simulations.	196
4.7	Predicted vacancy distribution with quasi-steady (a) and time-dependent (b) defect simulations.	197
4.8	Predicted defect difference ($C_I - C_V$) distribution with quasi-steady (a) and time-dependent (b) defect simulations.	198
4.9	199
4.10	Influence of the reduced heat of transport $Q_I^{**} = r_I \bar{H}_I^f$ on the $C_I - C_V$ distribution. All the other material parameters are the same as in the S-D model. The $C_I - C_V = 0$ isoline is in bold. Same growth conditions as in Fig. 4.8(a).	199
4.11	Comparison of the test- and S-D model predictions. Distributions of C_I (left) of $C_I - C_V$ (right) under the same growth conditions as in Fig. 4.8(a). The $C_I - C_V = 0$ isoline is in bold. At the height $H=2R$ the OSF ring location differs in the two solutions by 1 mm.	200

List of Tables

4.1	Non-dimensional coefficients.	170
4.2	Comparison table for material data (1).	185
4.3	Comparison table for material data (2).	186

Part I

General introduction

The ever-shrinking size of the microelectronic devices of our modern era imposes challenging restrictions on the quality of the silicon substrate used in the manufacturing of these devices (Kulkarni et al, 2004). It is known that most of the semiconductor single crystals including silicon, germanium, gallium arsenide, and indium phosphide crystals are grown by the Czochralski (CZ) method and some of its variants whose major problem is the formation of crystallographic imperfections resulting from large temperature gradients in the growing crystal. These gradients may cause the generation of thermal stresses and dislocations, while excess point-defects aggregate in various types of crystallographic defects during the crystal cooling period and the subsequent integrated circuit (IC) device processing (Wijaranakula, 1993). Various types of defects which are not related to ingot growth, but generated during wafer manufacturing, are also observed on and in silicon wafers, eg, damage due to mechanical processing, particles on the surface or dislocations originated by stress above the yield stress during thermal wafer treatment. Real crystals, as opposed to ideal crystals¹, incorporate a finite number of types of imperfections, such as impurities, self-interstitials, vacancies, grown-in microdefects and dislocations. These structural imperfections can be categorized according to their dimensional extension into point, line, surface and volume type defects. The different structural defects are summarised below and illustrated for silicon (Dornberger, 1998):

Point-defects. The class of point-defects comprises the mono-atomic defects. Point-defects are the fundamental building blocks for grown-in defects in silicon crystals. Self-interstitials and vacancies are intrinsic point-defects. Foreign atoms such as oxygen, boron, phosphorus, carbon and metal atoms are extrinsic point-defects. Some point-defects occupy interstitial sites, eg oxygen, while other defects are incorporated substitutionally, such as boron or carbon.

Line defects. Typical line defects are dislocations. Once generated during the growth of a silicon crystal, they can multiply instantaneously and generate networks of dislocations, that render the material unusable for device manufacturing.

Surface defects. Typical surface defects in crystals are grain boundaries, twin boundaries and stacking-faults. Interstitial type defects, such as extrinsic stacking fault, are formed in wafers by agglomeration of self-interstitials during heat treatments. Stacking faults consist of an additional double {111} lattice plane and are bordered by Frank-type partial dislocations.

Volume defects. Volume defects in silicon crystals are observed as polyhedral voids or precipitates of impurity atoms. Precipitating oxygen generates octahedral defects in CZ silicon crystals.

¹An ideal crystal is a perfectly symmetric and periodic arrangement of lattice atoms, whose elementary cell defines the geometrical configuration of the lattice elements and builds the basis of the crystal.

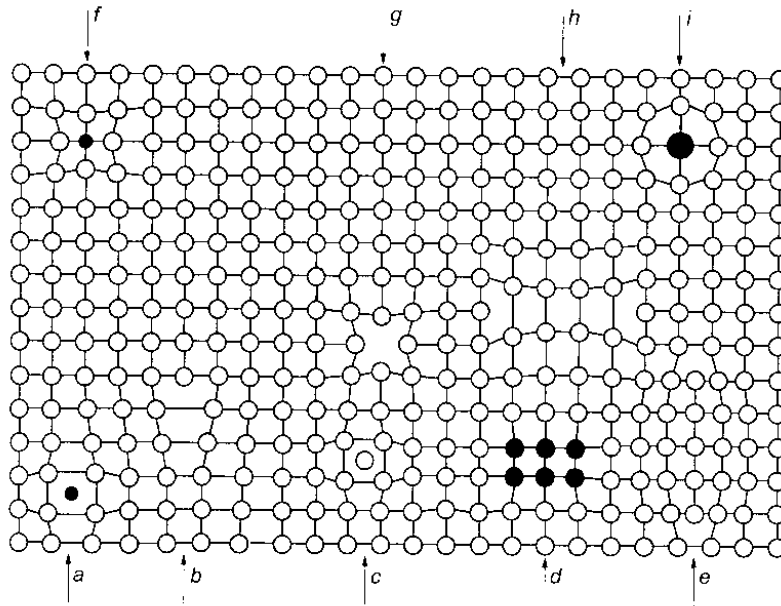


Figure 1: Crystal defects: a) impurity interstitial, b) dislocation, c) self-interstitial, d) cluster of impurity atoms, e) extrinsic dislocation loop, f) small substitutional impurity, g) vacancy, h) intrinsic dislocation loop, i) large substitutional impurity; from Föll and Kolbesen (1976).

Surface and volume defects, together with dislocations, are also termed “microdefects”. The most common microdefects in Czochralski silicon, are voids and dislocations loops, formed by the agglomeration of point-defects such as “vacancies” (formed by a missing silicon atom from the lattice) and “interstitials” (which are silicon atoms not bonded with the atoms forming the lattice). V. Voronkov (1982) was the first to describe the conditions leading to the formation of microdefects on the basis of an interplay between the transport of point-defects from the melt/crystal interface and the Frenkel pair reaction.

This thesis will give contributions to the fields of point- and line-defects, only. The approach followed for the point-defects (PD) analysis is essentially relying on the numerical simulation of “well-known” evolution equations, aiming at the solution of effective applications in the field of industrial crystal growth. Here, simulation results can be compared with real growth experiments, and the expectations from the growth industry are known and possibly fulfilled. In contrast, no satisfactory macroscopic

evolution model for dislocations in single crystals is known to us so far². Although huge contributions in this field for the last 5 decades, researchers still hamper on the intrinsic difficulties of the problem, viz. the complex dislocation geometries (including the effect of their conservation properties), the high tensorial orders of the involved fields (defect densities of order 2 meaning constitutive laws involving 4th-order tensors, etc.), letting apart the seeking of evolution laws for defect densities as a function of temperature, external and internal constraints, the identification of elastic and plastic contributions with their respective constitutive laws, the setting of appropriate boundary conditions, etc. Our initial aim was the creation of such a dislocation model, in the same spirit as for the PD model, but this objective soon appeared as non-realistic for two reasons, to be developed in the present thesis. First, the PD model has shown unexpected issues of phenomenological nature, in the sense that significant discrepancies (sometimes of several orders) between the physical parameters available in the literature were reported, and this made us at the very least suspicious for the passage to the (higher order) dislocation problem. Also, the reading of the known theories on dislocation modelling presented (in our opinion) some weaknesses, and the answers to these challenging problems took several years. Let us now briefly describe these two topics, and outline the structure of the thesis.

The structural properties of as-grown silicon are controlled by the type and concentration of intrinsic point-defects incorporated into the growing crystal. An incorporation model which is now commonly accepted, assumes the fast recombination of intrinsic point-defects in the vicinity of the crystal/melt interface. The annihilation stage is effectively complete when the temperature is below the melting point by about 100°[C]. After this stage, only one kind of point-defect, either vacancy or self-interstitial, remains present in supersaturated concentration while the competing defect rapidly disappears. There are five basic constants for the self-interstitials and the same for the vacancies: two for the equilibrium concentration (the melting point value and the formation energy), two for the diffusivity (the melting point value and the migration energy) and one for the drift velocity along a temperature gradient (to account for thermodiffusion). The problem in its simplest and conventionally accepted version (that is, when fast recombination of the point-defects is assumed) comprises 10 parameters. It has been emphasised by Voronkov & Falster (2003) that none of them is well defined (or well known) in the current state of knowledge. Moreover, in a simple approximation of a one-dimensional diffusion field, there is a universal critical value of the ratio of the growth rate (V) to the axial temperature gradient (G), generally referred to as V/G ratio, which separates the vacancy growth mode (at higher V/G) from the interstitial growth mode (at lower V/G). Due to the radial and axial non uniformity of G , the same crystal may contain both vacancy-type and interstitial-type regions sepa-

²Let us mention some recent progresses made in the theory of moving and interacting dislocations, as, eg, by Kubin (1992), Schwarz (1999) and Rodney (2004). Let us also mention other approaches to multiscale analysis, as found in Forest et al. (2001), Conti et al. (2002), Rodney et al. (2003).

rated by a well-defined boundary, known as “OSF ring”³. The critical V/G ratio is of fundamental importance to improve the growth of dislocation-free silicon crystals of controlled microdefect properties. For the standard interstitial growth mode the basic microdefects were found to be interstitial-type “dislocation loops” (Voronkov and Falster, 2002). For the standard vacancy growth mode the basic microdefects were found to be vacancy-type “microvoids”.

In fact, dislocations can be considered as the most undesirable and resistant class of defects for several kinds of single crystals (Maroudas & Brown, 1991; Jordan et al., 2000). Therefore, in order to improve crystal quality, the development of a relevant and accurate physical model represents a key issue with a view to reducing the dislocation density in the crystal by acting in an appropriate way on the temperature field and the solid-liquid interface shape during the growth process (Van den Bogaert & Dupret, 1997).

However the dislocation models available in the literature, such as the model of Alexander & Haasen (1968, 1986), are often based on a rather crude extension of models previously developed for polycrystals (such as usual metals and ceramics). In this case, some particular features of single crystals, such as material anisotropy or the existence of preferential glide planes, can be taken into account up to some extent, but the fundamental physics of dislocations in single crystals cannot be captured. In fact, dislocations are lines that either form loops, or end at the single crystal boundary, or join together at some locations, while each dislocation segment has a constant Burgers vector which exhibits additive properties at dislocation junctions. These properties play a fundamental role in the modelling of line defects in single crystals and induce key conservation laws at the macro-scale (typically defined by the crystal diameter). On the contrary, no dislocation conservation law exists at the macro-scale for polycrystals since dislocations can abruptly end at grain boundaries inside the medium without any conservation law holding across these interfaces.

Aware of these principles and of the pioneer works of Volterra (1907) and Cosserat (1909), Burgers (1939), Eshelby, Frank and Nabarro (1951, 1956), Kondo (1952), Nye (1953), and Kröner (1980) among other authors (Bilby, 1960; Mura, 1987) consider a tensorial density to model dislocations in single crystals at the macro-scale, in order to take into account both the dislocation orientation and the associated Burgers vector (cf the survey contributions of Kröner (1980, 1990) and Kleinert (1989)). However, in these works, the relationship between macro-scale crystal properties and the basic physics governing the atomic scale (defined by the inter-atomic distance) is not completely justified from a mathematical viewpoint. Therefore, to well define the concept of tensorial dislocation density, we will introduce in this thesis an additional scale to the macro-and atomic scales, viz. the meso-scale as defined by the average distance between dislocations. The laws governing dislocation behaviour are modelled

³The ring-like distributed oxidation-induced stacking fault appears with a high density on wafers after oxydation. A key reference is here Dornberger (1998).

at the atomic scale, while the meso-scale (defined from the atomic scale by ensemble averaging or by averaging over a representative volume (Kröner, 2001)) defines the "dislocated continuous medium", where each dislocation is viewed as a line and the interactions between dislocations can be modelled while the laws of linear elasticity govern the adjacent medium.

This thesis is twofold. The main part, viz. Chapters 1-3, is devoted to establish a "distributional approach" in order to analyse the geometry of 2D and 3D dislocations, aims at answering to the drawbacks of the "classical theories" (which essentially rely on the work done in the early 50ies by Eshelby, Frank, Nabarro, Kondo and Nye (1951-1956) and the review book on differential geometry by Schouten (1954)). These approaches are termed as "Kröner's" and "Kleinert's" approaches in Chapter 1, Section 1.8, where they are reviewed and criticised. In particular, Chapter 1 is devoted to be the toolcase for the understanding of both the motivations and the formal developments of Chapters 2 & 3. Chapter 2 focuses on the analysis of the 2D case, but since all the concepts are exposed in their full 3D generality, this chapter should be considered as the key chapter of our theoretical work on dislocations in this thesis. Chapter 3 provides an extension (obtained in Section 3.6) of the methods developed and used in the 2D case with a view to reaching a full generality for this "static", otherwise termed "geometric" analysis of dislocations.

The reader aware of these classical dislocation theories, including the non-Riemannian description of the defective crystal, can read Chapter 2 without consulting Chapter 1. He can also skip most of Chapter 3, which mainly consists of mathematical developments without new formal concepts, but is invited to glance to the new mesoscopic formulas for dislocation densities and strain incompatibility formulated in Section 3.5.1. On the other hand, Chapter 1 is really conceived for non-experts in the field. All the necessary concepts, of mechanical or mathematical nature, but also to some extent of "philosophical" nature, are exposed in an attempt of combined accuracy and pedagogy. Moreover, in case the reader is satisfied by the content of Chapter 1, he might skip Chapters 2 and 3 which appear as more specialised, without missing the point of this thesis.

The second and last part of this thesis is dedicated to the numerical simulation of point-defects in silicon crystals. Let us emphasise that no such theory can be considered as complete without comprising a combined model for point-defects, microdefects and dislocations, since these latter two are sinks and sources of point-defects. In fact, the scheme followed in Chapter 4 addresses problems which are common to both PD and dislocation modelling, viz. the nature of the evolution equations as a balance between transport, diffusion and recombination, to which nucleation equation should be added in the case of line and volume defects (see, eg, Nicola et al. (2006) for an analysis of nucleation in the framework of discrete dislocation plasticity). This chapter also includes a discussion on the PD formation and migration energies as well as

their equilibrium concentration values. It also comprises a discussion on the nature of diffusion, including the combined effects of self- and thermodiffusion, the transient effects, the asymptotic analysis leading to the observation of regions where a particular mechanism is preponderant with respect to others, and eventually the thermodynamic analysis of the complete problem including the setting of appropriate boundary conditions.

All these aspects of the PD problem were not completely clear, and Chapter 4 provides a contribution to the field, consisting in the following steps. Section 4.1 is a review of the evolution coupled equations between interstitials and vacancies in the case of Si CZ growth, while Section 4.2 describes more intensively the various mechanisms of diffusion, addressing the unclear and sensitive “thermodiffusion” issue. Section 4.3 proposes to set the problem in terms of non dimensional variables and aims at showing that the commonly accepted 1D model is probably not satisfactory if the sole “Damkohler number” effect is introduced. In fact, while the so-called “outer region” is well understood, the “far-field” region is more delicate since, on the one hand, the “freezing” of all thermo-dependent parameters should not prevent the however slow mechanisms of diffusion, nucleation etc. to progress, even very slightly and, on the other hand, the existence of a boundary layer where information from the lower regions is transported and which gets thinner as temperature decreases should be included in this asymptotic analysis. Briefly, this section outlines the difficulties of an asymptotic treatment of the exponentially decreasing and interrelated mechanisms of point-defect evolution. Section 4.4 follows a discussion with N. Stolwijk (Lerner & Stolwijk, 2005) who obtained, via direct measurements, values for the vacancy equilibrium concentration in silicon, in dramatic contradiction with the commonly accepted values in the crystal growth community. This section aims at summarising the various proposed values with a view to enlightening questionable aspects of the fitting approach in numerical simulation, while showing the resulting lack of physical understanding of the underlying mechanisms. Our contributions to the field from an applied point of view are explained in Sections 4.5 and 4.7. In Section 4.5 we present the results of time-dependent simulations of point-defects in Si crystals, identifying regions that were not correctly treated by quasi-steady approach, while Section 4.7 aims at proposing a reconciliation between “Stolwijk values” and the classical model by highlighting the possible role of thermodiffusion. Finally, Section 4.6.3 is a small complement to the abundant literature on OSF ring.

As a conclusive remark, let us claim the benefit of our twofold approach, where the first approach is the target of the second one. Point-defects are indeed not separable from dislocations, neither from a conceptual physical viewpoint, nor in terms of application to the effective calculation of defective matter. Since dislocations are intrinsically more complex structures because lines are of dimension 1 and codimension 2 in the 3D ambient space, and hence may exhibit complex geometries, it is natural to spend much effort on their understanding, and to be patient for the blooming of a complete model for their behaviour. However, PD analysis in the mean time has

shown the milestones for such a model, and simultaneously the dangers and issues to address for its elaboration. Much work remains to be done, probably mostly from an experimental viewpoint, but combination of modelling and experimental approaches is surely the best way to facilitate physical understanding. Finally, the rich nature of the phenomena involved in defect modelling, is for sure an immense field to be explored by mathematicians, and their contributions to the field has the advantage of being not programmable, leading to unexpected solutions or to the proposal of new approaches.

Part II

Mesosopic modelling of the geometry of dislocations

Nomenclature

Acronyms

2D: two-dimensional
3D: tri-dimensional
Pf.: pseudo-function
Fp.: finite part
BV: bounded variation
LHS: left-hand side
RHS: right-hand side

Variables

t : time
 x or x_i : position vector
 x_0 or x_{0i} : reference point
 x^L or x_i^L : position vector on the line L
 ξ_i : vector (mainly position vector on a curve)
 r, θ, z : cylindrical coordinates
 z or Z : variable of the complex plane

Fields

Classical fields of the multiscale linear Elasticity theory

\mathcal{E}_{ij} : macroscopic elastic strain tensor
 \mathcal{E}_{ij}^* : mesoscopic elastic strain tensor
 σ_{ij} : macroscopic stress tensor
 σ_{ij}^* : mesoscopic stress tensor
 \mathcal{E}^* : elastic energy density (compliance)

\mathcal{E}° : concentrated energy term
 $\mathcal{E}^{*\circ}$: corrected elastic energy
 η_{ij} : macroscopic elastic strain incompatibility tensor
 η_{ij}^* : mesoscopic elastic strain incompatibility tensor
 u_i : macroscopic displacement field
 u_i^* : mesoscopic displacement field
 u_i^{**} : atomic displacement field
 ω_i : macroscopic rotation or Bravais rotation field
 ω_i^* : mesoscopic rotation field
 ω_i^{**} : atomic rotation field

Fields introduced for the purpose of the distributional approach to dislocations

b_j^* : mesoscopic Burgers field
 β_{ij} : macroscopic distortion (i.e. displacement gradient $\partial_i u_j$) or Bravais distortion
 $\bar{\partial}_i \omega_j^*$: mesoscopic Frank tensor
 $\bar{\partial}_i b_j^*$: mesoscopic Burgers tensor
 $\bar{\partial}_i \bar{\partial}_j u_k^*$: tensor related to second order derivatives of the mesoscopic displacement
 $\bar{\partial}_i \omega_j$: macroscopic Bravais rotation gradient
 $\bar{\partial}_i \bar{\partial}_j u_k$: macroscopic Bravais distortion gradient
 $\bar{\partial}_i \omega_j^*$: mesoscopic Bravais rotation gradient
 $\bar{\partial}_i \bar{\partial}_j u_k^*$: mesoscopic Bravais distortion gradient

Defect densities

Θ_{ij} : macroscopic disclination density
 Λ_{ij} : macroscopic dislocation density
 α_{ij} : macroscopic displacement jump density
 κ_{ij} : macroscopic contortion
 Θ_{ij}^* : mesoscopic disclination density
 Λ_{ij}^* : mesoscopic dislocation density
 α_{ij}^* : mesoscopic displacement jump density
 κ_{ij}^* : mesoscopic contortion

Symbols

General symbols

ε, δ : small nonnegative numbers
 $i, j \dots$ and all Latin indices: indices taking their values in $\{1, 2, 3\}$
 $\alpha, \beta \dots$ and all Greek indices: indices taking their values in $\{1, 2\}$
 δ_{ij} : Kronecker symbol in 3D

$\delta_{\alpha\beta}$: Kronecker symbol in 2D
 ε_{ijk} : permutation (pseudo-)tensor (Levi-Civita symbol) in 3D
 $\varepsilon_{\alpha\beta}$: permutation (pseudo-)tensor (Levi-Civita symbol) in 2D
 \underline{e}_i : Cartesian base vector
 $\underline{e}_r, \underline{e}_\theta, \underline{e}_z$: cylindrical base vectors

Geometrical symbols

L: dislocation line
 \mathcal{L} : set of dislocation line
 s or t : arc parameter
 τ_i : tangent vector to L
 ν_i, σ_i : other Frenet's unit normal vectors
 C: circuit or loop (a closed curve)
 C_ε : circuit of radius epsilon
 $\hat{\nu}_i(x)$: unit vector joining the points x and \hat{x}
 $\hat{\sigma}_i$: tangent vector to C or C_ε
 Ω : dislocated crystal
 Ω_L : dislocated crystal without the dislocation lines
 Ω_i^* : mesoscopic Frank vector
 d_i : distance vector
 dx_i : tangent line element
 dC_i : line element multiplied by the external unit normal
 dS_i : area element multiplied by the external unit normal
 A, B, D, E, G, U, V, ϕ , S_j : point or subsets
 K: compact subset

Physical symbols

B_i^* : mesoscopic Burgers vector
 B_i^{**} : atomic Burgers vector
 \mathcal{R}_0 : macroscopic reference crystal
 \mathcal{R}_0^* : mesoscopic reference crystal
 \mathcal{R}_0^{**} : atomic reference crystal
 $\mathcal{R}(t)$: macroscopic crystal at time t
 $\mathcal{R}^*(t)$: mesoscopic crystal at time t
 $\mathcal{R}^{**}(t)$: atomic crystal at time t

Mathematical symbols

∂_i : partial derivative in the smooth classical or distributional sense
 $\partial_i^{(s)}$: partial derivative for defect multifunctions
 F: Riemann set

μ or ν : measures

$\phi, \varphi, \psi_i, \underline{\psi}$: test functions

$F, f, \tilde{f}, \hat{f}, g, h$: functions or real or complex variables

$[\cdot]$: jump of a function around the dislocation L or along the circuit C

δ_0 : Dirac mass

δ_L : concentrated measure on the line L

δ_S : concentrated measure on the surface S

Function spaces

$\mathcal{D}(\Omega)$ or $\mathcal{C}_c^\infty(\Omega)$: smooth functions with compact support over Ω

$\mathcal{D}'(\Omega)$: distribution space over Ω

$\mathcal{C}_c(\Omega)$: continuous functions with compact support over Ω

$L^1(\Omega, \mu)$: Lebesgue space over Ω with respect to the measure μ

$\mathcal{M}(\Omega)$: space Radon measures

Chapter 1

Ingredients for a multiscale analysis of the geometry of dislocations

1.1 Introduction

This chapter is devoted to provide a toolbox for the understanding of both the motivations and the formal developments of Chapters 2 and 3. In fact, the viewpoint of our approach is to study the geometry of dislocations at the *mesoscale*, where linear elasticity is assumed away from the dislocation line. Since, with this approach, a single dislocation is viewed as a line (i.e. as a set of vanishing volume and surface), all the effects which do not strictly pertain to linear elasticity, and in particular the elastic strain incompatibility, will be assumed to be concentrated along this line. However, in contrast with the Gravitation theory, where massive bodies are also modelled as concentrated Dirac masses, it will be shown that the theory of line-defects in single crystals also involves the gradient of such concentrated masses, therefore requiring a particular treatment which is not fulfilled by classical mathematical tools. Moreover, since in a single crystal the defect lines can sometimes form very complex aggregates, the multivaluedness of some fields (such as the displacement or rotation fields) is an issue to be addressed in its full generality, with a view to provide appropriate tools for the homogenisation of various (including fractal-like) dislocation clusters. Let us emphasise that this particular difficulty is not encountered if polycrystals are considered

instead of single crystals, since the existence of internal grains renders these effects much less critical.

The combination of field multivaluedness outside these defect lines together with concentration effects along these lines is a difficult task, requiring, at least in our approach, the use of mathematical concepts which are described in the present chapter. This chapter also aims at introducing the defects from a physical viewpoint, which, of course, is prior to the choice of the mathematical tools. Therefore, we have decided to organise this chapter in the form of small sections, each of them being divided in smaller subsections where a single issue is addressed independently. These sections alternatively address physical descriptions and the introduction of mathematical objects. Eventually, all the objects are combined together in order to provide a clear description of the physics of defects in single crystals.

The ingredients for a multiscale analysis of the geometry of dislocations are addressed as follows. In the first section the basic physics of dislocation formation is described, while in the second section, the question of a multiscale model is raised. Then, in the third section, the physical field multivaluedness is described in mathematical terms, while the fundamental invariance properties of the Burgers and Frank vectors are stated and proved. The fourth section is a complement to the two previous ones, aiming at discussing the consequences of the displacement and rotation multivaluedness in single crystals, and at proposing an appropriate basic approach for the mesoscopic modelling of dislocations which avoids the use of a reference configuration (noting that the latter is not required and arbitrary). This approach will be completed along the 3 last sections of the present chapter and further detailed in all the subsequent chapters. The next ingredient of this chapter is a collection of examples of rectilinear dislocations, devoted to validate the general results. The sixth ingredient of this chapter is an introduction to several concepts of differential geometry, which will all be encountered in the presentation of the results of Chapters 2 and 3. Here, the reader might not be interested in the reading all technical details, which are presented actually for the sake of completeness. We have chosen to mention all the particular difficulties encountered in terms of a geometric description of the defects, in order to highlight the full complexity of the problem, and hence the need for a complete clarification of the topic from a mathematical viewpoint. The seventh section is a discussion of previous approaches published in the literature, as compared to the approach described in this thesis. This section must be understood as providing the motivation for the development of the present theory. Finally, the last section is an introduction to the distribution theory and to other related concepts aiming at a rigorous description of concentration mechanisms.

1.2 Dislocations and disclinations

This section aims at describing the basic physics of dislocations and disclinations and contains the following subsections:

- Atomic formation of dislocations
- Interaction of dislocations with point-defects
- Five families of line-defects
- A selection of dislocations and disclinations

1.2.1 Atomic formation of dislocations

The formation of a dislocation line such as an “edge” dislocation, as illustrated in Figure 1.1, takes its origin in the removal (due to thermal activation or the supply of external forces) not only of isolated atoms, but of a connected set A of atoms originally located at regular lattice sites. These atoms change location inside the crystal lattice by occupying “interstitial” sites and leaving vacancies (which are the abandoned lattice sites) behind them. Atoms might also leave the crystal across its boundary or, reversely, penetrate from the external world into the crystal, thereby perturbing its perfect atomic order. A rearrangement of the atoms in the vicinity of A tending to suppress the vacancies follows in any case, but unless the periodicity of the upper and lower layers is maintained, the crystal is not anymore “perfect” in a region D surrounding the boundary of A , thereby forming a dislocation line, identified as D . A similar mechanism can be associated with the formation of an additional connected layer A of interstitial atoms whose boundary forms a dislocation line. In fact, the dislocation line at the atomic scale cannot be determined uniquely, since the removal of several distinct atom lines from the perfect crystal can produce an identical dislocated atomic picture. Therefore it seems preferable to use the term dislocation “region” instead of dislocation “location” at the atomic scale. Related to this, in Figure 1.2, it is pointed out that given a dislocated crystal, the atoms may be considered as having moved from a perfect lattice, but their displacement in the perturbed region is not uniquely defined. On the contrary, the deformation field around the dislocation region may be considered as uniquely defined. More exactly, we have a “multiple-valued” atomic map $x_i := \chi_i^{**}(X_i)$, $i = 1, 2, 3$, where $X_i \in \mathcal{R}_0^{**}$ denotes position in the reference body and $x_i \in \mathcal{R}^{**}(t)$ denotes position in the actual crystal at time t . In Figs. 1.1 and 1.2, multivaluedness results from a displacement of the order of the interatomic distance.

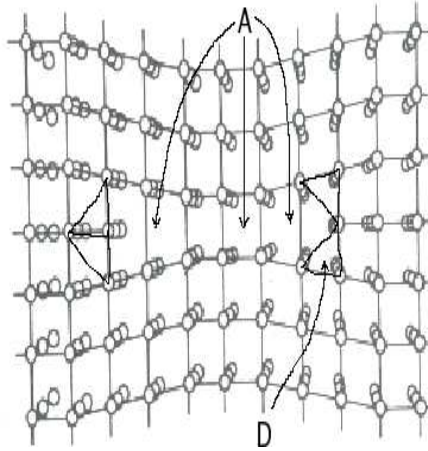


Figure 1.1: Example of a dislocation loop (“edge dislocation”). In general the dislocation is a loop or an open curve ending at the crystal rim; from (Kleinert, 1989).

Let us emphasise that this general situation does not allow us, neither to uniquely define some important dynamical fields such as displacement or rotation, nor to identify the precise location of the dislocation lines. In fact, addressing these issues will govern the mathematical model construction at higher scales, according to the present chapter review.

1.2.2 Interaction of dislocations with point-defects

The most common microdefects in Czochralski silicon growth are voids and dislocation loops, as formed by the agglomeration of point-defects, vacancies and interstitials. The Frenkel interstitial-vacancy recombination reaction, and the transport of point-defects occur simultaneously (cf Chapter 4 for further details). Moreover microdefects are submitted to the diffusion of point-defects from and to their surface according to the nucleation theory, in such a way that a complete picture of the dislocation dynamics should allow for a point-defect mass balance including diffusion, recombination, convection and consumption by the loops. Since in the case of silicon growth, nucleation occurs at lower temperatures, where point-defect recombination and diffusion have been damped out, it is accepted that the region above the melt/solid interface is concerned with “pure” point-defect dynamics as described in Chapter 4, whereas microdefect, or dislocation dynamics is rather observed in an upper region, where several physical parameters are submitted to slow variations or completely frozen.

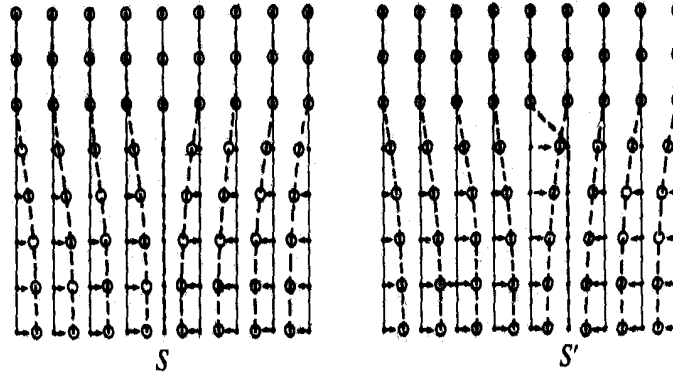


Figure 1.2: Multiple definition of the atomic dislocation location and displacement field multivaluedness; from (Kleinert, 1989).

More precisely, it has been mentioned in the Introduction that the magnitude of the V/G ratio just above the solidification interface, where V is the pulling rate and G , the thermal gradient, determines whether interstitial or vacancies will be the surviving point-defect species in the “far field” region. In fact at this stage the other species has been almost completely consumed, and hence, a microdefect of interstitial or vacancy type will be formed¹. Let us go back to Figure 1.1, and to the atomic formation of the associated edge dislocation. It has been explained how a void could be reduced to a dislocation loop by atomic movements. Moreover, the displacement or enlargement of such a loop occurs together with the creation or consumption of vacancies (or interstitials) along its edge part in the Burgers vector direction, and it results that dislocation dynamics is intrinsically related to point-defect evolution and should be associated to appropriate conservation laws. Finally, let us mention that, in actual crystals, it should be taken into account that extrinsic point-defects, such as oxygen, can segregate at a dislocation core, leading sometimes to its immobilisation (Senkader et al., 2000).

Since a proper analysis of all these interrelated phenomena represents a very complex task, it is beyond the scope of this thesis to describe these interactions and to analyse the complete set of conservation laws for multisized defects. However, although the approach followed to describe dislocations is here purely static, it should be kept in mind that only a coupled description of point-and line-defect evolution could provide a complete picture of the dislocation behaviour, and hence at every occasion it will be stressed that from both formal and computational viewpoints, these two classes of

¹Interstitial microdefects have been identified by various studies and termed A-clusters and B-clusters, or A-swirl and B-swirl defects, as associated with interstitial-related dislocation loops and globular structures, respectively. The vacancy agglomerates, or voids, are termed D-clusters (Kulkarni and Falster, 2003).

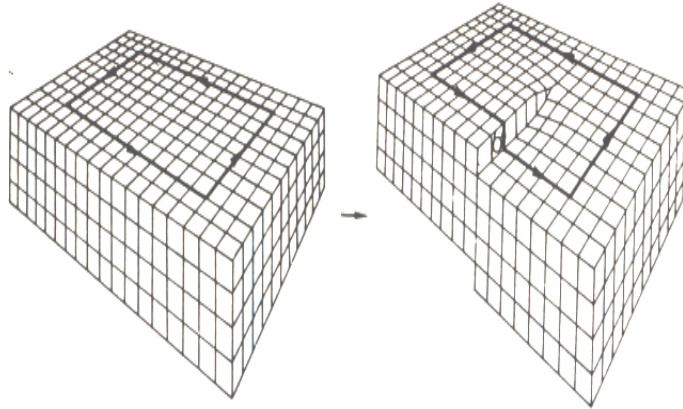


Figure 1.3: Screw dislocation; from Kleinert(1989).

defects are per se inseparable.

1.2.3 Five families of line-defects

In the above description of the atomic formation of a dislocation, one immediately distinguishes two classes of defects. If the lattice displacement is perpendicular to line D , the line is known as an *edge dislocation* (this was the case in the above Figures). If otherwise the lattice displacement is parallel to D , the line is called a *screw dislocation* as depicted in Figure 1.3. Let us however here cite H. Kleinert (1989). “Another type of defect called *disclinations* is capable of destroying the global rotational order while maintaining it locally. To describe the formation of a *wedge disclination* as depicted in Figure 1.4(a), take a regular crystal in the form of a cheese and remove a section subtending an angle Ω . The free surfaces can be forced together. For large Ω this requires considerable energy. Still, if the atomic layers on the free surfaces match together perfectly, the crystal can re-establish locally its periodic structure. We can imagine also the opposite procedure. We may cut the crystal, force the lips open by Ω and insert new undistorted crystalline matter to match the atoms in the free surfaces. These are wedge disclinations of negative angle. As for the dislocations case, if the vector Ω , instead of pointing in the direction of the line, now points orthogonal to D , two other types of defects appear, namely the *splay* and *twist* disclinations”, as depicted in Figure 1.4(b). The edge and screw dislocations, and the wedge disclination can be computed as rectilinear defects in planar elasticity, while the two other disclinations are fully 3D defects. These three 2D examples will be computed in Section 1.6 and

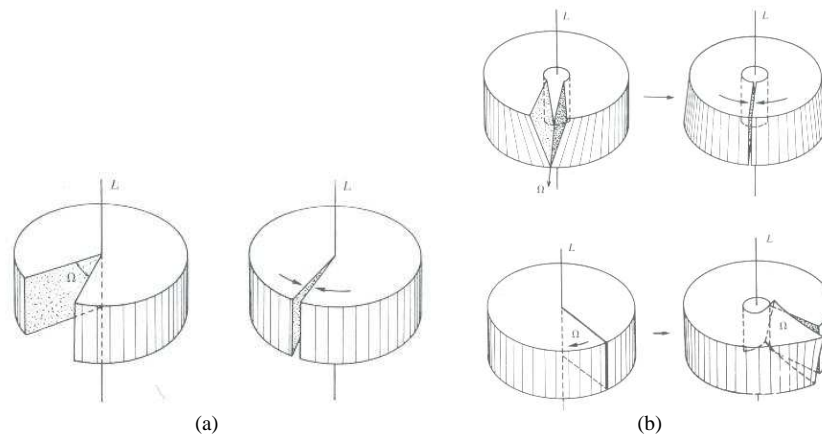


Figure 1.4: (a) Wedge disclination; (b) Splay (top) and twist (bottom) disclinations; from Kleinert (1989).

will allow us to validate our theory in the three first Chapters.

1.2.4 A selection of dislocations and disclinations

Figures 1.5-1.8 are chosen to show a variety of dislocations in single crystals. Whereas Figure 1.5 clearly illustrates the geometry of dislocation lines, which either form loops or end at the crystal rim, Figure 1.6 shows an array of rectilinear dislocations in silicon-germanium layers – which are crystals of interest in our work (cf Chapter 4 for a point-defect analysis). Figure 1.7 shows a collection of dislocations in gallium arsenide, which can be considered (together with indium phosphide dislocations) as a particularly resistant class of defects and Figure 1.8 shows a typical network of dislocations, with interactions, branching points and cluster regions. Let us point out that it is typical of single crystals to exhibit dislocations which can freely evolve while forming complex geometrical structures (cf Section 3.6.3).

1.3 The multiscale problem

The present work focuses on the mesoscale modelling of line-defects, but one should keep in mind that our ultimate objective is the obtention of homogenised defect den-

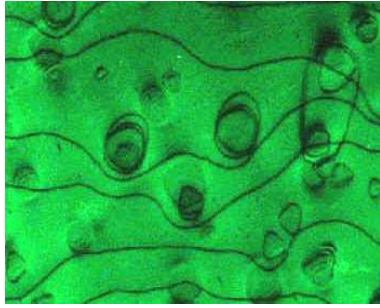


Figure 1.5: Dislocations in nickel observed by TEM. “The Transmission Electron Microscope is a powerful tool for materials science. A high energy beam of electrons is shone through a very thin sample, and the interactions between the electrons and the atoms can be used to observe features such as the crystal structure and features in the structure like dislocations and grain boundaries.”

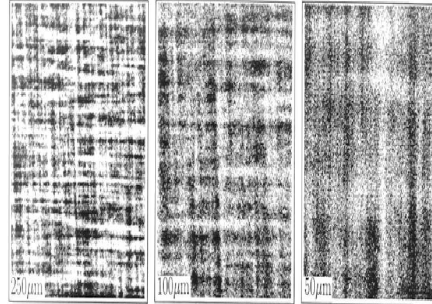


Figure 1.6: IBIC images of dislocations in relaxed silicon-germanium layers: “Ion Beam Induced Charge analysis of devices provides a unique method of studying fully functioning circuits beneath their thick surface layers without the need to remove any surface layers prior to analysis. This is due to the high penetrating power and low lateral scattering of the focused MeV ion beam used for analysis” (cf Dr. M. Breese, Univ. of Surrey).

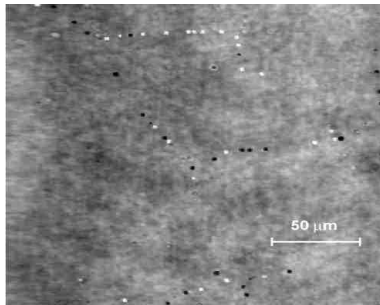


Figure 1.7: As precipitates decorating dislocations in a GaAs sample (from SEMILAB).

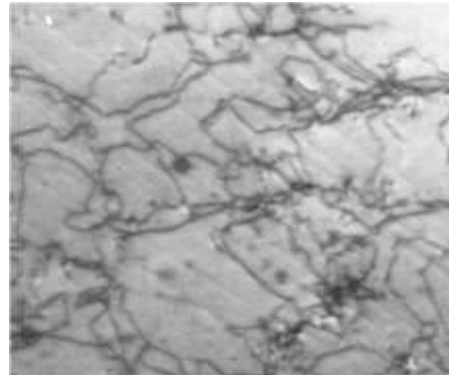


Figure 1.8: Dislocations in aluminum.

sities and the associated laws at the macro-scale. Moreover, it should also be recalled that some aspects of the fundamental physics of dislocations can only be handled at the atomic scale. Therefore, this section will briefly introduce these 3 scales of matter description and the relations between them. In particular, we will discuss the Burgers and Frank vectors, which are the basic defect properties associated to line-defects. This section contains the following subsections:

- The 3 scales of matter description
- Burgers and Frank vectors and tensors
 - Burgers circuit size
 - Dislocations and disclinations at the meso-scale
- Atomic scale analysis: crystalline lattice
- Meso-scale analysis: dislocated continuous medium
- Macro-scale analysis: continuous medium
- Defect densities

1.3.1 The 3 scales of matter description

To address the modelling of single crystals with line-defects, the various scales relevant for matter description and their interrelations are here briefly reviewed.

- At the atomic scale (generally indicated in the sequel by a double $\star\star$) the characteristic length is the interatomic distance. At time t , the body is referred to as $\mathcal{R}^{\star\star}(t)$ and the reference body is a perfect lattice $\mathcal{R}_0^{\star\star}$.
- At the meso-scale (indicated in the sequel by a single \star) the characteristic length is the average distance between two neighbour dislocation lines. At time t , the body is referred to as $\mathcal{R}^\star(t)$, to be interpreted as a random sample corresponding to a given growth experiment. The reference body \mathcal{R}_0^\star is a perfect crystal, i.e. a body without dislocations or disclinations.
- At the macro-scale (indicated without stars) the characteristic length is the diameter of the crystal and the body $\mathcal{R}(t)$ has a physical meaning related to $\mathcal{R}^\star(t)$ and $\mathcal{R}^{\star\star}(t)$ in terms of ensemble average; the reference body \mathcal{R}_0 can be, or not, a perfect crystal. The difficulty of selecting this reference configuration will be discussed at a later stage.

1.3.2 Burgers and Frank vectors and tensors

According to the above classification, the Burgers and Frank vectors associated with a line-defect can be defined at every scale:

- The *atomic Burgers vector* is, in the absence of disclinations, equal to the lattice displacement created by the dislocation. More exactly, it is equal to the closure failure in the reference configuration of the image of a closed loop enclosing once the dislocation in the actual crystal, that is, is defined as

$$B_i^{**}(C) = \sum_{\text{closed loop}} \Delta d_i(x_n) \quad (1.3.1)$$

where $\Delta d_i(x_n)$ denote the increments of the displacement vector between \mathcal{R}_0^{**} and \mathcal{R}^{**} along the closed loop C. Figure 1.9 shows how a closed circuit in the actual crystal is deformed into an open circuit in the reference configuration, while preserving the number of atomic steps (contrarily to the curve length) along this circuit in the presence of an edge dislocation. On the other hand, the

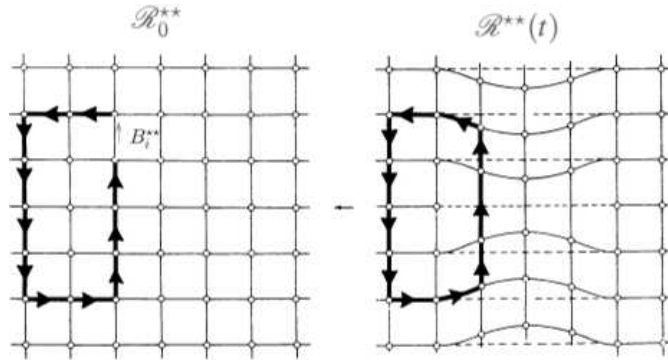


Figure 1.9: Atomic reference (left) and dislocated (right) crystal configurations for an edge dislocation. The Burgers circuit and vector are defined by atomic step counting; from Kleinert(1989).

atomic Frank vector is the total rotation experienced by a vector field parallelly transported (that is, transported while keeping a fixed angle with respect to the lattice lines) along a circuit enclosing the disclination line (which is also a dislocation since the deformation of a closed loop from actual to reference crystal will be an open curve if the number of atomic steps is preserved). Figure 1.10 illustrates the case of a wedge disclination.

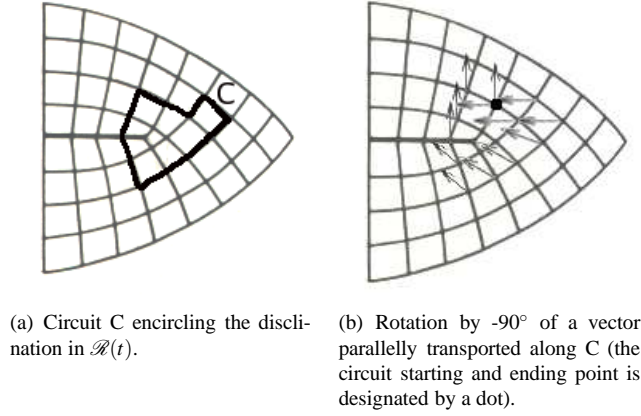


Figure 1.10: Atomic scale observation of a crystal with a wedge disclination; from Kleinert (1989).

- Considering now the mesoscopic scale (the “dislocated continuous medium”), the *mesoscopic Frank vector* along a circuit (i.e. a closed loop C in the actual crystal $\mathcal{R}^*(t)$) encircling once a disclination is defined as follows:

$$\Omega_k^* := [\omega_k^*](C) = \int_C \bar{\partial}_m \omega_k^* d\xi_m, \quad (1.3.2)$$

where the *Frank tensor* is introduced as

$$\bar{\partial}_m \omega_k^*(x) := \varepsilon_{kpn} \partial_p \mathcal{E}_{mn}^*(x). \quad (1.3.3)$$

while \mathcal{E}_{mn}^* denotes the (assumed) linear strain, ε_{kpn} stands for the permutation symbol and ∂_p for the gradient operator, while $[\omega_k^*](C)$ is the jump over C of the multivalued linear rotation vector ω_k^* . The classical summation convention of Einstein over repeated indices is used.

The symbol $\bar{\partial}_m$ is here introduced and it should be emphasised that, for reasons that will become clear at a later stage, it does not indicate a true derivative. In fact, $\bar{\partial}_m \omega_k^*$ simply represents a 2nd order tensor defined from the linear strain by Eq. (1.3.3) and related to the gradient of the multivalued field ω_k^* .

Similarly, the *mesoscopic Burgers vector* along a circuit encircling once a dislocation is defined from the knowledge of the linear strain \mathcal{E}_{ij}^* and a reference point x_0 as follows:

$$B_i^*(C; x_0) := [u_i^*](x; C; x_0) - \varepsilon_{ilm} [\omega_l^*](C) (x_m - x_{0m}) = \int_C \bar{\partial}_l b_i^* d\xi_l, \quad (1.3.4)$$

where the *Burgers tensor* is introduced as

$$\bar{\partial}_l b_i^*(x; x_0) := \mathcal{E}_{ii}^*(x) + \varepsilon_{ipq} (x_p - x_{0p}) \bar{\partial}_l \omega_q^*(x), \quad (1.3.5)$$

with the same remark as before concerning symbol $\overline{\partial}_l$.

Expressing the Burgers vector in terms of the strain, instead of the displacement gradient, is here of fundamental importance (such as for the Frank vector). Indeed, contrarily to the linear rotation and displacement fields, the strain is single-valued and hence can be homogenised to provide at the macro-scale the so-called *elastic strain*. The precise justification and detailed computation of Eqs. (1.3.2)-(1.3.5) is given in Section 1.5, while its main application to the validation of Weingarten's theorems is given in Section 1.4.4.

From Stokes theorem and strain incompatibility outside the defect lines, i.e. from the relation

$$\varepsilon_{jlm}\partial_l\partial_l\omega_k^* = \varepsilon_{jlm}\partial_l\varepsilon_{kpn}\partial_p\varepsilon_{nm}^* = 0 \quad (1.3.6)$$

away from L, it turns out that the mesoscopic Burgers and Frank tensors are equal for any pair of curves C and C' which are continuously deformable into each other. This is the well-known Weingarten's theorem, which states that the Frank and Burgers vectors are invariant vectors attached to a given defect line L (cf Section 1.4.4).

- Finally, at the macroscopic level, the *macroscopic Burgers and Frank vectors* associated to any surface S of $\mathcal{R}(t)$ are in turn defined from the dislocation and disclination densities over S:

$$\Omega_k(S) := \int_S \Theta_{ik} dS_i, \quad (1.3.7)$$

$$B_k(S) := \int_S \Lambda_{ik} dS_i, \quad (1.3.8)$$

where Λ_{ik} and Θ_{ik} stand for the dislocation and disclination density tensors, respectively, to be defined at a later stage (cf Section 1.3.6).

Burgers circuit size

Since the macro-scale Burgers/Frank circuit (or surface) diameter is much larger than the mesoscopic average distance between the defect lines, the macroscopic densities only provide information on the average defect densities. In particular these densities only provide the excess of defects of a given sign over the other sign defects in the selected region, whereas the crystal microstructure strongly depends on the positively and negatively oriented defects; for example the resulting Burgers vector turns out to be zero if an equal number of dislocations of both signs are present in a given region, even if this number is very high². Moreover, experience shows that often the

²A prominent example is tension, where for reasons of symmetry equal numbers of positive and negative dislocations are produced, so that $B_i(C) = 0$ for each C (Kröner, 2001).

material state can change in spite of the absence of a non-zero macroscopic dislocation density, while in some other cases (such as bending and torsion), excess dislocations of a given sign are produced, but their number is usually so small that the resulting change of state is much lower than that resulting from the simultaneously produced dislocations of both signs (Kröner, 2001). In fact, this indicates that the second-order defect densities (introduced in Section 1.3.6) are not sufficient to completely describe the matter behaviour in such cases and that higher-order tensors should be considered in addition.

Dislocations and disclinations at the meso-scale

The Frank vector of a defect line L is the invariant jump $\Omega_k^* := [\omega_k^*]$, while for a given reference point x_0 its Burgers vector is the invariant $B_k^* := [u_k^*](x) - \varepsilon_{klm}\Omega_l^*(x_m - x_{0m})$. A defect line with non-vanishing Frank vector is called a disclination, while a defect line with non-vanishing Burgers vector is called a dislocation. Clearly a disclination should always be considered as a dislocation by an appropriate choice of x_0 while the reverse statement is false since Ω_k^* might vanish. This is why, in the present work, the word “dislocation” means in the general sense a dislocation and/or a disclination. A pure dislocation is a dislocation with vanishing Frank vector. Moreover, let us remark that a purely rotational defect (i.e. such that $[\omega_k^*] \neq 0$ while $[u_k^*]$ vanishes) does not truly exist, by the invariance of the Burgers vector which shows that an appropriate selection of the reference point x_0 can always provide a non-vanishing B_k^* if $\Omega_k^* \neq 0$. This can be observed on Figure 1.10 where the perfect lattice dimensions have been modified by the presence of a disclination.

1.3.3 Atomic scale analysis: crystalline lattice

Given a dislocation in the general sense, the atomic arrangement $\mathcal{R}^{**}(t)$ differs from the reference lattice \mathcal{R}_0^{**} , and in addition the atom displacements from \mathcal{R}_0^{**} to $\mathcal{R}^{**}(t)$ are not uniquely defined (Kleinert, 1989). More exactly, a discrete *multivalued* (cf Section 1.4 for details) mapping $x_i := \chi_i^{**}(X_i), i = 1, 2$ or 3 applying the reference atom positions onto the actual atom positions, is defined with $X_i \in \mathcal{R}_0^{**}$ and $x_i \in \mathcal{R}^{**}(t)$. In general, to understand the meaning of the mapping χ_i^{**} , it should be first recalled that the dislocation position cannot be determined precisely at the atomic level since several dislocation locations in the actual crystal can be associated with the same picture of the atom positions (in fact the defect should be understood as located inside a nanoscopic lattice region). Moreover, as already explained, there is no way to uniquely define the displacement field at the atomic scale. Indeed any atom of \mathcal{R}_0^{**} can in princi-

ple be selected to define the displacement of a given atom of $\mathcal{R}^{**}(t)$ which is therefore a multivalued discrete mapping. In fact, the atom locations are unchanged in the left and right parts of Figure 1.2, both in \mathcal{R}_0^{**} and $\mathcal{R}^{**}(t)$, while the displacement definition and hence the dislocation line location are differently defined (the distinct atomic planes S or S', pictured on Figure 1.2, are filled with vacancies and the dislocation is at the boundary of this set of vacancies).

1.3.4 Meso-scale analysis: dislocated continuous medium

This scale is the one on which Chapters 2 and 3 of this work mainly focus, in the framework of linear elasticity. Let us here describe some general and basic field properties at the meso-scale level.

- Outside the defect line L, *displacement field* is a *multivalued function* (cf Section 1.4) such that for any point $X_l \in \mathcal{R}_0^*$ (the perfect crystal) one has

$$u_i^*(X_l) = x_i - X_i, \quad \text{with} \quad x_i := \chi_i^*(X_l),$$

and where $\chi_i^*(X_l)$ is a multivalued mapping from \mathcal{R}_0^* to $\mathcal{R}^*(t)$. Displacement multivaluedness represents an important difficulty to address at the meso-scale in dislocation modelling. As opposed to multiple-valued fields, single-valued fields will also be called uniform.

- The *linear strain* will be denoted by \mathcal{E}_{ij}^* . In general, the Lagrange deformation tensor is given by

$$\mathcal{E}_{ij}^* := \frac{1}{2}(\partial_j u_i^* + \partial_i u_j^* + \partial_j u_m^* \partial_i u_m^*), \quad \text{with} \quad \partial_j u_i^* := \frac{\partial u_i^*}{\partial X_j}.$$

In the sequel, linear elasticity will be assumed and hence the nonlinear terms are not taken into account at the meso-scale. This fundamental hypothesis relies on the assumption³ that all nonlinear deformation effects take place around the dislocation in an atomic scale region whose diameter is small compared to the meso-scale characteristic distance between the dislocations. Therefore, using a singular perturbation asymptotic treatment, the nonlinear effects become concentrated inside the defect line at the meso-scale and hence the strain can be assumed to be the single-valued linear symmetric tensor given by

$$\mathcal{E}_{ij}^* := \frac{1}{2}(\partial_j u_i^* + \partial_i u_j^*) \tag{1.3.9}$$

³In practise this assumption is certainly valid in single crystal growth.

outside the defect line and arbitrarily set to 0 on the defect line (noting that concentrated deformation effects inside this line do not play any role in displacement integration at the meso-scale).

- Outside the defect line L , the *infinitesimal rotation tensor* is a possibly multiple-valued field given by $\omega_{ij}^* := \frac{1}{2}(\partial_j u_i^* - \partial_i u_j^*)$ with the associated rotation vector given by

$$\omega_k^* = -\frac{1}{2}\varepsilon_{ijk}\omega_{ij}^* = \frac{1}{2}\varepsilon_{ijk}\partial_j u_i^*$$

and the identity $\omega_{ij}^* = -\varepsilon_{ijk}\omega_k^*$. The Frank and Burgers vectors Ω_k^* and B_i^* associated with a defect line are commonly defined as functions of the jumps of ω_k^* and u_i^* around this line. From Weingarten's theorems (cf Chapter 2 Section 2.2.2 or Kleinert (1989)), these vectors are shown as invariants of the defect line (Eqs. (1.3.2) & (1.3.4)). In general at the meso-scale a dislocation or a disclination is a defect line (i.e. a singular line for the strain) to which non-vanishing Burgers and/or Frank vectors are attached.

- The mesoscopic strain is said to be *compatible* on a region U if the *incompatibility tensor* as defined by

$$\eta_{ik}^* := \varepsilon_{lmn}\varepsilon_{kpq}\partial_m\partial_p\mathcal{E}_{qn}^* \quad (1.3.10)$$

vanishes on U . The dislocated crystal cannot be globally described by a compatible deformation field derived from a single-valued displacement field and hence the incompatibility tensor is concentrated in the defect lines.

This work is devoted to provide a clarification of the relation between mesoscopic incompatibility and defect densities.

1.3.5 Macro-scale analysis: continuous medium

At this level, a point x_i of the actual body $\mathcal{R}(t)$, with $x_i = \chi_i(X_i)$, $X_i \in \mathcal{R}_0$, will be called a material point – to be understood as a certain representative volume of matter of mesoscopic size located around point x_i .

In order to define macroscopic concepts such as temperature or stress, one needs to give a meaning to the temperature and stress at any point. The rigorous definition is obtained from an ergodicity argument and hence, at the macroscopic level, the fields on $\mathcal{R}(t)$ are defined as “ensemble averages” of the fields defined on $\mathcal{R}^*(t)$ (see Section 1.3.6 for a short review of this issue). By this operation these fields are smoothed, which means that concentration effects at the meso-scale level along the defect lines are erased. To this end, a weak limiting procedure (or homogenisation) is needed in order to define the dislocation and disclination densities Λ_{ij} and Θ_{ij} at the macro-scale

level from the knowledge of the meso-scale fields Λ_{ij}^* and Θ_{ij}^* .

To justify that homogenisation of mesoscopic concentrated terms results in continuous macroscopic counterparts of these terms, the following 1D analogy can be made. Consider the continuous function $g(x)$ on the interval $(a, b) \subset \mathbb{R}$ discretised by n points $x^{(k)}$ and define the distribution

$$g^{(n)}(x) = \sum_{k=0}^n \delta(x - x^{(k)}) g(x^{(k)}) \Delta^{(n)} x^{(k)},$$

with $\Delta^{(n)} x^{(k)}$ representing the lengths of small intervals covering (a, b) and which tend to 0 as $n \rightarrow \infty$, while $\delta(x - x^{(k)})$ is the shifted Dirac measure. Then, for any appropriate test functions ψ , one finds that

$$\lim_{n \rightarrow \infty} \langle g^{(n)}, \psi \rangle = \lim_{n \rightarrow \infty} \sum_{k=0}^n \psi(x^{(k)}) g(x^{(k)}) \Delta^{(n)} x^{(k)} =: \int_a^b g(x) \psi(x) dx,$$

and hence the atomic measures $g^{(n)}$ weakly converge to the continuous function g .

In this context, the macroscopic reference body \mathcal{R}_0 is basically arbitrary and can, or not, be a perfect crystal. Indeed, at the macro-scale, the displacement u_i must be a single-valued function, whereas the displacement field u_i^* is multivalued at the meso-scale (cf Section 1.4.2). Consequently the ensemble averaging procedure is forbidden for multivalued fields such as u_i^* and hence u_i is not the ensemble average of u_i^* . It should also be observed that removing the field multivaluedness by performing appropriate cuts is of no use here, since by derivation these cuts introduce arbitrary distributional contributions without physical meaning. In general, it is important to make it clear that the only fields which can be obtained at the macro-scale by ensemble averaging from the meso-scale are the so-called extensive fields associated with additive physical properties (such as specific mass, stress, specific internal energy... and the dislocation and disclination densities).

1.3.6 Defect densities.

- At the meso-scale, the dislocation line L has an arbitrary orientation, while the Frank and Burgers circuits are always defined in the sequel in order to encircle L in the right-handed sense, in such a way that choosing the opposite direction for the line orientation will let the Burgers and Frank vectors change sign. However the products $B_j^* \tau_j$ and $\Omega_j^* \tau_j$, where τ_j is the tangent vector to L , will keep the same sign. Since this quantity simultaneously accounts for the defect orientation and the resulting local crystal structure modification with respect to the

reference perfect crystal, the following geometric tensors are introduced:

$$\begin{aligned}
\text{DISCLINATION DENSITY:} & \quad \Theta_{ij}^* := \Omega_j^* \delta_{iL} \\
\text{DISLOCATION DENSITY:} & \quad \Lambda_{ij}^* := B_j^* \delta_{iL} \\
\text{DISPLACEMENT JUMP DENSITY:} & \quad \alpha_{ij}^* := \Lambda_{ij}^* + \varepsilon_{jlm} \Theta_{il}^* (x_m - x_{0m}) \\
\text{CONTORTION:} & \quad \kappa_{ij}^* := \alpha_{ij}^* - \frac{1}{2} \alpha_{mm}^* \delta_{ij},
\end{aligned}$$

where x_{0m} is a reference point for rotation and displacement integration. Here, symbol δ_{iL} is used to represent the concentrated vectorial measure density on the defect region L (in case of an isolated regular defect line it will be equal to $\tau_i \delta_L$, where δ_L is the “line-Delta measure”, cf Section 1.10.2).

Notice that not only the Burger and Frank vectors do not depend on the position x on L (by Weingarten’s theorem, cf Section 1.4.4) but also in practice the number of Burgers and Frank vector types is finite, often small, all being however connected to the lattice structure (Kröner, 2001). The disclination and dislocation density tensors Θ_{ij}^* and Λ_{ij}^* are measure densities related to the strain incompatibility η_{ij}^* as it will be shown later. Therefore, the tensors Λ_{ij}^* and Θ_{ij}^* are basic physical tools to model defect density at the meso-scale while η_{ij}^* plays a key role to understand their behaviour. The displacement jump density and mesoscopic “contortion” (otherwise termed lattice curvature, cf Section 1.7.3) tensors α_{ij}^* and κ_{ij}^* are combinations of these basic density tensors, with $\alpha_{ij}^* = \Lambda_{ij}^*$ when the disclination density tensor vanishes. Measuring the densities Θ_{ij}^* and Λ_{ij}^* can be performed at every spatial point x of the actual crystal, by scrutating the presence of a defect line at x , its orientation and the type and length of the associated Burgers and Frank vectors. This should provide the exact internal mechanical state of the crystal.

- At the macro-scale defect densities are introduced by *homogenisation* of their mesoscopic counterparts. In other words, we do not observe a single specimen (as in the mesoscopic approach) but study the behaviour of an ensemble consisting of several repetitions of the real (mesoscopic) system. To obtain a manageable statistical theory it is necessary to assume the validity of an ergodic hypothesis, which in our case of a static (geometric) approach, states that the *volume average* of a random function (as performed on a so-called “representative volume”) equals the *ensemble average* of the same function (Kröner, 2001), that is, in the case of defect densities:

$$\begin{aligned}
\underbrace{\Theta_{ij} := \frac{1}{\Delta V} \int_{\Delta V} \Theta_{ij}^* dV}_{\text{volume average}} & \stackrel{\text{ergodicity}}{=} \underbrace{\lim_{N \rightarrow \infty} \sum_N \Theta_{ij}^*}_{\text{ensemble average}} \\
\Lambda_{ij} := \frac{1}{\Delta V} \int_{\Delta V} \Lambda_{ij}^* dV & = \lim_{N \rightarrow \infty} \sum_N \Lambda_{ij}^*.
\end{aligned}$$

Here ΔV is the representative, or macroscopic, volume element which is infinitesimal at the macro-scale, but very large at the mesoscale, while N is the number of members of the statistical ensemble on which the test measurements are performed (Kröner, 2001).

1.4 Mesoscopic field multivaluedness

This technical section introduces the concept of multivalued functions in precise mathematical terms and allows us to correctly introduce the multivalued displacement and rotation fields. Its main results, termed as Weingarten's theorems, show the rotation and displacement jumps as obeying to invariance properties on the associated defect line.

The present section contains the following subsections:

- Basic properties of multivalued functions
- The space of defect multifunctions
- Single-valued strain and multivalued rotation and displacement fields
- Weingarten's theorems and strain multivalued decomposition
- Geometry of the dislocation lines

1.4.1 Basic properties of multivalued functions

Let us here start by introducing the meaning of some mathematical concepts. A “function”

$$f : \Omega \rightarrow \mathbb{R}^N$$

is referred to as a “multifunction” if the image set $f(x)$ for $x \in \Omega$ contains more than one element of \mathbb{R}^N . Let us already point out that the space of *multiple-valued* functions cannot be considered as a vector space.

In the presence of a cut surface $S \subset \Omega$ passing by the defect line L , a multifunction f could sometimes be written as

$$f(x; C) = f^{(S)}(x) + K[f](x),$$

where $K \in \mathbb{Z}$, $[f](x)$ is the jump of the function at x due to the presence of the line L , and where $f^{(S)}(x)$ denotes a simple function related to the arbitrary choice of S . However, it is precisely one of the key aspects of this work to avoid any kind of arbitrary introduction of a cut surface without precise justification, since this procedure appears in general as an artificial trick and does not really bring a tractable way to handle multifunctions. In particular, no homogenisation to the macroscale is possible when such cut surfaces are used. On the other hand, we will show that the multivaluedness of the elastic displacement and rotation fields can be taken into account in a rigorous manner. To this end, a general notion of multiple-valued functions is given below in the case of line-defects in linear elasticity.

Exact definition of a multivalued function. In the sequel, symbol Ω will denote the entire crystal, whereas Ω_L will denote the crystal without its dislocation lines. A multivalued function

$$f : \Omega_L \subset \mathbb{R}^N \rightarrow \mathbb{R}^N$$

consists of a set F with a topological structure (usually called Riemann set or *Riemann foliation*) and with two maps

$$\hat{f} : F \rightarrow \Omega_L \quad \text{and} \quad \tilde{f} : F \rightarrow \mathbb{R}^N$$

such that

- \hat{f} is a surjective map
- for every $\phi \in F$, there is a neighbourhood V of ϕ s.t.
 - $\hat{f}(V)$ is a neighb. of $\hat{f}(\phi)$
 - the restriction $\hat{f}|_V$ of \hat{f} s.t. $\hat{f}|_V : V \rightarrow \hat{f}(V)$ is an homeomorphism (i.e. one-to-one, continuous, and with a continuous reciprocal).

This definition can be summarised by the following scheme:

$$\Omega_L \leftarrow F \rightarrow \mathbb{R}^N,$$

where only the introduction of a cut surface can bring out the classical representation of f as a single-valued function associated with the scheme $\Omega_L \xleftarrow{f} F \rightarrow \mathbb{R}^N$.

Example. To understand the multivaluedness of the position vector $x_i = \chi_i^*(X_I)$, let us observe the analogy between χ_i^* and the multivalued function of a complex variable $z = f(Z) = \log Z = \log R + i\Theta$ where $Z = Re^{i\Theta}$. The set of image points of $Z = 1$ is $\{2k\pi i, k \in \mathbb{Z}\}$ and the difference between two elements of this set is an entire multiple of the jump $[z] = 2\pi i$. It is possible however to make f single-valued by cutting the complex Z -plane for instance along the positive

real half-axis. Hence, $Z = 1$ does no more belong to the domain of the single-valued function f but can be approached by letting $\Theta \rightarrow 0^+$ or $\Theta \rightarrow 2\pi^-$ with $R = 1$.

A selection of multivalued functions. Figure 1.11 pictures a multivalued function with two branches. Note that the notion of branch only appears as soon as a cutting surface has been introduced, otherwise one can pass from one branch to the other one without observing any particular change. Figure 1.12 shows the real and imaginary parts of the multivalued complex cubic root function, which has a 3-branch Riemann set. Let us remark that Riemann sets can exhibit infinitely many branches and can differ from the sole superpositions of identical sheets around a branching line, and hence can exhibit complex topological structures.

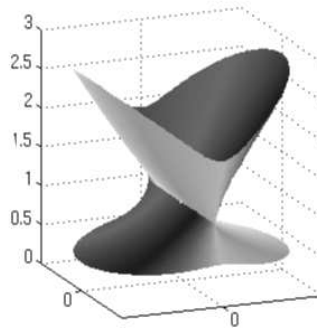


Figure 1.11: Example of multivalued function, with two branches.

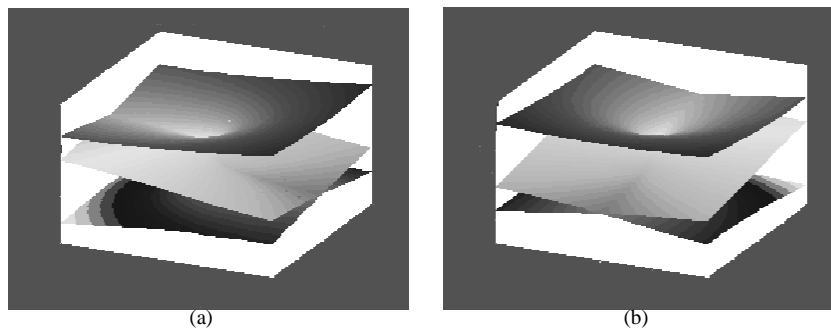


Figure 1.12: Cubic root function on the complex plane. (a): Real part; (b): Imaginary part; from MIT OpenCourseWare

1.4.2 The space of defect multifunctions

In this work, the following particular subclass of multivalued functions called “defect multifunctions” will only be considered.

Defect multifunctions. The multiple-valued scalar or vector function f belongs to the defect multifunction class if the single-valued $\mathcal{C}^\infty(\Omega_L)$ -differential form $\bar{\partial}_l f d\xi_l$ is closed on Ω_L (that is, if it verifies $\varepsilon_{jkl} \partial_k \bar{\partial}_l f = 0$ on Ω_L), where $\bar{\partial}_l f$ is defined on Ω and equal to $\partial_l f$ on Ω_L , while it is extended in some way on Ω . The same definition can be applied to distributions as well.

If $x_0 \in \Omega_L$ is a point where $f(x_0) := f_0$ is known and if $C \subset \Omega_L$ is a continuous curve joining the endpoints $x_0, x \in \Omega_L$ for a given $x \in \Omega_L$, the “function”

$$f(x; C) = f_0 + \int_C \bar{\partial}_l f(\xi; x) d\xi_l,$$

is multiply defined, since it depends on the choice of C . Since two homotopic (i.e. continuously deformable into each other) curves give the same value to $f(x; C)$, a so-called *defect multifunction* of index 1 is associated with

$$f(x; \#C),$$

where the equivalence class $\#C$ of C is the class of all curves homotopic to C . We observe that the Riemann set related to this class of functions is the set

$$F := \left\{ (x, \#C) \text{ for every } x \in \Omega_L \text{ and for every continuous curve joining } x_0 \text{ to } x \right\},$$

while the canonical projection $(x, \#C) \mapsto x$ defines the map \hat{f} and where the map \tilde{f} designates for instance the elastic displacement or rotation field in the forthcoming discussion.

It is crucial to observe that single-valued functions can be added since they share the same domain, whereas a multivalued function is defined on its specific Riemann foliation and cannot be added to a multivalued function defined on another Riemann foliation, thereby showing f as not belonging to a (linear) Banach space.

Moreover, a defect multifunction will be called of *index n* if its n th differential is single-valued. Typically, the rotation field ω_k^* is a defect multifunction of index 1, while the displacement field u_k^* is a defect multifunction of index 2.

The *jump* of a defect multifunction of index 1 (such as the rotation or the Burgers fields, as introduced below) is computed along the equivalence class $\#C$ of the closed curve C encircling once the line L as follows:

$$[f](C) = \int_C \bar{\partial}_l f(\xi; x) d\xi_l,$$

and also termed jump of f around L . The principal mathematical difficulty associated with multivalued functions results from the fact that they cannot be derived on the entire domain Ω , even in the distributive sense. This is why the notation $\bar{\partial}_i$ is introduced to represent in some sense the gradient of a defect multifunction of index 1. In the same way, the notation $\bar{\partial}_i \bar{\partial}_j$ is used for defect multifunctions of index 2. The notations $\bar{\partial}_i$ and ∂_i coincide away from L and it is one of the concerns of this work to distinguish between the gradient $\partial_i w_k^*$ of a single-valued field w_k^* and the single-valued second-order (resp. third-order) tensors $\bar{\partial}_m \omega_k^*$ (resp. $\bar{\partial}_j \bar{\partial}_l u_k^*$), whose first (resp. second) line integral is the index 1 (resp. index 2) multivalued rotation field ω_k^* (resp. displacement field u_k^*).

In addition, ∂_i will usually mean partial derivation w.r.t. $x_i \in \mathcal{R}^*(t)$ or $x_i \in \mathcal{R}(t)$. The notation $\partial_j^{(s)}$ is used for partial derivation of a single- or multiple-valued function whose domain is restricted to Ω_L . Locally around $x \in \Omega_L$, for smooth functions, the meanings of $\partial_j^{(s)}$ and the classical ∂_j are the same, whereas on the entire Ω the partial derivation operator ∂_j only applies to single-valued fields and must be understood in the distributive sense. A *defect-free* subset U of Ω is an open set such that $U \cap L = \emptyset$, in such a way that $\partial_j^{(s)}$ and ∂_j coincide on U for every single- or multiple-valued function of index 1.

1.4.3 Single-valued strain and multivalued rotation and displacement fields

For obvious physical reasons, it is indispensable to assume that the strain and all its derivatives are single-valued on Ω_L , whatever definition is selected for the reference configuration \mathcal{R}_0^* . From Eqs. (1.3.2) & (1.3.3), the rotation vector is a defect multifunction of index 1 defined on Ω_L as

$$\omega_k^*(x) := \omega_{0k}^* + \int_{x_0}^x \varepsilon_{kpn} \partial_p \mathcal{E}_{mn}^*(\xi) d\xi_m, \quad (1.4.1)$$

where $\varepsilon_{kpn} \partial_p \mathcal{E}_{nm}^*$ is denoted by $\bar{\partial}_m \omega_k^*$, while the displacement vector is a defect multifunction of index 2, which is obtained on Ω_L by recursive line integration of $\partial_j^{(s)} \partial_l^{(s)} u_k^* = \partial_j^{(s)} (\mathcal{E}_{kl}^* + \omega_{kl}^*)$ and hence by recursive integration of (cf Section 1.5 for details)

$$\bar{\partial}_j \bar{\partial}_l u_k^* = \partial_j \mathcal{E}_{kl}^* + \varepsilon_{kpl} \bar{\partial}_j \omega_p^*. \quad (1.4.2)$$

1.4.4 Weingarten's theorems and strain multivalued decomposition

The reader is invited to complement this section by reading Section 1.5, which specifically focuses on the obtention of the rotation and displacement fields by recursive line integrations of the linear strain only.

Weingarten's theorem for the rotation field. The rotation vector ω_k^* is a defect multifunction of index 1 whose jump $\Omega_k^* := [\omega_k^*]$ is an invariant of the line L.

Proof. Referring to the notations of Figure 1.13, for two distinct points \hat{x} and \hat{x}' , it can be observed that

$$[\omega_k^*](C_\varepsilon) = \lim_{\delta \rightarrow 0} \int_{C_\varepsilon^\delta(\hat{x})} \bar{\partial}_m \omega_k^* d\xi_m \quad \text{and} \quad [\omega_k^*](C'_\varepsilon) = \lim_{\delta \rightarrow 0} \left(- \int_{C_\varepsilon^\delta(\hat{x}')} \bar{\partial}_m \omega_k^* d\xi_m \right),$$

where C_ε and C'_ε stand for two circles of radius ε encircling L and defining a tube enclosing L, while δ denotes the thickness of a small strip removed from this tube parallel to L. Since the Frank tensor is a single-valued continuous function away from L,

$$\lim_{\delta \rightarrow 0} \int_{L_\varepsilon^\delta} \bar{\partial}_m \omega_k^* d\xi_m = 0,$$

in such a way that

$$[\omega_k^*](C_\varepsilon) - [\omega_k^*](C'_\varepsilon) = \lim_{\delta \rightarrow 0} \int_{C_\varepsilon^\delta(\hat{x}) \cup C_\varepsilon^\delta(\hat{x}')} \bar{\partial}_m \omega_k^* d\xi_m = \lim_{\delta \rightarrow 0} \int_{\Gamma_\varepsilon^\delta} \bar{\partial}_m \omega_k^* d\xi_m,$$

where $\Gamma_\varepsilon^\delta = C_\varepsilon^\delta(\hat{x}) \cup C_\varepsilon^\delta(\hat{x}') \cup L_\varepsilon^\delta$. By application of Stokes theorem,

$$[\omega_k^*](C_\varepsilon) - [\omega_k^*](C'_\varepsilon) = \lim_{\delta \rightarrow 0} \int_{\Sigma_\varepsilon^\delta} \varepsilon_{qlm} \partial_l \bar{\partial}_m \omega_k^* dS_q.$$

for any surface $\Sigma_\varepsilon^\delta$ enclosed by $\Gamma_\varepsilon^\delta$. By strain compatibility on Ω_L , the vanishing of the integrand for every $\delta > 0$ yields $[\omega_k^*](C_\varepsilon) = [\omega_k^*](C'_\varepsilon)$, both terms being denoted by Ω_k^* , where Ω_k^* is called the Frank vector of the line. \square

Multivalued displacement field. From the symmetric smooth linear strain tensor \mathcal{E}_{ij}^* , the multiple-valued displacement field u_i^* of index 2 is defined on Ω_L . Moreover, the symmetric part of the distortion tensor $\partial_j^{(s)} u_i^*$ is the single-valued strain tensor \mathcal{E}_{ij}^* on Ω_L , while its skew-symmetric part is the multiple-valued rotation tensor $\omega_{ij}^* = -\varepsilon_{ijk} \omega_k^*$.

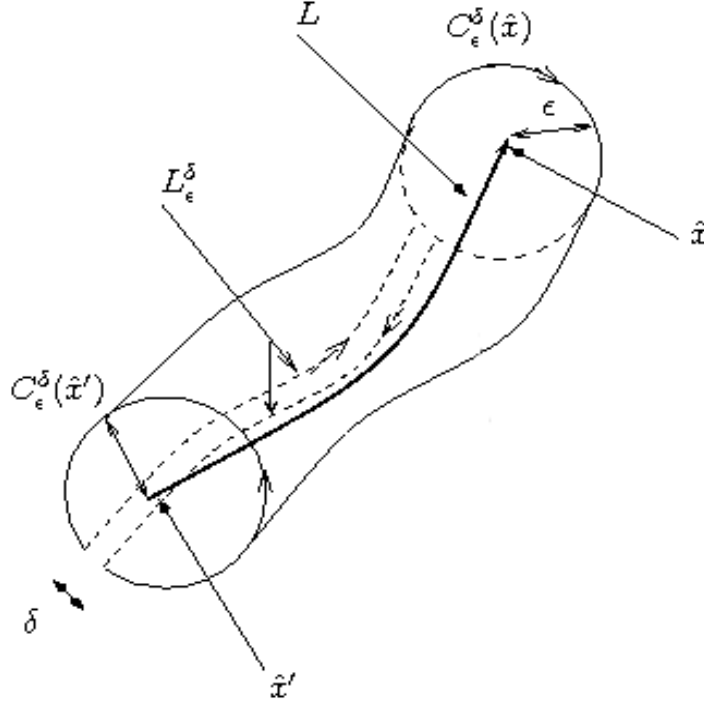


Figure 1.13: Scheme of a tube around L.

Proof. By Eq. (1.4.1), the rotation field $\omega_p^*(x; \Gamma)$ is defined for every smooth curve Γ joining x_0 to $x \in \Omega_L$, in such a way that its gradient is the known expression $\partial_m \omega_k^* = \varepsilon_{kpq} \partial_p \mathcal{E}_{qm}^*$ in the framework of the infinitesimal displacement theory. The displacement vector u_i^* is defined as the equivalence class of

$$u_i^*(x; \Gamma) = u_{0i}^* + \int_{\Gamma} [\mathcal{E}_{il}^* + \varepsilon_{lpq} (\xi_p - x_{0p}) \bar{\partial}_l \omega_q^*] d\xi_l + \varepsilon_{lpq} \omega_p^*(x; \Gamma) (x_q - x_{0q}), \quad (1.4.3)$$

for all curves homotopic to Γ . From the definition of the Burgers field

$$b_i^*(x) := u_i^*(x) - \varepsilon_{lpq} \omega_p^*(x_q - x_{0q})$$

where $x \in \Omega_L$, and of the Burgers tensor

$$\bar{\partial}_l b_i^*(x) := \mathcal{E}_{il}^*(x) + \varepsilon_{lpq} (x_p - x_{0p}) \bar{\partial}_l \omega_q^*(x),$$

the jump of the displacement field at $x \in \Omega_L$ writes as

$$[u_i^*](x) := \varepsilon_{ipq} \Omega_p^*(x_q - x_{0q}) + \int_{C_\varepsilon(x_L)} \bar{\partial}_l b_i^*(\xi) d\xi_l.$$

Since $\partial_l^{(s)} \omega_q^* = \bar{\partial}_l \omega_q^*$ and $\partial_l^{(s)} b_i^* = \bar{\partial}_l b_i^*$ away from L, the (s)-partial derivatives of the multifunction u_i^* at $x \in \Omega_L$ write as

$$\partial_j^{(s)} u_i^*(x) = (\mathcal{E}_{ij}^* - \varepsilon_{ijp} \omega_p^*)(x),$$

in such a way that the symmetric part of this multivalued distortion on Ω_L is the single valued strain $\frac{1}{2}(\partial_j^{(s)} u_i^* + \partial_i^{(s)} u_j^*) = \mathcal{E}_{ij}^*$, while its skew-symmetric part is the multivalued $\frac{1}{2}(\partial_j^{(s)} u_i^* - \partial_i^{(s)} u_j^*) = -\varepsilon_{ijp} \omega_p^*$, thereby proving the statement. \square

Weingarten's theorem for the displacement field. It turns out that the jump of the multiple-valued displacement field is a constant vector plus a fixed rotation term $\varepsilon_{ipq} \Omega_p^*(x_q - x_{0q})$, which is the cross product of the rotation jump Ω_p^* by the position vector $x - x_0$. In fact, by the same arguments as in the above proofs, it can be observed that

$$[b_k^*](C_\varepsilon) - [b_k^*](C'_\varepsilon) = \lim_{\delta \rightarrow 0} \int_{\Gamma_\varepsilon^\delta} \bar{\partial}_m b_k^* d\xi_m = \lim_{\delta \rightarrow 0} \int_{\Sigma_\varepsilon^\delta} \varepsilon_{qlm} \bar{\partial}_l \partial_m b_k^* dS_q$$

for any surface $\Sigma_\varepsilon^\delta$ enclosed by $\Gamma_\varepsilon^\delta$. By strain compatibility on Ω_L , it follows from Eqs.(1.3.5) and (1.3.3) that the integrand is zero, in such a way that $[b_k^*](C_\varepsilon) = [b_k^*](C'_\varepsilon)$ defines the invariant Burgers vector B_k^* of L as given by Eq. (1.3.4). \square

1.4.5 Geometry of the dislocation lines

From Weingarten's theorem proofs it immediately appears that dislocation lines are either closed loops or end at the crystal rim.

In fact, if the line had an endpoint $A \in \Omega$, then a surface Σ enclosed by $C_\varepsilon(x)$ and contained inside Ω_L could be found entirely inside Ω in such a way that, by application of Stokes' theorem and strain compatibility away from L,

$$[\omega_k^*](C_A) := \int_{C_\varepsilon(A)} \bar{\partial}_m \omega_k^* d\xi_m = \int_\Sigma \varepsilon_{qlm} \varepsilon_{kpn} \partial_l \partial_p \mathcal{E}_m^* dS_q = 0,$$

Moreover, by strain compatibility on Ω_L and since $\bar{\partial}_m \omega_m^* = 0$, it readily follows from Eqs. (1.3.5) and (1.3.3) that

$$B_j^* := [b_j^*](C_A; x_0) = \int_{C_\varepsilon(A)} \bar{\partial}_m b_j^* d\xi_m = \int_\Sigma \varepsilon_{qlm} \partial_l \partial_m b_j^* dS_q = 0,$$

thereby proving that either $A \in \partial\Omega$ or the line is closed.

1.5 Expression of the Burgers vector in terms of the elastic strain only

This section is devoted to justifying the use of the sole linear (elastic) strain and Frank tensor in the expression of the multivalued displacement field, of the Burgers vector and the associated defect densities at the meso-scale. The reason is that, using this approach, no reference configuration is needed at the meso-scale because the strain is in fact defined from the stress tensor and the temperature field (whose existence can of course be assumed) by the equations of linear elasticity. On the contrary, starting from the displacement field requires to define a reference configuration (the displacement being defined from some reference position to some actual position), and this represents a problem for several reasons:

- There is arbitrariness in the selection of the reference configuration (in particular, in single crystal growth from the melt, no privileged reference configuration exists since the crystal grows dislocated). Any further physical development then requires to show that the obtained result is independent of the reference configuration. In fact, passing by the objective strain field (as related to the displacement by Eq. (1.3.9)) solves the problem. However, at this stage, it turns out that the displacement field is not required anymore and that all developments can be carried out from the strain only. Considering the strain without reference configuration might seem contradictory, but this is not the case because this strain is in fact the elastic strain (at the meso-scale, the strain is purely elastic, except within the defect line). Both at the meso- and macro-scales, the elastic strain is directly defined from stress and temperature without requiring a reference configuration.
- There are complex issues related to displacement field multivaluedness, since in the presence of disclinations, the rotation field is itself multiple-valued. In particular, let us emphasise that no homogenization is allowed for multivalued fields whereas the single-valued elastic strain, stress, temperature, and defect density fields can all be homogenized from meso- to macro-scale. Moreover, our approach is not devoted to avoid the treatment of multivalued fields, but to carry out the developments in a sound mathematical framework. As a main benefit, this approach will allow us to rigorously demonstrate the Kröner fundamental identity “ $\text{inc } \mathcal{E} = \text{curl } \kappa$ ” relating the elastic strain incompatibility to defect densities, as explained in the remaining of this Chapter.

Let us now give the precise justification and detailed computation of Eqs. (1.3.2)-(1.3.5) and Eq. (1.4.3). Starting from the mesoscopic displacement field u_i^* , all the required quantities are successively defined as follows on Ω_L :

Strain

$$\mathcal{E}_{ij}^* = \frac{1}{2} (\partial_j u_i^* + \partial_i u_j^*) \quad (1.5.1)$$

Rotation tensor

$$\omega_{ij}^* = \frac{1}{2} (\partial_j u_i^* - \partial_i u_j^*) \quad (1.5.2)$$

Rotation vector

$$\omega_i^* = \frac{1}{2} \varepsilon_{ijk} \omega_{kj}^* = \frac{1}{2} \varepsilon_{ijk} \partial_j u_k^* \quad (1.5.3)$$

and hence

$$\omega_{ij}^* = -\varepsilon_{ijk} \omega_k^* \quad (1.5.4)$$

It results that Eqs. (1.5.1) & (1.5.3) imply that

$$\partial_m \omega_k^* = \varepsilon_{kpn} \partial_p \mathcal{E}_{mn}^* \quad (1.5.5)$$

and hence imply strain compatibility on Ω_L . Now, from classical elasticity, Eq. (1.5.5) implies that the rotation field is defined as

$$\omega_k^* := \omega_{k0}^* + \int_{x_0}^x \varepsilon_{kpn} \partial_p \mathcal{E}_{mn}^* d\xi_m. \quad (1.5.6)$$

From Eqs. (1.5.1), (1.5.2), (1.5.4), it results that

$$\partial_l u_i^* = \mathcal{E}_{il}^* + \omega_{il}^* = \mathcal{E}_{il}^* - \varepsilon_{ilk} \omega_k^* \quad (1.5.7)$$

and hence by integration that

$$u_i^*(x) = u_{0i}^* + \int_{x_0}^x (\mathcal{E}_{il}^*(\xi) - \varepsilon_{ilk} \omega_k^*(\xi)) d\xi_l,$$

and by partial integration (where the brackets denote the variation of a quantity between positions x_0 and x) that

$$\begin{aligned} u_i^*(x) &= u_{0i}^* + \int_{x_0}^x (\mathcal{E}_{il}^*(\xi) + \varepsilon_{imk} (\xi_m - x_{0m}) \partial_l \omega_k^*(\xi)) d\xi_l \\ &\quad - [\varepsilon_{imk} \omega_k^*(\xi) (\xi_m - x_{0m})]_{\xi=x_0}^{\xi=x}, \end{aligned}$$

which shows the displacement field as equal to

$$u_i^*(x) := u_{0i}^* + \int_{x_0}^x [\mathcal{E}_{il}^* + \varepsilon_{imk} (\xi_m - x_{0m}) \partial_l \omega_k^*] d\xi_l - \varepsilon_{imk} \omega_k^*(x) (x_m - x_{0m}). \quad (1.5.8)$$

Let us remark that, when disclinations are present in addition to dislocations, the displacement jump around the defect line is not an invariant of this line. Nonetheless the jump of the quantity b_i^* defined as follows is an invariant of the line and can be used to define the Burgers vector B_i^* :

$$b_i^* := u_i^* - \varepsilon_{ikm} \omega_k^*(x_m - x_{0m}), \quad (1.5.9)$$

and therefore

$$b_i^* := u_{0i}^* + \int_{x_0}^x [\mathcal{E}_{il}^* + \varepsilon_{imk}(\xi_m - x_{0m}) \partial_l \omega_k^*] d\xi_l, \quad (1.5.10)$$

in such a way that

$$\partial_l b_i^* = \mathcal{E}_{il}^* + \varepsilon_{imk}(\xi_m - x_{0m}) \partial_l \omega_k^*. \quad (1.5.11)$$

When disclinations are absent, the displacement jump around the defect line is an invariant of this line and can be used to define the Burgers vector B_i^* . In fact, since

$$[\varepsilon_{imk} \omega_k^*(x)(x_m - x_{0m})]_C = \varepsilon_{imk} [\omega_k^*(x)]_C (x_m - x_{0m}) = 0,$$

where the brackets here denote the the jump of a quantity along a closed curve C, it can be observed from Eq. (1.5.8) that

$$[u_i^*]_C = B_i^* = \int_C [\mathcal{E}_{il}^* + \varepsilon_{imk}(\xi_m - x_{0m}) \partial_l \omega_k^*] d\xi_l. \quad (1.5.12)$$

On the other hand, let us compute the displacement derivative, as obtained from Eq. (1.5.8) as

$$\begin{aligned} \partial_l u_i^*(x) &= \mathcal{E}_{il}^* + \varepsilon_{imk}(x_m - x_{0m}) \partial_l \omega_k^* + \varepsilon_{ikm} \partial_l \omega_k^*(x_m - x_{0m}) + \varepsilon_{ikl} \omega_k^* \\ &= \mathcal{E}_{il}^* + \omega_{il}^* \end{aligned}$$

which, after integration around C, provides the Burgers vector B_i^* . Hence in the presence of disclinations, the Burgers vector writes as

$$B_i^* := [b_i^*]_C = \int_C [\mathcal{E}_{il}^* + \varepsilon_{imk}(\xi_m - x_{0m}) \partial_l \omega_k^*] d\xi_l,$$

while in the absence of disclinations it writes as

$$B_i^* := [b_i^*]_C = [u_i^*]_C = \int_C \mathcal{E}_{il}^* + \varepsilon_{imk}(\xi_m - x_{0m}) \partial_l \omega_k^* d\xi_l = \int_C \partial_l u_i^*(\xi) d\xi_l.$$

As a consequence, the jumps of b_i^* and u_i^* are exactly the same in the absence of disclinations.

However, and this is the key justification of the present work, there are important reasons to use b_i^* instead of u_i^* in any case:

- This approach is more general since it is adapted to both the absence or the presence of disclinations.
- This approach allows us to define the Burgers vector from the strain \mathcal{E}_{ij}^* only (noting that, at the meso-scale, the strain is elastic everywhere along the integration paths defining b_i^* and B_i^* since non-elastic effects are concentrated within the defect lines). Indeed the rotation gradient $\partial_l \omega_k^*$ is itself related to the strain gradient by Eq. (1.5.6) and hence Eq. (1.5.10) defines b_i^* from the strain only.

1.6 Computation of 2D rectilinear dislocations

In the present section, the computation of 3 well-known examples of line-defects (2 dislocations and 1 disclination) is carried out in the planar case, that is, in the case of a rectilinear defect associated with an elastic strain which is independent of the 3rd coordinate z (as defined along the defect line). Let us precise that the conservation and constitutive laws involving strain and stress are only considered in the present section for the computation of explicit expressions of rectilinear dislocations, and no more in the remaining of this thesis⁴. In the sequel, in order to handle 2D (planar) and 3D computations together, Greek indices ($\alpha, \beta \dots$) will be assumed to take their values from 1 to 2, while Latin indices take their values from 1 to 3.

The present section contains the following subsections:

- First group of solutions: planar displacement field
- Second group of solutions: vertical displacement field
- Three 2D examples of rectilinear line-defects
- Screw and edge dislocations, and wedge disclination

⁴The goal is to clarify the geometrical theory of dislocations without introducing any restricting and superfluous assumption on the body forces and the temperature field in order to address a maximum physical generality.

1.6.1 First group of solutions: planar displacement field

From the elastic constitutive law $\sigma_{ij}^* = \lambda \mathcal{E}_{kk}^* \delta_{ij} + 2\mu \mathcal{E}_{ij}^*$ with λ, μ the Lamé coefficients and since $\mathcal{E}_{kk}^* = \mathcal{E}_{\gamma\gamma}^*$, the following planar law holds:

$$\sigma_{\alpha\beta}^* = \kappa^* \mathcal{E}_{\gamma\gamma}^* \delta_{\alpha\beta} + 2\mu \mathcal{E}_{\alpha\beta}^{*D}, \quad (1.6.1)$$

with the planar compressibility modulus κ^* defined by $\kappa^* := \lambda + \mu$ and the planar deviatoric strain given by $\mathcal{E}_{\alpha\beta}^{*D} = \mathcal{E}_{\alpha\beta}^* - \frac{1}{2} \mathcal{E}_{\gamma\gamma}^* \delta_{\alpha\beta}$, with $\delta_{\alpha\beta}$ the Kronecker symbol. From the equilibrium conditions $\partial_\beta \sigma_{\beta\gamma}^* = 0$ it follows that

$$\sigma_{\alpha\beta}^* = \varepsilon_{\alpha\gamma} \varepsilon_{\beta\delta} \partial_\gamma \partial_\delta F, \quad (1.6.2)$$

for a smooth enough Airy function F , in such way that

$$\sigma_{\alpha\alpha}^* = \partial_\alpha^2 F = \Delta F. \quad (1.6.3)$$

The relations between stress and strain are

$$\mathcal{E}_{\alpha\beta}^* = \frac{1+\nu^*}{E^*} \sigma_{\alpha\beta}^* - \frac{\nu^*}{E^*} \sigma_{\gamma\gamma}^* \delta_{\alpha\beta}, \quad (1.6.4)$$

with the 3D and planar elastic coefficients

$$E = \frac{\mu(3\lambda + 2\mu)}{\lambda + \mu}, \nu = \frac{\lambda}{2(\lambda + \mu)}, E^* := \frac{E}{1 - \nu^2}, \quad \text{and} \quad \nu^* := \frac{\nu}{1 - \nu}.$$

The first compatibility condition Eq. (2.3.1) writes from Eqs. (1.6.3) and (1.6.4) as

$$\Delta \Delta F = 0.$$

In this and the following sections, functions of the complex variable $Z = x + iy$ and its conjugate \bar{Z} are introduced. Remembering that, compared to holomorphic functions, analytical functions may be multivalued, it is easily seen that given two analytic functions f and g , all real functions of the form

$$F = \Re\{\bar{Z}f + g\}$$

satisfy Eq. (1.6.2) and vice-versa. Eq. (1.6.3) then shows that

$$\sigma_{xx}^* + \sigma_{yy}^* = 4\Re\{f'(Z)\}.$$

From Eqs. (1.6.3) and (1.6.4) the deformation tensor is given by

$$\begin{cases} \mathcal{E}_{xx}^* + \mathcal{E}_{yy}^* = \frac{4(1-\nu^*)}{E^*} \Re\{f'(Z)\}, \\ \mathcal{E}_{yy}^* - \mathcal{E}_{xx}^* + 2i\mathcal{E}_{xy}^* = \frac{2(1+\nu^*)}{E^*} (\bar{Z}f''(Z) + g''(Z)), \end{cases} \quad (1.6.5)$$

yielding after integration

$$\begin{aligned} E^*(u_x^* - iu_y^*) &= (3 - \nu^*)\bar{f}(Z) - (1 + \nu^*)(\bar{Z}f'(Z) + g'(Z)), \\ E^*\omega_z^* &= 4\Im\{f'(Z)\}. \end{aligned} \quad (1.6.6)$$

It should be recalled that $\mathcal{E}_{\alpha\beta}^*$ must be a single-valued field.

1.6.2 Second group of solutions: vertical displacement field

Another solution concerns the particular case where $u_\alpha^* = 0$, noting that each solution of 2D elasticity can be decomposed into a purely planar and a purely vertical solution. In fact, since stress equilibrium shows that

$$(\lambda + \mu)\partial_i\partial_j u_j^* + \mu\Delta u_i^* = 0,$$

it is easy to infer for $i=z$ that

$$u_z^* = \frac{(1+\nu)}{E} \Re\{h(Z)\}, \quad (1.6.7)$$

with $h(Z)$ an analytic function. Then

$$\mathcal{E}_{xz}^* - i\mathcal{E}_{yz}^* = \frac{(1+\nu)}{2E} h'(Z). \quad (1.6.8)$$

The function $h'(Z)$ must be uniform. The complex rotation is

$$\omega^* := \omega_x^* + i\omega_y^* = -\frac{i(1+\nu)}{2E} \overline{h'(Z)}. \quad (1.6.9)$$

In 2D isothermal linear elasticity without body forces, every displacement solution has planar components given by Eq. (1.6.6) and a vertical component given by Eq. (1.6.7) while the rotation vector has planar components given by Eq. (1.6.9) and a vertical component given by Eq. (1.6.7) (cf Sokolnikoff (1946) and Knopp (1996)).

1.6.3 Three 2D examples of rectilinear defects

In this section we consider the two typical multivalued analytic functions $\log(Z)$ and $Z\log(Z)$. Starting from the general uniform strain expressions Eq. (1.6.5) or Eq. (1.6.8) it is easily observed that any of the holomorphic functions f'' (with $\Re\{f'\}$ single-valued), g'' and h' can provide a solution to the 2D problem. Since these functions can be expanded in Laurent series:

$$f''(Z) = \sum_{-\infty}^{+\infty} a_n Z^n, \quad g''(Z) = \sum_{-\infty}^{+\infty} b_n Z^n, \quad h'(Z) = \sum_{-\infty}^{+\infty} c_n Z^n,$$

inside their respective convergence annuli, primitivation shows that

$$\left\{ \begin{array}{l} f(Z) = \sum_{\substack{-\infty \\ n \neq -1, -2}}^{+\infty} \frac{a_n}{(n+1)(n+2)} Z^{n+2} - a_{-2} \ln(Z) + a_{-1} Z \ln(Z) + A_1 Z + A_0, \\ g(Z) = \sum_{\substack{-\infty \\ n \neq -1, -2}}^{+\infty} \frac{b_n}{(n+1)(n+2)} Z^{n+2} - b_{-2} \ln(Z) + b_{-1} Z \ln(Z) + B_1 Z + B_0, \\ h(Z) = \sum_{\substack{-\infty \\ n \neq -1}}^{+\infty} \frac{c_n}{n+1} Z^{n+1} + c_{-1} \ln(Z) + C_0, \end{array} \right.$$

with a_{-1} real in order that $\Re\{f'\}$ be uniform. The relevant cases are those which give rise to a dislocation or a disclination, i.e. such that the functions $\bar{f}, f', g', \Re\{h\}$ or $\Im\{f'\}$ are multivalued. Hence, in order to obtain non-vanishing rotation or displacement jumps, one needs to consider the following cases:

$$f(Z) = -a_{-2} \ln\left(\frac{Z}{R}\right) + a_{-1} Z \ln\left(\frac{Z}{R}\right), \quad a_{-1} \in \mathbb{R}, \quad (1.6.10)$$

$$g(Z) = b_{-1} Z \ln\left(\frac{Z}{R}\right), \quad (1.6.11)$$

$$h(Z) = c_{-1} \ln\left(\frac{Z}{R}\right), \quad c_{-1} \in i\mathbb{R}, \quad (1.6.12)$$

where R is a constant length and to which any purely elastic term may always be added. In fact, from Eqs. (1.6.6), (1.6.7), (1.6.7) and (1.6.9), and from the definition $B^* := B_x^* + iB_y^*$ with B_k^* given by Eq. (3.3.4), it follows that:

$$\left\{ \begin{array}{l} \Omega_z^* = \frac{4}{E^*} [\Im\{f'\}], \\ \bar{B}^* : = B_x^* - iB_y^* = [u_x^*] - i[u_y] - \Omega_z^*(iz) \\ \quad = \frac{3-\nu^*}{E^*} [\bar{f}] - \frac{1+\nu^*}{E^*} \{Z[f'] + [g']\} + \frac{4i\bar{Z}}{E^*} [\Im\{f'\}], \\ \Omega^* : = \Omega_x^* + i\Omega_y^* = -\frac{i(1+\nu)}{2E} [\bar{h'}], \\ B_z^* = [u_z^*] - \Re\{i\bar{Z}\Omega^*\} = \frac{1+\nu}{E} [\Re\{h\}] - \frac{1+\nu}{2E} \Re\{Z[\bar{h'}]\} = \frac{1+\nu}{E} [\Re\{h\}]. \end{array} \right.$$

It should immediately be noted that Ω^* vanishes identically since h' cannot be multivalued. From Eqs. (1.6.10)-(1.6.12) and some easy computations, the only possible solutions are given by the following proposition (in summary): for a straight defect line L in 2D elasticity, there are no more than three distinct defect classes. The two dislocation classes are the screw dislocation which has a vertical Burgers vectors B_z^* and is generated by the analytical function h (with $f = g = 0$), and the edge dislocation which has a planar complex Burgers vector $B_x^* + iB_y^*$, and is generated by the analytical function g (with $f = h = 0$). There is a single class of disclinations, the wedge

disclination, which has a vertical Frank vector Ω_z^* and is generated by the analytical function f (with $g = h = 0$). These functions are:

$$\text{WEDGE DISCLINATION} \quad f(Z) = \frac{E^* \Omega_z^*}{8\pi} z \ln\left(\frac{Z}{R}\right) \quad (1.6.13)$$

$$\text{EDGE DISLOCATION} \quad g(Z) = \frac{E^* (B_y^* + iB_x^*)}{2(1+\nu^*)\pi} Z \ln\left(\frac{Z}{R}\right) \quad (1.6.14)$$

$$\text{SCREW DISLOCATION} \quad h(Z) = \frac{iEB_z^*}{2\pi(1+\nu)} \ln\left(\frac{Z}{R}\right). \quad (1.6.15)$$

For the edge dislocation, a detailed derivation was given by Eshelby (1966).

1.6.4 Screw and edge dislocations, and wedge disclination

The remaining of this section is devoted to present the three classical examples of 2D line-defects for a medium assumed to be body force free and isothermal.

- *Pure screw dislocation.* From Eq. (1.6.7), (1.6.9), and (1.6.15), the displacement and rotation vectors write as

$$u_i^* \underline{e}_i = \frac{B_z^* \theta}{2\pi} \underline{e}_z \quad \text{and} \quad \omega_i^* \underline{e}_i = \frac{1}{2} \nabla \times u_i^* \underline{e}_i = \frac{B_z^*}{4\pi r} \underline{e}_r, \quad (1.6.16)$$

with $\{\underline{e}_i\}$ the Cartesian unit base vectors and $\{\underline{e}_r, \underline{e}_\theta, \underline{e}_z\}$ the cylindrical unit base vectors, in such a way that the jump $[\omega_i^*]$ vanishes identically, while from Eq. (1.6.8) the Cartesian strain writes as

$$[\mathcal{E}_{ij}^*] = \frac{-B_z^*}{4\pi r^2} \begin{bmatrix} 0 & 0 & y \\ 0 & 0 & -x \\ y & -x & 0 \end{bmatrix}. \quad (1.6.17)$$

Moreover, in Ω_L , appealing to Eq. (1.6.17), the Frank tensor writes as

$$[\bar{\partial}_m \omega_k^*] = \frac{-B_z^*}{4\pi r^2} \begin{bmatrix} \cos 2\theta & \sin 2\theta & 0 \\ \sin 2\theta & -\cos 2\theta & 0 \\ 0 & 0 & 0 \end{bmatrix}. \quad (1.6.18)$$

- *Pure edge dislocation.* From Eq. (1.6.6), (1.6.7), and (1.6.14), the displacement is the vector

$$u_i^* \underline{e}_i = \frac{-B_y^* (\log \frac{r}{R} + 1)}{2\pi} \underline{e}_x + \frac{B_y^* \theta}{2\pi} \underline{e}_y,$$

while the rotation ω_i^* vanishes together with its jump. The Cartesian strain writes from Eq. (1.6.5) as

$$[\mathcal{E}_{ij}^*] = \frac{-B_y^*}{2\pi r^2} \begin{bmatrix} x & y & 0 \\ y & -x & 0 \\ 0 & 0 & 0 \end{bmatrix}, \quad (1.6.19)$$

noting that the tensor $\bar{\partial}_m \omega_k^*$ vanishes identically in Ω_L .

- *Wedge disclination.* From Eqs. (1.6.7), (1.6.6), and (1.6.13), the rotation vector is

$$\omega_i^* e_i = \frac{\Omega_z^* \theta}{2\pi} e_z,$$

with the multiple-valued planar displacement field given by

$$\begin{aligned} u_x^* - iu_y^* &= \frac{\Omega_z^*}{4\pi}(1 - \nu^*)x \ln\left(\frac{r}{R}\right) - \frac{\Omega_z^*}{8\pi}(1 + \nu^*)x - \frac{\Omega_z^*}{2\pi}y\theta \\ &- i \left[\frac{\Omega_z^*}{4\pi}(1 - \nu^*)y \ln\left(\frac{r}{R}\right) - \frac{\Omega_z^*}{8\pi}(1 + \nu^*)x + \frac{\Omega_z^*}{2\pi}x\theta \right] \end{aligned} \quad (1.6.20)$$

and a vanishing Burgers vector:

$$B_x^* - iB_y^* = [u_x^*] - i[u_y^*] + \Omega_z^*(y + ix) = 0.$$

The Cartesian strain writes from Eq. (1.6.5) as

$$\begin{aligned} [\mathcal{E}_{ij}^*] &= \frac{\Omega_z^*(1 - \nu^*)}{4\pi} \begin{bmatrix} (\log \frac{r}{R} + 1) & 0 & 0 \\ 0 & (\log \frac{r}{R} + 1) & 0 \\ 0 & 0 & 0 \end{bmatrix} \\ &- \frac{\Omega_z^*(1 + \nu^*)}{8\pi} \begin{bmatrix} \cos 2\theta & \sin 2\theta & 0 \\ \sin 2\theta & -\cos 2\theta & 0 \\ 0 & 0 & 0 \end{bmatrix}, \end{aligned} \quad (1.6.21)$$

and hence

$$[\bar{\partial}_m \omega_k^*] = -\frac{\Omega_z^*}{2\pi r} \begin{bmatrix} 0 & 0 & \sin \theta \\ 0 & 0 & -\cos \theta \\ 0 & 0 & 0 \end{bmatrix}. \quad (1.6.22)$$

1.7 Geometry of the dislocated crystal

The theory of defects in single crystals at the macroscale can be compared in several aspects to the physics describing our universe, as governing for instance the gravitation and electromagnetic fields (defect densities are however of a higher tensorial

order). In fact, defects behave in an analogous way to the massive bodies curving the space-time geometry of the universe as described by the General Relativity of A. Einstein. However, defects are properly described by a geometry in which curvature (in the presence of disclinations) coexists with torsion (in the presence of dislocations), and, last but not least, where metric and connexion are not necessarily compatible (to account for the possible presence of point-defects).

The present section contains the following subsections, each of which pointing out and describing a particular geometrical property of the dislocated crystal.

- Metric tensors and the elastic strain
 - Riemannian and Euclidian metrics
 - Compatible elastic strain metric
- Space connexion and the internal observer
 - Parallel transport and curvature
 - Differential geometric connexion
 - Parallel transport of vector fields
 - External and internal observer
- Non-Riemannian geometry of dislocated crystals
 - Metric compatible connexion

Since this technical section does not provide crucial informations from a physical viewpoint, the reader might wish to skip it and directly go to Section 1.8, which addresses specific and key physical issues.

1.7.1 Metric tensors, and the elastic strain

The perfect crystal. Following Kondo (1954), by calling a crystal “perfect”, it is meant that the atoms form, in its stress-free configuration, a regular pattern proper to the prescribed nature of the matter.

The defective crystal. Citing again Kondo (1954), “the defective crystal is, by contrast, an aggregation of an immense number of small pieces of perfect crystals (i.e. small pieces of the defective crystal brought to their natural state in which

the atoms are arranged on the regular positions of the perfect crystal) that cannot be connected with one another so as to form a finite lump of perfect crystals as an organic unity”.

This property of defective crystals is due to the presence of line-defects as it appeared in the description of dislocation and disclination formation at the atomic scale (Section 1.2.1). In order to introduce the geometry of defective crystals, let us now cite Elie Cartan in his lecture on the geometry of Riemannian spaces: “The Riemannian space is for us an ensemble of small pieces of Euclidian space, lying however to a certain degree amorously” (Cartan, 1922). Before giving the definitions of some specific concepts of differential geometry, let us also observe the analogy between a perfect crystal and a Euclidian space, whereas dislocated crystals will be compared with a non-Euclidian space as endowed with a Riemannian metric while being submitted to inner torsion and curvature (because of the presence of torsion, this geometry was called after Einstein *non-Riemannian*⁵).

Riemannian and Euclidian metrics

When curved coordinate systems are used, the best approach is to start from contravariant (with upper indices) and covariant (with lower indices) tensor components and to introduce orthogonal coordinates and physical tensor components at a later stage. In general, Einstein’s summation convention holds for every covariant-contravariant pair of repeated indices. When physical components are used, this convention simply holds for every pair of repeated indices.

A *Riemannian metric* is a smooth symmetric and positive definite tensor field g_{ij} such that the length ξ of vector ξ^i is computed as $\xi^2 = g_{ij}\xi^i\xi^j$, while the scalar product between two vectors ξ^i and η^j is given by $\xi \cdot \eta = g_{ij}\xi^i\eta^j$. From the Riemannian metric definition (positive and symmetric properties) there is a smooth transformation a_i^j such that $g_{ij} = a_i^m a_j^n \delta_{mn}$. Let us note that the metric g_{ij} is called Euclidian if a_i^j is a global coordinate change to a Cartesian coordinate system $x^i = \hat{x}^i(x'^j)$ (x'^j being the “old” coordinates and x^i the Cartesian coordinates used for the description of the actual body), that is if⁶ $a_i^j = \partial_i x'^j$ in such a way that the metric writes as δ_{mn} in this new coordinate system.

⁵Following a remark of Unzicker (2000), some modern texts simply mean by a Riemannian geometry, a geometry endowed with a Riemannian metric.

⁶The operators ∂_i and ∂'_i always denote the partial derivative with respect to x^i and x'^i , respectively.

Compatible elastic strain metric

In our work the reference crystal \mathcal{R}_0 is not necessarily a perfect crystal at the macro-scale. It is generally a body where all the external (thermal and gravitational) stresses have been released, thereby defining, by an elastic reverse deformation of $\mathcal{R}(t)$, the body denoted by \mathcal{R}_0 . The metric of the “external observer” on $\mathcal{R}(t)$ is the Euclidian metric δ_{ij} . However, as soon as the linear elastic strain \mathcal{E}_{ij} is given, another Riemannian metric can be defined on $\mathcal{R}(t)$, i.e. the *elastic metric*

$$g_{ij}^E = \delta_{ij} - 2\mathcal{E}_{ij}. \quad (1.7.1)$$

The use of this metric on defect-free regions U of $\mathcal{R}(t)$ implies the existence of a one-to-one coordinate change between $\mathcal{R}(t)$ and \mathcal{R}_0 , whose deformation gradient writes as

$$a_i^{Em} = \delta_i^m - \partial_i u^{Em}. \quad (1.7.2)$$

This relation can be easily checked since the absence of defects implies elastic strain compatibility, which in turn precisely implies the existence of a displacement field u^{Em} such that, in the linear approximation, the metric tensor equals $g_{ij}^E = \delta_{mn} (\delta_i^m - \partial_i u^{Em}) (\delta_j^n - \partial_j u^{En})$. In case of compatibility the coordinates on \mathcal{R}_0 are $x^{0j} = x^j - u^{Ej}$, where x^j denote the Cartesian coordinates on $\mathcal{R}(t)$ and u^{Ei} the elastic displacement field.

1.7.2 Space connexion and the internal observer

Citing Einstein "To take into account (...) gravitation, we assume the existence of Riemannian metrics. But in nature we also have electromagnetic fields, which cannot be described by Riemannian metrics. The question arises: How can we add to our Riemannian spaces in a logically natural way an additional structure that provides all this with a uniform character?" This additional notion is precisely related to the so-called “Columbus connexion”: for Columbus, navigating straight right meant going westwards, that is, on a sphere, to keep a fixed angle with respect to the lines of constant latitude. In fact, the *connexion* is the differential geometric property which governs the law of *parallel transport* of vectors (Unzicker, 2000), which is a notion generalising Euclidian parallelism. Whereas in Euclidian geometry the parallelism of two vectors is equivalent to equaling the vector components, in Riemannian geometry this is no longer true and the parallelism of two vectors depends on the vector origin locations, on the choice of a curve joining these two points and of the space connexion. In order to define a space connexion, it is required to introduce the *Christoffel symbols* related

to a given choice of coordinates. Basically, the space connexion aims at defining an operation of covariant differentiation of tensors generalising the Euclidian differential in such a way that the gradient of any tensor still behaves as a tensor under arbitrary coordinate changes.

Parallel transport and curvature

In the ordinary 3D Euclidean space, we can tell whether two vectors originating at distant points are parallel, by moving one of these vectors without rotating it in order to try to let it coincide (at its origin) with the other one. However, if a space is curved, it is impossible to compare two distant vectors without some method of parallel transport of the vectors throughout the curved space. The intuitive difference between Euclidian geometry and curved non-Euclidian spaces is emerging from this consideration: if we parallelly transport a single vector along two curves with the same endpoints, depending on the path choice, this vector can end up as different after the two transports (as in the case of the black path as compared to the white path on Figure 1.14(a)). To let this comparison be possible, the vector must be parallelly transported along both curves, and any “rotation” must be due to the space curvature encountered along the circuit. The parallel transport is provided by a structure which is added to the manifold, namely the connexion.

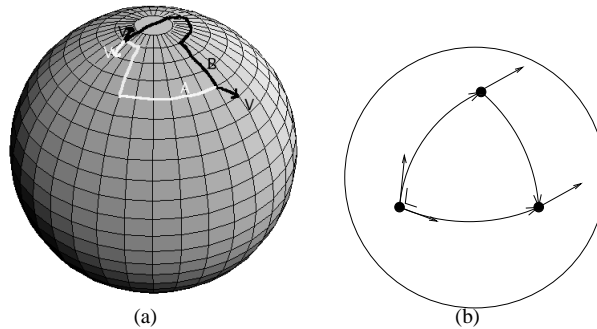


Figure 1.14: Rotation of 180° of a vector parallelly transported along path B (black path), while it keeps its south-east orientation along path A (white path) (a); Parallel transport along geodesics on a sphere (b).

Differential geometric connexion

Let v_l and w^l denote a vector and $\nabla_i v_l$ and $\nabla_i w^l$ stand for two tensors given in terms of Euclidian coordinates x^i as $\partial_i v_l$ and $\partial_i w^l$. Then, in terms of arbitrary curvilinear coordinates x'^i the transformed components $\nabla'_i v'_l$ and $\nabla'_i w'^l$ are given by the formulas (Dubrovin et al., 1992):

$$\nabla'_i v'_l = \frac{\partial v'_l}{\partial x'^i} - \Gamma_{li}^m v'_m, \quad (1.7.3)$$

$$\nabla'_i w'^l = \frac{\partial w'^l}{\partial x'^i} + \Gamma_{im}^l w'^m, \quad (1.7.4)$$

where the *Christoffel symbols* are defined as

$$\Gamma_{ij}^n = \frac{\partial x'^n}{\partial x^m} \frac{\partial^2 x^m}{\partial x'^i \partial x'^j}. \quad (1.7.5)$$

Formulas (1.7.3) & (1.7.4) directly result from the definitions $v'_l = (\partial x^m / \partial x'^l) v_m$ and $w'^l = (\partial x'^l / \partial x^m) w^m$ and the assumption that $\{x^i\}$ denotes a system of Euclidian coordinates.

Now, considering a second set of curvilinear coordinates x''^i , it is possible to show that the new Christoffel symbols Γ''^n_{ij} are related to the previous Christoffel symbols Γ^m_{ki} by the relation

$$\Gamma''^n_{ij} = \frac{\partial x''^n}{\partial x'^m} \left(\Gamma^m_{ki} \frac{\partial x'^k}{\partial x''^l} \frac{\partial x'^i}{\partial x''^j} + \frac{\partial^2 x'^m}{\partial x''^l \partial x''^j} \right). \quad (1.7.6)$$

It is important to note that because of the last term inside the parenthesis, the Christoffel symbol is not a tensor. Moreover, it appears that in the case of an Euclidian coordinate system $\{x^i\}$ associated to an affine, hence vanishing Γ^m_{ki} , Eq. (1.7.6) reduces to Eq. (1.7.5):

$$\Gamma''^n_{ij} = \frac{\partial x''^n}{\partial x'^m} \left(\Gamma^m_{ki} \frac{\partial x'^k}{\partial x''^l} \frac{\partial x'^i}{\partial x''^j} + \frac{\partial^2 x'^m}{\partial x''^l \partial x''^j} \right),$$

and so on for every change of curvilinear coordinates. As a consequence, the covariant gradients of any covariant vector v_l or contravariant vector w^l is well-defined by Eqs. (1.7.3) & (1.7.4), whose use only requires a proper definition of the Christoffel symbols, which are constrained to satisfy Eq. (1.7.6) for any coordinate transform.

Parallel transport of vector fields

To understand the meaning of the gradients $\nabla_i v_l$ and $\nabla_i w^l$ in a general non-necessarily Euclidian space, the vectors v_l and w^l are defined as being parallelly transported along a given path if, for any infinitesimal displacement dx_i along this path, the following identities are satisfied:

$$\delta v_l = \nabla_i v_l dx_i = 0 \quad (1.7.7)$$

$$\delta w^l = \nabla_i w^l dx_i = 0 \quad (1.7.8)$$

of v_l and w^l along the infinitesimal segment dx_i whose calculation must take into account the space curvature and torsion.

In the present case, appropriate Christoffel symbols will be introduced to represent the defective crystal internal structure, with the associated parallel transport meaning that the vectors are dragged along the crystallographic lines. Two different effects can be represented by this way:

- In the presence of dislocations, the Christoffel symbols Γ_{ki}^m are not symmetric w.r.t. i and k . This mathematical feature is associated with the “torsion” experienced by an internal observer along the cristallographic lines as resulting from the effect of the dislocations and the internal crystal structure.
- In the presence of disclinations, in addition the space curvature will not vanish.

External and internal observer

Citing Kröner (1990): “In our universe we are internal observers who do not possess the ability to realize external actions on the universe, if there are such actions at all. Here we think of the possibility that the universe could be deformed from outside by higher beings. A crystal, on the other hand, is an object which certainly can deform from outside. We can also see the amount of deformation just by looking inside it, eg, by means of an electron microscope. Imagine some crystal being who has just the ability to recognize crystallographic directions and to count lattice steps along them. Such an *internal observer* will not realize deformations from outside, and therefore will be in a situation analogous to that of the physicist exploring the world. The physicist clearly has the status of an internal observer”.

The *external observer* observes the crystal actual configuration $\mathcal{R}(t)$ with the Euclidian metric $g_{ij}^{ext} = \delta_{ij}$ while the elastic metric g_{ij}^E allows him to locally define a reference configuration by releasing all elastic strains. The defect-free regions of

$\mathcal{R}(t)$ are Euclidan regions since there is a coordinate change $a_m^n = \partial_m x^{En}$ such that $g_{ij}^{ext} = a_i^m a_j^n g_{mn}^E$. The internal observer, in turn, can only count atom steps while moving in $\mathcal{R}(t)$, and parallelly transport a vector along crystallographic lines⁷. Since he does not feel the body torsion, he will observe defective regions by analysing the effect of parallel transport (to observe curvature) while moving along closed curves, and compare path lengths (to observe torsion).

1.7.3 Non-Riemannian geometry of dislocated crystals

Let us point out the following remark by Kröner (1992): “When a lattice vector is parallelly displaced using $\Gamma_{m;kl}$ along itself, say 1000 times, then its start and goal are separated by 1000 atomic spacings, as measured by g_{kl} ”. Because the result of the measurement by parallel displacement and by counting lattice steps is the same, we say that the space is “metric with respect to the connexion $\Gamma_{m;kl}$ ”.

Metric compatible connexion

Let us here precise the meaning of having a perfect crystal in every defect-free region of $\mathcal{R}(t)$. Although in the motivation for introducing a metric and a connexion, these two concepts appear as independent, it is aimed at having a flat space in every defect-free region, that is, to have simultaneously

- a Euclidian metric
- an affine connexion, that is, vanishing Christoffel symbols.

This is provided by requiring the connexion to be compatible with the metric, hence requiring that

$$\nabla_k g_{ij} = \partial_k g_{ij} - \Gamma_{ik}^l g_{lj} - \Gamma_{jk}^l g_{il} = 0. \quad (1.7.9)$$

Let us describe how a compatible connexion can be defined as a function of the arbitrary metric g_{ij} and the connexion torsion defined as $\Gamma_{[ik]}^l := \Gamma_{ik}^l - \Gamma_{ki}^l$. It is well known (cf eg Dubrovin et al. (1992)) that a symmetric compatible connexion $\tilde{\Gamma}_{jk}^i$

⁷We remark that noncrystallographic coordinate systems have no meaning for the description of a crystal from the stand point of an internal observer who sees the atoms but not the space in between.

writes as $\tilde{\Gamma}_{jk}^i = \frac{1}{2}g^{im}(\partial_j g_{mk} + \partial_k g_{mj} - \partial_m g_{jk})$, while for any compatible connexion Γ_{ik}^l , $\Delta\Gamma_{ik}^l = \tilde{\Gamma}_{ik}^l - \Gamma_{ik}^l$ is introduced in such a way that

$$\Delta\Gamma_{k;ij} = \frac{1}{2}(\Gamma_{j;[ik]} + \Gamma_{i;[jk]} - \Gamma_{k;[ji]}), \quad (1.7.10)$$

where $\Delta\Gamma_{k;ij} := g_{km}\Delta\Gamma_{ij}^m$, in such a way that the compatible connexion writes as

$$\Gamma_{k;ij} = \frac{1}{2}(\partial_i g_{kj} + \partial_j g_{ki} - \partial_k g_{ij}) - \frac{1}{2}(\Gamma_{j;[ik]} + \Gamma_{i;[jk]} - \Gamma_{k;[ji]}), \quad (1.7.11)$$

where the term on the right hand-side expressed as a combination of the connexion torsion is called the *contortion tensor* (cf the next paragraph for a proof). Therefore, it is one of the objectives of this analysis (this will be detailed in Chapter 2, Section 2.5) to provide the following inter-dependent objects, viz.

- a metric which is Euclidian in the defect-free regions of $\mathcal{R}(t)$: this metric is for instance given by g_{ij}^E (by strain compatibility and Eqs. (1.7.1)-(1.7.2)).
- a connexion compatible with this metric and whose torsion vanishes in the absence of dislocations: if this torsion is chosen to be the defect quantity $-\frac{1}{2}\varepsilon_{pij}\Lambda_{pk}$, it defines by Eq. (1.7.11) a compatible connexion and vanishes as soon as the Burgers vector vanishes.

1.8 Classical and new approaches to the geometry of dislocations

This section summarises two approaches from the literature as described by H. Kleinert and E. Kröner. Our goal is to enlighten some inconsistencies of these approaches and to thereby justify the description of the method developed in this thesis, in order to provide not only a complete justification of the geometry of dislocations, but also a manner to handle and improve the existing theories, in order to develop a manageable macroscopic model for single crystals.

The present section contains the following subsections:

- Kleinert's approach
 - Multivaluedness and the cut surface

- Mesoscopic geometry with macroscopic fields?
- Elastic-plastic decomposition
- Mathematical assumptions on the physical fields and defect lines
- Kröner’s approach
 - The “ $inc\mathcal{E} = curl\kappa$ ” fundamental relation
 - Discussion about Kröner’s approach
- Proposal for a multiscale programme
 - Passage from atomic to meso-scale
 - Defect measures at the meso-scale
 - Main 2D result: mesoscopic incompatibility of a set of isolated defect lines
 - Passage from the meso- to the macro-scale
 - Conservation laws for defect densities
 - Unbounded mesoscopic energy
 - New formulas for 3D dislocations

1.8.1 Kleinert’s approach

The content of this paragraph originates from a monograph by Hagen Kleinert (1989), “Gauge fields in condensed matter, vol.2: Stresses and defects”, which summarises the classical approach developed by G.I. Taylor (1934), J.M. Burgers (1939), F.C. Frank (1958), J.D. Eshelby (1966), F.R.N. Nabarro (1967), T. Mura (1987) and others. In this section we will point out the elements of this approach which appear in our mind as drawbacks, in particular the lack of a rigorous mathematical setting, but also some doubtful physical statements.

Multivaluedness and the cut surface

Although Kleinert refers to the displacement and rotation fields as multivalued at the meso-scale, he identifies the “non-integrability” situation at a given point x as

$$\alpha_{ij}(x) := \varepsilon_{ikl} \partial_k \partial_l u_j(x) \neq 0 \quad (1.8.1)$$

for the displacement, and

$$\Theta_{ij}(x) := \varepsilon_{ikl} \partial_k \partial_l \omega_j(x) \neq 0 \quad (1.8.2)$$

for the rotation field, which we believe is not correct for two reasons:

- Any field multivaluedness implies the existence of an underlying Riemann foliation with branching lines, for which no such derivation operation in the classical sense can be rigorously justified. In particular, obviously no derivation of the multivalued function is possible on the branching line (which is in fact the defect line). Moreover partial derivations commute outside this line, except if the symbol ∂_k is replaced by the gradient ∇_k and the space is non-Euclidian, but this meaning was not intended by the author.
- In Kleinert's approach to multivaluedness, an arbitrary "cutting surface" S is chosen to contain the defect line L and to obstruct the introduction of a closed path around L , therefore preventing any abrupt passage from one branch to the other one on the Riemann set. Of course this surface is a trick, and is often removed after a couple of applications of Stokes' theorem, thereby recovering a concentrated quantity on L . However, let us point out that crude applications of Stokes' theorem are often not justified.

But the more serious reproach to the introduction of S is probably its lack of physical justification, such as, eg, as the author introduces "plastic distortion" as a concentrated term on S . In fact, as explained in Section 1.7.3, while there is a distortion decomposition, on the one-hand, one cannot conclude that it necessarily consists of an "elastic" and "plastic" part and, on the other hand, that such a decomposition should not depend on any arbitrarily chosen surface.

Often, the introduction of S aims at bypassing the difficulties of the treatment of multiple fields and, as soon as a physical justification is sought, S is either removed (because of its arbitrariness), or is interpreted as containing some non-well-localised, non-well defined physical field.

Mesoscopic geometry with macroscopic fields?

In the classical approach described by Kleinert, the line L is always present, which involves that the considered scale relates to the mesoscopic dislocated crystal. This suggests that linear elasticity is assumed everywhere away from L , since diffuse plastic effects are only macroscopic. But the definition of $\partial_m \omega_k$ (apart from the problem of derivation justification) is not clear. If this quantity were in fact elastic then Θ_{ij} as defined by Eq. (1.8.2) would identically vanish by strain compatibility away from L since $\partial_m \omega_k = \varepsilon_{kpn} \partial_p \mathcal{E}_{mn}$. However, Θ_{ij} is also computed (by introduction of the surface S) as being equal to the non vanishing tensor $\Omega_j \tau_i \delta_L$, where Ω_j is the Frank vector and τ_i the tangent vector to L , while the strain incompatibility η_{ij} appears as distinct from $\Omega_j \tau_i \delta_L$. On the other hand, if displacement and rotation are thought as macroscopic fields (apart from their crude definition), then the distinction between the disclination density Θ_{ij} and the incompatibility η_{ij} can be justified by the author's formalism. Moreover, if the macroscopic scale is intended, displacement and rotation are

necessarily thought as non-smooth (otherwise Θ_{ij} and α_{ij} as given by Eqs. (1.8.1) & (1.8.2) would identically vanish), but then the lack of justification of their derivation as macroscopic entities re-appears: are they still multivalued (which again raises the question of their physical interpretation), or just single-valued and non-smooth (which raises the question of the specification of this irregularity in view of their mathematical treatment)?

Surprisingly enough, this incorrect formalism can lead to the correct formulas, but it does not provide any correct physical interpretation of these formulas.

In contrast, the present work aims at distinguishing between the different matter scales, at considering appropriate mathematical tools for each of them, and at clarifying the passage from one to another scale, specifying the quantities which may be homogenised and those for which this is forbidden while giving a precise meaning to the macroscopic fields.

Elastic-plastic decomposition

The author's justification for displacement and rotation "non-integrability" property still remains connected to the classical elastic/plastic decomposition of the displacement gradient, while the total strain, rotation, and displacement are macroscopically smooth. We only accept this decomposition as a postulate, and only for the distortion and strain decompositions in the absence of disclinations (cf Section 1.7.3). This approach is followed by Kröner (among others) and will briefly be reviewed in Section 1.8.2. As we will see, this technique provides the correct formulas with a correct formalism, but the results are obtained by focussing on the macro-scale only, therefore missing the key connection between the defect densities across the different matter scales. Let us emphasise that the discussion about such decomposition is not only a matter of words. In fact, some authors (as reviewed by Kleinert (1989)) develop an expression for the "elastic" displacement field involving the postulated elastic distortion and the "Green's elastic function", and consequently develop a non-justified formalism for the energy and mutual interactions between the dislocations.

The objective of the present work is to clarify the mathematical framework (in particular the working assumptions) and the physical meaning of the macroscopically relevant fields for building the physical model of a "defective crystal continuum" leaning on a multiscale analysis.

Mathematical assumptions on the physical fields and defect lines

In general no assumption is ever made in the literature neither on the regularity of the involved fields, nor on the defect line regularity. However at the meso-scale, strain, rotation, displacement, and even compliance (or energy) are singular along L (as observed on the 2D examples of dislocations and disclinations of Section 1.6). This singularity can be reasonable, or very strong, thereby forbidding any classical treatments. Moreover, it is justified to raise the question whether all defects show the same type and order of singularity. Since the issue of well treating any field multivaluedness is raised in the context of singular fields, the present work will show how a “distributional approach” might help resolve the problem, under reasonable strain regularity assumptions.

Another issue relates to the homogenisation from meso- to macro-scale, requiring in particular the averaging of non-multivalued fields. How can then the macroscopic displacement and rotation fields be defined, since the latter are multivalued at the meso-scale? Moreover, no assumption is ever made on the defect line regularity, and on the possible clustering of defect lines in very irregular sets, raising the question of the selection of a formalism, such as the so-called “geometric measure theory”, to allow for the presence of fractal effects as resulting from the defective matter physical behaviour.

For general 3D lines, another question is the presence, or not, of their curvature and torsion in the expressions of the defect densities and incompatibility (these effects being clearly absent in the classical formulas). Again, the answer could depend on the assumptions made on the admissible strain and defect line regularity for the mesoscopic dislocated crystal, and highlight the need of a well-defined mathematical framework.

1.8.2 Kröner’s approach

This paragraph is devoted to very briefly summarise the review paper by Ekkehart Kröner (1981) entitled “Continuum theory of defects”. The author here clearly situates his developments at the macro-scale and speaks of a “continuized crystal”, in the sense that the lattice parameter is considered as a small parameter a , while the microscopic Burgers vector is re-scaled accordingly in order to keep the same defect content during homogenisation from micro- to macro-scale as $a \rightarrow 0$. Since the Frank vector is a rotational jump (instead of a translational jump), it cannot be re-scaled as $a \rightarrow 0$ without modifying the crystal structure, and the author therefore does not consider the presence of disclinations.

The “ $inc\mathcal{E} = curl\kappa$ ” fundamental relation

As soon as an elastic/plastic decomposition of the distortion (i.e. the displacement gradient) is postulated, namely

$$\beta_{ij}^T = \beta_{ij} + \beta_{ij}^P, \quad (1.8.3)$$

where superscripts “T” and “P” here stand for “total” and “plastic”, while no superscript means “elastic”, the dislocation density is defined as the curl of the plastic part of β_{ij}^T or, equivalently, as

$$\alpha_{ij} = -\varepsilon_{ikl}\partial_k\beta_{lj}, \quad (1.8.4)$$

since the curl of the total distortion vanishes by macroscopic strain compatibility. By application of Stokes theorem the macroscopic Burgers vector over a surface S with normal v_i is introduced as the integral on S of the dislocation density, namely

$$B_j(S) = \int_S \alpha_{ij} dS_i. \quad (1.8.5)$$

Now, from the relation $\mathcal{E}_{ij} = \varepsilon_{ijk}\omega_k + \beta_{ij}$, it immediately follows that

$$\partial_m\omega_k = \varepsilon_{klm}\partial_l\mathcal{E}_{mn} + \left(\alpha_{km} - \frac{1}{2}\alpha_{pp}\delta_{km} \right), \quad (1.8.6)$$

where the term inside the parenthesis is called contortion and denoted by κ_{km} . The author interprets ω_k as a rigid rotation of the volume element which “carries along the lattice orientation” (instead of a purely elastic rotation, as suggested by the strain decomposition), and postulates that the absence of disclinations implies that $d\omega_k$ be an exact differential, in such a way that a further application of Stokes’ theorem yields the relation

$$\varepsilon_{jpm}\partial_p\varepsilon_{kln}\partial_l\mathcal{E}_{mn} = \varepsilon_{jpm}\partial_p\kappa_{km}, \quad (1.8.7)$$

hence providing the announced statement “ $inc\mathcal{E} = curl\kappa$ ”.

To tell the truth, by introducing differential geometry concepts (as detailed in Section 1.7), the author is more precise concerning the definition of the elastic distortion. In fact, $d\beta_{ik}$ is defined as the opposite of the variation by parallel displacement⁸ of the lattice triad, hence verifying by Eq. (1.7.8) $d\beta_{ik} = -\Gamma_{k;ij}dx_j$. Since $\Delta\Gamma_{k;ij}$ is skew-symmetric in k and i while $\frac{1}{2}\partial_j g_{ki}$ is the symmetric part of $\Gamma_{k;ij}$, the following identification easily follows:

$$g_{ik} = \delta_{ik} - 2\mathcal{E}_{ik}, \quad (1.8.8)$$

⁸ given by the connexion $\Gamma_{i;jk} = \tilde{\Gamma}_{i;jk} + \Delta\Gamma_{i;jk}$ (cf Section 1.9)

where g_{ij} is the chosen metric, while

$$d\omega_{ik} = -(\Delta\Gamma_{k:ij} - \varepsilon_{pik}\varepsilon_{pqm}\partial_q\mathcal{E}_{mj})dx_j. \quad (1.8.9)$$

Writing $\Delta\Gamma_{k:ij} = \varepsilon_{pki}\kappa_{pj}$ and $\varepsilon_{pqm}\partial_q\mathcal{E}_{mj} = \bar{\partial}_j\omega_p$, Eq. (1.8.9) shows that

$$\partial_j\omega_p = \bar{\partial}_j\omega_p - \kappa_{pj}, \quad (1.8.10)$$

where the term κ_{pj} depends on both the metric and $\Delta\Gamma_{k:ij}$. By identification with Eq. (1.8.6), the contortion (this terminology originating from the so-called connexion contortion $\Delta\Gamma_{k:ij}$) is related to the dislocation density.

Discussion about Kröner's approach

The validity of Eq. (1.8.3) has already been discussed. Let us remark that the introduction of a distortion decomposition (instead of a displacement decomposition) is always possible in the absence of disclinations, the only question being the arbitrariness of the choice of what might be called, or not, a “plastic” part. We believe that this specification should have a precise meaning inherited from the defect content at lower scales. Here again we consider that this physical meaning is not clear in the work of Kröner, and therefore Eq. (1.8.3) still defines an ambiguous defect quantity. Then, Eq. (1.8.5), which is devoted to define the macroscopic Burgers vector, hence suffers from the lack of possible identification between $B_j(S)$ and the Burgers vector at lower scales as computed by Burgers circuit procedures around dislocations (cf Section 1.3). Although Eq. (1.8.5) reminds us of an expression for the dislocation density such as $\alpha_{ij} = B_j\tau_i$, where τ_i is the mesoscopic dislocation line orientation, thereby providing a way to identify $B_j(S)$ with the mesoscopic $B_j^*(L)$ as soon as L is perpendicular to S , the introduction of a defect line orientation at the macroscopic scale (where the singularities have been smoothed) seems not to be very appropriate. The question remains to understand the link between the dislocation density defined by Eq. (1.8.4) and the mesoscopic defect measure, as given by α_{ij}^* or Λ_{ij}^* . Moreover, Eq (1.8.6) is very ambiguous as well since, according to the preceding decomposition, there is apparently no reason why the term on left-hand side and the first term on the right-hand side should not be equal. Actually, Kröner's comments appeal to another interpretation of the rotation (and hence of the distortion), but then these fields should be noted differently and the fact that the disclination density vanishing implies its existence should be better justified. Coming back to Eqs. (1.8.8)-(1.8.10), the relation “ $inc\mathcal{E} = curl\kappa$ ” now clearly appears as an existence condition for the rotation vector in Eq. (1.8.10) and at the same time the meaning of the rotation is given as an elastic rotation minus the contortion term, to be interpreted as a lattice rotation (as shown by Nye (1952)). However, the link between the absence of disclinations and the relation “ $inc\mathcal{E} = curl\kappa$ ” is not clarified at this stage, since a relation showing that the

disclination density writes as $\Theta_{ij} := \varepsilon_{ikl} \partial_k \partial_l \omega_j$ is still needed (apart from the crude use of classical derivation on non-smooth rotation field). Similarly α_{ij} remains to be explicitly expressed in terms of the observed mesoscopic Frank and Burgers vectors. Moreover, the use of a connexion raises the question of its definition. In Kröner's approach the contortion appears as a defect measure defined from the knowledge of a law of parallel transport, which is itself defined by the motion of an internal observer in a Bravais lattice. Although the link between dislocation density and connexion is clear, the ambiguity resulting from the dislocation density definition also affects the connexion definition. In particular, the link between the parallel displacement of an internal observer and the defect microstructure observation is still missing.

1.8.3 Proposal for a multiscale programme

After the presentation of some physical prerequisites, of some tools from differential geometry and of a multiscale analysis of our problem, together with a brief commented review of the classical approaches used to describe the geometry of dislocations, let us now expose our programme, as developed in Chapters 2 and 3.

Passage from atomic to meso-scale

Here homogenisation is not used in the sense of a small parameter converging to zero, such as the lattice characteristic length, since the theory should include disclinations as well as dislocations (cf Section 1.8.2). The required physics here deals with the reversible dynamical interactions between atoms, and homogenisation means the volume averaging, or ensemble averaging, of a family of atomic pictures. This is a rough homogenisation, but it mainly allows us to obtain an average mesoscopic model, in which the crystal is everywhere a continuous medium except on the dislocation/disclination lines, where the physical fields are singular.

Defect measures at the meso-scale

At the meso-scale, displacement and rotation are defined by recursive line integrations of the strain curl. Due to the presence of defect lines (which are either loops or open curves ending at the crystal rim), these fields are multivalued and hence are not appropriate for homogenisation to the macro-scale. Therefore, in a first stage, only the single-valued strain curl $\bar{\partial}_m \omega_k^* := \varepsilon_{kpn} \partial_p \mathcal{E}_{mn}^*$ will be considered, with such assump-

tions on the strain regularity that $\bar{\partial}_m \omega_k^*$ can be defined in the *sense of distributions* (cf Section 1.10) on the entire crystal domain, including the singular lines. Since the displacement and rotation jumps around the defect lines are identified as the invariant Burgers and Frank vectors and since the mesoscopic crystal shows a limited number of such vectors according to its underlying atomic structure, it seems relevant to seek a relation between the strain incompatibility as defined by $\eta_{lk} = \varepsilon_{lmn} \partial_n \bar{\partial}_m \omega_k^*$ and the Frank and Burgers vectors.

Actually, the objective of Chapter 2 is not only to obtain such a relation, which was obtained by other authors before us, but better to develop a correct validation of this relation. By validation it is here meant a rigorous proof and, above all, the determination of the restrictions needed to apply these formulas. For instance, the minimal regularity of the strain, stress divergence, and defect line shape required for their obtention have to be specified. In fact, under such a set of assumptions, the following theorem will be proved in the 2D case (cf Section 3.5 of Chapter 2).

Main 2D result: mesoscopic incompatibility of a set of isolated defect lines

For a set \mathcal{L} of isolated dislocations parallel to the z -axis and located at the positions x_β^L , $L \in \mathcal{L}$, incompatibility is the vectorial first-order distribution

$$\eta_k^* = \delta_{kz} \eta_z^* + \delta_{k\kappa} \eta_\kappa^*,$$

where

- its vertical component is

$$\eta_z^* = \sum_{L \in \mathcal{L}} \left(\Omega_z^* \delta_L + \varepsilon_{\alpha\gamma} \left(B_\gamma^* + \varepsilon_{\beta\gamma} (x_\beta^L - x_{0\beta}) \Omega_z^* \right) \partial_\alpha \delta_L \right), \quad (1.8.11)$$

- its planar components are

$$\eta_\kappa^* = \sum_{L \in \mathcal{L}} \frac{1}{2} \varepsilon_{\kappa\alpha} B_z^* \partial_\alpha \delta_L, \quad (1.8.12)$$

and in which equations the quantities on the right hand-side are concentrated “measures” (cf Section 1.10.2) on the defect lines.

Passage from the meso- to the macro-scale

The preceding formulas include mesoscopic dislocation and disclination densities in their right-hand side. These physical quantities are defect measures and will be the first objects to be homogenised, thereby defining their macroscopic counterparts Θ_{ij} and α_{ij} , as introduced in Section 1.3.6, together with the macroscopic Frank and Burgers vector, as given in Eqs. (1.3.7)-(1.3.8) as the macroscopic counterparts of the mesoscopic defect measures. The following tensors are introduced,

$$\begin{aligned}\bar{\partial}_m \omega_k &:= \varepsilon_{kpq} \partial_p \mathcal{E}_{qm} - \kappa_{km} \\ \bar{\partial}_l \bar{\partial}_m u_k &:= \partial_l \mathcal{E}_{km} + \varepsilon_{kpm} \bar{\partial}_l \omega_p,\end{aligned}\quad (1.8.13)$$

where \mathcal{E}_{km} and κ_{km} are the macroscopic elastic strain and contortion tensors, defined as homogenisations of their mesoscopic counterparts \mathcal{E}_{km}^* and κ_{km}^* (the mesoscopic contortion was introduced in Section 1.3.6). Notice that symbol $\bar{\partial}_i$ has been intentionally introduced to be distinguished from a derivation operator, and will be shown to be a proper derivative only in particular situations. Here we assume that all homogenised fields are smooth at the macro-scale.

Now, instead of being postulated, the three following relations appear as resulting from the homogenisation of their validated mesoscopic counterparts:

$$\begin{array}{ll} \text{KRÖNER'S IDENTITY} & \eta_{ij} = \Theta_{ij} + \varepsilon_{ipq} \partial_p \kappa_{kq} \\ \text{MACROSCOPIC DISCLINATION DENSITY} & \Theta_{ij} = \varepsilon_{ipq} \partial_p \bar{\partial}_q \omega_j \end{array}\quad (1.8.14)$$

$$\text{MACROSCOPIC DISLOCATION DENSITY} \quad \alpha_{ij} = \varepsilon_{ipq} \bar{\partial}_p \bar{\partial}_q u_j, \quad (1.8.15)$$

together with the existence of a ‘‘Bravais’’ rotation ω_j^B and distortion $\beta_{kl}^B = \mathcal{E}_{kl} - \varepsilon_{klj} \omega_j^B$ as proved if the disclination density vanishes, thereby clarifying the macroscopic elastic strain decomposition. Moreover, the geometric interpretations of the above relations will be exposed in Section 1.9, showing for instance the connexion as defined by homogenisation of mesoscopic defect measurements. To close the present discussion, let us finally address in the following sections the existence of meso- and macroscopic conservation laws for line-defect densities and raise the question of the treatment of the mesoscopic unbounded elastic energy density.

Conservation laws for defect densities

The mesoscopic disclination, dislocation and displacement jump densities verify the relations

$$\partial_i \Theta_{ij}^* = 0, \quad \partial_i \Lambda_{ij}^* = 0, \quad \partial_i \alpha_{ij}^* = -\varepsilon_{jmn} \Theta_{mn}^*,$$

as easily verified, since for every smooth test-function ϕ , it results from Weingarten's theorem and from the formalism to be introduced in Section 1.10.1, that considering a single defect line L ,

$$\langle \partial_i \Theta_{ij}^*, \phi \rangle = - \langle \Theta_{ij}^*, \partial_i \phi \rangle = \Omega_j^* \int_L \partial_i \phi dx_i = \phi(A) - \phi(B)$$

where $\langle \cdot, \cdot \rangle$ denotes the distribution by the test-function product, while A and B are the endpoints of L , which have been shown in Section 1.4.5 to either coincide, or belong to the crystal boundary where the test-function ϕ vanishes.

By homogenisation it therefore results that

$$\partial_i \Theta_{ij} = 0, \quad \partial_i \Lambda_{ij} = 0, \quad \partial_i \alpha_{ij} = -\varepsilon_{jmn} \Theta_{mn},$$

which can be otherwise verified by Eqs. (1.8.13)-(1.8.15) and the assumed smoothness of the macroscopic densities.

We believe that one of the key issues of dislocation/disclination modelling in single crystal growth is to take these conservation laws into account.

Unbounded mesoscopic energy

It should be noted from the computed examples of Section 1.6 that the energy density (or compliance) $\mathcal{E}^* = \frac{1}{2} \sigma_{ij}^* \mathcal{E}_{ij}^*$ is not L^1 -integrable for both kinds of dislocations, while it is finite for the wedge disclination. Therefore, a Hadamard finite part distribution (Schwartz, 1957; Estrada and Kanwal, 1989) is needed to represent the compliance at the meso-scale (another approach makes use of strain mollification by a so-called core tensor (Koslowski et al., 2002)). This issue, whose solution requires to develop matched asymptotic expansions around the singular line in accordance with the infinitesimal displacement hypothesis, will not be addressed further in this work, which only focuses on the geometry of dislocations. A short introduction to these concepts and an interpretation in terms of energy concentration will be given in Section 1.10.1.

New formulas for 3D dislocations

It will be proven in Chapter 3 that using the approach just described for a collection \mathcal{L} of 3D defect lines verifying certain assumptions, and allowing for the formation of certain kinds of cluster regions, the elastic strain incompatibility as defined by Eq. (1.3.10) is the vectorial first order distribution

$$\eta_{mn}^* = \sum_{L \in \mathcal{L}} (G_{mij}(\hat{x}^L) \Theta_{ij}^*(x^L) + H_{mij}(\hat{x}^L) \varepsilon_{jlk} \partial_l \kappa_{ik}^*(\hat{x}^L))$$

where $\langle f \delta_{iL}, \varphi \rangle = \int_L f \varphi(\hat{x}^s) dL(\hat{x}^s)$ for any test-function φ , $L^1(L, \mathcal{H}^1)$ -integrable function f and defect line $L \in \mathcal{L}$ (cf Section 1.10 for some details concerning these notions), and where the geometrical tensors G_{mni} and H_{mni} write as

$$\begin{aligned} G_{mni} &:= \left[\left(\frac{1}{2} \tau_n \tau_j + v_n v_j + \sigma_n \sigma_j \right) \delta_{mi} \right]_{m \leftrightarrow n} \\ H_{mni} &:= \left[-\frac{1}{2} \tau_m \tau_n \delta_{ij} + \tau_n \tau_j \delta_{mi} \right]_{m \leftrightarrow n}, \end{aligned}$$

with $[S_{mn}]_{m \leftrightarrow n}$ indicating that twice the expression symmetric part $(S_{mn} + S_{nm})$ is taken.

1.9 Non-Riemannian objects in the dislocated crystal

The present section is devoted to summarise the dislocated crystal properties from the viewpoint of differential geometry and to define an admissible distortion decomposition. It is divided in the following subsections:

- Bravais distortion decomposition
- Non-existence of the Bravais displacement field

Dislocations show to be in some way translational defects, in the sense that a closed curve in $\mathcal{R}(t)$ might, because of the presence of dislocations, be seen as an open curve by an internal observer as soon as this curve encloses a dislocated region S . If disclinations are present together with dislocations a transported vector along a circuit will end up as translated and rotated⁹. Therefore, the presence of dislocations and/or disclinations, on the one hand, and, on the other hand, the choice of the elastic metric together with a connexion which has the property of being torsion-free in the absence of dislocations, will endow the crystal with a structure of non-Riemannian space (that is, possibly curved and twisted). Before giving all the related details, let us here summarise the basic concepts associated with the non-Riemannian crystal as

⁹Disclinations have shown in Section 1.3, Figure 1.10 to provide vector rotation effect by parallel transport at the atomic scale. By homogenisation, the macroscopic crystal filled with disclinations will therefore have a non-vanishing curvature tensor, called the Riemann curvature tensor.

follows.

$$\begin{aligned}
\text{EXTERNAL OBSERVER METRIC TENSOR: } g_{ij}^{ext} &:= \delta_{ij} \\
\text{ELASTIC METRIC TENSOR: } g_{ij} &:= \delta_{ij} - 2\mathcal{E}_{ij} \\
\text{DISLOCATION TORSION: } T_{k;ij} &:= -\frac{1}{2}\varepsilon_{pij}\Lambda_{pk} \\
\text{SYMMETRIC CHRISTOFFEL SYMBOLS: } \tilde{\Gamma}_{k;ij} &:= \frac{1}{2}(\partial_i g_{kj} + \partial_j g_{ki} - \partial_k g_{ij}) \\
\text{CONNEXION CONTORTION: } \Delta\Gamma_{k;ij} &:= T_{j;ik} + T_{i;jk} - T_{k;ji} \\
\text{NON SYMMETRIC CHRISTOFFEL SYMBOLS: } \Gamma_{k;ij} &:= \tilde{\Gamma}_{k;ij} - \Delta\Gamma_{k;ij}.
\end{aligned}$$

1.9.1 Bravais distortion decomposition

It is one of the aims of this work to explain why the choice of a non-affine connexion compatible with the elastic metric is needed. The goals are:

- to well-define the *Bravais rotation* ω_j (which appears as a combination of elastic and lattice rotations) and the *Bravais distortion* β_{kl} as

$$\begin{aligned}
\text{BRAVAIS ROTATION} \quad \omega_j(x) &:= \omega_j^0 + \int_{x_0}^x d\omega_j \\
\text{BRAVAIS DISTORTION} \quad \beta_{kl}(x) &:= \mathcal{E}_{kl}(x^0) - \varepsilon_{klj}\omega_j^0 + \int_{x_0}^x d\beta_{kl},
\end{aligned}$$

where $d\beta_{kl}$ is defined as $-\Gamma_{l;km}dx_m$, while $d\omega_j := \bar{\partial}_m\omega_j dx_m$ with an appropriate definition of $\bar{\partial}_m\omega_j$ accounting for mesoscale effects, and where the connexion contortion vanishes as soon as the *dislocation contortion* κ_{jm} (which is a defect measure) vanishes. Moreover, in Chapter 2 it will also be shown that the elastic infinitesimal rotation $\bar{\partial}_m\omega_j dx_m$ is the sum of the Bravais infinitesimal rotation $d\omega_j$ and of the lattice infinitesimal rotation (or contortion) $\kappa_{jm}dx_m$.

- to obtain the connexion torsion from the crystal internal torsion, namely $\Delta\Gamma_{m;[kl]} = T_{m;kl}$. It is fundamental to remark that, by Eq. (1.7.6), $T_{m;kl}$ is a tensor.
- to prove that the dislocation density is the Bravais distortion curl¹⁰:

$$\int_C du_k = \int_S \varepsilon_{\beta\alpha} \partial_\beta \beta_{k\alpha} dS = \alpha_k(S). \quad (1.9.1)$$

¹⁰Note that the relation $\int_C d\omega_k = \Theta_k(S)$ is independent of the metric and connexion choice, but only on the homogenisation of mesoscopic elastic strain and contortion.

- to associate the defect density measurements of an external observer with the parallel transport along Burgers circuits of an internal observer who is provided with a connexion computed from density measurements.
- to avoid an a-priori distortion decomposition in “elastic” and “plastic” parts. In fact, in the literature Eq. (1.9.1) is generally postulated and the fields β_{kl} together with ω_i are referred to as elastic distortion and rotation fields (cf Section 1.8.1 for a discussion on this topic). However, while the symmetric part of the Bravais distortion shows to be the elastic strain, there is no reason why its skew-symmetric part should be the elastic rotation tensor $-\varepsilon_{ijk}\omega_k$ where ω_k is obtained from a line integration of $\bar{\partial}_j\omega_k := \varepsilon_{kpq}\partial_p\mathcal{E}_{jq}$. This crucial point justifies the efforts of the present work to clarify the classical theory.

1.9.2 Non-existence of the Bravais displacement field

By *Bravais displacement*, we here mean the part of the macroscopic global displacement whose gradient is the Bravais distortion. In contrast with the existence postulate of an “elastic” displacement in the dislocated crystal, our work aims at explaining why no such decomposition is justified from a physical viewpoint. Moreover, it is explained why the index 2 multivaluedness of the mesoscopic displacement field is too strong to provide a Bravais displacement at the macro-scale (which could have been defined by a line integration of du_k), even in the case of flat crystals. In fact, multivaluedness is recovered at the macro-scale, as immediately seen from the relation

$$u_k(x) = u_k(x^0) + \int_{x^0}^x \beta_{kl} dx_l,$$

which is meaningless as soon as x is contained in a defective region of $\mathcal{R}(t)$, even with the introduction of (arbitrary) jump surfaces at x .

1.10 Elementary notions of distribution and geometric measure theories

This section provides the basic notions of distribution theory, in order to handle Dirac masses, and their derivatives. It also provides an introduction to the notion of generalised function, otherwise termed as Hadamard pseudo-functions and to the geometric measure theory, aimed at generalising the results of Chapter 2 to Chapter 3. The

notions of this section will also allow the reader to understand the global strain assumption as proposed in Chapter 2. The present section is divided in the following subsections:

- Distribution theory and Hadamard finite parts
 - Distributions
 - 1D examples of diverging integrals: Hadamard finite parts and pseudo-functions
 - 2D examples of radial functions
 - Singular elastic energy decomposition
- Line integration and Hausdorff measures
 - Radon measure and Radon-Nykodým decomposition
 - Gauss-Green's theorem for BV-functions and Frank tensor global regularity assumptions

1.10.1 Distribution theory and Hadamard finite parts

Distributions

Let us denote by $\mathcal{D}(\Omega) := \mathcal{C}_c^\infty(\Omega)$ the space of smooth functions with compact support in the open set Ω , also known as the space of *test-functions* ϕ . The space of distributions is the dual space of $\mathcal{D}(\Omega)$ and, since $\mathcal{D}(\Omega)$ is a very “small” function space, its dual is known to be very large, thereby containing many of the objects appearing in physical modelling. In fact the distribution space $\mathcal{D}'(\Omega)$ is defined as

$$\mathcal{D}'(\Omega) := \{f : \mathcal{D}(\Omega) \rightarrow \mathbb{R} : f \text{ is linear and continuous}\},$$

where continuity here means that $\langle f, \phi_n \rangle \rightarrow 0$ as soon as $\phi_n \rightarrow 0$ in appropriate spaces (Willem, 1995) and where symbol $\langle f, u \rangle$ here simply means the application of a distribution f against the test-function ϕ . Let us here mention an important property concerning the derivation of distributions: any distribution can be derived to any order, since derivation simply means that

$$\langle \partial_i f, \phi \rangle := - \langle f, \partial_i \phi \rangle,$$

which can be seen as a generalized partial integration property over Ω .

Moreover, the *order* of a distribution f is known as the smallest integer m such that f is linear and continuous over $\mathcal{C}_c^m(\Omega)$.

1D examples of diverging integrals: Hadamard finite parts and pseudo-functions

As an introductory example, let us consider the function $1/x$ which is not integrable on $]0, +\infty[$. Similarly, the function $\phi(x)/x$ is in general not integrable on $]0, +\infty[$ for $\phi \in \mathcal{C}_c^\infty(\mathbb{R})$. Nevertheless $(1/x)_{x>0}$ can be associated with a distribution by taking the *finite part in the Hadamard sense* of the divergent integral. This distribution is called the *pseudo-function* $1/x$ for $x > 0$. Indeed, by partial integration one easily obtains the relation

$$\int_{\varepsilon}^{\infty} \phi(x)/x dx = -\phi(\varepsilon) \ln \varepsilon - \int_{\varepsilon}^{\infty} \phi'(x) \ln x dx,$$

the last integral being convergent as $\varepsilon \rightarrow 0$. Therefore it appears as quite natural to define a pseudo-function as being equal to the finite part of a divergent integral (concisely written as “*Pf.* = *Fp.*”!), viz.

$$\langle Pf.(1/x)_{x>0}, \phi(x) \rangle := Fp. \int_0^{\infty} \phi(x)/x dx := \lim_{\varepsilon \rightarrow 0} \left(\int_{\varepsilon}^{\infty} \phi(x)/x dx + \phi(0) \ln \varepsilon \right),$$

where ϕ has been expanded around the origin with $\lim_{\varepsilon \rightarrow 0} (\phi(\varepsilon) - \phi(0)) \ln \varepsilon = 0$. Moreover, it should be observed that by the right-hand side linearity in ϕ of the previous relation, the pseudo-function $Pf.(1/x)_{x>0}$ defines a distribution.

In general a divergent integral “DI” can be decomposed into three parts, viz. a *divergent part* “DP”, a *finite part* “FP” and a *concentrated part* “CP” as illustrated here below by the partial integration of $1/x^2$ for $x > 0$. Since the limit

$$\lim_{\varepsilon \rightarrow 0} \left(\int_{\varepsilon}^{\infty} \phi(x)/x^2 dx - \phi(\varepsilon)/\varepsilon + \phi'(\varepsilon) \ln \varepsilon \right)$$

exists¹¹, letting $\phi_{r=\varepsilon} = \phi_{r=0} + \varepsilon \phi'_{r=0} + O(\varepsilon^2)$ and defining the finite part of the divergent integral as

$$Fp. \int_0^{\infty} \phi(x)/x^2 dx := \lim_{\varepsilon \rightarrow 0} \left(\int_{\varepsilon}^{\infty} \phi(x)/x^2 dx - \phi(0)/\varepsilon + \phi'(0) \ln \varepsilon \right),$$

shows the following relation “DI=DP+FP+CP” to hold:

$$\int_0^{\infty} \phi(x)/x^2 dx = \lim_{\varepsilon \rightarrow 0} \left(\phi(0)/\varepsilon - \phi'(0) \ln \varepsilon \right) + Fp. \int_0^{\infty} \phi(x)/x^2 dx - \phi'(0).$$

Defining the pseudo-function $Pf.(1/x^2)_{x>0}$ as the distribution

$$\langle Pf.(1/x^2)_{x>0}, \phi \rangle := Fp. \int_0^{\infty} \phi/x^2 dx,$$

¹¹and equals $-\int_0^{\infty} \phi'(x) \ln x dx$

for every test function $\phi \in \mathcal{C}_c^\infty(\mathbb{R}, \mathbb{R})$, it can be checked, from the definition and by partial integration, that

$$\begin{aligned} \left\langle \frac{d}{dx} Pf.(1/x)_{x>0}, \phi \right\rangle &= - \left\langle Pf.(1/x)_{x>0}, \phi' \right\rangle = -Fp. \int_0^\infty \phi'(x)/x dx \\ &= -Fp. \int_0^\infty \phi(x)/x^2 dx - \langle \delta_0', \phi \rangle, \end{aligned}$$

showing the following remarkable relations¹²:

$$\left\langle \frac{d}{dx} (Pf.(1/x)_{x>0} + \delta_0), \phi \right\rangle = \left\langle -Pf.1/x^2, \phi \right\rangle,$$

where symbol δ_0 denotes the Dirac measure.

2D examples of radial functions

Let us shortly analyse the pseudo-function $Pf.1/r^2$ where $r = \sqrt{x_i^2}$ in the plane. By partial integration,

$$\int_0^{2\pi} \int_\varepsilon^\infty \phi/r dr d\theta = -2\pi\phi(0) \ln \varepsilon - \int_0^{2\pi} \int_\varepsilon^\infty \partial_r \phi \ln r dr d\theta,$$

where the last integral is convergent as $\varepsilon \rightarrow 0$. The pseudo-function is as usual introduced as

$$\langle Pf.1/r^2, \phi \rangle := Fp. \int_{\mathbb{R}^2} \frac{\phi}{r^2} dV := \lim_{\varepsilon \rightarrow 0} \left(\int_0^{2\pi} \int_\varepsilon^\infty \frac{\phi}{r} dr d\theta + 2\pi\phi(0) \ln \varepsilon \right), \quad (1.10.1)$$

for every test function $\phi \in \mathcal{C}_c^\infty(\mathbb{R}^2, \mathbb{R})$. It can be shown that

$$\nabla Pf.1/r = -Pf.1/r^2 \underline{e}_r - 2\pi\delta_0,$$

where δ_0 denotes the 2D Dirac measure centred at the origin.

As last example, let us analyse the gradient of $Pf.1/r^2$:

$$\langle \nabla Pf.1/r^2, \underline{\psi} \rangle := - \langle Pf.1/r^2, \nabla \cdot \underline{\psi} \rangle,$$

where $\underline{\psi} \in \mathcal{C}_c^\infty(\mathbb{R}^2, \mathbb{R}^2)$ and hence $\underline{\psi}$ is a 2D vector test-function whose radial and azimuthal components are denoted by ψ_r and ψ_θ . Consider first the set $B_{R,\varepsilon} :=$

¹²where the left-hand side defines the “generalised derivative” D_x with the good property that $D_x Pf.(1/x)_{x>0} = -Pf.(1/x^2)_{x>0}$.

$B(0, R) \setminus B(0, \varepsilon)$, where $B(0, \varepsilon)$ is the disk of radius ε centred at 0 and with R large enough in order to contain the support of $\underline{\psi}$. By the Gauss–Green theorem we have

$$\int_{B_{R,\varepsilon}} (\nabla \cdot \underline{\psi})/r^2 dV = - \int_{B_{R,\varepsilon}} (\nabla(1/r^2)) \cdot \underline{\psi} dV - \int_{\partial B_\varepsilon} \underline{\psi}_r/r^2 dS.$$

Passing to the limit $\varepsilon \rightarrow 0$ and since $\lim_{\varepsilon \rightarrow 0} \int_{\partial B_\varepsilon} \underline{\psi}_r/r^2 dS = \pi \nabla \cdot \underline{\psi}(0)$ ¹³, it results that

$$Fp. \int_{B_{R,0}} \nabla \cdot \underline{\psi}/r^2 dV = -Fp. \int_{B_{R,0}} \nabla(1/r^2) \cdot \underline{\psi} dV - \pi \nabla \cdot \underline{\psi}(0),$$

equivalently written in the form

$$\langle \nabla P f.1/r^2, \underline{\psi} \rangle = Fp. \int_{B_{R,0}} \nabla(1/r^2) \cdot \underline{\psi} dV + \pi \nabla \cdot \underline{\psi}(0),$$

and resulting, since the finite part on the right hand-side defines the pseudo-function $-2P f.1/r^3 \underline{e}_r$, in the concise expression

$$\nabla P f.1/r^2 = -2P f.1/r^3 \underline{e}_r - \pi \nabla \delta_0.$$

Singular elastic energy decomposition

It was already announced in Section 1.8.3 that the elastic energy density need not be bounded. Let us take the screw dislocation as an example, which exhibits the singular term¹⁴

$$\mathcal{E} = \frac{1}{2} \mathcal{E}_{ij}^* \sigma_{ij}^* = \frac{E}{2(1+\nu)} \mathcal{E}_{ij}^* \mathcal{E}_{ij}^* = \frac{E B_z^2}{32\pi^2(1+\nu)r^2}.$$

The fundamental reason for this singularity is due to the inadequacy of the linear elastic model in the vicinity of the defect line. In fact, the strain is predominantly nonlinear in a neighbourhood of the order of length $|B_z|$ around the defect line. This is the reason why the energy required to create the dislocation line is infinite if the model is restricted to linear elasticity. A concentrated energy term \mathcal{E}° will be subtracted from the divergent integral, as an increasing function of r , viz.

$$\mathcal{E}^\circ = \frac{E B_z^2}{16\pi(1+\nu)} \delta_0 |\ln r|,$$

¹³This can be easily checked: from the divergence expression in the cylindrical base, it follows that $\underline{\psi}_r/r^2 = \nabla \cdot \underline{\psi}/r - \partial_r \underline{\psi}_r/r - 1/r^2 \partial_\theta \underline{\psi}_\theta$ where the last term vanishes after integration over the circle of radius ε , while $\partial_r \underline{\psi}_r = \cos^2 \theta \partial_x \underline{\psi}_x + \sin^2 \theta \partial_y \underline{\psi}_y$ is integrated up to an $O(\varepsilon)$ -term as $\pi \nabla \cdot \underline{\psi}(0)$ and the first term as $2\pi \nabla \cdot \underline{\psi}(0)$.

¹⁴It is here meant for r the non-dimensional radius $r \leq 1$.

for $r < 1$. More precisely, if the unbounded total energy \mathcal{E} is considered as a distributional pseudo-function $\text{Pf.}(EB_z^2)/(32\pi^2(1+\nu)r^2)$, the following interpretation can be proposed from Eq. (1.10.1). With φ a test-function, δ_0 the concentrated Dirac mass at the origin and Ω_ε the planar section from which a disk of radius ε around the defect line has been removed, a diffuse term $\mathcal{E}^{elast.} = (EB_z^2)/(32\pi^2(1+\nu)) \int_{\Omega_\varepsilon} \varphi/r^2 dV$ accounts for the energy of the dislocation creation at the distance $r = \varepsilon$, and a concentrated term \mathcal{E}° is to be introduced and interpreted as a correction to the linear approximations near the line. The subtraction of \mathcal{E}° from $\mathcal{E}^{elast.}$ while letting $\varepsilon \rightarrow 0$ results in a finite “corrected elastic energy” $\mathcal{E}^{*\circ}$ writing as

$$\mathcal{E}^{*\circ} = -\frac{EB_z^2}{32\pi^2(1+\nu)} \int_{\Omega} \partial_r \phi \ln r / r dV.$$

Let us emphasise that this approach only consists in an attempt of an interpretation in terms of the above introduced distributional objects, without proper physical justification.

1.10.2 Line integration and Hausdorff measures

The length of the graph G of a smooth function $g : [0; 1] \rightarrow \mathbb{R}^3$ is classically defined as the integral over $[0; 1]$ of the jacobian $\sqrt{\dot{x}_i^2}$ where $x_i = g'_i(t)$ since length is proved to be independent of the parametrisation of G . This classical formula is not adapted if such a parametrisation is unknown, if the function g is irregular, or as soon as the length of a curve other than a graph is sought. The solution has been found by F. Hausdorff, who introduced in 1918 an “ m -dimensional measure in \mathbb{R}^n defined on all subsets A of \mathbb{R}^n ”¹⁵. In order to compute the “ m -dimensional measure” of A , the idea is very simple, and very geometric indeed: it suffices to cover the set A by small subsets $S_j \in \mathbb{R}^n$ whose diameter $\delta(S_j)$ is known (usually S_j are n -dimensional balls) and to estimate the so-called *m -dimensional Hausdorff measure* of A by the measure of an “optimal” collection of covering small sets.

Let us give the precise definition of this concept for general m and n (where n will be equal to 2 or 3 in our work, whereas m will generally be equal to 1 or 2). Notice that m is any positive real number.

The set A is covered by a collection $\{S_j\}$ of small sets of diameter $\delta(S_j)$ lower than a given $\delta > 0$. Clearly, the measure of A will be as accurate as δ is chosen small. The (possibly infinite) m -dimensional Hausdorff measure of A is defined as

$$\mathcal{H}^m(A) := \alpha(m) \lim_{\delta \rightarrow 0} \inf_{A \subset \cup S_j} \sum_j (\delta(S_j))^m, \quad (1.10.2)$$

¹⁵Which turns out to be equal, up to a known constant, to the Lebesgue measure if $m=n$.

where $\alpha(m)$ is the volume of the closed unit m -dimensional ball as given by $\frac{\pi^{m/2}}{\Gamma(m/2 + 1)}$, where Γ is the usual “gamma function” (Evans and Gariepy, 1992).

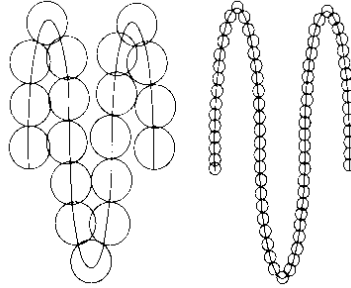


Figure 1.15: Here the length of the curve is well-estimated by the sum of the diameters of the tiny balls, but grossly under-estimated by the diameter of the huge ball; from Ambrosio et al. (2000).

Radon measure and Radon-Nykodým decomposition

Another type of measure, known as “Radon measure” will be used in this work. First of all, let us recall that a *measure* μ as applied to a subset¹⁶ $E \subset \mathbb{R}^n$ with value in $[0, \infty]$ verifies $\mu(\emptyset) = 0$ and $\mu\left(\bigcup_h E_h\right) = \sum_h \mu(E_h)$ for any collection of pairwise disjoint subsets $\{E_h\}$. Now, if for any compact subset K , $\mu(K) < \infty$, then μ is called a *Radon measure*.

Let us now define the *integral of a function with respect to a measure*. Any μ -measurable¹⁷ function $u : \mathbb{R}^3 \rightarrow \mathbb{R}^p$ can be approximated from below by μ -measurable step functions v , that is, linear combinations of the characteristic functions $\chi(E)$ of the subsets $E \subset \mathbb{R}^n$, thereby defining the integral of u w.r.t. μ as

$$\int_{\mathbb{R}^3} u d\mu := \sup\left\{\int_{\mathbb{R}^3} v d\mu\right\},$$

¹⁶By set and subset it is here always meant “Borel set” (Mattila, 1995), hence including a large variety of sets, such as the “closed”, “open” and “compact” sets.

¹⁷Which means that for any open $\mathcal{U} \subset \mathbb{R}^p$, $U := u^{-1}(\mathcal{U})$ is such that $\mu(U) = \mu(U \cap E) + \mu(U \setminus E)$ for all $E \subset \mathbb{R}^p$ (Evans, 1992; Mattila, 1995).

while the integral of the characteristic function is defined as

$$\int_{\mathbb{R}^3} v d\mu := \sum_{z \in Im(v)} z \mu(v^{-1}(z)),$$

where $Im(v)$ is the image set of v . A function f will be said to belong to the *Lebesgue space* $L^1(\mathbb{R}^3, \mu)$ if the norm $\|f\|_p := \int_{\mathbb{R}^3} |f| d\mu$ is finite, thereby defining the measure $f\mu(B)$ as $\int_B f d\mu$.

The *restriction* (or concentration) of μ to the subset L is denoted $\mu \llcorner L(B)$ and defined as by $\mu(B \cap L)$.

Riesz representation theorem. The Radon measure is a particular kind of distribution in the sense that for any test-function ϕ , $\langle \mu, \phi \rangle$ as defined by $\int_{\mathbb{R}^3} \phi d\mu$ is linear and continuous in ϕ . The *Riesz representation theorem* gives a finer statement, namely that any linear and continuous functional over the space of continuous functions with compact support (instead of the infinitely differentiable test-functions) has a measure representation μ such that

$$\langle \mu, \phi \rangle = \int_{\mathbb{R}^3} \phi d\mu \quad (1.10.3)$$

for all $\phi \in \mathcal{C}_c(\Omega)$ where Ω is an open subset of the Euclidian 3D space. Let us remark that the space of Radon measures is much smaller than the space of distributions and that a measure is a distribution of order 0.

Radon-Nykodým decomposition theorem. Actually, it appears as more interesting to work with a measure μ in the context of the “geometric measure theory”, instead of the full distributional context, which, although wider, is not able to provide a fine analysis of μ . For introducing the next crucial theorem, let us precise that a Radon measure μ is said singular w.r.t. the Lebesgue measure $|\cdot|$ if there exists a set $A \subset \mathbb{R}^3$ such that $\mu(A) = 0 = |\mathbb{R}^3 \setminus A|$. For instance, the Dirac measure at the origin is singular w.r.t. the Lebesgue measure as seen by the choice $A = \mathbb{R}^3 \setminus \{0\}$. Now, for every Radon measure μ , there exists a Lebesgue-integrable function f and a singular measure ν such that for any subset B :

$$\mu(B) = \int_B f d\mu + \nu(B).$$

This decomposition theorem will play an important role in the demonstrations of Chapters 2 and 3.

Hausdorff concentrated measures. The 1D Hausdorff measure concentrated on the line L is denoted by

$$\delta_L := \mathcal{H}^1 \llcorner L,$$

while the 2D Hausdorff measure concentrated on the surface S is written as

$$\delta_S := \mathcal{H}^2 \llcorner S.$$

Notice that δ_L is not a Radon measure (nor is δ_S) since $\delta_L(A) = \infty$ for all sets A whose dimension is strictly higher than 1 (as, eg, surfaces).

Gauss-Green's theorem for BV-functions and Frank tensor global regularity assumptions

A function f is said (to be) of *bounded variation* (a “BV function”) on $\Omega \subset \mathbb{R}^3$ if it is a $L^1(\Omega)$ -integrable function whose derivatives are all Radon measures. One of the interesting properties of BV functions is that they provide an extension of the Gauss-Green theorem.

Gauss Green's theorem for BV-functions. Letting $f \in BV(\Omega, \mathbb{R})$ and Ω with a regular boundary $\partial\Omega$, then

$$\int_{\Omega} \partial_i \psi_i f dV = - \int_{\Omega} \psi_i d(\partial_i f) + \int_{\partial\Omega} \psi_i f dS_i,$$

for all $\underline{\psi} \in \mathcal{C}_c^1(\Omega, \mathbb{R}^3)$. Here, dS_i denotes the vectorial measure on $\partial\Omega$, which equals $v_i dS$ when the outer unit normal v_i to $\partial\Omega$ exists.

Incompatibility and disclination density. This paragraph aims at showing that the Frank tensor $\bar{\partial}_m \omega_k^*$ is not of bounded variation and consequently that Gauss Green's theorem cannot be applied in a simple manner to globally relate the incompatibility tensor and the disclination density. To this end, let us consider a defect line L , enclosed by a tube of radius ε , and a cross-section $C_\varepsilon(\hat{x})$ with $\hat{x} \in L$ and with dC_q the infinitesimal vector normal to $C_\varepsilon(\hat{x})$, which equals $v_q dC$ when the outer normal v_q to $C_\varepsilon(\hat{x})$ exists. In fact, by the relations $\langle \Theta_{ij}^*, \phi_i \rangle = \int_L \Omega_j^* \phi_i dx_i$ and $\Omega_j^* = \int_{C_\varepsilon(\hat{x})} \bar{\partial}_m \omega_j^* d\xi_m$ for every $\hat{x} \in L$ and from $d\xi_m = \varepsilon_{mpq} \tau_p dC_q$, where we recall that τ_p is the tangent vector to L at \hat{x} , it results that for a regular line L ,

$$\langle \Theta_{ij}^*, \phi_i \rangle = \int_{\Sigma_\varepsilon} \phi_\varepsilon \tau_i \tau_p \bar{\partial}_m \omega_j^* \varepsilon_{mpq} dS_q,$$

where $\phi_\varepsilon(\xi) = \phi(\xi - \varepsilon e_r)$ and where Σ_ε stands for a surface enclosed by C_ε (since the defect line is closed or ends at the boundary, this surface is either a torus, or a tube ending at the boundary), in such a way that application of Gauss-Green's theorem (with the integrand vanishing on the tube extremities and with V_ε denoting the volume bounded by Σ_ε) yields the formula

$$\langle \Theta_{ij}^*, \phi_i \rangle = \int_{V_\varepsilon} \phi_\varepsilon \tau_i \tau_p d \left(\varepsilon_{mpq} \partial_q \bar{\partial}_m \omega_j^* \right) + O(\varepsilon),$$

thereby identifying by letting $\varepsilon \rightarrow 0$ and by Eq. (1.3.10) the disclination density Θ_{ij}^* with the incompatibility $\tau_i \tau_p \eta_{pj}^*$. Since, referring to Eq. (1.8.11), the expression $\Theta_z^* = \eta_z$ is false in the 2D case, we observe that a “simple” BV assumption for the Frank tensor global regularity is not valid¹⁸.

It is one of the objectives of Chapter 2 to provide correct global assumptions allowing us to validate Eqs. (1.8.11)-(1.8.12).

¹⁸Let us notice that referring to our previous explicit computations of the rectilinear edge and screw dislocations (resp. wedge disclination), the Frank tensor shows a dependence upon the variable r in $1/r^2$ (resp. $1/r$), and hence is not even L^1 in the case of the two dislocations, and, for the disclination, its gradient in $1/r^2$ which, considered as a pseudo-function, has been shown in Section 1.10.1 to be a distribution of order 1 instead of a measure.

Chapter 2

A distributional approach to the geometry of 2D dislocations at meso-scale

2.1 Introduction

The present chapter focuses on mesoscale modelling with a view to clarifying the homogenisation process from meso- to macroscale. Since dislocations are lines at the mesoscale, concentrated effects, as governed by the distribution theory (a key reference is here Schwartz (1957)), must be introduced in the mesoscopic model. In addition, since integration around the dislocations generates a multivalued displacement field with the dislocations as branching lines, multivalued functions must be considered (Almgren, 1986; Knopp, 1996; Remmert, 1996). This combination of distributional effects and multivaluedness is a key feature of the dislocation theory at the meso-scale but, unfortunately, the difficulties resulting from this mathematical association have not well been addressed so far in the literature (Thom, 1980). As an example, non-commuting differentiation operators are freely introduced without any justification by Kleinert (1989). Therefore, the principal objective of this chapter is to provide a strong mathematical foundation to the meso-scale theory of dislocations, showing how the distribution and geometric measure theories can be correctly used with multiple-valued fields. In particular, the application limits of Stokes' theorem are clarified. For the sake of generality, disclinations, which represent a second but

rarer kind of line defect, with in addition a multiple-valued rotation field, are here considered together with dislocations.

After homogenisation from meso- to macro-scale, no concentrated effects remain anymore present in the macroscopic model, which consists of a set of evolution PDE's governing scalar or tensorial defect density fields in the framework of elasto- or viscoplasticity (Kratohvil and Dillon, 1969). However, it should be pointed out that homogenisation from meso- to macro-scale has no meaning for multiple-valued fields such as displacement and rotation, since this operation is exclusively allowed for additive (or extensive) fields such as stress, energy density or heat flux. This consideration becomes obvious when homogenisation is defined by an ensemble averaging procedure, since multiple-valued fields are mathematically defined as extended functions which cannot be added since their "domains" depend on the defect line locations. This issue is clarified in the present chapter. Moreover, since the macroscopic displacement and rotation fields are not defined as ensemble averages of their mesoscopic counterparts, no unique privileged reference configuration can be defined at the macro-scale for single crystals with dislocations. Having in mind that displacement and rotation fields are defined with respect to the selected reference configuration (which can be, or not, defect-free), the invariance laws governing the behaviour of single crystals with line defects at the macro-scale are constructed in accordance with this observation.

In the literature the macroscopic dislocation density is classically defined as the curl of the plastic distortion (Head et al., 1993; Cermelli and Gurtin, 2001; Gurtin, 2002; Koslowski et al., 2002; Ariza and Ortiz, 2005), following a postulated distortion decomposition into elastic and plastic parts. However, this approach cannot be rigorously justified (contrarily to the strain decomposition) since elastic and plastic rotations cannot be set apart. In contrast, the present chapter introduces the macroscopic dislocation density by homogenisation of well-defined mesoscopic fields, under precise geometric-measure model assumptions, from which the distortion decomposition is obtained together with its relationship with the dislocation density. Since dislocations and disclinations represent body torsion and curvature, respectively, these concepts also appear as macroscopic counterparts of well-defined mesoscopic defect measures.

The present chapter is restricted to the 2D theory. Extension to the 3D case is under investigation and will be addressed in Chapter 3. A complete link between the mesoscopic and macroscopic behaviours of single crystals with line defects should be derived from these developments. In Section 1.3.1 of Chapter 1, the scaling analysis summarised in this introduction has been detailed and the basic concepts used to represent the dislocated continuous medium have been introduced. In this chapter, classical invariance theorems are recalled in Section 2.2. In Section 2.3, the 2D distributional theory of the dislocated continuous medium is established in the case of a single dislocation, while Section 2.4 treats the more general case of an ensemble of isolated

dislocations. Finally, Section 2.5 introduces the non-Riemannian macroscopic body by homogenisation from the mesoscale, and conclusions are drawn in Section 2.6.

Since our multiscale analysis of dislocations has already been explained in Chapter 1, Section 1.3, let us simply recall that the 3 scales of interest for our analysis are the *atomic scale* whose characteristic length is the interatomic distance, the *meso-scale* which defines the dislocated continuous medium and whose characteristic length is the average distance between two neighbour dislocation lines, and the *macro-scale* whose characteristic length is the diameter of the crystal. Moreover, the mesoscopic reference body \mathcal{R}_0^* is a perfect crystal, while the macroscopic reference body \mathcal{R}_0 can be, or not, a perfect crystal. Let us also recall that the displacement field is a multivalued function such that for any point $X_l \in \mathcal{R}_0^*$ one has $u_i^*(X_l) = x_i - X_i$ where $X_i \in \mathcal{R}_0^*$ and $x_i \in \mathcal{R}^*(t)$, while the single-valued strain tensor is denoted by \mathcal{E}_{ij}^* , with $\mathcal{E}_{ij}^* := \frac{1}{2}(\partial_j u_i^* + \partial_i u_j^*)$ outside the defect line and with \mathcal{E}_{ij}^* arbitrarily set to 0 on the defect line. Finally, the possibly multivalued infinitesimal rotation tensor is denoted by ω_{ij}^* , with $\omega_{ij}^* := \frac{1}{2}(\partial_j u_i^* - \partial_i u_j^*)$ outside the defect line, with the associated rotation vector given by

$$\omega_k^* = -\frac{1}{2}\varepsilon_{ijk}\omega_{ij}^* = \frac{1}{2}\varepsilon_{ijk}\partial_j u_i^*$$

and the identity $\omega_{ij}^* = -\varepsilon_{ijk}\omega_k^*$. The Frank and Burgers vectors Ω_k^* and B_i^* associated with a defect line are commonly defined as functions of the jumps of ω_k^* and u_i^* around this line. From Weingarten's theorems, these vectors are shown as invariants of the defect line (Kleinert, 1989). The following geometric tensors are also introduced:

Definition 2.1.1

$$\text{DISCLINATION DENSITY:} \quad \Theta_{ij}^* := \Omega_j^* \delta_{iL} \quad (2.1.1)$$

$$\text{DISLOCATION DENSITY:} \quad \Lambda_{ij}^* := B_j^* \delta_{iL} \quad (2.1.2)$$

$$\text{DISPLACEMENT JUMP DENSITY:} \quad \alpha_{ij}^* := \Lambda_{ij}^* + \varepsilon_{jlm}\Theta_{il}^*(x_m - x_{0m}) \quad (2.1.3)$$

$$\text{CONTORTION:} \quad \kappa_{ij}^* := \alpha_{ij}^* - \frac{1}{2}\alpha_{mm}^* \delta_{ij} \quad (2.1.4)$$

where x_{0m} is a reference point for rotation and displacement integration.

Here, symbol δ_{iL} is used to represent the concentrated vectorial measure density on the defect line L. In particular, when L is a rectifiable curve, δ_{iL} is equal to $\tau_i \delta_L$ with τ_i the unit tangent vector to L and δ_L the one-dimensional Hausdorff measure density concentrated on L.

The disclination and dislocation density tensors Θ_{ij}^* and Λ_{ij}^* are measure densities (cf Evans and Garipey, 1992; Mattila, 1995) related to the so-called strain incompatibility

η_{ij}^* to be defined later. In general at the meso-scale a dislocation or a disclination is a defect line (i.e. a singular line for the strain) to which non-vanishing Burgers and/or Frank vectors are attached. The tensors Λ_{ij}^* and Θ_{ij}^* are basic physical tools to model defect density at the meso-scale while η_{ij}^* plays a key role to understand their behaviour. The displacement jump density and mesoscopic contortion (or lattice curvature) tensors α_{ij}^* and κ_{ij}^* are combinations of these basic density tensors, with $\alpha_{ij}^* = \Lambda_{ij}^*$ when the disclination density tensor vanishes. Moreover, let us also recall that the macroscopic dislocation and disclination densities Λ_{ij} and Θ_{ij} are defined by homogenization from the knowledge of the mesoscopic fields Λ_{ij}^* and Θ_{ij}^* , whose analysis is devoted to establish the properties of these homogenised fields.

2.2 Multiple-valued fields and line invariants; distributions as a modelling tool at meso-scale

Notations 2.2.1 *In the following sections, the assumed open domain is denoted by Ω (in practice but not necessarily Ω is bounded), and the set of defect line(s) is denoted by $\mathcal{L} \subset \Omega$. When considered alone, a defect line is indicated by $L \subset \Omega$, and Ω_L is the chosen symbol for $\Omega \setminus L$, which is also assumed to be open without loss of generality. Focussing on the meso-scale, symbol \hat{x} or \hat{x}_i denotes a generic point of the defect line(s), x or x_i is a generic point of Ω_L and x_0 or x_{0i} is a given fixed reference point of Ω_L . When x and \hat{x} are used together, \hat{x} denotes the projection of x onto the defect line L in a appropriate sense and $\hat{v}_i := v_i(\hat{x}, x)$ is the unit vector joining \hat{x} to x . The symbol \odot_ε is intended for a set of diameter 2ε enclosing the line L . More precisely, \odot_ε is defined as the intersection with Ω of the union of all closed spheres of radius ε centred on L :*

$$\odot_\varepsilon := \Omega \cap \bigcup_{\hat{x} \in L} B[\hat{x}, \varepsilon].$$

In case L is an isolated line, \odot_ε is a tube of radius ε enclosing L . In the sequel, considering a surface S of Ω crossed by L at \hat{x} and bounded by the curve C , symbols dC , dL , and dS will denote the 1D Hausdorff measures on C and L , and the 2D Hausdorff measure on S , respectively, with $\hat{\sigma}_j$ and τ_j the unit tangent vectors to C at x and to L at \hat{x} (when they exist). In some cases (having fractal curves in mind) the symbols dx_k and $dS_i := \varepsilon_{ijk} dx_j^{(1)} dx_k^{(2)}$ will stand for infinitesimal vectors oriented along C and normal to S , respectively, with in addition $dC_l(x) := \varepsilon_{lmn} dx_m \tau_n$ denoting an infinitesimal vector normal to C when $\tau_n = \tau_n(\hat{x})$ exists.

Assumption 2.2.1 (Mesoscopic elastic strain) *Henceforth we will assume that the linear strain \mathcal{E}_{mn}^* is a given symmetric $\mathcal{C}^\infty(\Omega_L, \mathbb{R}^{3 \times 3})$ -tensor prolonged by 0 on the*

line L , L^1 -integrable on Ω and compatible on Ω_L . In other words, the equality

$$\varepsilon_{qlm}\varepsilon_{kpn}\partial_l\partial_p\mathcal{E}_{mn}^* = 0 \quad (2.2.1)$$

is assumed everywhere on Ω_L .

2.2.1 Distributional analysis of the multiple-valued fields

In general, a multivalued function from Ω_L to \mathbb{R}^N consists of a pair of single-valued mappings with appropriate properties:

$$F \rightarrow \Omega_L \quad \text{and} \quad F \rightarrow \mathbb{R}^N,$$

where F is the associated Riemann foliation (Almgren, 1986; Knopp, 1996; Remmert, 1996). In the present case of meso-scale elasticity, we limit ourselves to multivalued functions obtained by recursive line integration of single-valued mappings defined on Ω_L . Reducing these multiple line integrals to simple line integrals, the Riemann foliation shows to be the set of equivalence path classes in Ω_L from a given $x_0 \in \Omega_L$ with the homotopy as equivalence relationship. Accordingly, a multivalued function will be called of index n on Ω_L if its n -th differential is single-valued on Ω_L . No other kinds of multifunctions are considered in this work, whether L is a single line alone or belongs to a more complex set of defect lines (with possible branchings, etc).

Notations 2.2.2 The notation $\partial_j^{(s)}$ is used for partial derivation of a single- or multiple-valued function whose domain is restricted to Ω_L . Locally around $x \in \Omega_L$, for smooth functions, the meanings of $\partial_j^{(s)}$ and the classical ∂_j are the same, whereas on the entire Ω the partial derivation operator ∂_j only applies to single-valued fields and must be understood in the distributive sense. A defect-free subset U of Ω is an open set such that $U \cap L = \emptyset$, in such a way that $\partial_j^{(s)}$ and ∂_j coincide on U for every single- or multiple-valued function of index 1.

In the following essential definition the strain is considered as a distribution on Ω :

Definition 2.2.1 [Frank tensor] The Frank tensor $\bar{\partial}_m\omega_k^*$ is defined on the entire domain Ω as the following distribution:

$$\bar{\partial}_m\omega_k^* := \varepsilon_{kpq}\partial_p\mathcal{E}_{qm}^*, \quad (2.2.2)$$

in such a way that

$$\langle \bar{\partial}_m\omega_k^*, \varphi \rangle := - \int_{\Omega} \varepsilon_{kpq}\mathcal{E}_{qm}^*\partial_p\varphi dV, \quad (2.2.3)$$

with φ a smooth test-function with compact support in Ω .

In fact, the tensorial distribution $\bar{\partial}_m \omega_k^*$ is the finite part of an integral when acting against test-functions. Indeed, since $\partial_p \mathcal{E}_{qm}^*$ might be non- $L^1(\Omega)$ -integrable in view of its possibly too strong singularity near the defect line, instead of being directly calculated as an integral, $\langle \varepsilon_{kpq} \partial_p \mathcal{E}_{qm}^*, \varphi \rangle$ must be calculated on Ω as the limit

$$\lim_{\varepsilon \rightarrow 0} \left(\int_{\Omega \setminus \odot_\varepsilon} \varepsilon_{kpq} \partial_p \mathcal{E}_{qm}^* \varphi dV + \int_{\partial \odot_\varepsilon \cap \Omega} \varepsilon_{kpq} \mathcal{E}_{qm}^* \varphi dS_p \right), \quad (2.2.4)$$

where the second term inside the parenthesis is precisely added in order to achieve convergence. One readily sees after integration by parts that expression (2.2.4) is equal to Eq. (2.2.3) provided $\lim_{\varepsilon \rightarrow 0} \Omega \setminus \odot_\varepsilon = \Omega_L$ (which is a general hypothesis limiting the acceptable defect lines together with the assumption that L is of vanishing 2D Hausdorff measure). Considering the possibly multivalued (with index 1) rotation vector ω_k^* , it should be observed from Definition 2.2.1 that $\bar{\partial}_m \omega_k^* = \partial_m^{(s)} \omega_k^*$ on Ω_L . This results from the classical relationship provided by elasticity theory between infinitesimal rotation and deformation derivatives. However, $\bar{\partial}_m \omega_k^*$ is defined by Eq. (2.2.2) as a distribution on Ω and therefore concentrated effects on L and its infinitesimal vicinity are added to $\partial_m^{(s)} \omega_k^*$, justifying the use of the symbol $\bar{\partial}_m \omega_k^*$ instead of $\partial_m \omega_k^*$ without giving to $\bar{\partial}_m$ the meaning of a derivation operator. In particular, it may be observed that the identical vanishing of $\partial_m^{(s)} \omega_k^*$ on Ω_L does not necessarily imply that the distribution $\bar{\partial}_m \omega_k^*$ vanishes as well. In fact from Eq. (2.2.4), it can be shown in this particular case that

$$\langle \bar{\partial}_m \omega_k^*, \varphi \rangle = \lim_{\varepsilon \rightarrow 0} \int_{\partial \odot_\varepsilon \cap \Omega} \varepsilon_{kpq} \mathcal{E}_{qm}^* \varphi dS_p = - \int_{\Omega} \varepsilon_{kpq} \mathcal{E}_{qm}^* \partial_p \varphi dV, \quad (2.2.5)$$

which is generally non-vanishing. Finally, as soon as the definition of the tensor distribution $\bar{\partial}_m \omega_k^*$ is given, so are the distributional derivatives of $\bar{\partial}_m \omega_k^*$:

$$\langle \partial_l \bar{\partial}_m \omega_k^*, \varphi \rangle = - \langle \bar{\partial}_m \omega_k^*, \partial_l \varphi \rangle = \int_{\Omega} \varepsilon_{kpn} \mathcal{E}_{nm}^* \partial_p \partial_l \varphi dV. \quad (2.2.6)$$

2.2.2 Rotation and displacement vectors

The rotation vector is defined from the knowledge of the linear strain together with the rotation at a given reference point x_0 . From this construction follows an invariance property of ω_k^* as a multifunction (recalling that multivaluedness takes its origin from the existence of a defect line which renders the strain incompatible on the entire Ω). Starting from the distributive Definition 2.2.1 of $\bar{\partial}_m \omega_k^*$, the differential form $\bar{\partial}_m \omega_k^* d\xi_m$ is integrated along a regular parametric curve $\Gamma \subset \Omega_L$ with endpoints $x_0, x \in \Omega_L$. For selected x_0 and ω_{0k}^* , the multivalued rotation vector is defined as

$$\omega_k^* = \omega_k^*(\#\Gamma, \omega_0^*) = \omega_{0k}^* + \int_{\Gamma} \bar{\partial}_m \omega_k^* d\xi_m,$$

where $\#\Gamma$ is the equivalence class of all regular curves homotopic to Γ in Ω_L . Indeed, from strain compatibility in Ω_L , i.e. from relation (2.2.1), it is clear that ω_k^* is a function of $\#\Gamma$ only. Consider now a regular parametric loop C (in case C is a planar loop, it is called a Jordan curve) and the equivalence class $\#C$ of all regular loops homotopic to C in Ω_L . Here, the extremity points play no role anymore and two loops are equivalent if and only if they can be continuously transformed into each other in Ω_L . The jump of the rotation vector ω_k^* along $\#C$ depends on $\#C$ only and is defined as¹

$$[\omega_k^*] = [\omega_k^*](\#C) = \int_C \bar{\partial}_m \omega_k^* d\xi_m. \quad (2.2.7)$$

The following developments address the displacement field multivaluedness as a mere consequence of strain incompatibility. The procedure defining the displacement vector from the rotation vector by means of line integrals is classical in linear elasticity. The following tensor plays in the construction of the displacement field a role analogous to $\bar{\partial}_m \omega_k^*$ in the construction of the rotation field:

Definition 2.2.2 [*Burgers tensor*] For a selected reference point $x_0 \in \Omega_L$, the Burgers tensor is defined on the entire domain Ω as the distribution

$$\bar{\partial}_l b_k^*(x; x_0) := \mathcal{E}_{kl}^*(x) + \varepsilon_{kpq}(x_p - x_{0p}) \bar{\partial}_l \omega_q^*(x). \quad (2.2.8)$$

The Burgers tensor can be integrated in the same way as the Frank tensor along any parametric curve Γ , providing for selected x_0 , ω_{0k}^* and u_{0k}^* the multivalued displacement vector u_k^* of index 2:

$$u_k^* = u_k^*(\#\Gamma, \omega_0^*, u_0^*) = u_{0k}^* + \varepsilon_{klm} \omega_l^*(x; \Gamma)(x_m - x_{0m}) + \int_\Gamma \bar{\partial}_l b_k^*(\xi) d\xi_l,$$

which is a function of $\#\Gamma$ only. It may be observed that $\bar{\partial}_l b_k^*$ and the vector

$$b_k^* = u_k^* - \varepsilon_{klm} \omega_l^*(x_m - x_{0m})$$

are related in the same way as $\bar{\partial}_m \omega_k^*$ and ω_k^* , including the fact that $\bar{\partial}_l b_k^* = \partial_l^{(s)} b_k^*$ on Ω_L . The jumps of b_k^* along $\#C$ and of u_k^* at x along $\#C$ (which depends on $\#C$ only) are defined as

$$[b_k^*](\#C; x_0) = [u_k^*](x; \#C; x_0) - \varepsilon_{klm} [\omega_l^*](\#C)(x_m - x_{0m}) = \int_C \bar{\partial}_l b_k^* d\xi_k.$$

¹let us note that the curve C could be non rectifiable, i.e. of infinite length. In fact, integrals on fractal curves and the related Stokes' and Gauss-Green's theorems are analysed by Harrison and Norton (1992), where it is shown, by the \mathcal{C}^∞ -smoothness of the differential form $\bar{\partial}_m \omega_k^* dx_m$ on Ω_L that Eq. (2.2.7) still holds even when the Hausdorff dimension of C is higher than 1.

Let us now, for the sake of simplicity, focus on the case of a defect line L which (i) can itself be represented as a single \mathcal{C}^0 , closed or not, parametric line without multiple points except possibly its extremities and (ii) is isolated in the sense that each of its points \hat{x} is located inside a smooth surface $S(\hat{x})$ bounded by a loop $C(\hat{x})$ and such that $S(\hat{x}) \setminus \{\hat{x}\} \subset \Omega_L$. Such a defect line L will be called an isolated dislocation or disclination. The jump $[\omega_k^*]$ of the rotation vector ω_k^* around L is defined as the jump of ω_k^* along $\#C(\hat{x})$ and hence is the same for any \hat{x} and suitable $C(\hat{x})$. Similarly, the jump $[b_k^*]$ of the vector b_k^* around L is defined as the jump of b_k^* along $\#C(\hat{x})$ and is also the same for any \hat{x} and suitable $C(\hat{x})$, given x_0 . In fact, the following result is well-known (Kleinert, 1989):

Theorem 2.2.1 [Weingarten] *The rotation vector ω_k^* is a multifunction of index 1 on Ω_L whose jump $\Omega_k^* := [\omega_k^*]$ around L is an invariant of the defect-line L . Moreover, for a given x_0 , the vector b_k^* is a multifunction of index 1 on Ω_L whose jump $B_k^* := [b_k^*]$ around L is an invariant of the defect-line.*

Proposition 2.2.1 [Multiple-valued displacement field] *From a symmetric smooth linear strain tensor \mathcal{E}_{ij}^* on Ω_L and a point x_0 where the displacement and rotation are given, a multivalued displacement field u_i^* of index 2 can be constructed on Ω_L such that the symmetric part of the deformation gradient $\partial_j^{(s)} u_i^*$ is the single-valued strain tensor \mathcal{E}_{ij}^* on Ω_L while its skew-symmetric part is the multivalued tensor $\omega_{ij}^* := -\varepsilon_{ijk} \omega_k^*$.*

From this result, the Frank and Burgers vectors can be defined as invariants of the single isolated line L .

Definition 2.2.3 [Frank and Burgers vectors] *The Frank vector of the line L is the invariant*

$$\Omega_k^* := [\omega_k^*], \quad (2.2.9)$$

while for a given reference point x_0 its Burgers vector is the invariant

$$B_k^* := [b_k^*] = [u_k^*](x) - \varepsilon_{klm} \Omega_l^* (x_m - x_{0m}). \quad (2.2.10)$$

A defect line with non-vanishing Frank vector is called a disclination while a defect line with non-vanishing Burgers vector is called a dislocation.

Clearly a disclination should always be considered as a dislocation by appropriate choice of x_0 while the reverse statement is false since Ω_k^* might vanish. This is why in the present work, the word “dislocation” means in the general sense a dislocation and/or a disclination. A pure dislocation is a dislocation with vanishing Frank vector.

Remark 2.2.1 *Two distinct reference points x_0 and x'_0 define two distinct Burgers vectors, related by*

$$B_k^* - B_k'^* = \varepsilon_{klm}(x_{0m} - x'_{0m})\Omega_l^*,$$

in such a way that $B_k^\Omega_k^*$ is an invariant independent of the arbitrary choice of x_0 . Therefore, for a non-zero Frank vector, the vanishing of the Burgers vector depends on the arbitrary choice of x_0 .*

Definition 2.2.4 (Mesoscopic strain incompatibility) *According to Eq. (2.2.1) combined with Eq. (2.2.2), the incompatibility tensor is defined by*

$$\eta_{ik}^* := \varepsilon_{imn}\partial_m\bar{\partial}_n\omega_k^*.$$

The strain field is called compatible on the set U if the associated incompatibility tensor vanishes on U .

2.3 Distributional analysis of incompatibility for a single rectilinear dislocation

2.3.1 The 2D model for rectilinear dislocations

2D elasticity means that the strain \mathcal{E}_{ij}^* is independent of the “vertical” coordinate z . However this assumption introduces no restriction on the dependence of the multivalued displacement and rotation fields upon z .

Notations 2.3.1 *Henceforth the single defect line will be assumed to be located along the z -axis. The two planar coordinates will be denoted by x and y or x_α . The projection of $x = (x_\alpha, z)$ on L is $\hat{x} = (0, 0, z)$. By convention, Latin indices i, j, k, l, \dots take their values from 1 to 3 and are basically used for 3D elasticity, while Greek indices $\alpha, \beta, \gamma, \delta, \dots$ take the values 1 or 2 and are used for 2D elasticity. Symbols $(\underline{e}_x, \underline{e}_y, \underline{e}_z)$ or $(\underline{e}_\alpha, \underline{e}_\beta)$ denote the Cartesian base vectors, while $(\underline{e}_r, \underline{e}_\theta, \underline{e}_z)$ denote the local cylindrical base vectors. For a planar curve C , the notation $dC_\alpha(x) = \varepsilon_{\alpha\beta}dx_\beta$ will be used for the curve normal.*

Let us observe that many fields are singular at the origin and that Ω_L is in fact the domain where the laws of linear elasticity will apply. Moreover, the strain can be

decomposed into three tensors:

$$\mathcal{E}_{ij}^* = \underbrace{\delta_{\alpha i} \delta_{\beta j} \mathcal{E}_{\alpha\beta}^*}_{\text{planar strain}} + \underbrace{(\delta_{iz} \delta_{j\gamma} \mathcal{E}_{\gamma z}^* + \delta_{jz} \delta_{i\gamma} \mathcal{E}_{\gamma z}^*)}_{\text{3D shear}} + \underbrace{\delta_{iz} \delta_{jz} \mathcal{E}_{zz}^*}_{\text{pure vertical compression}}.$$

The following propositions can be readily proved from Assumption 2.2.1:

Proposition 2.3.1 [2D compatibility] *In Ω_L , from 2D strain compatibility, there are real numbers K , a_α and b such that*

$$\begin{cases} \varepsilon_{\alpha\gamma} \varepsilon_{\beta\delta} \partial_\alpha \partial_\beta \mathcal{E}_{\gamma\delta}^* = 0, \\ \varepsilon_{\alpha\beta} \partial_\alpha \mathcal{E}_{\beta z}^* = K, \\ \mathcal{E}_{zz}^* = a_\alpha x_\alpha + b. \end{cases} \quad (2.3.1)$$

Lemma 2.3.1 *Let $C(\hat{x})$ denote a family of 2D closed rectifiable curves. Then, in 2D elasticity, the Frank tensor and the strain verify the relation*

$$\lim_{C(\hat{x}) \rightarrow \hat{x}} \int_{C(\hat{x})} x_\alpha \bar{\partial}_\beta \omega_\kappa^* dx_\beta + \varepsilon_{\kappa\beta} \mathcal{E}_{\beta z}^* dx_\alpha = 0,$$

provided the length of C is uniformly bounded and as long as the convergence $C(\hat{x}) \rightarrow \hat{x}$ is understood in the Hausdorff sense, i.e. in such a way that

$$\max\{\|x - \hat{x}\|, x \in C(\hat{x})\} \rightarrow 0.$$

Proof. The second compatibility condition of Eq. (2.3.1) is equivalent to

$$\partial_\gamma \mathcal{E}_{\beta z}^* - \partial_\beta \mathcal{E}_{\gamma z}^* = K \varepsilon_{\gamma\beta},$$

from which, so far as 2D elasticity is concerned,

$$\bar{\partial}_\beta \omega_\kappa^* := \varepsilon_{\kappa\gamma} \partial_\gamma \mathcal{E}_{\beta z}^* = \varepsilon_{\kappa\gamma} \partial_\beta \mathcal{E}_{\gamma z}^* - K \delta_{\kappa\beta},$$

and

$$\left(x_\alpha \bar{\partial}_\beta \omega_\kappa^* + \delta_{\alpha\beta} \varepsilon_{\kappa\gamma} \mathcal{E}_{\gamma z}^* \right) = \partial_\beta \left(x_\alpha \varepsilon_{\kappa\gamma} \mathcal{E}_{\gamma z}^* \right) - x_\alpha K \delta_{\kappa\beta}.$$

Since, under the limit assumptions of this lemma,

$$\lim_{C(\hat{x}) \rightarrow \hat{x}} \int_{C(\hat{x})} x_\alpha dx_\kappa = 0,$$

and since the strain is a single-valued tensor, the proof is achieved. \square

Lemma 2.3.2 *In 2D elasticity the planar Frank vector Ω_α^* vanishes.*

Proof. Since

$$\bar{\partial}_\beta b_\tau^* = \mathcal{E}_{\beta\tau}^* + \varepsilon_{\tau\gamma}(x_\gamma - x_{0\gamma})\delta_\beta \omega_z^* - \varepsilon_{\tau\gamma}(z - z_0)\delta_\beta \omega_\gamma^*,$$

the planar Burgers vector simply writes as

$$B_\tau^* = \int_C \left(\mathcal{E}_{\beta\tau}^* + \varepsilon_{\tau\gamma}(x_\gamma - x_{0\gamma})\delta_\beta \omega_z^* \right) dx_\beta - \varepsilon_{\tau\gamma}(z - z_0)\Omega_\gamma^*,$$

where C is any planar loop. By Weingarten's theorems the Burgers vector is a constant while the integrand is independent of z , from which the result obviously follows. \square

In general, the present theory does not make any use of the linear elasticity constitutive laws and of the momentum and energy conservation laws, since in the framework of Continuum Mechanics arbitrary body forces and heat supply could be applied. Before entering into the heart of this chapter, let us recall that three explicit examples of rectilinear dislocations have been computed in Section 1.6.

2.3.2 Mesoscopic incompatibility for a single defect line

For 2D problems the incompatibility vector contains all the information provided by the general incompatibility tensor. The latter expresses on the one hand the non-commutative action of the defect line over the second derivatives of the rotation vector and on the other hand is related to concentrated effects of the Frank and Burgers vectors along the defect line.

Definition 2.3.1 *In the 2D case, the mesoscopic incompatibility vector is defined by*

$$\eta_k^* := \varepsilon_{\alpha\beta} \partial_\alpha \bar{\partial}_\beta \omega_k^*. \quad (2.3.2)$$

A strain field is compatible if the associated incompatibility vector vanishes.

As shown in the following sections, concentration effects on the defect line L will be represented by means of first- and second-order distributions.

Notations 2.3.2 *Recalling Notations 2.3.1, Ω_z and Ω_z^0 stand for the sets $\Omega_z := \{x \in \Omega \text{ such that } x = (x_\alpha, z)\}$ and $\Omega_z^0 := \Omega_z \setminus L$, while the radius $r = \|x - \hat{x}\|$ is the distance from a point x inside Ω to L. Then, the 1D Hausdorff measure concentrated on L is denoted by δ_L (cf Ambrosio et al. (2000), Evans and Garipey (1992) and Mattila (1995) for general definitions and properties on the geometric measure theory).*

In what follows the hypothesis consists in assuming that the strain radial dependence in the vicinity of L is less singular than a critical threshold. This is verified for instance by the wedge disclination whose strain radial behaviour is $O(\ln r)$ and by the screw and edge dislocations whose strains are $O(r^{-1})$.² For a straight defect-line L , according to these examples, the hypotheses on the strain and Frank tensors read as follows:

Assumption 2.3.1 [2D strain for line defects] *The strain tensor \mathcal{E}_{ij}^* is independent of the vertical coordinate z , is compatible on Ω_L in the sense that conditions (2.3.1) hold, is smooth on Ω_L and L^1 -integrable on Ω .*

Assumption 2.3.2 [Local behaviour] *The strain tensor \mathcal{E}_{ij}^* is assumed to be $o(r^{-2})$ ($\varepsilon \rightarrow 0^+$) while the Frank tensor is assumed to be $o(r^{-3})$ ($\varepsilon \rightarrow 0^+$).*

Theorem 2.3.1 [Main result for a single defect line] *Under Assumptions 2.3.1 and 2.3.2, for a dislocation located along the z -axis, incompatibility as defined by Eq. (2.3.2) is the vectorial first order distribution*

$$\eta_k^* = \delta_{kz} \eta_z^* + \delta_{k\kappa} \eta_\kappa^*,$$

where its vertical component is

$$\eta_z^* = \Omega_z^* \delta_L + \varepsilon_{\alpha\gamma} (B_\gamma^* - \varepsilon_{\beta\gamma} x_{0\beta} \Omega_z^*) \partial_\alpha \delta_L, \quad (2.3.3)$$

while its planar components are

$$\eta_\kappa^* = \frac{1}{2} \varepsilon_{\kappa\alpha} B_z^* \partial_\alpha \delta_L. \quad (2.3.4)$$

Proof. For some small enough $\varepsilon > 0$ and using Notations 2.2.1 a tube \odot_ε can be constructed around L and inside Ω . Assuming that the smooth 3D test-function φ has its compact support containing part of L , $\Omega_{\varepsilon,z}$ denotes the slice of $\Omega \setminus \odot_\varepsilon$ obtained for a given $\hat{x} \in L$, i.e.

$$\Omega_{\varepsilon,z} := \{x \in \Omega_z \text{ such that } \|x_\alpha\| > \varepsilon\},$$

while the boundary circle of $\Omega_{\varepsilon,z}$ is designated by $C_{\varepsilon,z}$.

▲ Let us firstly treat the left-hand side of Eq. (2.3.3). Indeed, from Definition 2.3.1 with Eq. (2.2.2), Definition 2.2.1, and Eqs. (2.2.3) and (2.2.4), it follows that

$$\langle \eta_k^*, \varphi \rangle = \int_L dz \lim_{\varepsilon \rightarrow 0^+} \Pi_k(z, \varphi, \varepsilon),$$

²A function $f(\varepsilon)$ is said to be $O(g(\varepsilon))$ ($\varepsilon \rightarrow 0^+$) if there exists $K, \varepsilon_0 > 0$ s.t. $0 < \varepsilon < \varepsilon_0 \Rightarrow |f(\varepsilon)| \leq K|g(\varepsilon)|$. A function $f(\varepsilon)$ is said to be $o(g(\varepsilon))$ ($\varepsilon \rightarrow 0^+$) if $\lim_{\varepsilon \rightarrow 0^+} \frac{f(\varepsilon)}{g(\varepsilon)} = 0$.

where

$$\Pi_k(z, \varphi, \varepsilon) := - \int_{\Omega_{\varepsilon, z}} \varepsilon_{\alpha\beta} \bar{\partial}_\beta \omega_k^* \partial_\alpha \varphi dS - \int_{C_{\varepsilon, z}} \varepsilon_{\alpha\beta} \varepsilon_{k\gamma n} \mathcal{E}_{\beta n}^* \partial_\alpha \varphi dC_\gamma.$$

The boundedness of $|\partial_\tau \partial_\delta \varphi|$ on Ω_L provides the following Taylor expansions of φ and of $\partial_\alpha \varphi$ around \hat{x} :

$$\varphi(x) = \varphi(\hat{x}) + r \hat{v}_\alpha \partial_\alpha \varphi(\hat{x}) + \frac{r^2}{2} \hat{v}_\tau \hat{v}_\delta \partial_\tau \partial_\delta \varphi(\hat{x} + \gamma_1(x - \hat{x})), \quad (2.3.5)$$

$$\partial_\alpha \varphi(x) = \partial_\alpha \varphi(\hat{x}) + r \hat{v}_\tau \partial_\tau \partial_\alpha \varphi(\hat{x} + \gamma_2(x - \hat{x})), \quad (2.3.6)$$

with $0 < \gamma_1(x - \hat{x}), \gamma_2(x - \hat{x}) \leq 1$.

▲ Consider the first term of Eq. (2.3.5), noted $\hat{\Pi}_k$. By virtue of strain compatibility on Ω_L and Gauss-Green's theorem, this term writes as

$$\hat{\Pi}_k(z, \varphi, \varepsilon) := - \int_{\Omega_{\varepsilon, z}} \partial_\gamma (\varepsilon_{\gamma\beta} \bar{\partial}_\beta \omega_k^* \varphi) dS = \int_{C_\varepsilon} \varepsilon_{\gamma\beta} \bar{\partial}_\beta \omega_k^* \varphi dC_\gamma.$$

Since by Notations 2.3.1 $r \hat{v}_\alpha := x_\alpha - \hat{x}_\alpha = x_\alpha$, then Eq. (2.3.5) and Assumption 2.3.2 show that, for $\varepsilon \rightarrow 0^+$,

$$\hat{\Pi}_k = \int_{C_{\varepsilon, z}} \varepsilon_{\gamma\beta} \bar{\partial}_\beta \omega_k^* (\varphi(\hat{x}) + x_\alpha \partial_\alpha \varphi(\hat{x})) dC_\gamma + o(1).$$

▲ Consider the second term of Eq. (2.3.5), noted Π_k^* . On account of Assumption 2.3.2 and by expansion (2.3.6), this term may be rewritten as

$$\begin{aligned} \Pi_k^*(z, \varphi, \varepsilon) &:= - \int_{C_{\varepsilon, z}} \varepsilon_{\alpha\beta} \varepsilon_{k\gamma n} \mathcal{E}_{\beta n}^* \partial_\alpha \varphi dC_\gamma \\ &= - \partial_\alpha \varphi(\hat{x}) \int_{C_{\varepsilon, z}} \varepsilon_{\alpha\beta} \varepsilon_{k\gamma n} \mathcal{E}_{\beta n}^* dC_\gamma + o(1). \end{aligned}$$

▲ From Weingarten's theorem, recalling that $dC_\gamma = \varepsilon_{\gamma\tau} dx_\tau$, the expression $\Pi_k = \hat{\Pi}_k + \Pi_k^*$ writes as

$$\begin{aligned} \Pi_k &= \partial_\alpha \varphi(\hat{x}) \int_{C_{\varepsilon, z}} (x_\alpha \bar{\partial}_\tau \omega_k^* - \varepsilon_{\alpha\beta} \varepsilon_{k\gamma n} \varepsilon_{\gamma\tau} \mathcal{E}_{\beta n}^*) dx_\tau \\ &+ \Omega_k^* \varphi(\hat{x}) + o(1). \end{aligned} \quad (2.3.7)$$

▲ Consider the first term of Eq. (2.3.7), noted Π'_k , and take $\delta = \gamma$ in the identity

$$\varepsilon_{k\delta n} \varepsilon_{\gamma\tau} = \delta_{kz} (\delta_{\gamma\delta} \delta_{n\tau} - \delta_{n\gamma} \delta_{\tau\delta}) - \delta_{nz} (\delta_{\gamma\delta} \delta_{k\tau} - \delta_{k\gamma} \delta_{\tau\delta}) \quad (2.3.8)$$

in such a way that

$$\Pi'_k = \partial_\alpha \varphi(\hat{x}) \int_{C_{\varepsilon, z}} (x_\alpha \bar{\partial}_\tau \omega_k^* - \delta_{kz} \varepsilon_{\alpha\beta} \mathcal{E}_{\beta\tau}^* + \delta_{k\tau} \varepsilon_{\alpha\beta} \mathcal{E}_{\beta z}^*) dx_\tau. \quad (2.3.9)$$

▲ The cases $k = z$ and $k = \kappa$ are treated separately.

- When $k = z$, Definition 2.2.2 shows that

$$\bar{\partial}_\beta b_\tau^* := \mathcal{E}_{\beta\tau}^* + \varepsilon_{\tau\gamma}(x_\gamma - x_{0\gamma})\bar{\partial}_\beta \omega_z^* - \varepsilon_{\tau\gamma}(z - z_0)\bar{\partial}_\beta \omega_\gamma^*$$

which, after multiplication by $\varepsilon_{\tau\alpha}$ and using Eq. (2.3.8) with τ, α and z substituted for k, δ and n , is inserted into Eq. (2.3.9), thence yielding:

$$\Pi'_z = \partial_\alpha \varphi(\hat{x}) \int_{C_{\varepsilon, z}} \left(\varepsilon_{\tau\alpha} \bar{\partial}_\beta b_\tau^* + x_{0\alpha} \bar{\partial}_\beta \omega_z^* + (z - z_0) \bar{\partial}_\beta \omega_\alpha^* \right) dx_\beta, \quad (2.3.10)$$

and consequently, from the definitions of the Frank and Burgers vectors,

$$\lim_{\varepsilon \rightarrow 0^+} \Pi'_z = \ll \left\{ \varepsilon_{\alpha\tau} B_\tau^* - (z - z_0) \Omega_\alpha^* - x_{0\alpha} \Omega_z^* \right\} \partial_\alpha \delta_0, \varphi_z \gg, \quad (2.3.11)$$

where δ_0 is the 2D Dirac measure located at 0 and $\varphi_z(x_\alpha) := \varphi(x_\alpha, z)$, while symbol $\ll \cdot, \cdot \gg$ denotes the 2D distribution by test-function product.

- When $k = \kappa$, Definition 2.2.2 shows that

$$\bar{\partial}_\beta b_z^* := \mathcal{E}_{\beta z}^* + \varepsilon_{\gamma\tau}(x_\gamma - x_{0\gamma})\bar{\partial}_\beta \omega_\tau^*,$$

from which, after multiplication by $\varepsilon_{\kappa\alpha}$, it results that:

$$x_\alpha \bar{\partial}_\tau \omega_\kappa^* = -\varepsilon_{\kappa\alpha} \bar{\partial}_\tau b_z^* + \varepsilon_{\kappa\alpha} \mathcal{E}_{\tau z}^* + x_{0\alpha} \bar{\partial}_\tau \omega_\kappa^* + (x_\kappa - x_{0\kappa}) \bar{\partial}_\tau \omega_\alpha^*.$$

Then, by Lemma 2.3.1 with a permutation of indices κ and α , Eq. (2.3.9) also writes as

$$\begin{aligned} \Pi'_\kappa &= \partial_\alpha \varphi(\hat{x}) \int_{C_{\varepsilon, z}} \left(-\varepsilon_{\kappa\alpha} \bar{\partial}_\beta b_z^* + \varepsilon_{\kappa\alpha} \mathcal{E}_{\beta z}^* + x_{0\alpha} \bar{\partial}_\beta \omega_\kappa^* - x_{0\kappa} \bar{\partial}_\beta \omega_\alpha^* \right) dx_\beta \\ &\quad + o(1). \end{aligned}$$

On the other hand, from Eq. (2.3.9) and Lemma 2.3.1 (i.e. from strain compatibility) it follows that:

$$\begin{aligned} \Pi'_\kappa &= \partial_\alpha \varphi(\hat{x}) \int_{C_{\varepsilon, z}} \left(-\varepsilon_{\kappa\beta} \mathcal{E}_{\beta z}^* dx_\alpha + \varepsilon_{\alpha\beta} \mathcal{E}_{\beta z}^* dx_\kappa \right) + o(1) \\ &= \partial_\alpha \varphi(\hat{x}) \int_{C_{\varepsilon, z}} \varepsilon_{\alpha\kappa} \mathcal{E}_{\beta z}^* dx_\beta + o(1). \end{aligned} \quad (2.3.12)$$

By summing this latter expression of Π'_κ with Eq. (2.3.12), from the definitions of the Frank and Burgers vector it follows that

$$\Pi'_\kappa = \frac{1}{2} \partial_\alpha \varphi(\hat{x}) \varepsilon_{\alpha\kappa} \left(B_z^* - \varepsilon_{\gamma\beta} \Omega_\gamma^* x_{0\beta} \right) + o(1). \quad (2.3.13)$$

Hence, in the limit $\varepsilon \rightarrow 0^+$ Eq. (2.3.13) writes as

$$\lim_{\varepsilon \rightarrow 0^+} \Pi'_\kappa = \ll \left\{ \frac{1}{2} \varepsilon_{\kappa\alpha} B_z^* - \frac{1}{2} \varepsilon_{\kappa\alpha} \varepsilon_{\gamma\beta} \Omega_\gamma^* x_{0\beta} \right\} \partial_\alpha \delta_0, \varphi_z \gg. \quad (2.3.14)$$

Therefore, the result is proved on Ω_z^0 , since

$$\lim_{\varepsilon \rightarrow 0^+} \Pi_k(z, \varphi, \varepsilon) = \lim_{\varepsilon \rightarrow 0^+} \Pi'_k(z, \varphi, \varepsilon) + \ll \Omega_k^* \delta_0, \varphi_z \gg. \quad (2.3.15)$$

▲ As suggested by Eq. (2.3.5), to obtain the result for the entire domain Ω it suffices to integrate Eqs. (2.3.10) and (2.3.13) and expression $\Omega_k^* \varphi(\hat{x})$ over L , in order to replace δ_0 by the line measure δ_L in Eqs. (2.3.11), (2.3.14) and (2.3.15). By Eqs. (2.3.5), (2.3.11), (2.3.14) and (2.3.15), the proof is achieved. \square

2.3.3 Applications of the main result

Throughout this section (x, y, z) denotes a generic point of Ω_L and all tensors are written in matrix form in the Cartesian base (e_x, e_y, e_z) .

- *Screw dislocation.* Since $B_y^* = \Omega_z^* = 0$, Eq. (2.3.4) yields

$$[\eta_k^*] = \frac{B_z^*}{2} \begin{bmatrix} \partial_y \delta_L \\ -\partial_x \delta_L \\ 0 \end{bmatrix}.$$

This result is easily verified with use of Eq. (2.2.6). One needs to compute $\int_{\Omega} \varepsilon_{kpn} \varepsilon_{\alpha\beta} \varepsilon_{\beta n}^* \partial_p \partial_\alpha \varphi dV$, that is to calculate the integral of

$$\frac{B_z^*}{4\pi} \begin{bmatrix} \partial_y \partial_x \varphi \frac{x}{r^2} + \partial_y^2 \varphi \frac{y}{r^2} \\ -\partial_x^2 \varphi \frac{x}{r^2} - \partial_x \partial_y \varphi \frac{y}{r^2} \\ 0 \end{bmatrix}.$$

By integration by parts, using Gauss-Green's theorem on Ω , and recalling that test-functions have compact supports and that $\partial_m \log r = x_m/r^2$, these integrals become

$$-\frac{B_z^*}{4\pi} \int_{\Omega} \begin{bmatrix} \partial_y \varphi \left(\partial_x \frac{x}{r^2} + \partial_y \frac{y}{r^2} \right) \\ -\partial_x \varphi \left(\partial_x \frac{x}{r^2} + \partial_y \frac{y}{r^2} \right) \\ 0 \end{bmatrix} dV = \frac{B_z^*}{4\pi} \int_{\Omega} \begin{bmatrix} -\partial_y \varphi \partial_m^2 \log r \\ \partial_x \varphi \partial_m^2 \log r \\ 0 \end{bmatrix} dV.$$

Hence, from $\Delta(\log r) = 2\pi \delta_L$, with Δ the Laplacian operator, the first statement is verified.

- *Edge dislocation.* Whereas $\bar{\partial}_m \omega_k^*$ identically vanishes on Ω_L , it is easily seen that Eqs. (2.3.3) and (2.3.4) with $B_z^* = \Omega_z^* = 0$ yield

$$[\eta_k^*] = B_y^* \begin{bmatrix} 0 \\ 0 \\ \partial_x \delta_L \end{bmatrix}.$$

We must compute $[\eta_k^*] = \int_{\Omega} \varepsilon_{pmk} \varepsilon_{\alpha\beta} \mathcal{E}_{\beta n}^* \partial_p \partial_{\alpha} \varphi dV$. For $k = 1$ and 2 and with $n \neq 3$, the tensor $\varepsilon_{\alpha\beta} \mathcal{E}_{\beta n}^* \partial_p \partial_{\alpha} \varphi$ equals $\mathcal{E}_{yx}^* \partial_z \partial_y \varphi - \mathcal{E}_{yy}^* \partial_z \partial_x \varphi$ and $\mathcal{E}_{xy}^* \partial_z \partial_x \varphi - \mathcal{E}_{xx}^* \partial_z \partial_y \varphi$ respectively. By integration by parts, the related integrals vanish. For $k = 3$, the integrand is

$$\varepsilon_{pmz} \varepsilon_{\alpha\beta} \mathcal{E}_{\beta n}^* \partial_p \partial_{\alpha} \varphi = \mathcal{E}_{xx}^* \partial_y \partial_y \varphi + \mathcal{E}_{yy}^* \partial_x \partial_x \varphi - 2\mathcal{E}_{xy}^* \partial_y \partial_x \varphi.$$

Integration by parts provides the expression $\int_{\Omega} -\frac{B_y}{2\pi} \partial_x \varphi \Delta(\log r) dV$, achieving the second verification.

- *Wedge disclination.* Incompatibility reads

$$[\eta_k^*] = \Omega_z^* \begin{bmatrix} 0 \\ 0 \\ \delta_L \end{bmatrix}.$$

We must calculate $\langle \eta_k^*, \varphi \rangle$. For $k = 1, k = 2, n \neq 0$ and $p = 3$ the integrand vanishes. For $k = 3$, one computes

$$\begin{aligned} \varepsilon_{\alpha\beta} \varepsilon_{\gamma\tau} \mathcal{E}_{\tau\beta}^* \partial_{\alpha} \partial_{\gamma} \varphi &= \frac{\Omega_z^*(1 - \nu^*)}{4\pi} \varphi \Delta(\log \frac{r}{R}) + \frac{\Omega_z^*(1 - \nu^*)}{4\pi} \varphi \Delta(\log \frac{r}{R}) \\ &= \frac{\Omega_z^*}{4\pi} (4\pi \delta_L), \end{aligned}$$

achieving the third verification.

2.4 Distributional analysis of incompatibility for a set of isolated dislocations

In the previous section, a single defect line was considered. However, to address the macro-scale physics, homogenisation must be performed on a set of dislocation lines whose number tends to infinity in order to define regular defect density tensors. Therefore, our goal is to introduce appropriate hypotheses that can easily be applied to a set of defect lines and to a regular defect density as well.

2.4.1 Governing assumptions for the strain and Frank tensors

Besides the strain Assumptions 2.3.1 two measure hypotheses on the strain derivatives are introduced to replace the local Assumptions 2.3.2 in order to validate Theorem 2.3.1 in a global framework.

Assumption 2.4.1 *The strain divergence and trace gradient $\partial_\alpha \mathcal{E}_{\alpha i}^*$ and $\partial_\gamma \mathcal{E}_{\kappa \kappa}^*$ are finite Radon measures on Ω .³*

Remark 2.4.1 *No assumption could be made on the complete Lebesgue integrable strain gradient without contradicting the 2D examples of Chapter 1, Section 1.6.3. On the other hand, it can be shown that the sharp Assumptions 2.4.1 are required to demonstrate Lemma 2.4.4 and hence Theorem 2.3.1.*

Remark 2.4.2 *Assumption 2.4.1 is natural in infinitesimal elasticity if one considers the strain-stress constitutive law and the equilibrium laws. As a consequence, the stress divergence must be a measure on Ω .*

The following Lemmas are needed for the proof of Lemma 2.4.4.

Lemma 2.4.1 • *A solenoidal distributional vector field a_α on Ω_z writes as*

$$a_\alpha = \varepsilon_{\alpha\gamma} \partial_\gamma \phi, \quad (2.4.1)$$

with $\phi \in \mathcal{D}'(\Omega_z)$.

• *A symmetric solenoidal distribution tensor $a_{\alpha\beta}$ on Ω_z writes as*

$$a_{\alpha\beta} = \varepsilon_{\alpha\gamma} \varepsilon_{\beta\tau} \partial_\gamma \partial_\tau \psi, \quad (2.4.2)$$

with $\psi \in \mathcal{D}'(\Omega_z)$.

Proof.

- *First statement.* Let ϕ_0 be any x_2 -primitive distribution of a_1 (Schwartz, 1957). Then $\partial_2 \phi_0 = a_1$ and, from the solenoidal property of a_α , there exists a distribution $G(x_1)$ s.t. $\partial_1 \phi_0 + a_2 = G(x_1)$. By x_1 -primitivation of $G(x_1)$, it is easy to find $F(x_1)$ s.t. $\partial_1 F = G(x_1)$, and to verify that $\phi = \phi_0 + F(x_1)$ solves the problem.

³A (finite) Radon measure on Ω is a measure bounded on compact subsets of Ω .

- *Second statement.* From $\partial_\alpha a_{\alpha\beta} = 0$, there is a distribution ϕ_β s.t. $a_{\alpha\beta} = \varepsilon_{\alpha\gamma} \partial_\gamma \phi_\beta$. Then $\varepsilon_{\alpha\gamma} \partial_\gamma (\partial_\beta \phi_\beta) \partial_\beta a_{\alpha\beta} = 0$ and hence $\partial_\beta \phi_\beta$ is a constant C or equivalently $\partial_\beta (\phi_\beta - \frac{1}{2} C x_\beta) = 0$. From Eq. (2.4.1), there exists a distribution ψ such that $\phi_\beta - \frac{1}{2} C x_\beta = \varepsilon_{\beta\tau} \partial_\tau \psi$, and hence $a_{\alpha\beta} = \varepsilon_{\alpha\gamma} \varepsilon_{\beta\tau} \partial_\gamma \partial_\tau \psi + \frac{1}{2} \varepsilon_{\alpha\beta} C$. The symmetry of $a_{\alpha\beta}$ implies that $C=0$. \square

Lemma 2.4.2 • For a given $L^1(\Omega_z)$ -scalar function f , there exists an irrotational distribution field g_β such that

$$\partial_\beta g_\beta = f. \quad (2.4.3)$$

- For a given $L^1(\Omega_z)$ -vector function f_β such that $\partial_\beta f_\beta = \Delta g$ where g is a $L^1(\Omega_z)$ function, there exists a symmetric compatible tensor $g_{\alpha\beta}$ on Ω_z such that

$$\partial_\alpha g_{\alpha\beta} = f_\beta. \quad (2.4.4)$$

Proof.

- *First statement.* It is sufficient to consider an ultra-weak solution (Brezis, 1983) of $\Delta H = f$ and to define $g_\beta = \partial_\beta H$.
- *Second statement.* By primitivation, there is a non-compatible $L^1(\Omega_z)$ -field $g_{\alpha\beta}^*$ such that $f_1 = \partial_1 g_{11}^*, f_2 = \partial_2 g_{22}^*$ and $0 = g_{21}^* = g_{12}^*$. A necessary condition for $g_{\alpha\beta}$ to exist is that $\hat{g}_{\alpha\beta} = g_{\alpha\beta} - g_{\alpha\beta}^*$ verifies $\partial_\alpha \hat{g}_{\alpha\beta} = 0$, or by Lemma 2.4.1 that $\hat{g}_{\alpha\beta} = \varepsilon_{\alpha\gamma} \varepsilon_{\beta\tau} \partial_\gamma \partial_\tau \phi$ for some gauge distribution ϕ . In order that $g_{\alpha\beta}$ be compatible on Ω_z , ϕ must satisfy the following equation, equivalent to the 2D compatibility of $g_{\alpha\beta}$ on Ω_z :

$$\Delta \Delta \phi = \Delta g_{\kappa\kappa}^* - \partial_\beta \partial_\alpha g_{\alpha\beta} = \Delta (g_{\kappa\kappa}^* - g). \quad (2.4.5)$$

Up to a harmonic and hence smooth function on Ω_z , the solution of Eq. (2.4.5) is the solution of $\Delta \phi = g_{\kappa\kappa}^* - g$. Since the right-hand side is $L^1(\Omega_z)$, a solution ϕ exists in the ultra-weak sense and hence the existence of a symmetric compatible distribution field $g_{\alpha\beta}$ on Ω_z verifying Eq. (2.4.4) follows. \square

Lemma 2.4.3 For constant C and C_β , there are a vector g_κ and a symmetric, compatible tensor $G_{\alpha\beta}$ on Ω_z such that

$$\partial_\kappa g_\kappa = C \delta_0, \quad (2.4.6)$$

$$\partial_\alpha G_{\alpha\beta} = C_\beta \delta_0. \quad (2.4.7)$$

Proof. The solutions are given by $g_\kappa = (2\pi)^{-1} \partial_\kappa \log r$ and $G_{\alpha\beta} = \frac{1}{2} (\partial_\alpha H_\beta + \partial_\beta H_\alpha)$, where

$$\begin{aligned} H_1 &= \frac{C_1}{2\pi} \left(\frac{3}{2} \log r - \frac{x_1^2}{2r^2} \right) - C_2 \frac{x_1 x_2}{4\pi r^2}, \\ H_2 &= \frac{C_2}{2\pi} \left(\frac{3}{2} \log r - \frac{x_2^2}{2r^2} \right) - C_1 \frac{x_1 x_2}{4\pi r^2}. \end{aligned}$$

□

Lemma 2.4.4 *Under Assumptions 2.3.1 and 2.4.1, the strain components can be put in the form:*

$$\mathcal{E}_{\kappa z}^* = E_\kappa + e_\kappa, \quad (2.4.8)$$

$$\mathcal{E}_{\alpha\beta}^* = E_{\alpha\beta} + e_{\alpha\beta}, \quad (2.4.9)$$

where vector E_κ has a vanishing curl on Ω_z for any given z while vector e_κ is $o(r^{-2})$ as $r \rightarrow 0^+$, and where tensor $E_{\alpha\beta}$ is compatible on Ω_z for any given z while tensor $e_{\alpha\beta}$ is $o(r^{-2})$ as $r \rightarrow 0^+$.

Proof. By Assumption 2.4.1, $\partial_\kappa \mathcal{E}_{\kappa i}^*$ is a Radon measure on Ω_z , and hence writes by Radon-Nykodým's decomposition theorem as

$$\partial_\kappa \mathcal{E}_{\kappa i}^* = f_i + \phi_i, \quad (2.4.10)$$

where $f_i \in L^1(\Omega_z)$ and where ϕ_i is a Radon measure on Ω_z singular with respect to Lebesgue's measure. As a mere consequence of the smoothness of $\partial_\kappa \mathcal{E}_{\kappa i}^*$ on Ω_z^0 , ϕ_i is a concentrated measure on Ω_z and hence is proportional to the Dirac mass δ_0 ,

$$\phi_i = C_i \delta_0 = (2\pi)^{-1} C_i \partial_\kappa^2 \log r. \quad (2.4.11)$$

▲ *First statement.*

- By Eqs. (2.4.10), (2.4.11) with $i = z$, and Lemma 2.4.2, there exists an irrotational g_κ such that

$$\partial_\kappa (\mathcal{E}_{\kappa z}^* - g_\kappa - (2\pi)^{-1} C_z \partial_\kappa \log r) = 0,$$

in such a way that, by Lemma 2.4.1,

$$\mathcal{E}_{\kappa z}^* - g_\kappa - (2\pi)^{-1} C_z \partial_\kappa \log r = \varepsilon_{\kappa\gamma} \partial_\gamma \psi, \quad (2.4.12)$$

where ψ is a distribution. Apply the curl operator to Eq. (2.4.12) and take into account the irrotational property of g_κ in such a way that $\Delta \psi = \varepsilon_{\kappa\beta} \partial_\beta \mathcal{E}_{\kappa z}^*$. Since

$\mathcal{E}_{\kappa z}^*$ is a L^1 -vector, its curl is a first-order distribution⁴ and hence, by the strain compatibility which ensures the curl of $\mathcal{E}_{\kappa z}^*$ to be a constant K on Ω_z^0 and a combination of the Dirac mass and its first-order derivatives at the origin (Schwartz, 1957), writes as $K + c\delta + c_\gamma\partial_\gamma\delta$.

- Now in the resulting equation

$$\partial_\beta \left(\varepsilon_{\kappa\beta} \mathcal{E}_{\kappa z}^* - (2\pi)^{-1} c \partial_\beta \log r - \frac{K}{2} x_\beta \right) = c_\gamma \partial_\gamma \delta, \quad (2.4.13)$$

the term on the left-hand side is the divergence of a L^1 -vector, and hence Eq. (2.4.13) has no distributional solution unless $c_\gamma = 0$.

- It results that $\Delta\psi = K + (2\pi)^{-1}c\Delta(\log r)$ provides a gauge field ψ which writes as

$$\psi = h + (2\pi)^{-1}c \log r, \quad (2.4.14)$$

where h is a solution of $\Delta h = K$ on Ω_z . It is easily verified that the curl of ψ is $o(r^{-2})$ as $r \rightarrow 0^+$.

- Defining $E_\kappa = g_\kappa + (2\pi)^{-1}C_z\partial_\kappa \log r$ and $e_\kappa = \varepsilon_{\kappa\gamma}\partial_\gamma\psi$ in Eq. (2.4.12) achieves the first statement proof.

▲ *Second statement.*

- Let us prove that the divergence of f_i is the Laplacian of an $L^1(\Omega_z)$ function. In fact, since η_z^* writes as

$$\eta_z^* = \partial_\alpha \left(\partial_\alpha \mathcal{E}_{\kappa\kappa}^* - \partial_\beta \mathcal{E}_{\alpha\beta}^* \right), \quad (2.4.15)$$

it is from Assumption 2.4.1 a concentrated first-order distribution writing as a combination of the Dirac mass and its first-order derivatives. Hence:

$$\begin{aligned} \partial_\beta f_\beta &= \partial_\alpha \partial_\beta \mathcal{E}_{\alpha\beta}^* - \partial_\beta \phi_\beta = \Delta \mathcal{E}_{\kappa\kappa}^* - \eta_z^* - \partial_\beta \phi_\beta = \Delta \mathcal{E}_{\kappa\kappa}^* - \hat{c}\delta_0 - \hat{c}_\gamma \partial_\gamma \delta_0 \\ &= \Delta \left(\mathcal{E}_{\kappa\kappa}^* - \bar{c} \log r - \bar{c}_\gamma \partial_\gamma \log r \right), \end{aligned} \quad (2.4.16)$$

where $\hat{c}, \hat{c}_\gamma, \bar{c}, \bar{c}_\gamma$ are constants.

⁴Following Schwartz (1957), a distribution is of order 1 if it defines a linear continuous map on $\mathcal{C}_c^1(\Omega)$.

- From Eqs. (2.4.10), (2.4.7), (2.4.4) and Lemma 2.4.2, there exists a compatible $g_{\kappa\beta}$ such that

$$\partial_\kappa \left(\mathcal{E}_{\kappa\beta}^* - g_{\kappa\beta} - G_{\kappa\beta} \right) = 0, \quad (2.4.17)$$

in such a way that, by Lemma 2.4.1,

$$\mathcal{E}_{\kappa\beta}^* - g_{\kappa\beta} - G_{\kappa\beta} = \varepsilon_{\kappa\gamma} \varepsilon_{\beta\tau} \partial_\gamma \partial_\tau A, \quad (2.4.18)$$

for some gauge field $A \in \mathcal{D}'(\Omega_z)$ verifying, by the compatibility of $g_{\kappa\beta}$ and $G_{\kappa\beta}$ on Ω_z , the relation

$$\eta_z^* = \Delta \Delta A \quad \text{on} \quad \Omega_z. \quad (2.4.19)$$

Hence, since the left-hand side writes as a combination of derivatives of δ_0 of order lower or equal to 1, the field A is the solution of $\Delta A = (a + a_\gamma \partial_\gamma) \log r$ with constant a, a_γ , up to a smooth harmonic function on Ω_z . It follows that $A = (a + a_\gamma \partial_\gamma) \left(\frac{r^2}{4} (\log r - 1) \right)$ is a $\mathcal{C}^0(\Omega_z)$ solution of Eq. (2.4.19) such that:

$$\partial_\kappa \partial_\beta A \quad \text{is} \quad o(r^{-2}) \quad \text{as} \quad r \rightarrow 0^+. \quad (2.4.20)$$

- The proof is complete with the definitions $E_{\kappa\beta} = G_{\kappa\beta} + g_{\kappa\beta}$ and $e_{\kappa\beta} = \varepsilon_{\kappa\gamma} \varepsilon_{\beta\tau} \partial_\gamma \partial_\tau A$ in Eqs. (2.4.18) and (2.4.20). \square

2.4.2 Mesoscopic incompatibility for a set of isolated defect lines

Theorem 2.4.1 [Main 2D result] *Under Assumptions 2.3.1 and 2.4.1, for a set \mathcal{L} of isolated dislocations parallel to the z -axis and located at the positions x_β^L , $L \in \mathcal{L}$, incompatibility as defined by Eq. (2.3.2) is the vectorial first order distribution*

$$\eta_k^* = \delta_{kz} \eta_z^* + \delta_{k\kappa} \eta_\kappa^*, \quad (2.4.21)$$

where

- its vertical component is

$$\eta_z^* = \sum_{L \in \mathcal{L}} \left(\Omega_z^* \delta_L + \varepsilon_{\alpha\gamma} \left(B_\gamma^* + \varepsilon_{\beta\gamma} (x_\beta^L - x_{0\beta}) \Omega_z^* \right) \partial_\alpha \delta_L \right), \quad (2.4.22)$$

- its planar components are

$$\eta_\kappa^* = \sum_{L \in \mathcal{L}} \frac{1}{2} \varepsilon_{\kappa\alpha} B_z^* \partial_\alpha \delta_L. \quad (2.4.23)$$

102 A distributional approach to the geometry of 2D dislocations at meso-scale

Proof. From Lemma 2.4.4 the strain $\mathcal{E}_{\beta n}^*$ ($n = \alpha$ or z) is decomposed in compatible parts (E_β and $E_{\alpha\beta}$) and $o(r^{-2})$ parts (e_β and $e_{\alpha\beta}$) to which the demonstration may be limited by linearity. Since from Eqs. (2.4.14) and (2.4.20) the gradients $\partial_\gamma e_\beta, \partial_\gamma e_{\alpha\beta}$ are $o(r^{-3})$ for $r \rightarrow 0^+$, the proof of Theorem 2.3.1 can be followed for every $L \in \mathcal{L}$ as soon as $\mathcal{E}_{\beta z}^*$ is replaced by e_β and $\mathcal{E}_{\beta\tau}^*$ by $e_{\beta\tau}$. However, since the dislocations are located at positions x_β^L instead of 0, an additional shift x_β^L is required in Eq. (2.4.22). \square

2.4.3 Mesoscopic defect densities in 2D incompatible elasticity

Since the tensors $\Theta_{ik}^*, \Lambda_{ik}^*, \alpha_{ik}^*$ vanish for $i \neq z$, the 2D densities for an ensemble \mathcal{L} of rectilinear dislocations write as follows⁵:

Definition 2.4.1

$$\Theta_k^* := \sum_{L \in \mathcal{L}} \delta_{kz} \Omega_z^{*L} \delta_L \quad (2.4.24)$$

$$\Lambda_k^* := \sum_{L \in \mathcal{L}} B_k^{*L} \delta_L, \quad (2.4.25)$$

$$\alpha_k^* := \alpha_{zk}^* = \Lambda_k^* - \delta_{k\alpha} \varepsilon_{\alpha\beta} \Theta_z^* (x_\beta - x_{0\beta}). \quad (2.4.26)$$

Moreover, in the 2D case, the contortion tensor writes as:

$$\kappa_{ij}^* = \delta_{iz} \alpha_j^* - \frac{1}{2} \alpha_z^* \delta_{ij}. \quad (2.4.27)$$

The following result expresses the incompatibility in terms of κ_{ij}^* :

Theorem 2.4.2 *Under Assumptions 2.3.1 and 2.4.1, the mesoscopic strain incompatibility for a set \mathcal{L} of rectilinear dislocations writes as*

$$\eta_k^* = \Theta_k^* + \varepsilon_{\alpha\beta} \partial_\alpha \kappa_{k\beta}^*, \quad (2.4.28)$$

or equivalently as $\eta_k^* = \Theta_k^* + \varepsilon_{k\alpha l} \partial_\alpha \kappa_{zl}^*$. \square

⁵Various notations are used in the literature to represent the defect densities. In particular, Nye (1953), Kröner (1980) and Kleinert (1989) give different definitions of the dislocation density and contortion tensors (without considering disclinations in the first two cases). We here follow Kröner's and Kleinert's notations for α_{ij}^* and Nye's original definition of κ_{ij}^* , with Nye's α_{ij}^* here denoted by α_{ji}^* . It should be recalled that the term "contortion" was introduced by Kondo (1952).

Proof. Consider any straight dislocation $L \in \mathcal{L}$ located at a given $x^L \in \Omega$. From Theorem 2.4.1, incompatibility writes as

$$\begin{aligned} \eta_k^* &= \delta_{kz} (\Omega_z^* \delta_L + \varepsilon_{\alpha\gamma} (B_\gamma^* + \varepsilon_{\beta\gamma} (\hat{x}_\beta - x_{0\beta}) \Omega_z^*) \partial_\alpha \delta_L) \\ &+ \delta_{k\kappa} \frac{1}{2} \varepsilon_{\kappa\alpha} B_z^* \partial_\alpha \delta_L. \end{aligned} \quad (2.4.29)$$

Taking into account Eqs. (2.4.24), (2.4.25), (2.4.26), and (2.4.27), and the relation

$$\partial_\alpha ((x_\beta - x_{0\beta}) \delta_L) = \partial_\alpha ((x_\beta^L - x_{0\beta}) \delta_L) = (x_\beta^L - x_{0\beta}) \partial_\alpha \delta_L,$$

it results from Theorem 2.4.1 that incompatibility can be written in the alternative formulation

$$\eta_k^*(x^L) = \Theta_k^*(x^L) + \varepsilon_{\alpha\beta} \partial_\alpha \kappa_{k\beta}^*(x^L), \quad (2.4.30)$$

or equivalently as $\eta_k^*(x^L) = \Theta_k^*(x^L) + \varepsilon_{k\alpha l} \partial_\alpha \kappa_{z l}^*(x^L)$. The result follows after summation on $L \in \mathcal{L}$ and using Eqs. (2.4.24), (2.4.25), (2.4.26), and (2.4.27). \square

In a next step, the tensor $\bar{\partial}_j \bar{\partial}_l u_k^*$ is defined on the entire Ω in a similar way as $\bar{\partial}_j \omega_k^*$:

Definition 2.4.2

$$\bar{\partial}_j \bar{\partial}_l u_k^* := \partial_j \mathcal{E}_{kl}^* + \varepsilon_{kpl} \bar{\partial}_j \omega_p^*. \quad (2.4.31)$$

By Proposition 2.2.1, the displacement field u_k^* is a multivalued function of index 2, which is obtained on Ω_L by recursive line integration of $\partial_j^{(s)} \partial_l^{(s)} u_k^* = \partial_j^{(s)} (\mathcal{E}_{kl}^* + \omega_{kl}^*)$ and hence by recursive integration of $\bar{\partial}_j \bar{\partial}_l u_k^*$.

Remark 2.4.3 *In the situation where, for a particular selection of the reference point, the dislocations have vanishing Burgers vectors, the disclination density equals the incompatibility*

$$\varepsilon_{\alpha\beta} \partial_\alpha \bar{\partial}_\beta \omega_k^* = \Theta_k^* = \eta_k^*. \quad (2.4.32)$$

Using an arbitrary reference point, this expression is certainly false in the general case where disclinations coexist with dislocations. Moreover, the tensor $\bar{\partial}_j \bar{\partial}_l u_k^$ does not provide relevant information in terms of defect densities since $\varepsilon_{iji} \bar{\partial}_j \bar{\partial}_l u_k^* = 0$ on Ω .*

The mesoscopic vectors and tensors Θ_k^* , Λ_k^* , α_k^* , κ_k^* and η_k^* are concentrated distributions on the defect lines which provide all the information on dislocation and disclination densities. However, homogenisation to the macro-scale still requires to clarify

their link with the multivalued rotation and displacement fields. In order to resolve this problem, the tensors $\bar{\partial}_j \omega_k^*$ and $\bar{\partial}_j \bar{\partial}_l u_k^*$ are completed by appropriate concentrated effects in the defect lines, without however modifying their relationship with the multivalued displacement and rotation fields defined in Ω_L .

Definition 2.4.3

$$\bar{\partial}_\beta \omega_k^* := \bar{\partial}_\beta \omega_k^* - \kappa_{k\beta}^*, \quad (2.4.33)$$

$$\bar{\partial}_\alpha \bar{\partial}_\beta u_k^* := \bar{\partial}_\alpha \bar{\partial}_\beta u_k^* - \varepsilon_{kp\beta} \kappa_{p\alpha}^* = \partial_\alpha \mathcal{E}_{k\beta}^* + \varepsilon_{kp\beta} \bar{\partial}_\alpha \omega_p^*. \quad (2.4.34)$$

Theorem 2.4.3 *The vector and tensor distributions $\bar{\partial}_\beta \omega_k^*$ and $\bar{\partial}_\alpha \bar{\partial}_\beta u_k^*$ verify:*

$$\text{MESOSCOPIC DISCLINATION DENSITY} \quad \Theta_k^* = \varepsilon_{\alpha\beta} \partial_\alpha \bar{\partial}_\beta \omega_k^*, \quad (2.4.35)$$

$$\text{MESOSCOPIC DISLOCATION DENSITY} \quad \alpha_k^* = \varepsilon_{\alpha\beta} \bar{\partial}_\alpha \bar{\partial}_\beta u_k^*. \quad (2.4.36)$$

Proof. The first statement is a mere consequence of Eq. (2.4.28) while the second one follows from Eq. (2.4.33) by simple calculations, noting that $\bar{\partial}_m \omega_m^* = 0$ on Ω and that

$$\alpha_k^* = \kappa_{zk}^* - \kappa_{pp}^* \delta_{zk}. \quad (2.4.37)$$

□

Remark 2.4.4 *Eqs. (2.4.35) and (2.4.24) directly show that*

$$\int_S \varepsilon_{\alpha\beta} \partial_\alpha \bar{\partial}_\beta \omega_k^* dS = \int_S \Theta_k^* dS = \sum_{L \in \mathcal{L}_C} \Omega_k^{*L},$$

where the domain S is bounded by the counterclockwise-oriented Jordan curve C , which encloses once each defect line of the subset \mathcal{L}_C of \mathcal{L} . Similarly, Eqs. (2.1.2) and (2.4.26) show that

$$\begin{aligned} \int_S \varepsilon_{\alpha\beta} \bar{\partial}_\alpha \bar{\partial}_\beta u_k^* dS &= \int_S (\Lambda_k^* - \delta_{k\alpha} \varepsilon_{\alpha\beta} \Theta_z^* (x_\beta - x_{0\beta})) dS, \\ &= \sum_{L \in \mathcal{L}_C} \left(B_k^{*L} - \delta_{k\alpha} \varepsilon_{\alpha\beta} \Omega_z^{*L} (x_\beta^L - x_{0\beta}) \right). \end{aligned}$$

Remark 2.4.5 *The vector $\bar{\partial}_l \omega_z^*$ does not verify Stokes' theorem, neither in the classical sense, since $\varepsilon_{\alpha\beta} \partial_\alpha \bar{\partial}_\beta \omega_z^*$ is singular at x^L , nor in a measure theoretical sense, since $\varepsilon_{\alpha\beta} \partial_\alpha \bar{\partial}_\beta \omega_z^*$ is not a measure but a first-order distribution given by Eq. (2.4.22). As often observed in the literature, even in an inappropriate context, a formal use of Stokes' theorem may give a correct final result. We here prefer to avoid any confusion and hence to mention that, in view of a clarification of Stokes' theorem in the context*

of defective crystals, the following formula holds and can be proved as a consequence of the previous definitions:

$$\int_C \tilde{\partial}_l \omega_z^* dx_l = \int_{S_C} \varepsilon_{\alpha\beta} \partial_\alpha \tilde{\partial}_l \omega_z^* dS. \quad (2.4.38)$$

2.5 Macroscopic analysis

2.5.1 A first approach to homogenisation from meso- to macro-scale

The mesoscopic results given in the previous sections are now homogenised (cf Chapter 1, Section 1.7.1 and following). Indeed, in the context of linear elasticity, the macroscopic elastic strain \mathcal{E}_{ij} is obtained by averaging the mesoscopic stress σ_{ij}^* (and from the known elastic constitutive laws) and hence the macroscopic elastic incompatibility η_{ik} is obtained by averaging the mesoscopic incompatibility η_{ik}^* . Moreover the defect densities are homogenised and the macroscopic counterparts of Θ_k^* , Λ_k^* , α_k^* and κ_{ij}^* write as Θ_k , Λ_k , α_k , and κ_{ij} , with

$$\alpha_k = \kappa_{zk} - \kappa_{pp} \delta_{zk} \quad \text{and} \quad \kappa_{ij} = \delta_{iz} \alpha_j - \frac{1}{2} \alpha_z \delta_{ij}. \quad (2.5.1)$$

Definition 2.5.1 (Macroscopic Frank and Burgers tensors) *The Frank and Burgers vectors crossing a macroscopic surface S are defined as*

$$\Omega_k(S) := \int_S \Theta_k dS, \quad (2.5.2)$$

$$B_k(S) := \int_S \Lambda_k dS. \quad (2.5.3)$$

By homogenisation of Eqs. (2.4.33) and (2.4.34), the macroscopic counterparts of Definition 2.4.3 write as follows:

Definition 2.5.2

$$\tilde{\partial}_\beta \omega_k := \varepsilon_{kpq} \partial_p \mathcal{E}_{q\beta} - \kappa_{k\beta}, \quad (2.5.4)$$

$$\tilde{\partial}_\alpha \tilde{\partial}_\beta u_k := \partial_\alpha \mathcal{E}_{k\beta} + \varepsilon_{kp\beta} \tilde{\partial}_\alpha \omega_p, \quad (2.5.5)$$

where $\mathcal{E}_{k\beta}$ and $\kappa_{k\beta}$ define the macroscopic elastic strain and contortion.

Moreover, the macroscopic counterpart of Theorem 2.4.2 (i.e. the fundamental equation “inc $\mathcal{E} = \Theta + \text{curl } \kappa$ ” of the continuum theory of defects by Kröner (1980)⁶) together with Theorem 2.4.3 now follow from homogenisation of the mesoscopic defect densities and from Definition 2.5.2:

Theorem 2.5.1

$$\text{KRÖNER'S IDENTITY} \quad \eta_k = \Theta_k + \varepsilon_{\alpha\beta} \partial_\alpha \kappa_{k\beta}, \quad (2.5.6)$$

$$\text{MACROSCOPIC DISCLINATION DENSITY} \quad \Theta_k = \varepsilon_{\alpha\beta} \partial_\alpha \bar{\partial}_\beta \omega_k, \quad (2.5.7)$$

$$\text{MACROSCOPIC DISLOCATION DENSITY} \quad \alpha_k = \varepsilon_{\alpha\beta} \bar{\partial}_\alpha \bar{\partial}_\beta u_k. \quad (2.5.8)$$

Remark 2.5.1 *By Stokes' theorem, if S is a region enclosed by a curve C , which might have only fractal regularity (Harrison and Norton, 1992), then $\Omega_k(S) = \int_C \bar{\partial}_\beta \omega_k dx_\beta$.*

Moreover, in the absence of disclinations, $B_k(S) = \int_S \alpha_k dS$.

The macroscopic density tensors Λ_k and κ_{ij} , as obtained from the single-valued mesoscopic densities, have a geometrical interpretation (Kröner, 1980; Anthony, 1970) which will be discussed in the following section. Indeed, α_k is directly related to the torsion of a body submitted to an incompatible purely elastic deformation to which a non-Riemannian connexion is attached due to the contortion κ_{ij} .

2.5.2 The non-Riemannian macroscopic body

The following geometric objects are introduced after homogenisation of the well-defined mesoscopic elastic strain and defect densities, in order to provide the model of a macroscopic body endowed with a law of parallel displacement together with internal torsion accounting for the defective crystal structure.

Definition 2.5.3

$$\text{ELASTIC METRIC TENSOR:} \quad g_{ij} := \delta_{ij} - 2\mathcal{E}_{ij} \quad (2.5.9)$$

$$\text{DISLOCATION TORSION:} \quad T_{k;ij} := -\frac{1}{2} \varepsilon_{pij} \Lambda_{pk} \quad (2.5.10)$$

$$\text{SYMMETRIC CHRISTOFFEL SYMBOLS:} \quad \tilde{\Gamma}_{k;ij} := \frac{1}{2} (\partial_i g_{kj} + \partial_j g_{ki} - \partial_k g_{ij})$$

$$\text{CONNEXION CONTORTION:} \quad \Delta\Gamma_{k;ij} := T_{j;ik} + T_{i;jk} - T_{k;ji} \quad (2.5.11)$$

$$\text{NON SYMMETRIC CHRISTOFFEL SYMBOLS:} \quad \Gamma_{k;ij} := \tilde{\Gamma}_{k;ij} - \Delta\Gamma_{k;ij}. \quad (2.5.12)$$

⁶Note that different sign conventions for the rotation vector and incompatibility apply in Kröner's work.

Remark 2.5.2 *The metric of the actual configuration $\mathcal{R}(t)$ is δ_{ij} . Therefore, as required (cf Section 2.1 and Chapter 1, Section 1.3.5) the reference configuration \mathcal{R}_0 is nowhere used to introduce the above objects.*

Since small displacements are considered, no distinction is to be made between upper and lower indices.

Lemma 2.5.1 *The tensor g_{ij} defines a Riemannian metric. The symmetric Christoffel symbols $\tilde{\Gamma}_{k;ij}$ define a symmetric connexion compatible with this metric, while $T_{k;ij}$ and $\Delta\Gamma_{k;ij}$ are skew-symmetric tensors w.r.t. i and j and i and k , respectively. Moreover, the components of $T_{k;ij}$ for $i = z$ or $j = z$ vanish in the 2D case.*

Proof. The first statements follow from basic definitions (Dubrovin et al., 1992; Schouten, 1954) while the last one follows from the fact that, in the 2D case, $\alpha_{pk}(x^L)$ and $\Theta_{pm}(x^L)$ for $L \in \mathcal{L}$ are proportional to $\tau_p \delta_L(x^L)$ with τ_p standing for the tangent vector to the defect line. \square

Proposition 2.5.1 *The Cristoffel symbols $\Gamma_{k;ij}$ define a non-symmetric connexion compatible with the metric g_{ij} and whose torsion writes as $T_{k;ij}$.⁷*

Proof. It is easy to verify (Dubrovin et al., 1992) that $\Gamma_{k;ij}$ is a connexion since $\tilde{\Gamma}_{k;ij}$ is a connexion and $\Delta\Gamma_{k;ij}$ is a tensor. Denoting by ∇_k (resp. $\tilde{\nabla}_k$) the covariant gradient w.r.t. $\Gamma_{k;ij}$ (resp. $\tilde{\Gamma}_{k;ij}$), and recalling that a connexion is compatible with the metric g_{ij} if the covariant gradient of g_{ij} w.r.t. this connexion vanishes, we find by Eq. (2.5.12)

$$\begin{aligned} \nabla_k g_{ij} &= \partial_k g_{ij} - \Gamma_{l;ik} g_{lj} - \Gamma_{l;jk} g_{li} \\ &= \tilde{\nabla}_k g_{ij} + \Delta\Gamma_{l;ik} g_{lj} + \Delta\Gamma_{l;jk} g_{li}, \end{aligned} \quad (2.5.13)$$

where in the right-hand side, the 1st term vanishes by Lemma 2.5.1 while the 2nd and 3rd terms cancel each other since $\Delta\Gamma_{l;jk} g_{li} = \Delta\Gamma_{i;jk} = -\Delta\Gamma_{j;ik}$. It results that the connexion torsion, i.e. the skew-symmetric part of $\Delta\Gamma_{j;ik}$ w.r.t. i and k , writes as

$$\begin{aligned} \frac{1}{2} (\Delta\Gamma_{j;ik} - \Delta\Gamma_{j;ki}) &= -\frac{1}{2} (\Delta\Gamma_{i;jk} - \Delta\Gamma_{k;ji}) = \frac{1}{2} ((\Delta\Gamma_{k;ij} - \Delta\Gamma_{i;kj}) + \\ &\quad (\Delta\Gamma_{k;ji} - \Delta\Gamma_{k;ij}) - (\Delta\Gamma_{i;jk} - \Delta\Gamma_{i;kj})). \end{aligned} \quad (2.5.14)$$

Observing that the 1st term in the right-hand side of Eq. (2.5.14) writes as $\Delta\Gamma_{k;ij}$ while, by Definition 2.5.3 (Eq. (2.5.11)), the left-hand side and the two remaining terms of

⁷In the literature, a so-called Bravais' crystal is a macroscopic body endowed with a lattice where parallel displacement along the crystallographic lines is defined by the connexion $\Gamma_{k;ij}$ of Proposition 2.5.1 and where the metric is not defined by Eq. (2.5.9), but by the motion of an internal observer who would measure his own displacement by counting the atomic lattice steps, without feeling the body torsion (Kröner, 1980).

the right-hand side of Eq. (2.5.14) are equal to $T_{j;ik}, T_{k;ji}$ and $-T_{i;jk}$, respectively, the proof is complete. \square

The following result shows $\Delta\Gamma_{k;ij}$ as directly linked to the contortion κ_{ij} .

Proposition 2.5.2 *In the 2D case, the contortion tensor $\Delta\Gamma_{k;ij}$ writes in terms of κ_{ij} as*

$$\begin{aligned} \Delta\Gamma_{k;ij} = \delta_{k\kappa} (\delta_{i\alpha}\delta_{j\beta}\varepsilon_{\kappa\alpha}\kappa_{z\beta}) + \delta_{i\alpha}\delta_{jz}\varepsilon_{\alpha\tau}\kappa_{\tau\kappa} &+ \delta_{iz}\delta_{j\beta}\varepsilon_{\beta\tau}\kappa_{\tau\kappa} \\ &- \delta_{kz}\delta_{i\alpha}\delta_{j\beta}\varepsilon_{\alpha\beta}\kappa_{zz}. \end{aligned}$$

Proof. For $k = z$, by Definition 2.5.3, the last statement of Lemma 2.5.1, and Eq. (2.5.1), it is found that $\Delta\Gamma_{z;ij} = \Delta\Gamma_{z;\alpha\beta}\delta_{i\alpha}\delta_{j\beta}$, with

$$\begin{aligned} \Delta\Gamma_{z;\alpha\beta} = T_{z;\alpha\beta} = -\frac{1}{2}\varepsilon_{\alpha\beta}\alpha_z &= -\varepsilon_{\alpha\beta}\kappa_{zz} \\ &= -\frac{1}{2}\varepsilon_{\alpha\tau}\delta_{\tau\beta}\alpha_z = \varepsilon_{\alpha\tau}\kappa_{\tau\beta}. \end{aligned}$$

For $k = \kappa$, by Definition 2.5.3 and the last statement of Lemma 2.5.1, it is found that

$$\Delta\Gamma_{\kappa;ij} = \delta_{i\alpha}\delta_{j\beta} (T_{\kappa;\alpha\beta} + T_{\beta;\alpha\kappa} + T_{\alpha;\beta\kappa}) + \delta_{i\alpha}\delta_{jz}T_{z;\alpha\kappa} + \delta_{iz}\delta_{j\beta}T_{z;\beta\kappa},$$

with $T_{z;\xi\kappa} = \varepsilon_{\xi\tau}\kappa_{\tau\kappa}$ and $T_{\xi;\tau\nu} = -\frac{1}{2}\varepsilon_{\tau\nu}(\alpha_\xi + \varepsilon_{\xi\gamma}\Theta_z(x_\gamma - x_{0\gamma}))$. Since the combination of the terms in Θ_z vanish in $\Delta\Gamma_{\kappa;ij}$, the proof is completed by observing that $\varepsilon_{\alpha\beta}\alpha_\kappa + \varepsilon_{\kappa\alpha}\alpha_\beta = (\varepsilon_{\alpha\kappa}\varepsilon_{\tau\nu})\varepsilon_{\tau\beta}\alpha_\nu = \varepsilon_{\alpha\kappa}\alpha_\beta = \varepsilon_{\alpha\kappa}\kappa_{z\beta}$. \square

The following definition introduces two differential forms related, on the one hand (by Definitions 2.5.2 and 2.5.3, and Theorem 2.5.1 and Proposition 2.5.1) to the homogenisation of the well-defined mesoscopic defect measures and, on the other hand, as shown by the forthcoming theorem, to macroscopic incompatible rotation and distortion vectors.

Definition 2.5.4 *The following differential forms are introduced:*

$$d\omega_j := \bar{\partial}_\beta \omega_j dx_\beta, \quad (2.5.15)$$

$$d\beta_{kl} := -\Gamma_{l;k\beta} dx_\beta. \quad (2.5.16)$$

In the literature the existence of an elastic macroscopic distortion field is generally postulated (Mura, 1987; Head et al., 1993; Cermelli and Gurtin, 2001, 2002; Koslowski et al., 2002; Ariza and Ortiz, 2005) and the global distortion decomposition in elastic

and plastic parts follows⁸. The point of view of the present work is to avoid this kind of a-priori decomposition, which we believe cannot be rigorously justified. Nevertheless, the following theorem introduces rotation and distortion fields (which are not the global rotation and distortion related to the macroscopic strain) in the absence of disclinations. In contrast with the classical literature where it is basically postulated that dislocation density is the distortion curl, this relationship is here well-proved.

Theorem 2.5.2 [*Bravais rotation and distortion fields*] *If the macroscopic disclination density vanishes, there exists rotation and distortion fields defined as*

$$\text{BRAVAIS ROTATION} \quad \omega_j(x) := \omega_j^0 + \int_{x_0}^x d\omega_j, \quad (2.5.17)$$

$$\text{BRAVAIS DISTORTION} \quad \beta_{kl}(x) := \mathcal{E}_{kl}(x^0) - \varepsilon_{klj}\omega_j^0 + \int_{x_0}^x d\beta_{kl}, \quad (2.5.18)$$

with $\beta_{kl} = \mathcal{E}_{kl} - \varepsilon_{klj}\omega_j$, and where ω_j^0 is arbitrary and the integration is made on any line with endpoints x_0 and x . Moreover,

$$\partial_\alpha \beta_{k\beta} = \bar{\partial}_\alpha \bar{\partial}_\beta u_k \quad \text{and} \quad \varepsilon_{\alpha\beta} \partial_\alpha \beta_{k\beta} = \alpha_k. \quad (2.5.19)$$

Proof. By Definition 2.5.3, the symmetric part of the connexion writes as

$$-\Gamma_{(l;k)\beta} dx_\beta = -\frac{1}{2} \partial_\beta g_{kl} dx_\beta = -\frac{1}{2} \partial_m g_{kl} dx_m = \partial_m \mathcal{E}_{kl} dx_m = d\mathcal{E}_{kl},$$

while, by Definition 2.5.3 and Proposition 2.5.2, the skew-symmetric part writes as

$$-\Gamma_{[l;k]\beta} = -\frac{1}{2} (\partial_k g_{l\beta} - \partial_l g_{k\beta}) + \Delta \Gamma_{l;k\beta} = \partial_k \mathcal{E}_{l\beta} - \partial_l \mathcal{E}_{k\beta} + \Delta \Gamma_{l;k\beta}.$$

Observing, by Definitions 2.5.2 and 2.5.4 and Proposition 2.5.2, that $d\omega_j = \bar{\partial}_\beta \omega_j dx_\beta = -\frac{1}{2} \varepsilon_{lkj} \Gamma_{[l;k]\beta} dx_\beta$, it results that $d\beta_{kl} = d\mathcal{E}_{kl} - \varepsilon_{klj} d\omega_j$. Under the assumption of a vanishing macroscopic disclination density, the existence of well-defined Bravais rotation and distortion fields follows from Eqs. (2.5.15) and (2.5.19), Theorem 2.5.1, and Remark 2.5.1. Moreover, since $\partial_\alpha \beta_{k\beta} = \partial_\alpha \mathcal{E}_{k\beta} - \varepsilon_{k\beta j} \bar{\partial}_\alpha \omega_j$, by Eq. (2.5.5), this expression equals $\bar{\partial}_\alpha \bar{\partial}_\beta u_k$, completing the proof by Eq. (2.5.8). \square

Remark 2.5.3 *Referring to “Bravais” instead of “elastic” rotation and distortion fields is devoted to highlight that these quantities do not have a purely elastic meaning*

⁸In fact, the distortion is often considered as a constitutive variable in dislocation models (Davini, 1986; Gurtin, 2002; Ariza and Ortiz, 2005).

Remark 2.5.4 *The Bravais distortion does not derive from a Bravais displacement in the presence of dislocations. In fact, around a closed loop C , even if the macroscopic disclination density vanishes, the displacement differential as defined by $du_k := \beta_{k\alpha} dx_\alpha$ verifies by Theorem 2.5.2 the relationship:*

$$\int_C du_k = \int_S \varepsilon_{\beta\alpha} \partial_\beta \beta_{k\alpha} dS = \alpha_k(S). \quad (2.5.20)$$

Remark 2.5.5 *Eq. (2.5.17) indicates that symbol $\tilde{\partial}$ in Eq. (2.5.15) becomes a true derivation operator in the absence of disclinations.*

Remark 2.5.6 *Proposition 2.5.1 defines an operation of parallel displacement according to the Bravais lattice geometry. The parallel displacement of any vector v_i along a curve of tangent vector $dx_\alpha^{(1)}$ is such that $dx_\alpha^{(1)} \nabla_\alpha v_i = 0$ and hence that the components of v_i vary according to the law $d^{(1)}v_i = -\Gamma_{i;j\beta} v_j dx_\beta^{(1)}$ (Dubrovin et al., 1992). This shows the macroscopic Burgers vector and dislocation density together with the Bravais rotation and distortion fields as reminiscences of the defective crystal properties at the nanoscale. In fact, if $dx_\nu^{(1)}, dx_\xi^{(2)}$ are two infinitesimal vectors with the associated area $dS := \varepsilon_{\nu\xi} dx_\nu^{(1)} dx_\xi^{(2)}$, it results from Eq. (2.5.10), Remark 2.5.1, and the skew symmetry of $T_{k;\alpha\beta}$ that, in the absence of disclinations,*

$$dB_k = \alpha_k dS = -\varepsilon_{\alpha\beta} \Gamma_{k;\alpha\beta} dS = -\Gamma_{k;\alpha\beta} (dx_\alpha^{(1)} dx_\beta^{(2)} - dx_\beta^{(1)} dx_\alpha^{(2)}),$$

whose right-hand side appears as a commutator verifying the relation

$$dB_k = \varepsilon_{\alpha\beta} \tilde{\partial}_\alpha \tilde{\partial}_\beta u_k dS = -\varepsilon_{\alpha\beta} d^{(\alpha)}(dx^{(\beta)}).$$

2.6 Concluding remarks

In this work we have developed a 2D theory to analyse dislocated single crystals at the meso-scale by combining distributions with multivalued kinematic fields. The distributions are basically concentrated along the defect lines, which in turn form the branching lines of the multivalued fields. As a consequence of this analysis, a basic theorem relating the incompatibility tensor (as derived from the deformation field) to the Frank and Burgers vectors of the defect line has been established. This theory provides a framework for the homogenisation of the medium properties from meso- to macro-scale. In particular the macroscopic dislocation density is defined without stipulating an a-priori distortion decomposition into elastic and plastic parts (which does not exist, actually). The classical relationship between Bravais distortion and dislocation densities, instead of being a definition, now appears as a result taking its

origin from the meso-scale analysis. Moreover, the torsion and contortion tensors, which both describe the defective macroscopic crystal, are now properly understood as averages of concentrated mesoscopic tensors. Since the latter are the differentials (in an appropriate sense) of multivalued mesoscopic fields, we have shown how mesoscopic multivaluedness is recovered in the geometric properties of the non-Riemannian macroscopic crystal. In particular, in contrast with the mesoscale (where defects are due to the multivaluedness of the rotation and displacement fields) the macroscopic Burgers vector now appears as the commutator of a non-closed differential operator related to the body torsion.

Extension to the 3D case is the topic of Chapter 3, where the handling of non-rectilinear curves will be required in the framework of the geometric-measure theory. This should eventually make it possible to consider a set of defect curves, freely occupying the crystal with possible intersections and accumulation region-forming so-called dislocation clusters.

Chapter 3

Extension of the distributional approach to 3D dislocations

3.1 Introduction

This chapter is devoted to extend the results of Chapter 2 to the 3D case, by applying the method developed in Chapter 2 in order to validate Kröner's formulas in the 2D case. However, in a first step, we will restrict to the case of a Lipschitz line, and subsequently generalise the result to a set which is composed of possibly infinitely many lines, forming so-called 0D clusters. The application of the distributional approach to the 3D case will highlight new formulas relating strain incompatibility to the Frank and Burgers vectors. These formulas, as compared to the “ $\text{inc } \mathcal{E} = \Theta + \text{curl } \kappa$ ” formula, will exhibit two terms in the right hand-side which are related to the disclination and the dislocation densities, respectively (through the contortion tensor), both being weighted by a factor taking into account the line orientation, curvature and torsion. Global strain assumptions for these formulas are simply obtained by following the 2D case without the need for any new assumption of any kind on the elastic strain. The structure of this chapter follows the structure and methods of the 2D case, but the mathematical tools required, and the computational techniques appear to be slightly more complex.

The missing part of this chapter is the absence of homogenisation from meso-to macro-scale, which would show new macroscopic defect densities taking into account the

mesoscopic aspects of the 3D lines and clusters.¹

3.2 Geometrical analysis of the defect line L

This section is a discussion on the defect-line assumptions in order to determine the existence conditions for a tube surrounding the line L whose normal sections do not intersect. Let us recall that for a smooth curve the classical Frenet's formulas read

$$\tau'_m = \chi v_m, \quad v'_p = -\chi \tau_p - \zeta \sigma_p, \quad \sigma'_l = \zeta v_l, \quad (3.2.1)$$

where the derivation is intended with respect to the natural arc parameter along L, and where τ_i , v_i and σ_i denote the unit tangent vector, and the two natural normal vectors, respectively, while χ and ζ stand for the line intrinsic curvature and torsion.

Assumption 3.2.1 *Let us assume that the defect-line L is a simple² regular Lipschitz curve contained in $\overline{\Omega}$ where the set Ω is open, that is, a curve satisfying the following requirements:*

- i. *An admissible defect-line L is parametrically described by a continuous mapping*

$$\hat{x}_i : [0, 1] \rightarrow \overline{\Omega}$$

where its restriction to the open interval]0,1[takes its values in Ω .

- ii. *The tangent vector τ_i exists everywhere and is Lipschitz continuous on $\in [0, 1]$.*
- iii. *If $\hat{x}_i(t) = \hat{x}_i(t')$ then $t = t'$ or $\{t, t'\} = \{0, 1\}$. Moreover if $\{t, t'\} = \{0, 1\}$ then $\hat{x}_i(0) = \hat{x}_i(1) \in \Omega$ and $\tau_p(0) = \tau_p(1)$.*

The Lipschitz condition (ii) states that there is a uniform constant K which is the infimum of all reals $C > 0$ such that for every $t, t' \in [0, 1]$, $\|\tau_i(t) - \tau_i(t')\| \leq C|t' - t|$. By Frenet's two first formulas the Lipschitz conditions on the tangent vector guarantees the curvature χ to be bounded at those points of L where they are defined, that is almost everywhere on L (Lelong-Ferrand, 1963). Since the curve is Lipschitz continuous, the natural continuous and strictly increasing length parameter $s(t) \in [0; L]$ where $L < \infty$

¹Let me express my best thanks to Thierry Depauw and Jean Van Schaftingen for valuable discussions about some specific technical points of this chapter.

²"Simple" means that there are no distinct values of the length parameter other than the start- and end-points whose images may coincide on L.

will be used in the sequel, with the non-restrictive assumption that the length of the curve $|L|$ be equal to 1. Moreover, symbol $\hat{x}_i = \hat{x}_i^s = \hat{x}_i(s)$ (or \hat{x}) will always refer to a point of $L \in \Omega$, while $C_\varepsilon(\hat{x}^s)$ denotes the circle of radius ε centered at \hat{x}^s and whose plane is perpendicular to the tangent vector $\tau_i(s)$ to L at \hat{x}^s .

3.2.1 Existence of a regular tube

Proposition 3.2.1 *For every simple regular Lipschitz closed defect-line L and for every $\hat{x} \in L$ there exists $\delta > 0$ with δ independent of \hat{x} such that the closed disks $D_\delta(\hat{x})$ and $D_\delta(\hat{x}')$ for $\hat{x} \neq \hat{x}'$ have an empty intersection.*

Proof. We need prove that there is a $\delta > 0$ such that for every $t' \neq t \in [0, 1]$ with $\hat{x}'_i := \hat{x}_i(t')$ close to $\hat{x}_i := \hat{x}_i(t)$ and $\hat{x} \neq \hat{x}'$, the closed disc of radius δ perpendicular to $\tau'_i := \tau_i(t')$ at \hat{x}'_i belongs to Ω and does not intersect the closed disc of radius δ perpendicular to $\tau_i := \tau_i(t)$ at \hat{x}_i . Firstly, since the tangent vector is Lipschitz continuous, the curvature $\chi(t) := \left\| \frac{d\tau_i}{dt} \right\|$ exists almost everywhere on L and $\left\| \frac{d\tau_i}{ds} \right\|_\infty = \|\chi\|_\infty < \infty$, where $K = \|\chi\|_\infty$ is the uniform Lipschitz constant of the tangent vector τ_i . Moreover, let us define the set D as the intersection of the planes Π' and Π , perpendicular to $\tau_i(t')$ and $\tau_i(t)$ at \hat{x} and \hat{x}' , respectively.

Two preliminary steps and the main statement will now be proved.

- Proof steps.**
- (step1): $\exists \eta > 0$, s.t. $\forall (t' \neq t) \in [0; 1[$, if $M := \min\{|t - t'|, 1 - |t - t'|\} \leq \eta$ then Π' and Π are distinct (i.e. D is a line or the empty set).
 - (step2): Letting $\varepsilon > 0$, then $\forall (t' \neq t) \in [0; 1[$ s.t. $\bar{M} := \min\{|t - t'|, 1 - |t - t'|\} \geq \varepsilon$, $\exists \eta > 0$ such that $C'_\delta(\hat{x}') \cap C_\delta(\hat{x}) = \emptyset$ for every $\delta < \eta$.
 - (M): $\exists \delta > 0$, $\forall (t' \neq t) \in [0; 1[$, $C_\delta(\hat{x}') \cap C_\delta(\hat{x}) = \emptyset$.

Proof of (step1). If $t' \neq t$ and $\Pi' = \Pi$, then the vector $\hat{x}_i - \hat{x}'_i$ belongs to $\Pi' = \Pi$ and hence $(\hat{x}_i - \hat{x}'_i) \tau'_i = 0$. Define $\Delta\tau_i(t) := \tau_i(t) - \tau_i(t')$ where $t' \leq t$, in such a way that, from the Lipschitz assumption, $\|\Delta\tau_i(t)\| \leq K(t - t')$ and hence for $t' \leq \tau \leq t'$,

$$\Delta\tau_i(\tau) = \tau_i(\tau) - \tau_i(t') = \omega_i(\tau)K(\tau - t') \quad \text{with} \quad \omega_i := \omega_i^2(\tau) \leq 1, \quad (3.2.2)$$

where ω_i is a continuous function. Since

$$\hat{x}_i - \hat{x}'_i = \int_{t'}^t \tau_i d\tau = \int_{t'}^t (\tau_i(t') + \Delta\tau_i) d\tau = \tau'_i(t - t') + \omega_i(t^*)K(t^* - t'), \quad (3.2.3)$$

where $0 \leq t' \leq t^* \leq t < 1$, it results that its projection on τ'_i writes as

$$(\hat{x}_i - \hat{x}'_i)\tau'_i = (t - t')[1 + \Theta K]$$

where the scalar $\Theta = \tau'_i \omega_i(t^*) \frac{t-t'}{t^*-t'}$ verifies $0 \leq |\Theta| \leq 1$ and is non-negative, by continuity of the tangent vectors, for \hat{x}_i close enough to \hat{x}'_i , that is, for M close enough to 0, thereby proving (step1).

Proof of (step2). Basically, the property that the curve be simple and its compactness prove the statement. It is enough to prove the existence of a $\eta > 0$ such that the open balls centered at \hat{x}'_i and \hat{x}_i with radius η do not intersect. Let $\varepsilon > 0$ and $E_\varepsilon := \{(t', t) \text{ such that } \overline{M} \geq \varepsilon\}$ and $m = \inf_{E_\varepsilon} \|\hat{x} - \hat{x}'\|$. Assume that m vanishes. Then from those t', t corresponding to a sequence $\{(\hat{x}'_i, \hat{x}_i)\}_{i \geq 1}$ such that $\|\hat{x}_i - \hat{x}'_i\| \rightarrow 0$ as $i \rightarrow \infty$, one extracts a subsequence $\{(t'_i, t_i)\}_{i \geq 1}$ converging to $(t'_\infty, t_\infty) \in [0, 1]$. Clearly $\hat{x}(t'_\infty) = \hat{x}(t_\infty)$ which, since the line is simple, implies by Eq. (3.2.3) that either $t'_\infty = t_\infty$, or $(t'_\infty, t_\infty) = (0, 1)$, or $(t'_\infty, t_\infty) = (1, 0)$, hence contradicting the relation $\overline{M} \geq \varepsilon$. Taking $\eta := \frac{m}{2} > 0$ achieves the proof of (step2).

Proof of (M). Let $\varepsilon := \min\{\eta, \frac{1}{K}\}$. From the second step, it is sufficient to consider the case $M \leq \varepsilon$, while from the first step, the only relevant situation is the case where D is a line. All other situations trivially give the result. The plane Σ is defined (on the right of Figure 3.1) as the plane spanned by τ'_i and τ_i . Consider the picture on the left of Figure 3.1 and define d'_i (resp. d_i) as the vector from \hat{x}'_i (resp. from \hat{x}_i) to D . Moreover let $f_i := \hat{x}_i - \hat{x}'_i$, while e_i is the projection of f_i on the line D , in such a way that $f_i - e_i$ is the projection of f_i on Σ . Moreover, $d_i - d'_i = f_i - e_i$ and since $d'_i \subset \Pi'$ and $d_i \subset \Pi$, it results that $d'_i \tau'_i = d_i \tau_i = 0$ in such a way that $d_i \tau'_i = f_i \tau'_i$. Since the unit vectors τ_i and τ'_i are not perpendicular to each other, the decomposition $d_i = \alpha \tau'_i + \beta \tau_i$ follows, where $\alpha \tau'_i \tau_i + \beta = 0$ and $\alpha + \beta \tau'_i \tau_i = f_i \tau'_i$, and with

$$\alpha = \frac{f_i \tau'_i}{1 - (\tau'_i \tau_i)^2} \quad \text{and} \quad \beta = \frac{-\tau'_i \tau_i f_i \tau'_i}{1 - (\tau'_i \tau_i)^2}.$$

In order to prove (M), we need to compute the square of the distance $(d_i)^2 = \alpha^2 + \beta^2 + 2\alpha\beta(\tau'_i \tau_i)$ and show that it is bounded from below by a constant independent of t . Using Eq. (3.2.2), we firstly compute an accurate expression of $\tau'_i \tau_i$. Since $\tau_i^2 = (\tau'_i + \Delta \tau_i)^2 = 1 + 2\tau'_i \Delta \tau_i + (\Delta \tau_i)^2 = 1$, it results that $0 = 2\omega_i \tau'_i K(t - t') + \omega_i^2 K^2(t - t')^2$, in such a way that $2\omega_i \tau'_i = -\omega_i^2 K(t - t')$, and hence that

$$\tau'_i \tau_i = 1 + \omega_i \tau'_i K(t - t') = 1 - \frac{1}{2} \omega K^2(t - t')^2. \quad (3.2.4)$$

From Eqs. (3.2.4) and (3.2.2), the square norm of d_i writes as:

$$d_i^2 = \frac{(f_i \tau'_i)^2}{1 - (\tau'_i \tau_i)^2} = \frac{(1 - \Theta \frac{K}{2}(t - t'))^2}{\tilde{\Theta} K^2 - \frac{\Theta^2}{4} K^4 (t - t')^2} \geq \delta := \frac{(1 - \frac{K}{2} \varepsilon)^2}{K^2},$$

where $\delta > 0$ since $\varepsilon < \frac{2}{K}$. Since a uniform lower estimate δ has been found such

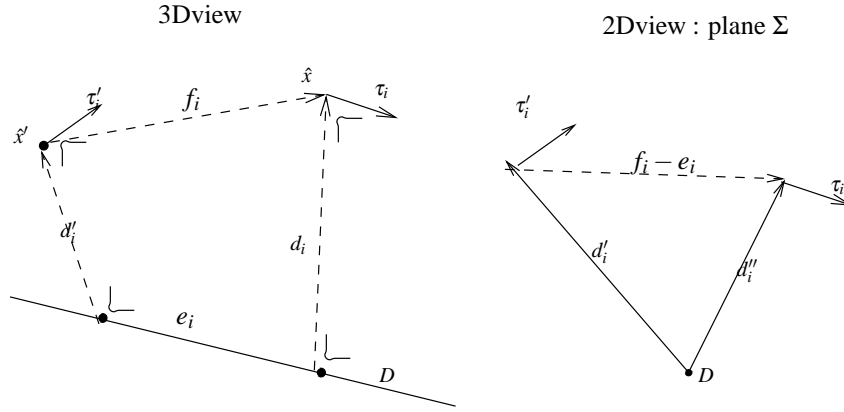


Figure 3.1: The sections of the tube do not intersect.

that, for every $\hat{x}_i \in L$ in the vicinity of any given $\hat{x}'_i \in L$, the disk $D_\delta(\hat{x})$ is contained in Ω and has an empty intersection with $D_\delta(\hat{x}')$, the proof is completed. \square

Remark 3.2.1 If the line L is open, let us denote by L_η the portion of the line corresponding to the interval $[\eta; 1 - \eta]$ for some given $\eta > 0$. The statement of Proposition 3.2.1 still holds for L_η instead of L . By the arbitrariness of η we can, in the remaining of this discussion, consider the case of an open line as well as the case of a closed line.

Definition 3.2.1 In the sequel, considering a surface S of Ω crossed by L at \hat{x}_i and \hat{x}_i only, and bounded by the curve C , symbols dC , dL , and dS will denote the 1D Hausdorff measures on C and L , and the 2D Hausdorff measure on S , respectively, with $\hat{\sigma}_j$ and τ_j the unit tangent vectors to C at x_i (when it exists) and to L at \hat{x}_i . In some cases (having fractal curves in mind) the symbols dx_k and $dS_i := \varepsilon_{ijk} dx_j^{(1)} dx_k^{(2)}$ will stand for infinitesimal vectors oriented along C and normal to S , respectively, with in addition $dC_i(x) := \varepsilon_{lmn} dx_m \tau_n$ denoting an infinitesimal vector normal to C .

Definition 3.2.2 We define $\odot_{\varepsilon,\eta}$, the tube of radius ε around the line L_η as

$$\odot_{\varepsilon,\eta} := \overline{\bigcup_{\hat{x} \in L_\eta} D_\varepsilon(\hat{x})} \cap \Omega.$$

Selecting $\varepsilon > 0$ according to Proposition 3.2.1 and Remark 3.2.1, let us observe that if the line is a closed loop the tube $\odot_\varepsilon := \odot_{\varepsilon,0}$ of radius ε around the line L has the same topology as a torus, while if the line is open $\odot_{\varepsilon,\eta}$ has the same topology as a cylinder. Moreover, by the regularity of the domain boundary $\partial\Omega$, for any $\eta > 0$, an $\varepsilon > 0$ can be found in such a way that $\odot_{\varepsilon,\eta} \subset \Omega$. The boundary of the disk $\partial D_\varepsilon(\hat{x})$ is denoted by $C_\varepsilon(\hat{x})$ or C_ε .

3.2.2 Geometrical properties of the defect line L

Definition 3.2.3 (Radial distance) The radial distance r of a point x (or x_i) in Ω_L to the line L is the minimal distance $\|x - \hat{x}\|$ from x to \hat{x} (or \hat{x}_i) in L . For this particular x , we define $v_i(\hat{x}, x) := \frac{x_i - \hat{x}_i}{\|\hat{x} - x\|}$ as the unit vector joining \hat{x} to x , in such a way that r is the positive number verifying

$$x_i = \hat{x}_i + r v_i(\hat{x}, x). \quad (3.2.5)$$

let us remark that in $\odot_{\varepsilon,\eta}$ the vector $v_i(\hat{x}, x)$ is orthogonal to $\tau_i(\hat{x})$. In the case where the point \hat{x} is uniquely defined for a given x in the vicinity of the defect line (which will generally be the case since the tube is used for local properties around L), the vector $v_i(\hat{x}, x)$ will be denoted without risk of confusion by $\hat{v}_i(x)$.

Planar curvature

Definition 3.2.4 (Planar curvature) Given $x \in \odot_{\varepsilon,\eta}$ and the associated $\hat{v}_i(x)$, the planar curvature of L for x is defined as

$$\chi(\hat{x}, x) = \chi(\hat{x}) v_i(\hat{x}) \hat{v}_i(x), \quad (3.2.6)$$

where $\chi(\hat{x})$ is the line intrinsic curvature at x .

Definition 3.2.5 (Projection plane and line) For $x \in \Omega_L$, the plane $\Sigma(x)$ is defined as the plane whose unit normal vector at $\hat{x} \in L$ writes as

$$\hat{\sigma}_i(x) := \sigma_i(\hat{x}, x) := \varepsilon_{ijk} \tau_j(\hat{x}) \hat{v}_k(x). \quad (3.2.7)$$

Then we introduce \tilde{L} as the projection of L on Σ , whose (non unit) tangent vector reads

$$\tilde{\tau}_k = \tau_k - \hat{\sigma}_k \hat{\sigma}_p \tau_p. \quad (3.2.8)$$

In what follows, \tilde{x}^t stands for the projection of $\hat{x}^t := \hat{x}(t)$ on \tilde{L} , while \tilde{v}_i stands for the (non-unit) normal vector at $\tilde{x}^t \in \tilde{L}$ defined as

$$\tilde{v}_i(\tilde{x}^t) := \varepsilon_{ijk} \sigma_j(\hat{x}, x) \tau_k(\tilde{x}^t). \quad (3.2.9)$$

Lemma 3.2.1 *The planar curvature of L on for x_0 equals to the curvature of \tilde{L} .*

Proof. For some given $x_0 \in \odot_{\varepsilon, \eta}$, let us consider the projection plane $\Sigma(x_0)$, where \hat{x}_0 stands for the projection of x_0 on L, and let a point of \tilde{L} be denoted by \tilde{x}^t , and $\hat{x}_0 = \hat{x}(t_0)$, where $0 \leq t_0 \leq 1$. By Frenet's first formula and from Eq. (3.2.8), it follows that

$$\frac{d}{dt} \tilde{\tau}_k = \chi (v_k - \hat{\sigma}_k \hat{\sigma}_p v_p) \quad (3.2.10)$$

in such a way that

$$\frac{d}{dt} \tilde{v}_i(\tilde{x}^t)|_{t=t_0} = \frac{d}{dt} (\varepsilon_{ijk} \sigma_j(\hat{x}_0, x_0) \tilde{\tau}_k(\tilde{x}^t))|_{t=t_0} = \chi(\hat{x}_0) \varepsilon_{ijk} \sigma_j(\hat{x}_0, x_0) v_k(\hat{x}_0).$$

Since by Eq. (3.2.7) $\varepsilon_{ijk} \sigma_j(\hat{x}_0, x_0) v_k(\hat{x}_0) = -v_j(\hat{x}_0) v_j(\hat{x}_0, x_0) \tau_i(\hat{x}_0)$, it results from Definition 3.2.4 that

$$\frac{d}{dt} \tilde{v}_i(\tilde{x}^t)|_{t=t_0} = -\chi(\hat{x}_0, x_0) \tau_i(\hat{x}_0), \quad (3.2.11)$$

while the unit vector $v_i(\tilde{x}^t)$ is such that

$$v_i(\tilde{x}^t) := \alpha(t) \tilde{v}_i(\tilde{x}^t) \quad (3.2.12)$$

with $|\alpha| \geq 1$. It remains to verify that the curvature $\chi(\hat{x}_0, x_0)$ is the curvature $\tilde{\chi}(\hat{x}_0)$ of the planar curve \tilde{L} at \hat{x}_0 . Firstly note that

$$\frac{d\tilde{t}}{dt}|_{t=t_0} = 1$$

while, by Frenet's first and second formulas for a planar curve, that

$$\frac{d}{d\tilde{t}} \tilde{v}_i(\tilde{x}^t) = \varepsilon_{ijk} \sigma_j(\hat{x}_0, x_0) \tilde{\chi}(\tilde{x}^t) v_k(\tilde{x}^t), \quad (3.2.13)$$

$$\frac{d}{d\tilde{t}} v_i(\tilde{x}^t) = -\tilde{\chi}(\tilde{x}^t) \tau_i(\tilde{x}^t) \quad (3.2.14)$$

It results from Eqs. (3.2.12), (3.2.13) and the unit property of $v_i(\tilde{x}^t)$, that

$$\frac{d\alpha}{dt} \Big|_{t=t_0} = \left(\tilde{v}_i(\tilde{x}^t) \frac{d}{dt} v_i(\tilde{x}^t) + v_i(\tilde{x}^t) \frac{d}{dt} \tilde{v}_i(\tilde{x}^t) \right) \Big|_{t=t_0} = 0. \quad (3.2.15)$$

Since $\alpha = \tilde{v}_i(\tilde{x}^t) v_i(\tilde{x}^t)$, it follows from Eq. (3.2.9) and from the fact that $\sigma_i(\hat{x}_0) = \sigma_i(\hat{x}_0, x_0)$ (since the line lies in $\Sigma(x_0)$), that $\alpha(t_0) = 1$, and hence by Eqs. (3.2.12), (3.2.14) and (3.2.15), that

$$-\tilde{\chi}(\hat{x}_0) \tau_i(\hat{x}_0) = \alpha(t_0) \frac{d\tilde{v}_i}{dt}(\hat{x}_0) + \frac{d\alpha}{dt}(t_0) \tilde{v}_i(\hat{x}_0) = \frac{d\tilde{v}_i}{dt}(\hat{x}_0)$$

which by Eq. (3.2.11) proves the statement. \square

Jacobian of the tube

Let s and ω denote the curvilinear coordinates associated with $x \in \odot_\varepsilon$ as chosen to verify the relations

$$v_i \hat{v}_i(x) = \cos \omega, \quad \text{and} \quad \sigma_i \hat{v}_i(x) = \sin \omega \quad (3.2.16)$$

in such a way that $\hat{\chi}(\hat{x}, x) = \chi(\hat{x}) \cos \omega$. Let us still denote by $\hat{v}_i(x)$ and $\hat{\sigma}_i(x)$ the vectors $v_i(s, \omega) = v_i(\hat{x}, x)$ and $\sigma_i(s, \omega) = \sigma_i(\hat{x}, x)$, respectively. By Eqs. (3.2.5) and (3.2.16), it results that

$$\begin{aligned} \frac{\partial x_i}{\partial s}(s, \omega) &= \tau_i(s) + \varepsilon \frac{\partial v_i(s, \omega)}{\partial s} \\ &= \tau_i(s) - \varepsilon (\chi(s) \cos \omega \tau_i(s) + \zeta(s) \cos \omega \sigma_i(s) - \zeta(s) \sin \omega v_i(s)) \\ \frac{\partial x_i}{\partial \omega}(s, \omega) &= \varepsilon (-\sin \omega v_i(s) + \cos \omega \sigma_i(s)), \end{aligned}$$

in such a way that, by Eq. (3.2.11), the metric tensor g_{ij} writes as the matrix (Dubrovin et al., 1992):

$$[g_{ij}] = \begin{bmatrix} (1 - \varepsilon \chi(\hat{x}, x))^2 + \varepsilon^2 \zeta^2 & -\varepsilon^2 \zeta \\ -\varepsilon^2 \zeta & \varepsilon^2 \end{bmatrix}.$$

Provided $\varepsilon < \frac{1}{K}$, where K is the Lipschitz constant of the curve, the discriminant of the metric tensor, that is, the square root of the determinant of g_{ij} writes as

$$g := \varepsilon(1 - \varepsilon \chi(\hat{x}, x)) > 0. \quad (3.2.17)$$

Definition 3.2.6 For a fixed $\varepsilon > 0$, the line $L_\varepsilon \subset \partial \odot_\varepsilon$ is defined as the set $\{x_i \in \odot_\varepsilon : x_i = \hat{x}_i + \varepsilon v_i(\hat{x}) \text{ where } \hat{x}_i \in L\}$. This line is described by means of the curvilinear coordinate s' , with the length element $dL(x)$ (ds') on L_ε defined as³

$$ds' = dL(x) := (1 - \varepsilon \chi(\hat{x}, x)) dL(\hat{x}), \quad (3.2.18)$$

where $dL(\hat{x}) := ds$ is the Lebesgue measure density on L , while the tangent vector on L_ε is given by

$$\tau_i^\varepsilon(x) = \tau_i(\hat{x}). \quad (3.2.19)$$

Moreover, $dC(x)$ denotes the Hausdorff measure density on $C_\varepsilon(x)$, symbol dx_k denotes an infinitesimal vector oriented along $C_\varepsilon(x)$, and

$$dC_l = \varepsilon_{lmn} dx_m \tau_n(\hat{x})$$

stands for an infinitesimal vector normal to $C_\varepsilon(x)$.

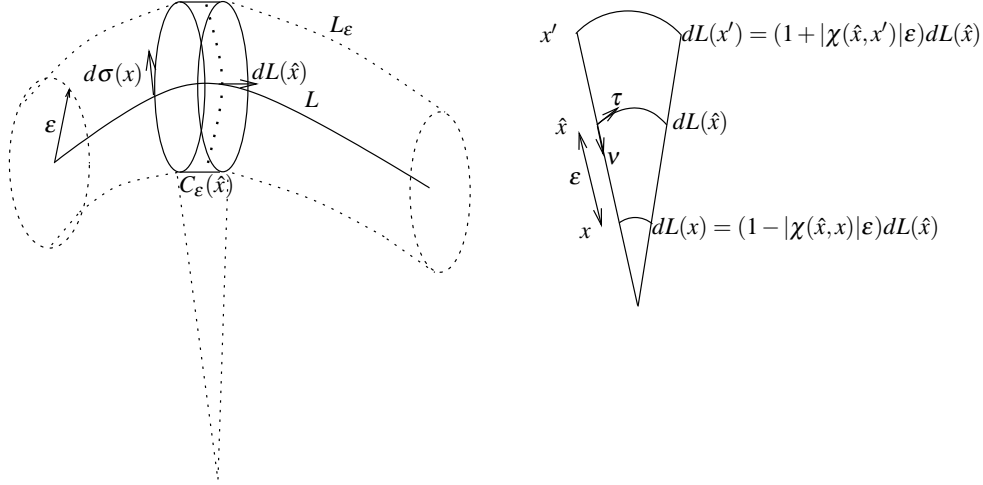


Figure 3.2: Curvature of the tube wrapped around L .

Lemma 3.2.2 In the vicinity of the line L , the following relation expressed in the general base holds:

$$\partial_j \hat{\tau}_i^\varepsilon(x) = \chi(\hat{x}) v_i(\hat{x}) \tau_j(\hat{x}) + o_{ij}(1). \quad (3.2.20)$$

Proof. For x in the vicinity of L , there exists a unique projection \hat{x} on L , defining τ_i, v_i and σ_i at $\hat{x} \in L$. Since $\partial_\tau s' = 1$ while $\partial_v s' = \partial_\sigma s' = 0$, it results that $\partial_j s' = \tau_j$,

³Note that s' is a function of x .

and hence from Eqs. (3.2.18), (3.2.19) and the first Frenet's formula (Eq. (3.2.1)), it immediately results that

$$\partial_j \hat{\tau}_i^e = (1 - \varepsilon \hat{\chi}) \chi v_i \tau_j, \quad (3.2.21)$$

proving the statement by Eq. (3.2.6) and the boundedness of the line curvature. \square

In the sequel of the chapter we make use of a local Cartesian base given by $\{v_i(\hat{x}^s), \sigma_i(\hat{x}^s), \tau_i(\hat{x}^s)\}$ at $\hat{x}^s \in L$, where s is the curvilinear abscissa on L , and a corresponding coordinate system given by $\{x_1^s, x_2^s, x_3^s\}$, where $x_3^s = z^s$ is the coordinate of the axis spanned by $\tau_i(\hat{x}^s)$. Greek subscripts always refer to the planar coordinates x_1^s or x_2^s of the axes spanned by $v_i(\hat{x}^s)$ and $\sigma_i(\hat{x}^s)$, respectively. By analogy with the planar case we also introduce the polar coordinates $r_s = \sqrt{x_1^{s2} + x_2^{s2}}$ and $\theta_s = \arctan \frac{x_2^s}{x_1^s}$, where subscript s indicates that the arc coordinate s is fixed. Moreover, partial derivation w.r.t. s will be denoted by ∂_s , and partial derivations w.r.t. r^s, θ^s, z^s by $\partial_{r^s}, \partial_{\theta^s}, \partial_{z^s}$, respectively. In general the notation ∂_i refers to partial derivation w.r.t. the i th coordinate of a 3D Cartesian base and coordinate system which, unless specified, is the general $\{\underline{e}_1, \underline{e}_2, \underline{e}_3\}$ -system attached to the origin. The notation $\hat{\partial}_i$ will, in turn, be used for partial derivation w.r.t. the local Cartesian system attached to $\hat{x}^s \in L$.

3.3 3D elasticity of the dislocated crystal

In this section, the crystal is dislocated by a single Lipschitz defect line and 3D linear elasticity applies everywhere away from the dislocation line.

3.3.1 Defect invariants and density tensors

In the following crucial definition the strain is considered as a distribution on Ω , where either the global Cartesian base $\{\underline{e}_1, \underline{e}_2, \underline{e}_3\}$, or the local Cartesian base $\{v_i(\hat{x}^s), \sigma_i(\hat{x}^s), \tau_i(\hat{x}^s)\}$ is considered, and where, for the sake of simplicity, the same notation \mathcal{E}_{ij}^* is adopted in all the following sections.

Let us firstly recall general notions and properties holding for any set of dislocation lines \mathcal{L} including the case of a single lines L .

Definition 3.3.1 [Frank and Burgers tensor] *The Frank tensor $\overline{\partial}_m \omega_k^*$ is defined on the entire domain Ω as the following distribution:*

$$\overline{\partial}_m \omega_k^* := \varepsilon_{kpq} \partial_p \mathcal{E}_{qm}^*, \quad (3.3.1)$$

in such a way that

$$\begin{aligned} \langle \bar{\partial}_m \omega_k^*, \varphi \rangle &:= - \int_{\Omega} \varepsilon_{kpq} \mathcal{E}_{qm}^* \partial_p \varphi dV \\ &= \lim_{\varepsilon \rightarrow 0} \left(\int_{\Omega \setminus \odot_{\varepsilon}} \varepsilon_{kpq} \partial_p \mathcal{E}_{qm}^* \varphi dV + \int_{\partial \odot_{\varepsilon} \cap \Omega} \varepsilon_{kpq} \mathcal{E}_{qm}^* \varphi dS_p \right), \end{aligned}$$

with φ a smooth test-function with compact support in Ω . Moreover, for a selected $x_0 \in \Omega_L$, the Burgers tensor is defined on the entire domain Ω as the distribution

$$\bar{\partial}_l b_k^*(x) := \mathcal{E}_{kl}^*(x) + \varepsilon_{kpq} (x_p - x_{0p}) \bar{\partial}_l \omega_q^*(x). \quad (3.3.2)$$

Definition 3.3.2 [Frank and Burgers vectors] The Frank vector of the line L is the invariant

$$\Omega_k^* := [\omega_k^*], \quad (3.3.3)$$

where the brackets here mean the jump of the considered quantity along a curve making a single loop around the defect line L . Moreover, the Burgers vector is defined as

$$B_k^* := [b_k^*] = [u_k^*](x) - \varepsilon_{klm} \Omega_l^* (x_m - x_{0m}). \quad (3.3.4)$$

Theorem 3.3.1 [Weingarten] The rotation vector ω_k^* is a multifunction of index 1 on Ω_L whose jump $\Omega_k^* := [\omega_k^*]$ around L is an invariant of the defect-line L . Moreover, the vector b_k^* is a multifunction of index 1 on Ω_L whose jump $B_k^* := [b_k^*]$ around L is an invariant of the defect-line.

Let us also recall the definition of the geometric density tensors as:

Definition 3.3.3

$$\text{DISCLINATION DENSITY:} \quad \Theta_{ij}^* := \Omega_j^* \delta_{iL} \quad (3.3.5)$$

$$\text{DISLOCATION DENSITY:} \quad \Lambda_{ij}^* := B_j^* \delta_{iL} \quad (3.3.6)$$

$$\text{DISPLACEMENT JUMP DENSITY:} \quad \alpha_{ij}^* := \Lambda_{ij}^* + \varepsilon_{jlm} \Theta_{il}^* (x_m - x_{0m}) \quad (3.3.7)$$

$$\text{CONTORTION:} \quad \kappa_{ij}^* := \alpha_{ij}^* - \frac{1}{2} \alpha_{mm}^* \delta_{ij}, \quad (3.3.8)$$

where x_{0m} is a reference point for rotation and displacement integration and $\delta_{iL} = \tau_i \delta_L$ for a Lipschitz curve L .

Notations 3.3.1 The notation $\partial_j^{(s)}$ is used for partial derivation of a single- or multiple-valued function whose domain is restricted to Ω_L . Locally around $x \in \Omega_L$, for smooth

functions, the meanings of $\partial_j^{(s)}$ and the classical ∂_j are the same, whereas on the entire Ω the partial derivation operator ∂_j only applies to single-valued fields and must be understood in the distributive sense. A defect-free subset U of Ω is an open set such that $U \cap L = \emptyset$, in such a way that $\partial_j^{(s)}$ and ∂_j coincide on U for every single- or multiple-valued function of index 1.

Proposition 3.3.1 [Multiple-valued displacement field] From a symmetric smooth linear strain tensor \mathcal{E}_{ij}^* on Ω_L and a point x_0 where the displacement is given, a multivalued displacement field u_i^* of index 2 can be constructed on Ω_L such that the symmetric part of the deformation gradient $\partial_j^{(s)} u_i^*$ on Ω_L is the single-valued strain tensor

$$\mathcal{E}_{ij}^* := \frac{1}{2} \left(\partial_j^{(s)} u_i^* + \partial_i^{(s)} u_j^* \right),$$

while its skew-symmetric part is the multivalued rotation tensor

$$-\varepsilon_{ijk} \omega_k^* := \omega_{ij}^* := \frac{1}{2} \left(\partial_j^{(s)} u_i^* - \partial_i^{(s)} u_j^* \right).$$

3.3.2 3D strain compatibility

Let us now fix the arc parameter s , and consider the corresponding local Cartesian base $\{v_i(\hat{x}^s), \sigma_i(\hat{x}^s), \tau_i(\hat{x}^s)\}$ attached to $\hat{x}^s \in L$, with the associated Cartesian coordinates denoted as $\{x_i^s\}$. Symbol ∂_i here has the meaning of $\frac{\partial}{\partial x_i^s}$ and symbol ∂_α the meaning of $\frac{\partial}{\partial x_\alpha^s}$ with $\alpha = 1$ or $\alpha = 2$. The strain \mathcal{E}_{ij}^* will be expressed in the components of the base $\{v_i(\hat{x}^s), \sigma_i(\hat{x}^s), \tau_i(\hat{x}^s)\}$ and for $i = 3$, will be written as \mathcal{E}_{sj}^* . In a first step, some notations and assumptions are made.

Notations 3.3.2 The planar sections of Ω are introduced by fixing the arc parameter s and defining

$$\Omega^s := \{x_i \in \Omega \text{ such that } (x_i - \hat{x}_i(s)) \tau_i(\hat{x}^s) = 0\},$$

while

$$\Omega_0^s := \{x_i \in \Omega^s \text{ such that } (x_\alpha - \hat{x}_\alpha(s))^2 = r_s > 0\}.$$

Moreover, the set Ω_ε^s is defined as

$$\Omega_\varepsilon^s := \{x_i \in \Omega^s \text{ such that } \|x_\alpha^s\| > \varepsilon\},$$

while the boundary circle of Ω_ε^s is designated by C_ε^s .

Assumption 3.3.1 *The strain local behaviour in Ω_L is assumed to be of the following form:*

$$\mathcal{E}_{\alpha\beta}^* \sim \frac{\hat{e}_{\alpha\beta}}{r_s} + \hat{e}'_{\alpha\beta} \log r_s + h_{\alpha\beta} \quad (3.3.9)$$

$$\mathcal{E}_{\alpha s}^* \sim \frac{\hat{e}_{\alpha s}}{r_s} + \hat{e}'_{\alpha s} \log r_s + h_{\alpha s} \quad (3.3.10)$$

$$\mathcal{E}_{ss}^* \sim \hat{e}'_{ss} \log r_s + h_{ss}, \quad (3.3.11)$$

where $\hat{e}_{\alpha s} = \hat{e} \hat{\sigma}_\alpha$ with \hat{e} , a function of s only, and where $\hat{e}_{\alpha\beta}$ and \hat{e}'_{ij} are functions of θ_s and s only, while h_{ij} is a smooth symmetric tensor on Ω . As a consequence of Eqs. (3.3.9)–(3.3.11) it results that

$$\mathcal{E}_{\alpha j}^* \quad \text{is} \quad o(r_s^{-2}) \quad (3.3.12)$$

$$\mathcal{E}_{ss}^* \quad \text{is} \quad o(r_s^{-1}), \quad (3.3.13)$$

as $r_s \rightarrow 0$.

Definition 3.3.4 *The 3D mesoscopic strain incompatibility tensor on Ω is defined by*

$$\eta_{lk}^* := \varepsilon_{lmn} \partial_m \bar{\partial}_n \omega_k^* = \varepsilon_{lmn} \varepsilon_{kpq} \partial_m \partial_p \mathcal{E}_{qn}^*, \quad (3.3.14)$$

while its restriction to Ω^s is denoted by $\hat{\eta}_{lk}^*(\hat{x}^s)$ or more briefly by $\hat{\eta}_{lk}^*$.

The general 3D strain compatibility condition in the local Cartesian base $\{v_i(\hat{x}^s), \sigma_i(\hat{x}^s), \tau_i(\hat{x}^s)\}$ reads:

$$\eta_{lk}^* = \varepsilon_{qlm} \varepsilon_{kpn} \partial_l \partial_p \mathcal{E}_{mn}^* = 0 \quad (3.3.15)$$

in Ω_L , where three different cases are identified.

Let $k = s$ and $q = s$. It results that

$$\hat{\eta}_{ss} = \varepsilon_{\alpha\beta} \varepsilon_{\gamma\tau} \partial_\alpha \partial_\gamma \mathcal{E}_{\beta\tau}^* = 0 \quad (3.3.16)$$

is the 2D compatibility in Ω^s .

Let $k = \kappa$ and $q = s$. It results that

$$\varepsilon_{\alpha\beta} \varepsilon_{\kappa pn} \partial_\alpha \partial_p \mathcal{E}_{\beta n}^* = \varepsilon_{\alpha\beta} \varepsilon_{\kappa\nu} \partial_\alpha \left[\partial_\nu \mathcal{E}_{\beta s}^* - \partial_{z^s} \mathcal{E}_{\beta\nu}^* \right] = 0$$

in Ω_L , and hence that

$$\partial_\nu \left(\varepsilon_{\alpha\beta} \partial_\alpha \mathcal{E}_{\beta s}^* \right) = \varepsilon_{\alpha\beta} \partial_\alpha \partial_{z^s} \mathcal{E}_{\beta\nu}^* \quad (3.3.17)$$

$$\partial_\alpha \mathcal{E}_{\beta s}^* - \partial_{z^s} \mathcal{E}_{\alpha\beta}^* = K_{\beta\alpha}(s) + \partial_\beta \phi_\alpha \quad (3.3.18)$$

in Ω_L , where $K_{\beta\alpha}(s)$ only depends on s and ϕ_α is an (arbitrary) gauge field. It results from strain symmetry that

$$\bar{\partial}_s \omega_s^* = \varepsilon_{\alpha\beta} \partial_\alpha \mathcal{E}_{\beta s}^* = K(s) + \varepsilon_{\alpha\beta} \partial_\beta \phi_\alpha, \quad (3.3.19)$$

where $K(s) := \varepsilon_{\beta\alpha} K_{\alpha\beta}(s)$.

Let $k = \kappa$ and $q = \alpha$. It results that

$$\begin{aligned} & \varepsilon_{\alpha\beta} \varepsilon_{\kappa\gamma} \left(\partial_{z^s}^2 \mathcal{E}_{\beta\gamma}^* + \partial_{z^s} \beta \partial_\gamma \mathcal{E}_{ss}^* - \partial_{z^s} \partial_\beta \mathcal{E}_{\gamma s}^* - \partial_{z^s} \partial_\gamma \mathcal{E}_{\beta s}^* \right) \\ &= \partial_{z^s}^2 \mathcal{E}_{\beta\gamma}^* + \partial_\beta \partial_\gamma \mathcal{E}_{ss}^* - \partial_{z^s} \partial_\beta \mathcal{E}_{\gamma s}^* - \partial_{z^s} \partial_\gamma \mathcal{E}_{\beta s}^* = 0 \end{aligned} \quad (3.3.20)$$

in Ω_L .

On properties of the strain and Frank tensors

Lemma 3.3.1 *From Assumption 3.3.1 it results that the displacement writes as*

$$u_\alpha^* = \hat{u}_\alpha \log r_s + h_\alpha \quad \text{and} \quad u_s^* = \hat{u}_s \log r_s + h_s, \quad (3.3.21)$$

on Ω^s , where $\hat{u}_\alpha, \hat{u}_s$ depend on θ and s only, while h_i is smooth on Ω^s .

Proof. Let u_r^*, u_θ^*, u_s^* denote the displacement components in the cylindrical base associated to $\{v_i(\hat{x}^s), \sigma_i(\hat{x}^s), \tau_i(\hat{x}^s)\}$ with the related coordinates r_s, θ_s, z^s . By Assumption 3.3.1, the radial component $\mathcal{E}_{rr}^* = \partial_{r_s} u_r^*$ writes as $\frac{\hat{e}_{rr}}{r_s} + \hat{e}'_{rr} \log r_s + h_{rr}$ where \hat{e}_{rr} depends on θ_s and z^s only, and h_{rr} is smooth on Ω^s , immediately proving, by primitivation, that $u_r^* = \hat{u}_r \log r_s + h_r$, where \hat{u}_r depends on θ_s and z_s only and h_r is smooth on Ω . The remaining of the proof immediately follows from Assumption 3.3.1 and from the formulas $\mathcal{E}_{\theta r}^* = \frac{1}{r_s} \partial_\theta u_r^* - \frac{u_\theta}{r_s}$ and $\mathcal{E}_{ss}^* = \partial_{z^s} u_s^*$. \square

Lemma 3.3.2 *Consider the local Cartesian base $\{v_i(\hat{x}^s), \sigma_i(\hat{x}^s), \tau_i(\hat{x}^s)\}$. From 3D compatibility on Ω_0^s , it results from Assumption 3.4.1 that*

$$2\partial_s \mathcal{E}_{\beta s}^* - \partial_\beta \mathcal{E}_{ss}^* \quad \text{is} \quad o(r_s^{-1}) \quad (3.3.22)$$

$$\bar{\partial}_s \omega_k^* \quad \text{is} \quad o(r_s^{-2}) \quad (3.3.23)$$

$$\bar{\partial}_s \omega_\kappa^* + \varepsilon_{\kappa\beta} \partial_{z^s} \mathcal{E}_{\beta s}^* \quad \text{is} \quad o(r_s^{-1}). \quad (3.3.24)$$

Proof. For a fixed arc parameter s let us consider the 2D set

$$\Lambda_s = \{(x_1^s, x_2^s) : 0 < r_s < \infty, \theta_s^1 < \theta_s < \theta_s^2\} \cap \Omega_L,$$

where $0 \leq \theta_s^1, \theta_s^2 \leq 2\pi$ with $\theta_s^2 - \theta_s^1 \neq 2\pi$ in such a way that Λ_s is a defect-free subset of Ω_L .

Proof of Eq. (3.3.22). Observe from Proposition 3.3.1 that

$$2\partial_s \mathcal{E}_{\beta s}^* - \partial_\beta \mathcal{E}_{ss}^* = \partial_s \partial_\beta^{(s)} u_s^* - \partial_\beta \partial_s^{(s)} u_s^* + \partial_s \partial_s^{(s)} u_\beta^*,$$

on Λ_s , which by the smoothness of u_k^* on Λ_s , i.e. from $\varepsilon_{ijk} \partial_i \partial_j^{(s)} u_k^* = \varepsilon_{ijk} \partial_i \partial_j u_k^* = 0$, shows that $2\partial_s \mathcal{E}_{\beta s}^* - \partial_\beta \mathcal{E}_{ss}^* = \partial_s^2 u_\beta^*$, thereby proving Eq. (3.3.22) by Eq. (3.3.21).

Proof of Eqs. (3.3.23) and (3.3.24). Observe that Eq. (3.3.23) with $k = \kappa$ and Eq. (3.3.24) immediately follow from Assumption 3.4.1. For the remaining assertions, observe from Proposition 3.3.1 and from the relation $\bar{\partial}_s \omega_s^* = \partial_s^{(s)} \omega_s^* = \partial_s \omega_s^*$ on Λ_s that

$$\partial_s \partial_\tau^{(s)} u_\beta^* = \partial_s \left(\mathcal{E}_{\beta\tau}^* + \omega_{\beta\tau}^* \right) = \partial_s \mathcal{E}_{\beta\tau}^* - \varepsilon_{\beta\tau} \partial_s \omega_s^*,$$

proving Eq. (3.3.23) with $k = s$, under the strain and displacement field local assumptions (Eqs. (3.3.9) and (3.3.21)).

Since θ_s^1, θ_s^2 can be selected arbitrarily in $[0, 2\pi]$ provided $\theta_s^2 - \theta_s^1 \neq 2\pi$, Eq. (3.3.22)-(3.3.24) have been proved in Ω_L . \square

Lemma 3.3.3 *Let x^s be a selected point on the line L and consider the local base attached to \hat{x}^s . If $C(\hat{x}^s)$ denote a family of 2D closed curves in Ω^s , then, in 3D elasticity, it results from Assumption 3.4.1 that the Frank tensor and the strain verify the relation*

$$\lim_{C(\hat{x}^s) \rightarrow \hat{x}^s} \int_{C(\hat{x}^s)} x_\alpha^s \bar{\partial}_\beta \omega_\kappa^* dx_\beta + \varepsilon_{\kappa\beta} \mathcal{E}_{\beta s}^* dx_\alpha = 0,$$

provided the length of C is uniformly bounded and as long as the convergence $C(\hat{x}) \rightarrow \hat{x}^s$ is understood in the Hausdorff sense, i.e. in such a way that

$$\max\{\|x - \hat{x}^s\|, x \in C(\hat{x}^s)\} \rightarrow 0$$

Proof. Since

$$\partial_\gamma \mathcal{E}_{\beta s}^* - \partial_\beta \mathcal{E}_{\gamma s}^* = \varepsilon_{\gamma\beta} \bar{\partial}_s \omega_s^*,$$

it results that

$$\bar{\partial}_\beta \omega_\kappa^* := \varepsilon_{\kappa\gamma} \partial_\gamma \mathcal{E}_{\beta s}^* - \varepsilon_{\kappa\gamma} \partial_{z^s} \mathcal{E}_{\beta\gamma}^* = \varepsilon_{\kappa\gamma} \partial_\beta \mathcal{E}_{\gamma s}^* - \bar{\partial}_s \omega_s^* \delta_{\kappa\beta} - \varepsilon_{\kappa\gamma} \partial_{z^s} \mathcal{E}_{\beta\gamma}^*,$$

and hence that

$$\left(x_\alpha^s \bar{\partial}_\beta \omega_\kappa^* + \delta_{\alpha\beta} \varepsilon_{\kappa\gamma} \mathcal{E}_{\gamma s}^* \right) = \partial_\beta \left(x_\alpha^s \varepsilon_{\kappa\gamma} \mathcal{E}_{\gamma s}^* \right) - x_\alpha^s \bar{\partial}_s \omega_s^* \delta_{\kappa\beta} - x_\alpha^s \varepsilon_{\kappa\gamma} \partial_{z^s} \mathcal{E}_{\beta\gamma}^*.$$

Let us now multiply the right-hand side by dx_β and integrate the result over $C(\hat{x}^s)$. Under the limit assumptions of this lemma, since the strain is single-valued and since $\bar{\partial}_s \omega_s^*$ and $\partial_{z^s} \mathcal{E}_{\alpha\beta}^*$ are $o(r_s^{-2})$ as $r_s \rightarrow 0$, the statement is proved. \square

Corollary 3.3.1 *Let \hat{x}^s be a selected point on the line L and consider the local base attached to \hat{x}^s . Then*

$$\int_{C_\varepsilon^s} \mathcal{E}_{\beta s}^* dx_\beta = \frac{1}{2} \hat{B}_s^* + \frac{1}{4} (\varepsilon_{\gamma\tau} x_{0\gamma} \hat{\Omega}_\tau^*) + o(1). \quad (3.3.25)$$

Proof. From the Burgers tensor definition in the local Cartesian base, it results that

$$x_\alpha \bar{\partial}_\beta \omega_\kappa^* - x_\kappa^s \bar{\partial}_\beta \omega_\alpha^* = \varepsilon_{kn\alpha} \bar{\partial}_\beta b_n^* - \varepsilon_{kn\alpha} \mathcal{E}_{\beta n}^* + x_{0\alpha}^s \bar{\partial}_\beta \omega_\kappa^* - x_{0\kappa}^s \bar{\partial}_\beta \omega_\alpha^*, \quad (3.3.26)$$

in such a way that, by Lemma 3.3.3 and for $k = \kappa$,

$$\begin{aligned} & - \varepsilon_{\kappa\alpha} B_s^* + \int_{C_\varepsilon^s} \varepsilon_{\kappa\alpha} \mathcal{E}_{\beta s}^* dx_\beta + x_{0\alpha}^s \Omega_\kappa^* - x_{0\kappa}^s \Omega_\alpha^* + o(1) = \\ & = \int_{C_\varepsilon^s} \varepsilon_{\alpha\beta} \mathcal{E}_{\beta s}^* dx_\kappa - \varepsilon_{\kappa\beta} \mathcal{E}_{\beta s}^* dx_\alpha = \int_{C_\varepsilon^s} \varepsilon_{\gamma\tau} \varepsilon_{\alpha\kappa} \varepsilon_{\gamma\beta} \mathcal{E}_{\beta s}^* dx_\tau = \int_{C_\varepsilon^s} \varepsilon_{\alpha\kappa} \mathcal{E}_{\beta s}^* dx_\beta, \end{aligned}$$

thereby proving the statement since

$$\int_{C_\varepsilon^s} \varepsilon_{\alpha\kappa} \mathcal{E}_{\beta s}^* dx_\beta = \frac{1}{2} (\varepsilon_{\alpha\kappa} B_s^* + x_{0\alpha}^s \Omega_\kappa^* - x_{0\kappa}^s \Omega_\alpha^*) + o(1). \quad \square$$

3.4 Governing assumptions for the strain and Frank tensors

Let us now fix the arc parameter s and consider the corresponding local Cartesian base $\{v_i(\hat{x}^s), \sigma_i(\hat{x}^s), \tau_i(\hat{x}^s)\}$. Besides the strain Assumptions 3.4.1 two measure hypotheses on the strain derivatives are introduced in order to replace the local Assumption 3.3.1 and to validate Kröner's identities in the global framework of a crystal dislocated by the effect of several Lipschitz defect lines.

Assumption 3.4.1 *The strain \mathcal{E}_{ij}^* is assumed to be a symmetric tensor of bounded L^1 -norm in Ω .*

Remark 3.4.1 *By the strain smoothness outside L , the strain components \mathcal{E}_{ij}^* and their derivatives $\partial_z^s \mathcal{E}_{ij}^*$ show to be of bounded L^1 -norm in Ω^s for every given $\hat{x}^s \in L$ and related Ω^s .*

Assumption 3.4.2 *The strain divergence and trace gradient $\partial_k \mathcal{E}_{kl}^*$ and $\partial_k \mathcal{E}_{pp}^*$ are finite Radon measures on Ω .^{4,5}*

The following Lemmas are needed for the proof of Proposition 3.4.1.

Lemma 3.4.1 • *A solenoidal distributional vector field a_α on Ω^s writes as*

$$a_\alpha = \varepsilon_{\alpha\gamma} \partial_\gamma \phi, \quad (3.4.1)$$

with $\phi \in \mathcal{D}'(\Omega^s)$.

• *A symmetric solenoidal distribution tensor $a_{\alpha\beta}$ on Ω^s writes as*

$$a_{\alpha\beta} = \varepsilon_{\alpha\gamma} \varepsilon_{\beta\tau} \partial_\gamma \partial_\tau \psi, \quad (3.4.2)$$

with $\psi \in \mathcal{D}'(\Omega^s)$.

Proof. The proof can be found in Chapter 2, Section 2.4.1.

Lemma 3.4.2 *For constant C and C_β , there are a vector g_κ and a symmetric compatible tensor $G_{\alpha\beta}$ on Ω^s such that*

$$\partial_\kappa g_\kappa = C \delta_0, \quad (3.4.3)$$

$$\partial_\alpha G_{\alpha\beta} = C_\beta \delta_0. \quad (3.4.4)$$

Proof. The proof can be found in Chapter 2, Section 2.4.1.

Lemma 3.4.3 *If the symmetric distribution tensor E_{ij} verifies the compatibility condition Eq. (3.3.15) on Ω , there exists a vectorial distribution field U_i such that*

$$E_{ij} = \frac{1}{2} (\partial_i U_j + \partial_j U_i). \quad (3.4.5)$$

⁴A Radon measure on Ω is a measure bounded on compact subsets of Ω (Evans and Gariepy, 1992; Mattila, 1995; Ambrosio et al., 2000).

⁵Assumption 3.4.2 is natural in infinitesimal elasticity if one considers the strain-stress constitutive law and the equilibrium laws. As a consequence, the stress divergence must be a measure on Ω .

Similarly, if the symmetric distribution tensor $E_{\alpha\beta}$ verifies the compatibility condition Eq. (3.3.16) on Ω^s , there exists a vectorial distribution field U_α such that

$$E_{\alpha\beta} = \frac{1}{2} (\partial_\alpha U_\beta + \partial_\beta U_\alpha). \quad (3.4.6)$$

Proof. Since $\varepsilon_{qlm} \partial_l (\varepsilon_{kpn} \partial_p E_{mn}) = 0$, it results that $\varepsilon_{kpn} \partial_p E_{mn} = \partial_m \phi_k$ for some distribution ϕ_k , which from the symmetry property of E_{mn} , turns out to be divergence-free and hence writes as $\phi_k = \varepsilon_{kpn} \partial_p \varphi_n$ for some distribution φ_n . Since $\varepsilon_{kpn} \partial_p (E_{mn} - \partial_m \varphi_n) = 0$ it results that $E_{mn} = \partial_m \varphi_n + \partial_n \varphi'_m$ for some distribution φ'_m . Posing $U_i = \frac{\varphi_i}{2} = \frac{\varphi'_i}{2}$ proves the statement. The proof of the second statement is similar. \square

Lemma 3.4.4 *Let the tensor $E_{\alpha i}$ be such that $E_{\alpha\beta}$ is a Radon measure on the open set $U \subset \Omega^s$. If $E_{\alpha i}$ verifies the compatibility conditions Eqs. (3.3.16)-(3.3.17) on U , then*

$$\varepsilon_{\alpha\beta} \partial_\alpha E_{\beta s} = \frac{1}{2} \varepsilon_{\alpha\beta} \partial_{z^s} \partial_\alpha U_\beta \quad (3.4.7)$$

is a Radon measure on U with U_β , the displacement field provided by Lemma 3.4.3.

Proof. Let $\psi \in \mathcal{C}_c(U)$ and h be the $\mathcal{C}_c^2(U)$ -solution of $\Delta h = \psi$ on U in such a way that $\psi_\nu := \partial_\nu h$ verifies $\partial_\nu \psi_\nu = \psi$ and $\partial_\alpha \psi_\nu \in \mathcal{C}_c(U)$. The form

$$\begin{aligned} \ll \varepsilon_{\alpha\beta} \partial_\alpha E_{\beta s}, \psi \gg &= - \ll \partial_\nu (\varepsilon_{\alpha\beta} \partial_\alpha E_{\beta s}), \psi_\nu \gg \\ &= - \ll \varepsilon_{\alpha\beta} \partial_\alpha \partial_{z^s} E_{\beta \nu}, \psi_\nu \gg = \ll \varepsilon_{\alpha\beta} \partial_{z^s} E_{\beta \nu}, \partial_\alpha \psi_\nu \gg \end{aligned}$$

is linear and continuous in $\psi = \partial_\nu \psi_\nu$ since $\ll \varepsilon_{\alpha\beta} \partial_{z^s} E_{\beta \nu}, \partial_\alpha \psi_\nu \gg$ is, from the strain assumption, linear and continuous in $\partial_\alpha \psi_\nu$. The proof is achieved by use of Eq. (3.4.6), since $\varepsilon_{\nu\beta} \partial_\nu \partial_\beta U_\beta = 0$ in the distribution sense.

Lemma 3.4.5 • *For a given $L^1(\Omega^s)$ -scalar function f and a given Radon measure μ , there exists a distribution g_β such that*

$$\partial_\beta g_\beta = f \quad (3.4.8)$$

$$\varepsilon_{\alpha\beta} \partial_\alpha g_\beta = \mu. \quad (3.4.9)$$

Moreover, if the restriction of μ on Ω_0^s is smooth, there exists a $L^1(\Omega^s)$ -function k_α such that $\mu = \partial_\alpha k_\alpha$.

• *For a given $L^1(\Omega^s)$ -vector function f_β such that $\partial_\beta f_\beta = \Delta g$ where g is a $L^1(\Omega^s)$ function, there exists a symmetric compatible tensor $g_{\alpha\beta}$ on Ω^s such that*

$$\varepsilon_{\alpha\beta} \partial_\alpha g_\beta = f. \quad (3.4.10)$$

Proof.

First statement. Consider first an ultra-weak solution (Brezis, 1983) of

$$\Delta H = f, \quad (3.4.11)$$

and define the particular solution $g_\beta^* = \partial_\beta H$ of Eq. (3.4.8). Since g_β^* is defined in the distributive sense up to a curl distribution $\varepsilon_{\beta\gamma} \partial_\gamma A$, Eq. (3.4.9) is verified by solving

$$\Delta A = -\mu. \quad (3.4.12)$$

Since μ is a Radon measure, Eq. (3.4.12) has a solution in an ultra-weak sense, and it suffices to take $g_\beta = g_\beta^* + \varepsilon_{\alpha\gamma} \partial_\gamma A$. Now, since the restriction of μ on Ω_0^s is smooth, the measure μ writes by Radon-Nykodym's theorem as $\mu = h + \phi$, where h is $L^1(\Omega^s)$ and ϕ is concentrated at the origin. Hence ϕ is as a Dirac mass writing as $\phi = c \varepsilon_{\alpha\beta} \partial_\alpha \varepsilon_{\gamma\beta} \partial_\gamma \log r$, while the $L^1(\Omega^s)$ -function h defines a linear and continuous form on $W^{1,p}(\Omega^s)$ for a given $p > 2$, hence writing, by its Hölder characterisation, as $\partial_\alpha h_\alpha$ where h_α is $L^1(\Omega^s)$. It results that

$$\varepsilon_{\alpha\beta} \partial_\alpha g_\beta = \partial_\alpha \varepsilon_{\alpha\beta} (\varepsilon_{\gamma\beta} h_\gamma + c \varepsilon_{\gamma\beta} \partial_\gamma \log r), \quad (3.4.13)$$

in such a way that the definition of $k_\alpha := \varepsilon_{\alpha\beta} (\varepsilon_{\gamma\beta} h_\gamma + c \varepsilon_{\gamma\beta} \partial_\gamma \log r)$ proves the first statement.

Second statement. The proof can be found in Chapter 2, Section 2.4.1. \square

Proposition 3.4.1 *Under Assumptions 3.4.1 and 3.4.2, the strain components can be put in the form:*

$$\mathcal{E}_{\alpha\beta}^* = E_{\alpha\beta} + e_{\alpha\beta} \quad (3.4.14)$$

$$\mathcal{E}_{\alpha s}^* = E_{\alpha s} + e_{\alpha s} \quad (3.4.15)$$

$$\mathcal{E}_{ss}^* = E_{ss} + e_{ss}, \quad (3.4.16)$$

where $E_{\alpha\beta}, E_{\alpha s}$ and E_{ss} are compatible on Ω , with $e_{\alpha j} = \frac{\hat{e}_{\alpha j}}{r_s} + \hat{e}'_{\alpha j} \log r_s + h_{\alpha j}$ and $e_{ss} = \hat{e}_{ss} \log r_s + h_{ss}$, and where $\hat{e}_{ij}, \hat{e}'_{\alpha j}$ are functions of θ_s and s only, while h_{ij} is a smooth tensor on Ω .

Proof of a preliminary result. By Assumption 3.4.2, $\partial_k \mathcal{E}_{ki}^*$ is a Radon measure on Ω^s , and hence writes by Radon-Nykodym's decomposition theorem (cf Chapter 1, Section 1.10.2) as

$$\partial_k \mathcal{E}_{ki}^* = \bar{f}_i + \phi_i, \quad (3.4.17)$$

where $\bar{f}_i \in L^1(\Omega^s)$ and where ϕ_i is a Radon measure on Ω^s singular with respect to Lebesgue's measure. By Assumption 3.4.1 and Remark 3.4.1, $\partial_{z^s} \mathcal{E}_{si}^*$ is $L^1(\Omega^s)$ and hence

$$\partial_\alpha \mathcal{E}_{\alpha i}^* = f_i + \phi_i,$$

where $f_i \in L^1(\Omega^s)$. As a mere consequence of the smoothness of $\partial_\alpha \mathcal{E}_{\alpha i}^*$ on Ω_0^s , ϕ_i is a concentrated measure on Ω^s and hence is proportional to the Dirac mass δ_0 , i.e.

$$\phi_i = C_i(s) \delta_0 = (2\pi)^{-1} C_i(s) \partial_\kappa^2 \log r_s. \quad (3.4.18)$$

Proof of Eq. (3.4.14). • Let us prove that $\partial_\beta f_\beta$ is the Laplacian of an $L^1(\Omega^s)$ function. In fact, since η_{ss}^* writes as

$$\eta_{ss}^* = \partial_\alpha \left(\partial_\alpha \mathcal{E}_{\kappa\kappa}^* - \partial_\beta \mathcal{E}_{\alpha\beta}^* \right), \quad (3.4.19)$$

where the term inside the parenthesis is by the previous Assumptions a Radon measure, $\hat{\eta}_{ss}^*$ is in turn a first-order distribution concentrated on \hat{x}^s , hence writing as a combination of the Dirac mass and its first-order derivatives (Schwartz, 1957), i.e.

$$\begin{aligned} \partial_\beta f_\beta &= \partial_\alpha \partial_\beta \mathcal{E}_{\alpha\beta}^* - \partial_\beta \phi_\beta = \Delta \mathcal{E}_{\kappa\kappa}^* - \eta_{ss}^* - \partial_\beta \phi_\beta = \Delta \mathcal{E}_{\kappa\kappa}^* - \hat{c} \delta_0 - \hat{c}_\gamma \partial_\gamma \delta_0 \\ &= \Delta \left(\mathcal{E}_{\kappa\kappa}^* - \bar{c} \log r - \bar{c}_\gamma \partial_\gamma \log r \right), \end{aligned} \quad (3.4.20)$$

where $\hat{c}, \hat{c}_\gamma, \bar{c}, \bar{c}_\gamma$ are functions of the curvilinear parameter s only, thereby proving the statement.

- From Eqs. (3.4.18), (3.4.4), (3.4.10) and Lemma 3.4.5, there exists a compatible $g_{\kappa\beta}$ such that

$$\partial_\kappa \left(\mathcal{E}_{\kappa\beta}^* - g_{\kappa\beta} - G_{\kappa\beta} \right) = 0, \quad (3.4.21)$$

in such a way that, by Lemma 3.4.1,

$$\mathcal{E}_{\kappa\beta}^* - g_{\kappa\beta} - G_{\kappa\beta} = \varepsilon_{\kappa\gamma} \varepsilon_{\beta\tau} \partial_\gamma \partial_\tau A, \quad (3.4.22)$$

for some gauge field $A \in \mathcal{D}'(\Omega^s)$ verifying, by the compatibility of $g_{\kappa\beta}$ and $G_{\kappa\beta}$ on Ω^s , the relation

$$\eta_{ss}^* = \Delta \Delta A \quad \text{on } \Omega^s. \quad (3.4.23)$$

Therefore, since the left-hand side writes as a combination of derivatives of δ_0 of order lower or equal to 1, the field A is the solution of $\Delta A = (a + a_\gamma \partial_\gamma) \log r_s$ with a, a_γ functions of s only, up to a smooth harmonic

function on Ω^s . It follows that $A = (a + a_\gamma \partial_\gamma) \left(\frac{r_s^2}{4} (\log r_s - 1) \right)$ is, up to a smooth harmonic function on Ω^s , a $\mathcal{C}^0(\Omega^s)$ solution of Eq. (3.4.23) verifying the relation:

$$\varepsilon_{\kappa\gamma} \varepsilon_{\beta\tau} \partial_\gamma \partial_\tau A = \frac{\hat{e}_{\kappa\beta}}{r_s} + \hat{e}'_{\kappa\beta} \log r_s + h_{\kappa\beta}, \quad (3.4.24)$$

where $\hat{e}_{\kappa\beta}$ and $\hat{e}'_{\kappa\beta}$ are a functions of θ and s only and $h_{\kappa\beta}$ is smooth on Ω^s .

- The proof of the first statement is complete with the definitions $E_{\kappa\beta} := G_{\kappa\beta} + g_{\kappa\beta}$ and $e_{\kappa\beta} := \varepsilon_{\kappa\gamma} \varepsilon_{\beta\tau} \partial_\gamma \partial_\tau A$ in Eqs. (3.4.22) and (3.4.24). It results from Assumption 3.4.1 that $\mathcal{E}_{\kappa\beta}^*$, $e_{\kappa\beta}$ and $E_{\kappa\beta}$ are $L^1(\Omega^s) \cap \mathcal{C}^\infty(\Omega_0^s)$ -symmetric compatible tensors. Moreover, from Lemma 3.4.3 there exists distribution fields U_α on Ω^s and $u_\alpha := u_\alpha^* - U_\alpha$ on Ω_0^s such that

$$E_{\kappa\beta} = \frac{1}{2} (\partial_\kappa U_\beta + \partial_\beta U_\kappa) \quad (3.4.25)$$

$$e_{\kappa\beta} = \frac{1}{2} (\partial_\kappa u_\beta + \partial_\beta u_\kappa), \quad (3.4.26)$$

noting in passing that u_α and u_α^* are multivalued and $e_{\kappa\beta}$ is incompatible at the origin.

Proof of Eq. (3.4.15). • By Eqs. (3.4.18), (3.4.18) with $i = s$, and Lemma 3.4.5 (Eq. (3.4.8)) with $E_{\alpha\beta}$ and U_α as found above, there exists a field g_κ such that

$$\partial_\kappa (\mathcal{E}_{\kappa s}^* - g_\kappa - (2\pi)^{-1} C(s) \partial_\kappa \log r_s) = 0,$$

and, by Lemma 3.4.5, such that

$$\varepsilon_{\beta\kappa} \partial_\beta g_\kappa = \frac{1}{2} \partial_{z^s} \varepsilon_{\alpha\beta} \partial_\alpha U_\beta = \varepsilon_{\alpha\beta} \partial_\alpha E_{\beta s}, \quad (3.4.27)$$

where the RHS is a measure by Lemma 3.4.4. Therefore, by Lemma 3.4.1,

$$\mathcal{E}_{\kappa s}^* - g_\kappa - (2\pi)^{-1} C(s) \partial_\kappa \log r_s = \varepsilon_{\kappa\gamma} \partial_\gamma \psi, \quad (3.4.28)$$

where ψ is a distribution. Apply the curl operator to Eq. (3.4.28) and take into account that, from Eq. (3.4.27),

$$\partial_\nu \varepsilon_{\beta\kappa} \partial_\beta g_\kappa = \frac{1}{2} \partial_{z^s} \varepsilon_{\alpha\beta} \partial_\alpha \partial_\nu U_\beta = \varepsilon_{\alpha\beta} \partial_\alpha \partial_{z^s} E_{\beta\nu}, \quad (3.4.29)$$

and hence, by Eqs. (3.4.28) and (3.4.29) and the compatibility condition Eq. (3.3.17), that

$$\begin{aligned} \partial_\nu \varepsilon_{\beta\kappa} \partial_\beta (\mathcal{E}_{\kappa s}^* - g_\kappa) &= \varepsilon_{\alpha\beta} \partial_\alpha \partial_{z^s} (\mathcal{E}_{\beta\nu}^* - E_{\beta\nu}) \\ &= \varepsilon_{\alpha\beta} \partial_\alpha \partial_{z^s} e_{\beta\nu} = \frac{1}{2} \partial_{z^s} \varepsilon_{\beta\kappa} \partial_\beta \partial_\nu^{(s)} u_\kappa \end{aligned} \quad (3.4.30)$$

on Ω_0^s . It follows that

$$\varepsilon_{\beta\kappa}\partial_\beta\left(\mathcal{E}_{\kappa s}^* - g_\kappa - \frac{1}{2}\partial_{z^s}u_\kappa\right) = K(z^s) \quad (3.4.31)$$

on Ω_0^s , for some scalar function K depending only on z^s . Let us remark that, from Lemma 3.3.1 and the first statement of this Lemma, it results that $u_\kappa = \hat{u}_\kappa \log r_s + h_\kappa$.

- Since the LHS of Eq. (3.4.31) is a distribution⁶ on Ω^s which is constant on Ω_0^s , it results from Schwartz (1957) that

$$\varepsilon_{\beta\kappa}\partial_\beta\left(\mathcal{E}_{\kappa s}^* - g_\kappa - \frac{1}{2}\partial_{z^s}u_\kappa\right) = K(z^s) + \sum_{p \geq 0} c_\alpha(s)\partial_\alpha^{(p)}\delta_0 \quad (3.4.32)$$

on Ω^s , where $\partial_\alpha^{(p)}$ denotes p -order derivatives with $\alpha \in \mathbb{N}^2$ such that $|\alpha| = p$. Now, by Lemma 3.4.5, Eq. (3.4.32) rewrites as

$$\partial_\beta\left(\varepsilon_{\beta\kappa}\mathcal{E}_{\kappa s}^* - k_\beta - \varepsilon_{\beta\kappa}\frac{1}{2}\partial_{z^s}u_\kappa\right) = K(z^s) + \sum_{p \geq 0} c_\alpha(s)\partial_\alpha^{(p)}\delta_0, \quad (3.4.33)$$

where the term inside the parentheses is a L^1 -vector, hence showing that $c_\alpha(s) = 0$ unless $\alpha = 0$.

- Applying the curl operator to Eq. (3.4.28) shows by Eq. (3.4.32) that

$$\Delta\left(\psi - \frac{c_0(s)}{2\pi}\log r_s\right) = \frac{1}{2}\partial_{z^s}\varepsilon_{\beta\kappa}\partial_\beta u_\kappa + K(z^s), \quad (3.4.34)$$

providing a gauge field ψ which writes as

$$\psi = h + \frac{c_0(s)}{2\pi}\log r_s + \varepsilon_{\beta\kappa}\partial_\beta\left(\hat{u}_\kappa(\theta, s)\frac{r_s^2}{8}(\log r_s - 1)\right), \quad (3.4.35)$$

where the smooth h is a solution of $\Delta h = K(z^s) + \varepsilon_{\beta\kappa}\partial_\beta h_\kappa$ on Ω^s . Therefore, $\varepsilon_{\kappa\gamma}\partial_\gamma\psi$ writes as $\frac{\hat{e}_{\kappa s}(s)}{r_s} + e'_{\kappa s}\log r_s + h_{\kappa s}$, where $h_{\kappa s}$ is smooth on Ω^s .

- By Eq. (3.4.29), it results that

$$2\varepsilon_{\beta\kappa}\partial_\beta g_\kappa - \partial_{z^s}\varepsilon_{\beta\kappa}\partial_\beta U_\kappa = B(z^s), \quad (3.4.36)$$

where the scalar function B is constant on Ω^s . Defining $E_{\kappa s} := g_\kappa + \frac{1}{2}\varepsilon_{\kappa\alpha}x_\alpha B(z^s)$ and $e_{\kappa s} := \varepsilon_{\kappa\gamma}\partial_\gamma\psi + (2\pi)^{-1}C(z^s)\partial_\kappa\log r_s - \frac{1}{2}\varepsilon_{\kappa\alpha}x_\alpha B(z^s)$ in Eq. (3.4.28) achieves the proof of the second statement.

⁶Defined for every test-function $\psi \in \mathcal{D}'(\Omega^s)$ as $-\int_{\Omega \setminus S}\left(\mathcal{E}_{\kappa s}^* - \frac{1}{2}\partial_{z^s}u_\kappa\right)\varepsilon_{\beta\kappa}\partial_\beta\psi dV + \langle g_\kappa, \varepsilon_{\beta\kappa}\partial_\beta\psi \rangle$, where S is an arbitrary cut set passing by the origin, which renders u_κ single-valued on $\Omega \setminus S$ (and hence the distribution is single-valued on Ω^s), while having no effect on the value of the integral, since S is chosen of vanishing Lebesgue measure.

- It results from Eq. (3.4.36) that equation

$$2g_\kappa - \partial_{z^s} U_\kappa + \frac{1}{2} \varepsilon_{\kappa\alpha} x_\alpha B(z^s) = \partial_\kappa U_s, \quad (3.4.37)$$

has a unique distribution solution U_s , in such a way that $E_{\kappa s}$ writes as

$$E_{\kappa s} = \frac{1}{2} (\partial_{z^s} U_\kappa + \partial_\kappa U_s). \quad (3.4.38)$$

Proof of the third statement. The definitions

$$E_{ss} := \partial_s U_s \quad \text{and} \quad e_{ss} := \mathcal{E}_{ss}^* - E_{ss} \quad (3.4.39)$$

provide a compatible E_{ij} on Ω^s . Moreover, since E_{ij} identically verifies the compatibility condition Eq. (3.3.20), it results from Eq. (3.3.20), Eqs. (3.4.14)-(3.4.16) and Eq. (3.4.39) that e_{ss} verifies the relation:

$$\begin{aligned} \partial_\beta \partial_\gamma e_{ss} &= \partial_{z^s} \partial_\beta \left(\frac{\hat{e}'_{\gamma s}}{r_s} + \hat{e}'_{\gamma s} \log r_s + h_{\gamma s} \right) \\ &+ \partial_{z^s} \partial_\gamma \left(\frac{\hat{e}'_{\beta s}}{r_s} + \hat{e}'_{\beta s} \log r_s + h_{\beta s} \right) - \partial_{z^s}^2 \left(\frac{\hat{e}'_{\beta\gamma}}{r_s} + \hat{e}'_{\beta\gamma} \log r_s + h_{\beta\gamma} \right) \end{aligned}$$

hence writing as $e_{ss} := \hat{e}_{ss} \log r_s + h_{ss}$, where \hat{e}_{ss} is a function of θ_s and z^s only, while h_{ss} is smooth on Ω^s , thereby completing the proof. \square

3.5 Mesoscopic incompatibility for an isolated 3D defect line

Lemma 3.5.1 [Preliminary 3D result] *For a 3D defect line verifying Assumption 3.2.1 and under Assumptions 3.4.1 and 3.4.2, let us fix a point $\hat{x}^s \in L$. Planar incompatibility in the local Cartesian base, as defined in Definitions 3.3.1 and 3.3.4, hence verifies the relations*

$$\hat{\eta}_{\alpha\kappa}^* = \hat{\eta}_{\kappa\alpha}^* = 0, \quad (3.5.1)$$

$$\hat{\eta}_{ss}^* = \hat{\Omega}_s^* \delta_{\hat{x}^s} + \varepsilon_{\alpha\gamma} (\hat{B}_\gamma^* - \varepsilon_{\gamma pq} (\hat{x}_p^s - x_{0p}^s) \hat{\Omega}_q^*) \hat{\partial}_\alpha \delta_{\hat{x}^s}, \quad (3.5.2)$$

$$\hat{\eta}_{s\kappa}^* = \hat{\eta}_{\kappa s}^* = \hat{\Omega}_\kappa^* \delta_{\hat{x}^s} + \frac{1}{2} \varepsilon_{\kappa\alpha} (\hat{B}_s^* - \varepsilon_{\beta\gamma} (\hat{x}_\beta^s - x_{0\beta}^s) \hat{\Omega}_\gamma^*) \hat{\partial}_\alpha \delta_{\hat{x}^s}, \quad (3.5.3)$$

where $\hat{\Omega}_i^*$, \hat{B}_i^* , and $\hat{\partial}_j$ denote the Frank and Burgers vectors, and the derivation operator in the local Cartesian base.

Proof. By Proposition 3.4.1, the remaining part of the strain in the expression of incompatibility is the sole $o(r^2)$ -part of Eqs. (3.4.14)-(3.4.16), in such a way that the global Assumptions 3.4.1 and 3.4.2 can be reduced to the sole Assumption 3.3.1⁷. Let φ , as a function of the coordinates (x_1^s, x_2^s, z^s) , denote any 3D test-function.

Proof of Eq. (3.5.1). By definition of incompatibility on Ω^s and Definition 3.3.2, integration by parts shows that

$$\begin{aligned} \langle \hat{\eta}_{\alpha\kappa}^*, \varphi \rangle &:= \langle \varepsilon_{\alpha lm} \partial_l \bar{\partial}_m \omega_\kappa^*, \varphi \rangle \\ &= \lim_{\varepsilon \rightarrow 0} \left(- \int_{\Omega_\varepsilon^s} \varepsilon_{\alpha lm} \bar{\partial}_m \omega_\kappa^* \partial_l \varphi dS - \int_{C_\varepsilon^s} \varepsilon_{\alpha lm} \varepsilon_{\kappa pn} \mathcal{E}_{mn}^* \partial_l \varphi dC_p \right), \end{aligned}$$

where the first and second terms inside the parenthesis are denoted by $\bar{\pi}_\varepsilon(\alpha, \kappa)$ and $\pi_\varepsilon^*(\alpha, \kappa)$, respectively, while their sum is written as

$$\pi_\varepsilon(\alpha, \kappa) = \bar{\pi}_\varepsilon(\alpha, \kappa) + \pi_\varepsilon^*(\alpha, \kappa). \quad (3.5.4)$$

After integration by parts of $\bar{\pi}_\varepsilon$ and from strain incompatibility on Ω_L , it results that

$$\bar{\pi}_\varepsilon(\alpha, \kappa) = \int_{C_\varepsilon^s} \varepsilon_{\alpha\beta} \bar{\partial}_s \omega_\kappa^* \varphi dC_\beta \quad \text{and} \quad \pi_\varepsilon^*(\alpha, \kappa) = - \int_{C_\varepsilon^s} \varepsilon_{\alpha li} \varepsilon_{\kappa\gamma} \mathcal{E}_{is}^* \partial_l \varphi dC_\gamma.$$

Computation of $\bar{\pi}_\varepsilon(\alpha, \kappa)$. This term writes as

$$\bar{\pi}_\varepsilon(\alpha, \kappa) := \int_{C_\varepsilon^s} \varepsilon_{\alpha\beta} \bar{\partial}_s \omega_\kappa^* \varphi \varepsilon_{\beta\tau} dx_\tau$$

which by Assumption 3.3.1 rewrites as

$$\bar{\pi}_\varepsilon(\alpha, \kappa) = - \int_{C_\varepsilon^s} \bar{\partial}_s \omega_\kappa^* (\varphi(\hat{x}^s) + (x_\gamma^s - \hat{x}_\gamma^s) \partial_\gamma \varphi(\hat{x}^s)) dx_\alpha + o_{\alpha\kappa}(1).$$

and also, using the relation $x_\gamma^s - \hat{x}_\gamma^s = \varepsilon \hat{v}_\gamma(x)$ and by Eqs. (3.3.23) & (3.3.24) (Lemma 3.3.2), as

$$\bar{\pi}_\varepsilon(\alpha, \kappa) := \bar{\Pi}_\varepsilon(\alpha, \kappa) + o_{\alpha\kappa}(1),$$

with

$$\bar{\Pi}_\varepsilon(\alpha, \kappa) = \varphi(\hat{x}^s) \int_{C_\varepsilon^s} \varepsilon_{\kappa\beta} \partial_{z^s} \mathcal{E}_{\beta s}^* dx_\alpha = \varphi(\hat{x}^s) \partial_{z^s} A_{\kappa\alpha}, \quad (3.5.5)$$

where $A_{\alpha\kappa} = \int_{C_\varepsilon^s} \varepsilon_{\alpha\beta} \mathcal{E}_{\beta s}^* dx_\kappa$.

⁷Let us recall that the strain components are here, for the sake of simplicity, still denoted by \mathcal{E}_{ij}^* . Moreover, the subscript $i = z^s$ is denoted by $i = s$, while $i = 1$ or 2 is denoted by a Greek subscript $i = \alpha, \beta, \gamma$ etc

Computation of $\pi_\varepsilon^*(\alpha, k)$. By Eq. (3.3.11) (Lemma 3.3.1), it results that

$$\pi_\varepsilon^*(\alpha, \kappa) := \int_{C_\varepsilon^s} \varepsilon_{\alpha l i} \mathcal{E}_{i s}^* \partial_l \varphi dx_\kappa = \Pi_\varepsilon^*(\alpha, \kappa) + o_{\alpha\kappa}(1)$$

where

$$\begin{aligned} \Pi_\varepsilon^{*s}(\alpha, \kappa) &:= - \int_{C_\varepsilon^s} \varepsilon_{\alpha\beta} \mathcal{E}_{\beta s}^* \partial_{z^s} \varphi dx_\kappa = \\ &= - \partial_{z^s} \left(\int_{C_\varepsilon^s} \varepsilon_{\alpha\beta} \mathcal{E}_{\beta s}^* \varphi dx_\kappa \right) + \int_{C_\varepsilon^s} \varepsilon_{\alpha\beta} \partial_{z^s} \mathcal{E}_{\beta s}^* \varphi dx_\kappa, \\ &= \partial_{z^s} (\varphi(\hat{x}^s) A_{\alpha\kappa}) + \varphi(\hat{x}^s) \partial_{z^s} A_{\alpha\kappa} + o_{\alpha\kappa}(1). \end{aligned} \quad (3.5.6)$$

Computation of $\pi_\varepsilon(\alpha, \kappa)$. By Eq. (3.3.10), $A_{\alpha\kappa} = \hat{\varepsilon}(s) \pi_\varepsilon \varepsilon_{\alpha\kappa}$ in such a way that both $A_{\alpha\kappa}$ and $\varphi(\hat{x}^s)$ are independent of z^s (they only depends on s but $\partial_{z^s} s = 0$ in the local base at \hat{x}^s). Therefore, from Eqs. (3.5.5) and (3.5.6), it results that $\pi_\varepsilon(\alpha, \kappa)$ writes as $\pi_\varepsilon(\alpha, \kappa) = \Pi_\varepsilon(\alpha, \kappa) + o_{\alpha\kappa}(1)$, where $\Pi_\varepsilon^s(\alpha, \kappa) = \bar{\Pi}_\varepsilon(\alpha, \kappa) + \Pi_\varepsilon^*(\alpha, \kappa) = o_{\alpha\kappa}(1)$, thereby completing the proof of the first statement, by letting $\varepsilon \rightarrow 0$.

Proof of Eqs. (3.5.2) & (3.5.3). By definition of incompatibility on Ω^s and Definition 2.5.17, integration by parts shows that

$$\begin{aligned} \hat{\eta}_{sk}^* &:= \langle \varepsilon_{\alpha\beta} \partial_\alpha \bar{\partial}_\beta \omega_k^*, \varphi \rangle \\ &= \lim_{\varepsilon \rightarrow 0} \left(- \int_{\Omega_\varepsilon^s} \varepsilon_{\alpha\beta} \bar{\partial}_\beta \omega_k^* \partial_\alpha \varphi dS - \int_{C_\varepsilon^s} \varepsilon_{\alpha\beta} \varepsilon_{kpn} \mathcal{E}_{\beta n}^* \partial_\alpha \varphi dC_p \right), \end{aligned}$$

where the first and second terms inside the parenthesis are denoted by $\bar{\pi}_\varepsilon(s, k)$ and $\pi_\varepsilon^*(s, k)$, respectively, while their sum is written as $\pi_\varepsilon(s, k) = \bar{\pi}_\varepsilon(s, k) + \pi_\varepsilon^*(s, k)$. After integration by parts of $\bar{\pi}_\varepsilon$ and by strain incompatibility on Ω_L , it results that

$$\bar{\pi}_\varepsilon(s, k) := \int_{C_\varepsilon^s} \varepsilon_{\alpha\beta} \bar{\partial}_\beta \omega_k^* \varphi dC_\alpha \quad \text{and} \quad \pi_\varepsilon^*(s, k) := - \int_{C_\varepsilon^s} \varepsilon_{\alpha\beta} \varepsilon_{kpn} \mathcal{E}_{\beta n}^* \partial_\alpha \varphi dC_p.$$

Computation of $\bar{\pi}_\varepsilon(s, k)$. This term writes as

$$\bar{\pi}_\varepsilon(s, k) := \int_{C_\varepsilon^s} \bar{\partial}_\beta \omega_k^* \varphi dx_\beta$$

which by Assumption 3.3.1 and since $x_\gamma - \hat{x}_\gamma^s = \varepsilon \hat{v}_\gamma(x)$, rewrites as

$$\bar{\pi}_\varepsilon(s, k) := \bar{\Pi}_\varepsilon(s, k) + o_k(1),$$

where

$$\bar{\Pi}_\varepsilon(s, k) = \varphi(\hat{x}^s) \hat{\Omega}_k^* + \varepsilon \partial_\gamma \varphi(\hat{x}^s) \int_{C_\varepsilon^s} \hat{v}_\gamma \bar{\partial}_\beta \omega_k^* dx_\beta.$$

Computation of $\pi_\varepsilon^*(s, k)$. By Lemma 3.3.1, it results that

$$\pi_\varepsilon^*(s, k) := - \int_{C_\varepsilon^s} \varepsilon_{\alpha\beta} \varepsilon_{k\gamma n} \varepsilon_{\gamma\tau} \mathcal{E}_{\beta n}^* dx_\tau \partial_\alpha \varphi(\hat{x}^s) + o_k(1),$$

and hence that $\pi_\varepsilon^*(s, k) := \Pi_\varepsilon^{*s}(s, k) + o_k(1)$, where,

$$\Pi_\varepsilon^{*s}(s, k) := \varepsilon_{\alpha\beta} \partial_\alpha \varphi(\hat{x}^s) \int_{C_\varepsilon^s} \left(\mathcal{E}_{\beta s}^* \delta_{k\tau} - \mathcal{E}_{\beta\tau}^* \delta_{ks} \right) dx_\tau.$$

Computation of $\pi_\varepsilon(s, k)$. From the preceding calculations, it results that $\pi_\varepsilon(s, k)$ writes as

$$\pi_\varepsilon(s, k) := \Pi_\varepsilon(s, k) + o_k(1),$$

where

$$\Pi_\varepsilon^s(s, k) := \bar{\Pi}_\varepsilon(s, k) + \Pi_\varepsilon^*(s, k).$$

By slightly adapting the proof of the 2D result as treated in Chapter 2 (in particular by considering non-vanishing Ω_α^* and writing the equations in the local Cartesian system attached to the point $\hat{x}_\beta^s \in L$), Eqs. (3.5.2)-(3.5.1) follow, thereby achieving the proof of all statements. \square

3.5.1 The 3D expression of Kröner's formulas at the mesoscale.

Let us recall Tee definitions and prove the following global result, for an arbitrary 3D Lipschitz defect line in Ω .

Theorem 3.5.1 [Main 3D result] *Under Assumptions 3.4.1 and 3.4.2, for a 3D defect line verifying Assumption 3.2.1, incompatibility as defined by Eq. (3.3.14) is the vectorial first order distribution*

$$\eta_{mn}^* = G_{mnij}(\hat{x}^s) \Theta_{ij}^*(\hat{x}^s) + H_{mnij}(\hat{x}^s) \varepsilon_{jlk} \partial_l \kappa_{ik}^*(\hat{x}^s) \quad (3.5.7)$$

where $\langle \delta_{iL}, \varphi \rangle = \int_L \varphi(\hat{x}^s) \tau_i dL(\hat{x}^s)$ for any test-function φ , and where the geometrical tensors G_{mnij} and H_{mnij} write as

$$G_{mnij} := \left[\left(\frac{1}{2} \tau_n \tau_j + \nu_n \nu_j + \sigma_n \sigma_j \right) \delta_{mi} \right]_{m \leftrightarrow n} \quad (3.5.8)$$

$$H_{mnij} := \left[-\frac{1}{2} \tau_m \tau_n \delta_{ij} + \tau_n \tau_j \delta_{mi} \right]_{m \leftrightarrow n}, \quad (3.5.9)$$

with the subscript $[S_{mn}]_{m \leftrightarrow n}$ indicating that the expression symmetric part $S_{mn} + S_{nm}$ is taken.

Proof. By Proposition 3.4.1, the remaining part of the strain \mathcal{E}_{ij}^* in the expression of incompatibility is the sole $o(r_s^2)$ -part of Eqs. (3.4.14)-(3.4.16), in such a way that the global Assumptions 3.4.1 and 3.4.2 might be reduced, by Proposition 3.4.1 to the sole Assumption 3.3.1. By definition of incompatibility, integration by parts shows that

$$\begin{aligned} \langle \eta_{mn}^*, \varphi \rangle &:= \langle \varepsilon_{mlq} \partial_l \bar{\partial}_q \omega_n^*, \varphi \rangle = - \lim_{\varepsilon \rightarrow 0} \left(\int_{\Omega \setminus \odot_\varepsilon} \varepsilon_{mlq} \bar{\partial}_q \omega_n^* \partial_l \varphi dV \right. \\ &\quad \left. - \int_{\partial \odot_\varepsilon} \varepsilon_{mlq} \varepsilon_{npk} \mathcal{E}_{qk}^* \partial_l \varphi dS_p \right), \end{aligned} \quad (3.5.10)$$

where the first and second terms inside the parenthesis write as $\bar{\pi}_\varepsilon(m, n)$ and $\pi_\varepsilon^*(m, n)$ while their sum writes as

$$\pi_\varepsilon(m, n) = \bar{\pi}_\varepsilon(m, n) + \pi_\varepsilon^*(m, n).$$

By integration by parts of $\bar{\pi}_\varepsilon$ and strain incompatibility on Ω_L , it follows that

$$\begin{aligned} \bar{\pi}_\varepsilon(m, n) &= \int_{\partial \odot_\varepsilon} \varepsilon_{mlq} \bar{\partial}_q \omega_n^* \varphi dS_l \\ \pi_\varepsilon^*(m, n) &= - \int_{\partial \odot_\varepsilon} \varepsilon_{mlq} \varepsilon_{npk} \mathcal{E}_{qk}^* \partial_l \varphi dS_p. \end{aligned}$$

By Definition 3.2.6, let us write the relations $\int_{\partial \odot_\varepsilon} dS_l(x) = \int_{L_\varepsilon} \int_{C_\varepsilon^s} dL(x) dC_l(x)$ which, from Lemma 3.2.1, rewrites as

$$\int_{\partial \odot_\varepsilon} dS_l(x) = \int_L dL(\hat{x}^s) \int_{C_\varepsilon^s} (1 - \varepsilon \hat{\chi}) dC_l(x), \quad (3.5.11)$$

for every $\varepsilon > 0$. Hence, by the boundedness of the line curvature and of $\hat{\eta}_{mn}^*$ on Ω^s and the line concentration property of $\hat{\eta}_{mn}^*$, it results from Eqs. (3.5.10) and (3.5.11), that

$$\langle \eta_{mn}^*, \varphi \rangle = \int_L \eta_{mn}^*(\hat{x}^s) \varphi(\hat{x}^s) dL(\hat{x}^s),$$

where $\eta_{mn}^*(\hat{x}^s)$ is the incompatibility on Ω^s , here expressed in the global Cartesian frame. Since from Lemma 3.5.1 $\eta_{mn}^*(\hat{x}^s)$ is known in the local Cartesian frame (denoted by $\hat{\eta}_{mn}^*$ and given in Lemma 3.5.1 by Eqs. (3.5.1)-(3.5.3)), it suffices to express $\hat{\eta}_{mn}^*$ in the global Cartesian coordinate system. The matrix required for change the coordinates from the local Cartesian system attached to a point \hat{x}^s of the line L to the global Cartesian system is given by:

$$a_{ij} := v_i \delta_{j1} + \sigma_i \delta_{j2} + \tau_i \delta_{j3},$$

in such a way that

$$\hat{\Omega}_l^* = a_{jl}\Omega_j^* \quad (3.5.12)$$

$$\hat{B}_l^* = a_{jl}B_j^* \quad (3.5.13)$$

$$\hat{\partial}_l = a_{jl}\partial_j \quad (3.5.14)$$

$$\left(x_\beta^s - x_{0\beta}^s\right) = a_{j\beta}(x_j - x_{0j}), \quad (3.5.15)$$

where $a_{jl} = (\delta_{l1}v_j + \delta_{l2}\sigma_j + \delta_{l3}\tau_j)$. Incompatibility hence writes as

$$\begin{aligned} \langle \eta_{mn}^*, \varphi \rangle &= \int_L a_{mi}a_{nj}\hat{\eta}_{ij}^*(\hat{x}^s)\varphi(\hat{x}^s)dL(\hat{x}^s) \\ &= \int_L (\tau_m\tau_n\hat{\eta}_{ss}^* + (\tau_m\nu_n\delta_{\kappa 1} + \tau_m\sigma_n\delta_{\kappa 2})_{m\leftrightarrow n}\hat{\eta}_{s\kappa}^*)dL(\hat{x}^s) \end{aligned}$$

where $m \leftrightarrow n$ indicates as before the symmetrisation of the term as performed by interchanging m and n in the expression inside the parenthesis. From Eqs. (3.5.1)-(3.5.3), let us consider the following 4 cases:

First term: $\hat{\eta}_{sl}^{*(1)} = \hat{\Omega}_l^*\delta_{\hat{x}^s}$. After some computations, it results that

$$\eta_{mn}^{*(1)}(\hat{x}^s) = \left(\frac{1}{2}\tau_m\tau_n\tau_j + \tau_m\nu_n\nu_j + \tau_m\sigma_n\sigma_j\right)_{m\leftrightarrow n}\Omega_j^*\delta_{\hat{x}^s}. \quad (3.5.16)$$

Second term: $\hat{\eta}_{sl}^{*(2)} = \delta_{ls}\varepsilon_{\alpha\gamma}\hat{B}_\gamma^*\hat{\partial}_\alpha\delta_{\hat{x}^s} + \delta_{l\kappa}\frac{1}{2}\varepsilon_{\kappa\alpha}\hat{B}_s^*\hat{\partial}_\alpha\delta_{\hat{x}^s}$. After some computations, it results that

$$\begin{aligned} \eta_{mn}^{*(2)}(\hat{x}^s) &= \frac{1}{2}(\tau_m(\tau_n\sigma_i\nu_j - \tau_n\sigma_j\nu_i + \tau_i\sigma_j\nu_n - \tau_i\sigma_n\nu_j))_{m\leftrightarrow n}B_i^*\partial_j\delta_{\hat{x}^s} \\ &= -\frac{1}{2}\varepsilon_{kuv}\varepsilon_{vjl}\tau_l\tau_u(\tau_m\varepsilon_{nik})_{m\leftrightarrow n}B_i^*\partial_j\delta_{\hat{x}^s}. \end{aligned} \quad (3.5.17)$$

Third term (a): $\hat{\eta}_{sl}^{*(3a)} = \delta_{ls}\varepsilon_{\alpha\gamma}\varepsilon_{\beta\gamma}\left((\hat{x}_\beta^s - x_{0\beta}^s)\hat{\Omega}_s^* - (\hat{z}^s - z_0^s)\hat{\Omega}_\beta^*\right)\hat{\partial}_\alpha\delta_{\hat{x}^s}$. After some computations, it results that

$$\begin{aligned} \eta_{mn}^{*(3a)}(\hat{x}^s) &= \tau_m\tau_n(\hat{x}_i^s - x_{0i}^s)\Omega_k^*[v_j(\nu_i\tau_k - \nu_k\tau_i) + \sigma_j(\sigma_i\tau_k - \sigma_k\tau_i)]\partial_j\delta_{\hat{x}^s} \\ &= \tau_n\tau_l\varepsilon_{lji}\varepsilon_{ipq}\tau_m\Omega_p^*(\hat{x}_q^s - x_{0q}^s)\partial_j\delta_{\hat{x}^s}. \end{aligned} \quad (3.5.18)$$

Third term (b): $\hat{\eta}_{sl}^{*(3b)} = -\delta_{l\kappa}\frac{1}{2}\varepsilon_{\kappa\alpha}\varepsilon_{\beta\gamma}(\hat{x}_\beta^s - x_{0\beta}^s)\hat{\Omega}_\gamma^*\hat{\partial}_\alpha\delta_{\hat{x}^s}$. After some computations, it results that

$$\eta_{mn}^{*(3b)}(\hat{x}^s) = \frac{1}{2}(\tau_m\varepsilon_{njl})_{m\leftrightarrow n}\tau_l\tau_i\varepsilon_{ipq}\Omega_p^*(\hat{x}_q^s - x_{0q}^s)\partial_j\delta_{\hat{x}^s}. \quad (3.5.19)$$

The combination of Eqs. (3.5.18) & (3.5.19) together with the identity

$$\frac{1}{2} \tau_l (\tau_m \tau_n \varepsilon_{ilj} - \tau_m \tau_i \varepsilon_{nlj}) = -\frac{1}{2} \tau_l \tau_m \varepsilon_{nik} \varepsilon_{kuv} \tau_u \varepsilon_{vjl}$$

results in the following expression:

Third term.

$$\begin{aligned} \eta_{mn}^{*(3)}(\hat{x}^s) &= \eta_{mn}^{*(3a)}(\hat{x}^s) + \eta_{mn}^{*(3b)}(\hat{x}^s) = \\ &= -\frac{1}{2} \tau_l \tau_m \varepsilon_{nik} \varepsilon_{kuv} \varepsilon_{vjl} \tau_u \varepsilon_{ipq} \Omega_p^*(\hat{x}_q^s - x_{0q}) \partial_j \delta_{\hat{x}^s}. \end{aligned} \quad (3.5.20)$$

By the definitions of the dislocation and disclination densities (viz. Eqs. (3.3.5) & (3.3.6)), Eq. (3.2.20) and identity $\varepsilon_{nik} \varepsilon_{kuv} = \delta_{nu} \delta_{iv} - \delta_{nv} \delta_{iu}$, it results that Eqs. (3.5.16), (3.5.17) and (3.5.20) rewrite as

$$\begin{aligned} \eta_{mn}^* &= \left[\left(\frac{1}{2} \tau_n \tau_j + v_n v_j + \sigma_n \sigma_j \right) \Theta_{mj}^* + \frac{1}{2} \varepsilon_{njl} \tau_l \tau_m \partial_j (\Lambda_{ii}^* + \varepsilon_{ipq} (\hat{x}_q^L - x_{0q}) \Theta_{ip}^*) \right. \\ &\quad \left. - \frac{1}{2} (\varepsilon_{ijl} \tau_l \tau_m \partial_j (\Lambda_{ni}^* + \varepsilon_{ipq} (\hat{x}_q^L - x_{0q}) \Theta_{np}^*)) \right]_{m \leftrightarrow n}. \end{aligned} \quad (3.5.21)$$

By Eq. (3.2.20) the last term is symmetric, and hence Eq. (3.5.21) rewrites as

$$\begin{aligned} \eta_{mn}^* &= \left[\left(\frac{1}{2} \tau_n \tau_j + v_n v_j + \sigma_n \sigma_j \right) \Theta_{mj}^* \right]_{m \leftrightarrow n} + \frac{1}{2} \varepsilon_{mjl} \tau_l \tau_m \partial_j (\Lambda_{ii}^* + \varepsilon_{ipq} (\hat{x}_q^L - x_{0q}) \Theta_{ip}^*) \\ &\quad - (\varepsilon_{kjl} \tau_l \tau_m \partial_j (\Lambda_{nk}^* + \varepsilon_{kpq} (\hat{x}_q^L - x_{0q}) \Theta_{np}^*)) \\ &\quad - \frac{1}{2} \varepsilon_{kjl} \tau_l \tau_m \partial_j \delta_{kn} (\Lambda_{ii}^* + \varepsilon_{ipq} (\hat{x}_q^L - x_{0q}) \Theta_{ip}^*) \Big]. \end{aligned}$$

By Eqs. (3.3.5)-(3.3.8) the two last terms rewrite as the contortion curl in the following manner:

$$\tau_m \tau_l \varepsilon_{ljk} \partial_j \kappa_{nk}^*,$$

while, from $\alpha_{ii}^* = -2\kappa_{ii}^*$, the second term rewrites as

$$\begin{aligned} \tau_n \tau_l \varepsilon_{ljm} \partial_j \kappa_{ii}^* &= \tau_n \tau_l \varepsilon_{ljk} \partial_j \kappa_{mk}^* - \tau_n \tau_l \varepsilon_{ljk} \partial_j \alpha_{mk}^* \\ &= \tau_n \tau_l \varepsilon_{ljk} \partial_j \kappa_{mk}^* - \tau_m \tau_n \varepsilon_{ljk} \partial_j \alpha_{lk}^* \\ &= \tau_n \tau_l \varepsilon_{ljk} \partial_j \kappa_{mk}^* - \tau_m \tau_n \varepsilon_{ljk} \partial_j (\kappa_{lk}^* + \kappa_{ii}^* \delta_{lk}) \\ &= \tau_n \tau_l \varepsilon_{ljk} \partial_j \kappa_{mk}^* - \tau_m \tau_n \varepsilon_{ljk} \partial_j \kappa_{lk}^*, \end{aligned}$$

in such a way that (3.5.21) rewrites as

$$\eta_{mn}^*(\hat{x}^s) = G_{mij}(\hat{x}^s) \Theta_{ij}^*(\hat{x}^s) + H_{mni}(\hat{x}^s) \varepsilon_{ilk} \partial_l \kappa_{jk}^*(\hat{x}^s),$$

where the geometrical tensors G_{mni} and H_{mni} read as

$$\begin{aligned} G_{mni}(\hat{x}^s) &:= \left[\left(\frac{1}{2} \tau_n \tau_j + v_n v_j + \sigma_n \sigma_j \right) \delta_{mi} \right]_{m \leftrightarrow n} \\ H_{mni}(\hat{x}^s) &:= \left[-\frac{1}{2} \tau_m \tau_n \delta_{ij} + \tau_n \tau_i \delta_{mj} \right]_{m \leftrightarrow n}. \end{aligned}$$

thereby proving the statement.

Remark 3.5.1 *In the 2D case, the lines are rectilinear along the z -axis and hence $\tau_i = \delta_{i3}$, $v_i = \delta_{i1}$, $\sigma_i = \delta_{i2}$, in such a way that $G_{3nij} = \delta_{n3} \delta_{i3} \delta_{j3} + \delta_{i3} \delta_{n\kappa} \delta_{j\kappa}$, while $H_{3nij} = \delta_{i3} \delta_{j3} \delta_{n3} \delta_{m3}$. Therefore, since Ω_κ^* and $\kappa_{\alpha s}^*$ vanish in the 2D case, it follows that:*

$$\eta_{3n}^* = \Theta_{3n}^* + \varepsilon_{\alpha\beta} \partial_\alpha \kappa_{n\beta}^*,$$

according to the results of Chapter 2.

3.6 Incompatibility of a discrete family of 3D dislocations

In this section, we will consider a family of 3D Lipschitz defect lines $\mathcal{L} \subset \Omega$, such that

- i. either all lines of \mathcal{L} are isolated or there is a finite number of contact points between these lines;
- ii. or there is a ‘‘OD dislocation cluster’’ in the sense that one of the lines of \mathcal{L} can be approached infinitely closely by a subset of \mathcal{L} .

Definition 3.6.1 *A Lipschitz defect line $L \in \mathcal{L}$ embedded in its tube \odot_ε^L is isolated if*

$$\lim_{\varepsilon \rightarrow 0} \odot_\varepsilon^L \cap \mathcal{L} = \{L\}.$$

If the latter condition is not verified, the set L is said to be a OD cluster and will be denoted by \mathbf{L} . In this case there exists a collection of isolated Lipschitz defect lines

$$L_j \subset \Omega \text{ such that } \mathbf{L} \subset \overline{\bigcup_{j=1}^{\infty} L_j}.$$

3.6.1 The case of an infinity of isolated dislocations

When the defect region \mathcal{L} consists of a finite number of isolated dislocations lines of arbitrary orientation the results extend in a straightforward manner by summing the densities of each line. If two lines intersect, the results also extend, by slightly adapting the proof of the single line situation: in fact it suffices to consider a small ball centered at the intersection points, to apply the result obtained for a single line except for the portion located inside the ball, and to let the radius of the ball tend to 0. In the case of infinitely many lines without accumulation regions, the summation of the incompatibility tensors of each single isolated line can also be performed. However, since the Burgers vector of a family of dislocations is defined by encircling this family inside a closed loop along which the total Burgers tensor is integrated, it should be noted that the following condition must hold: for every dislocation subset \mathcal{L}' of \mathcal{L} , the Burgers vectors of this subset $B_k^*(\mathcal{L}') := \sum_{j=1}^{\infty} B_k^*(L_j)$, $L_j \in \mathcal{L}'$, must be of finite norm. This condition restricts the possible situations where the crystal is filled with infinitely many dislocations.

3.6.2 Analysis of the 0D clustering

The purpose of this section is to show how the theory developed for isolated dislocations and disclinations extends in a natural manner to the simplest case of a dislocation cluster. Let us consider a 0D cluster $\mathbf{L} \in \mathcal{L}$. By definition, there is a set $T_\varepsilon^{\mathbf{L}}$ of radius $\varepsilon > 0$ containing both \mathbf{L} and an infinite family of L_j 's ($1 \leq j < \infty$). Moreover, $T_\varepsilon^{\mathbf{L}}$ and the family are chosen such that no defect line of the family is crossing the boundary of $T_\varepsilon^{\mathbf{L}}$ (this can be obtained either by just removing any line which crosses $\partial T_\varepsilon^{\mathbf{L}}$, or by changing ε , or by following the ‘escaping’ line with $T_\varepsilon^{\mathbf{L}}$). Consider now any non-isolated $\hat{x}^{\mathbf{L}} \in \mathbf{L}$ and define the set

$$\Omega^{\mathbf{L}}(\hat{x}) := \{x \in \Omega \quad s.t. \quad (x_i - \hat{x}_i^{\mathbf{L}})\tau_i(x^{\mathbf{L}}) = 0\}, \quad (3.6.1)$$

in such a way that $\hat{x}^{\mathbf{L}} = \lim_{j \rightarrow \infty} \hat{x}^{L_j}$ (in the Hausdorff sense) where $\hat{x}^{L_j} \in L_j \cap \Omega^{\mathbf{L}} \subset T_\varepsilon^{\mathbf{L}}$, and define a sequence of $\varepsilon_j > 0$ ($1 \leq j < \infty$), and $\varepsilon > 0$ such that

- $D(\hat{x}^{L_j}, \varepsilon_j) \subset D(\hat{x}^{\mathbf{L}}, \varepsilon)$
- $D(\hat{x}^{L_j}, \varepsilon_j) \cap \mathcal{L} = \{\hat{x}^{L_j}\}$,

where $D(x, r)$ denotes the open disk of radius r centred at x , hence such that the converging sequence consists of isolated points strictly contained in a bounded set of

radius ε . Define now

$$A_\varepsilon := \bigcup_{j=1}^{\infty} D(\hat{x}^L_j, \varepsilon_j) \quad (3.6.2)$$

and

$$A_\varepsilon^L := D(x^L, \varepsilon) \setminus A_\varepsilon \quad (3.6.3)$$

which both have bounded areas and verify $\hat{x}^L \in A_\varepsilon$, while A_ε^L is a defect free subset of Ω^L . Since A_ε^L has not necessarily a regular boundary $C_\varepsilon(\hat{x}^L)$ (in the sense of rectifiability properties, finite perimeter, etc) it is necessary to introduce the theory of line integrals along non smooth curves as developed by J. Harrison (1999) (see also (Harrison and Norton, 1992)).

3.6.3 Generalized Gauss-Green theorems and fractal clusters

The objective here is to give a very general version of Gauss-Green's⁸ formula

$$\int_{\partial A} (pdx + qdy) = \int_A (\partial_y p - \partial_x q) dS, \quad (3.6.4)$$

where A is a subset of \mathbb{R}^2 and p, q are smooth functions on A . Usual validations of Eq. (3.6.4) require the set A to have a finite perimeter (Evans, 1992), anyhow depending on the link between regularity (that is, measure) of ∂A and differentiability of p and q (Harrison and Norton, 1991). Here we restrict ourselves to the plane and seek to validate Eq. (3.6.4) for a ∂A that could be non-rectifiable, as for instance if ∂A is a fractal curve. Let us remark that the forthcoming statements are proved under the requirement that the left- and right-hand side of Eq. (3.6.4) be defined independently of each other, while integration is still intended in the Lebesgue sense. Since in 1935 H. Whitney (1935) (see also Harrison (1991, 1999)) constructed a famous $\mathcal{C}^1(\mathbb{R}^2, \mathbb{R})$ -function which appears to be “not constant on a connected set of critical points”, that is, which verifies $\nabla f \equiv 0$ on a (continuous) arc γ , even though f is increasing along γ . In particular, the fact that $f(\gamma(0)) = 0$ and $f(\gamma(1)) = 1$, implies a failure of the Fundamental Theorem of Calculus (“FTC”) “ $\int_\gamma df = f(\gamma(0)) - f(\gamma(1))$ ”. Of course, the reason for this failure is the too high *Hausdorff dimension*⁹ of γ w.r.t. the regularity of f . For instance, there exists curves whose ranges contain the entire 2-dimensional unit square. These space-filling curves are known as *Peano curves* and a such curve is illustrated on Figure 3.3. The relevance of this discussion in the context of line-

⁸The general Stokes theorem would involve a set $A \in \mathbb{R}^3$ whose “Hausdorff-dimension” is less than 3.

⁹The Hausdorff dimension is defined as $dim(\gamma) := \inf\{t : \mathcal{H}^t(\gamma) = 0\}$.

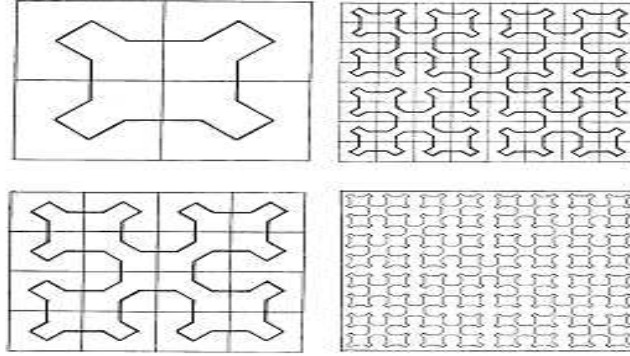


Figure 3.3: Example of a 2 dimensional (space-filling) Peano curve.

defect analysis appears as soon as one considers the implication of such a counter-example for the computation of the mesoscopic Frank and Burgers vectors as jumps of $f = \omega_k^*$ or $f = b_k^*$. For an “isolated” defect-line, neither Greens’ theorem, nor the FTC pose any kind of problem, since the Burgers circuit can always be taken smooth, while the Frank and Burgers tensors are smooth as well. But for clustering defect-lines instead, one ought to show that any Burgers vector as computed along a circuit enclosing an infinite collection of infinitely many nearby dislocations is the infinite sum of the single Burgers vectors of these lines. Actually, by the Frank and Burgers tensors smoothness away from the defect-line, the only issue is to find an optimal version of Eq. (3.6.4) accounting for the largest possible domains of integration, that is, allowing for pathological clustering processes. This class of domains is given by the so-called *chainlets* which are obtained by density of *polyhedral chains*, themselves defined as equivalence classes of *simplicial chains* (the equivalence relation permitting the cancellation of the overlap region of two simplicial chains), that is, finite sums of oriented convex envelopes σ_j of points in the plane. In fact, let us simply write the chainlet A as

$$A = \lim_{k \rightarrow \infty} \sum_j^k a_j \sigma_j, \quad (3.6.5)$$

where $a_j \in \mathbb{R}$. Chainlets appearing as domains of integration have the great advantage of being governed by an intuitive geometric construction as compared to the evaluation of a domain dimension. Let us denote by \mathcal{A}_2^r the space of chainlets in the plane, weighted with the 2-dimensional Lebesgue measure, and obtained by completion w.r.t. to an r -norm which will not be given here¹⁰, but which is chosen in such a way that \mathcal{A}_2^r will contain more and more strange and pathological limit points as $r \in \mathbb{Z}^+$ increases.

¹⁰Cf the paper of J. Harrison (1999) which develops the whole theory and the references therein.

By a continuity property, it can be shown that, for smooth p and q , the integral over a chainlet A as given by

$$\int_A (\partial_y p - \partial_x q) dS := \lim_{k \rightarrow \infty} \int_{A_k} (\partial_y p - \partial_x q) dS,$$

is well-defined, and that $\partial A = \lim_{k \rightarrow \infty} \partial A_k$ belongs to \mathcal{A}_1^{r+1} , thereby proving Eq. (3.6.4), which classically holds for the simplicial chain A_k , for any given $r > 0$ and for any chainlet A in \mathcal{A}_2^r .

The well-known “Von Koch snowflake” illustrated in Figure 3.4 is a fractal curve which belongs to \mathcal{A}_2^1 . If a dislocation line pierces the barycenter of each of the tri-

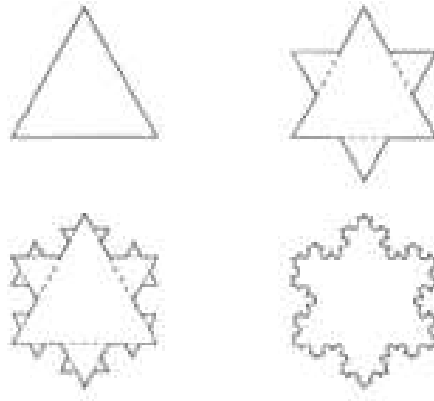


Figure 3.4: The snowflake as a sum of (oriented) simplexes (triangles) whose overlapping region has been cancelled (dotted lines).

angles arising in the construction of the snowflake, this curve is a *fractal cluster* of dislocations and the above mentioned Greens’ theorem allow us to define an equivalent Burgers vector for that region (cf Section 3.6.2 of Chapter 3).

On Figure 3.5(a) the simulation of a clustering process where dislocations move to each other is shown, while Fig. 3.5(b) shows the case of a growing cluster of dislocations, exhibiting fractal (or almost fractal) curves.

3.6.4 Incompatibility of a 0D cluster

It appears that the sets A_0 and A_0^L are chainlets as defined by completion using Eq. (3.6.5). Therefore, the Frank and Burgers vectors along $C(x^L, \varepsilon)$ and ∂A coincide

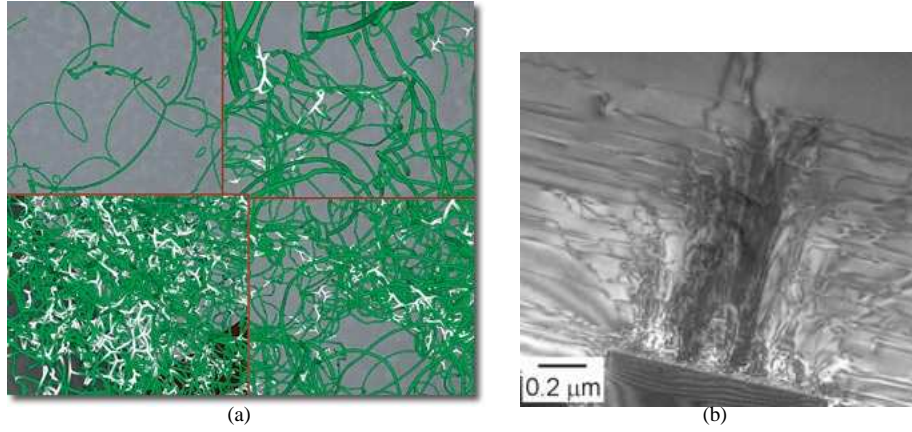


Figure 3.5: (a) Simulation of defect-line clustering (snapshot of dislocation network evolution using the Paradis code; from Science & Technology review, November 2005; (b) Growing dislocations in sapphire exhibit very complex geometric structures.

since, by the extended Green's theorem with $pdx + qdy = \bar{\partial}_\beta \omega_l^* dx_\beta$, it results that $\int_{A^L} \eta_k^* dS$ vanishes¹¹. Let us recall the necessary condition for OD clusters that

$$B_k^*(\mathbf{L}) := B_k^*(C(x^L, \varepsilon)) = \sum_{j=1}^{\infty} B_k^*(L_j) < \infty$$

$$\Omega_k^*(\mathbf{L}) := \Omega_k^*(C(x^L, \varepsilon)) = \sum_{j=1}^{\infty} \Omega_k^*(L_j) < \infty$$

in such a way that \mathbf{L} can be considered as an isolated Lipschitz line with Burgers and Frank vectors $B_k^*(\mathbf{L})$ and $\Omega_k^*(\mathbf{L})$, respectively. Incompatibility is therefore given by the following extended version of Theorem 3.5.1.

Theorem 3.6.1 [Extended 3D result] *Under Assumptions 3.4.1 and 3.4.2, for a collection \mathcal{L} of 3D defect lines verifying Assumption 3.2.1 and with possible OD clustering regions, incompatibility as defined by Eq. (3.3.14) is the vectorial first order distribution*

$$\eta_{mn}^* = \sum_{L \in \mathcal{L}} (G_{mij}(\hat{x}^L) \Theta_{ij}^*(x^L) + H_{mij}(\hat{x}^L) \varepsilon_{jlk} \partial_l \kappa_{ik}^*(\hat{x}^L))$$

¹¹Since dislocations of the same sign might not always be able, for energetical reasons, to form any cluster, the OD cluster often consists of an ensemble of dislocations of opposite sign.

where $\langle f \delta_{iL}, \varphi \rangle = \int_L f \varphi(\hat{x}^s) dL(\hat{x}^s)$ for any test-function φ , $L^1(L, \mathcal{H}^1)$ -integrable function f and defect line $L \in \mathcal{L}$, and where the geometrical tensors G_{mni} and H_{mni} write as

$$\begin{aligned} G_{mni} &:= \left[\left(\frac{1}{2} \tau_n \tau_j + v_n v_j + \sigma_n \sigma_j \right) \delta_{mi} \right]_{m \leftrightarrow n} \\ H_{mni} &:= \left[-\frac{1}{2} \tau_m \tau_n \delta_{ij} + \tau_n \tau_j \delta_{mi} \right]_{m \leftrightarrow n}. \end{aligned}$$

Let us remark that the cluster fine structure is considered with more accuracy for small values of ε .

3.7 Conclusive remarks

The results developed in this chapter did not require the introduction of any new concept. The same basic tools from geometric measure theory as in Chapter 2 have been used, while slightly adapting the mathematical technique, since the proof complexity increased quite much as a consequence of the treatment of the full 3D strain together with Lipschitz (instead of rectilinear) defect lines. On the other hand, restrictions have been introduced on the defect line regularity. In fact requiring the tangent vector to be Lipschitz continuous is equivalent to requiring the defect line to be described by means of a $W^{1,\infty}$ function of the arc parameter s . Moreover the line is assumed to be “simple” and its dimension will always be 1, therefore preventing the model from fractal curves, such as “space-filling” curves for instance. This is not a major restriction at this stage, since there is no specific interest in the defect line class per se, but rather in its completion class (in some appropriate sense which is beyond the scope of this work), which could have been reached by an even smoother class of curves (as analytical curves for instance).

However, the developments showed gauge fields in the treatment of global strain assumptions. In fact, the occurrence of gauges is very natural in the study of defective crystals, as a reminiscence of field multivaluedness.

The main interest of these developments is found in the “new” formulas relating strain incompatibility to defect densities, as showing the effective role played by the defect line curvature and torsion, by means of concentrated terms including the line tangent together with its normal vectors.

It would be even more interesting to obtain the macroscopic counterpart of these quantities by homogenisation in order to be able to compare our “new” result with Kröner’s general formula. This is a work under investigation.

Part III

Point-defect dynamics in single crystals

Chapter 4

Dynamic prediction of point-defect formation in silicon crystals

The silicon¹ (Si) single crystals used for device manufacturing are not ideal crystals, although they exhibit a high degree of perfection. Intrinsic point-defects, i.e. self interstitials and vacancies, impurity atoms and defect clusters or micro-voids are present in the crystal lattice at finite temperature due to energetic and entropic reasons. Understanding the behaviour of self-interstitials and vacancies in Si crystals during growth is of fundamental importance, as they are the basic building blocks for grown-in defects.

From a technological viewpoint, a major issue in Czochralski (CZ) Si growth is to reduce the defect density to the lowest possible level, especially when the aim is to produce defect-free crystals. Accordingly the effort paid for the last years to understand the mechanisms governing the formation and evolution of self-interstitials (I) and vacancies (V) in the growing crystal has brought reasonably good physical models on the basis of the Voronkov theory (1982). However numerical experiments reveal a very high sensitivity of the defect distribution in the crystal both to the material parameters governing point-defect diffusion and recombination and to the thermal gradient

¹Silicon is a group IV element with four valence electrons, two in the 3s-state and two in the 3p-state. The unit cell contains eight tetrahedral coordinated sites in the diamond structure, which can be described as two interpenetrating face-centered cubic (fcc) lattices displaced along the [111] direction by one-fourth of the diagonal length.

in the crystal along the solidification front. Therefore very accurate numerical tools are needed when the objective is to improve the crystal growth process on the basis of defect modeling.

4.1 Point-defects and grown-in defect modeling

4.1.1 Interstitial and vacancy equilibrium concentrations

Statistical thermodynamics can be used to calculate the concentration of point-defects, eg vacancies and interstitials (cf Fig. 4.1), in thermal equilibrium within a crystal. The spontaneous formation of point-defects above $T = 0[\text{K}]$ occurs because their presence decreases the Gibbs free energy (Glicksman, 2000), as given by

$$G_{I,V}^f = H_0 - TS_0 + n_{I,V} \left(\Delta H_{I,V}^f - T \Delta S_{I,V}^f \right) - k_b T \ln W, \quad (4.1.1)$$

where the first two terms represent the Gibbs free energy of the point-defects-free crystal, the third term stands for the formation free energy for interstitials or vacancies (which stems primarily from the energy of the free electrons and from the crystal frequency changes, as associated with the first and second term inside the parentheses, respectively (Shewmon, 1989)), while the last term is the configurational entropy, as expressed by Boltzmann's formula for the random mixing of the n_I interstitials and n_V vacancies among the N lattice sites (with $n_I, n_V \ll N$). The underlying atomic reaction for a pure crystal consisting of a lattice of atoms X is the so-called *Frenkel reaction*, where an atom leaves a lattice by simultaneously creating a vacancy V and an interstitial I (Philibert, 1988; Dornberger, 1998):



clearly showing that the formation of vacancies and interstitials is balanced in the crystal bulk. However, due to boundary and microdefect effects in the formation and annihilation of point-defects (eg if the solid crystal is adjacent to gas or liquid phases), the formation enthalpies and entropies slightly differ between vacancies and interstitials. In fact, related to these boundary mechanisms is the so-called *Schottky* mechanism, where a bulk lattice atom jumps to an interstitial site (thereby creating a vacancy) and diffuses to the surface, where it is added to the lattice, or, vice-versa, where a boundary lattice atom jumps to a bulk interstitial site (Philibert, 1988; Dornberger, 1998). Bulk sources or sinks for point-defects are microdefects (as eg clusters, voids and dislocations loops) (Falster and Voronkov, 2002; Kulkarni et al., 2004.) and need to be taken into account for accurate formation enthalpies and entropies. The (thermodynamic)

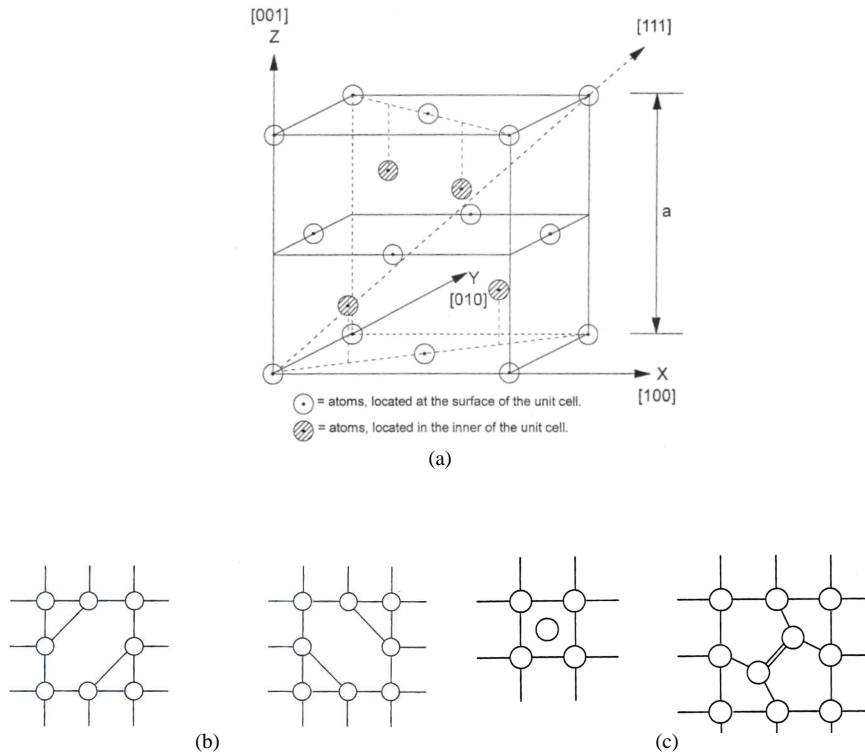


Figure 4.1: (a) Elementary cell of crystalline silicon, where $a=0.543$ [nm] is the lattice constant; (b) Two-dimensional schematic representation of a neutral single vacancy; Two dimensional representation of a free silicon self-interstitial (c)-left, and a dumbbell configuration (c)-right; from Dornberger (1998).

equilibrium concentrations of point-defects as defined by

$$C_{I,V}^{eq} := \frac{n_{I,V}^{eq}}{N},$$

can be computed by the minimization of G in Eq. (4.3.39) w.r.t. $n_{I,V}$ (Shewmon, 1989; Philibert, 1988), resulting in the Arrhenius-type formula $C_{I,V}^{eq} = \exp(-\Delta G_{I,V}^f)$ where $\Delta G_{I,V}^f = \Delta H_{I,V}^f - T\Delta S_{I,V}^f$.

However, let us remark that since point-defects are formed during the transient solidification process at the solid/liquid interface, thermodynamic equilibrium shows to be a simplifying assumption (Dornberger, 1998).

Non-dimensional expressions of the equilibrium concentrations

Letting the temperature-dependent formation enthalpies and entropies be expressed by the linear expressions $H_{I,V}^f = H_{I,V}^{f0} + H_{I,V}^{f1}T$ and $S_{I,V}^f = k_b (S_{I,V}^{f0} + S_{I,V}^{f1}T)$, respectively, effective enthalpies and entropies are defined as

$$\begin{aligned}\bar{H}_{I,V}^f &= H_{I,V}^{f0} + k_b S_{I,V}^{f1} T_m^2, \\ \bar{S}_{I,V}^f &= S_{I,V}^{f1} T_m,\end{aligned}$$

in such a way that the non-dimensional expressions of equilibrium concentrations reads:

$$C_{I,V}^{eq} = C_{I,V}^m \exp \left[-\frac{\bar{H}_{I,V}^f}{k_b T_m} \left(\frac{T_m}{T} - 1 \right) + \bar{S}_{I,V}^f \left(1 - \frac{T}{T_m} \right) \left(\frac{T_m}{T} - 1 \right) \right], \quad (4.1.3)$$

where the various parameter are given in a comparison Table in Section 4.4 compiled with a set of data from the crystal-growth literature.

Nowadays, after controversial discussions and considering the known presence of self-interstitial and vacancy related defects detected in silicon crystals, it is accepted by most researchers that vacancies and self-interstitials are simultaneously present in silicon crystals under thermal equilibrium not too far from the melting temperature (Dornberger, 1998; Tan & Gösele, 1985).

4.1.2 Transport of interstitials and vacancies

Obviously there is no convection inside the solid crystal and the transport is here created by the uniform vertical motion of the crystal with respect to the furnace (and the solidification interface), the pulling rate being denoted by V . The transport affects all atoms, of lattice or interstitial nature, and the vacancies as well. In addition, let us remark that convection in the liquid phase plays a prominent role, since it governs the melting interface shape and determines the rate and type of impurity penetration inside the solid phase. Moreover, since the crystal is cooled while being pulled, the hot region just above the interface is the most critical region in terms of the variety and rate of diffusion, recombination, creation and incorporation mechanisms. In contrast the “upper region”, termed as the “far field” in the sequel is “frozen” in terms of diffusion and recombination, and hence only submitted to transport without any other modification of the concentration isolines.

4.1.3 Recombination of interstitials and vacancies

The recombination rate clearly depends on the point-defect diffusivities, in the sense that high diffusivities will enhance the recombination mechanism. A linear law will here be assumed. Moreover, since recombination is a mechanism which globally releases energy while decreasing entropy, exponential laws of the Arrhenius type are introduced in the recombination rate expression to allow for the increasing energy and decreasing entropy contributions. The final expression writes as

$$K_{IV} = K_{I,V}^m \frac{D_I + D_V}{D_I^m + D_V^m} \exp \left[-\frac{\overline{H}^r}{k_b T_m} \left(\frac{T_m}{T} - 1 \right) \right] \exp \left[\overline{S}^r \left(\frac{T_m}{T} - 1 \right) \right] \left(1 - \frac{T}{T_m} \right), \quad (4.1.4)$$

where the equivalent enthalpies and entropies are defined as follows

$$\begin{aligned} \overline{H}^r &= H^r + k_b T_m^2 S^{r;1} \\ \overline{S}^r &= T_m S^{r;1}. \end{aligned}$$

4.1.4 Diffusion of interstitials and vacancies

The diffusion of interstitials and vacancies is driven by concentration gradients in the crystal and the flux of the diffusing species is basically in the direction of lower concentration. The diffusive flux is proportional to diffusion constants depending on temperature and concentration but as the concentration of point-defects is in practice lower than 1 ppma the concentration dependence can be neglected (Dornberger, 1998; Brown and Maroudas, 1991). Diffusivities can be computed theoretically or experimentally, both approaches suffering from the following drawbacks:

- The theoretical approach requires an accurate statistical analysis of the correlated atomic jumps and a description of the nano-physics accounting for a variety of diffusion mechanisms (where the predominance of a particular mechanism depends on the considered temperature range), mostly away from thermodynamic equilibrium. Moreover, the calculation of the formation or migration enthalpies and entropies relies on postulated diffusion and formation mechanism in the crystal bulk or boundary, which may interact and cancel each other. Even employing atomistic simulations (such as eg electronic density functional theory-DFT), which offer the advantage of letting a particular mechanism be isolated, there is too much uncertainty to provide all the parameters completely independently of experiments. In particular, atomistic simulations are handicapped by the inaccuracies caused by the crudeness of available interatomic potentials (Sinno et al; 1998.).

- The experimental approach for studying the properties of intrinsic point-defects can be based on self- or foreign- atom diffusion experiments (see Section 4.2.3), for properties in or away from thermodynamic equilibrium, respectively. Even though the experiments (as based on gold, zinc or iridium diffusion (Bracht et al., 1995; Lerner and Stolwijk, 2005), positron annihilation, or the use of radioactive isotopes) are carefully realised, there is always a deep lack of data for high temperature (ie, close to melting point) diffusivities and equilibrium concentration values.

Let us also mention “ab-initio” calculations, which also suffer from approximated interatomic potentials and are limited to small atomistic systems and short simulation times (Sinno et al., 1998). These difficulties justify to recall in the forthcoming chapter some basic properties of the diffusion in solids, enlightening as much as possible the successive approximations and postulates used when trying to determinate the diffusion coefficients.

They also explain why a new material data set based on updated values from the experiments by Lerner and Stolwijk (2005) will be considered in grown-in crystal processes without contradicting some unquestionable observations, such as the OSF-ring equilibrium and the V/G criterion (see Sections 4.6 and 4.7.2).

4.2 The mechanisms of diffusion

Diffusion occurs by means of molecular-scale entities moving sporadically over distances and directions determined by the internal structure of the material. These erratic motions are considered as elements of constrained random walks (limited to few directions, precisely specified by the material crystallography), because the probability of a motion occurring in a given direction and distance is biased by details of the material ultrastructure and the interatomic forces (Glicksman, 2000). However, the hypothesis of random walk (independence of the successive jumps) is not always appropriate, since the successive jumps of a particle can be, or not independent, depending on the nature of the particle and the jump mechanism. When these motions are not independent, the jumps are called correlated (cf Section 4.2.3); the jump frequencies of the particle in the different jump directions deviate from the probabilities calculated on the basis of a purely random walk, and the deviations depend on the nature of the preceding jump (Philibert, 1988). Figure 4.2 recalls the most simple mechanism by which migration can take place.

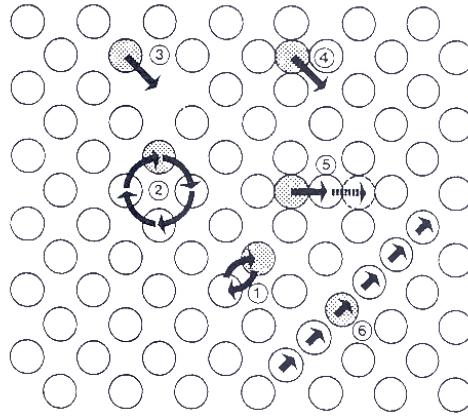


Figure 4.2: Scheme of the principal diffusion mechanisms: 1) direct exchange, 2) ring mechanism, 3) vacancy mechanism, 4) interstitial mechanism, 5) interstitialcy mechanism, 6) crowdion; from Philibert (1988).

4.2.1 Atomic analysis of diffusion

The analysis of random walk is not a simple problem, since it requires to go back and forth between the observed macroscopic diffusion coefficients and the jump frequencies and jump distances of the diffusing atoms. This analysis transforms the study of diffusion from the question of how fast a system will homogenise into the construction of a tool for studying the atomic processes involved in a variety of reactions in solids, and for studying defects in solids (Shewmon, 1989). In fact the atomic theory of diffusion provides an expression for the diffusive flux J of a foreign- or a self-atom as proportional to:

- the concentration gradient (assuming that concentration varies slowly w.r.t. the position),
- the diffusion coefficient D , itself basically dependent on
 - a geometrical factor g dependent on the crystallographic nature of the lattice,
 - the probability ω that a given atom (being an interstitial or a lattice site) will jump to a neighbour site,
 - the probability p that a particular diffusion mechanism occurs at this neighbour site (cf next paragraph).

The flux of the defect A (in a lattice X) hence writes as

$$\text{Fick's law:} \quad J_{AX} = -D_{AX}\nabla C_A,$$

where

$$D_{AX} = g_{AX}\omega_{AX}p_{AX} \quad (4.2.1)$$

is in general a second rank tensor depending essentially on temperature. For *self-diffusion*, ie the migration of a self-interstitial atom I, the coefficients write as D_I, g_I, ω_I and p_I . By the conservation of these migrating self-atoms, the diffusion of I implies the diffusion of its counterpart defect, the vacancy V, for which D_V, g_V, ω_V and p_V symbols are used. Self-diffusion and the particular diffusion mechanisms involved at the atomic scale are briefly described in Section 4.2.3.

4.2.2 General expression for the flux and the diffusion equation

The flow of particles within the medium can, in fact, be due to two causes: one is the effect of a concentration gradient, and the other one is the action of a driving force. Under the influence of such an external force the particles move with a certain average velocity \bar{v} , which gives rise to a flux $\bar{v}C$. Thus the general expression for the flux is (Philibert, 1988):

$$J = -D\nabla C + \bar{v}C, \quad (4.2.2)$$

where the first term on the right-hand side is called the Fickian flux and the second term the drift (or mass flow). The general diffusion equation (with respect to the crystal) is a second-order partial differential equation reading as

$$\frac{\partial C}{\partial t} = -\nabla \cdot J = \nabla \cdot (D\nabla C - \bar{v}C). \quad (4.2.3)$$

The relation between drift and diffusion is provided by the so-called *Nerst-Einstein* equation

$$\frac{\bar{v}}{D} = \frac{F}{k_b T}, \quad (4.2.4)$$

where F is a driving force, whose nature and analytical expression can only be determined from an analysis governed by the thermodynamics of irreversible processes (Philibert, 1988). In bulk crystal growth, thermal diffusion turns out to be a non-negligible phenomenon (see Section 4.7.2) modelled as a driving thermomigration force given by

$$F = -\frac{Q^*}{T}\nabla T = Q^*T\nabla\frac{1}{T}, \quad (4.2.5)$$

where the significance of the heat of transport Q^* is not obvious at all (cf Section 4.7 and Philibert (1988)).

It should be noted that Fick's law appears as presenting some limits since it is written for a continuous medium and hence neglects the discontinuous structure of real materials (which include dislocations), and since, for short times or in the presence of a large gradient, the linear equation seems to represent a gross oversimplification (Philibert, 1988).

4.2.3 Basic features of bulk diffusion in silicon crystals

Diffusion of intrinsic point-defects in silicon has been extensively studied since it has major influence on their aggregation into grown-in defects. Moreover, self-interstitials and vacancies control the diffusion of dopants which is an important process in device manufacturing. The conceptually simplest mechanisms of bulk diffusion in crystals are the so-called *direct mechanisms* (labeled "1", "2" and "4" on Fig. 4.9), where the interstitial mechanism ("4") is presumably responsible for the diffusion of foreign atoms (such as hydrogen for instance) in silicon, while the two others have not been observed so far (Frank and Gösele, 1984.). By contrast, *indirect diffusion* of self- or foreign-atoms requires intrinsic defects as diffusion vehicles. The best known indirect diffusion mechanisms are the *vacancy mechanism* (labeled "3" on Fig. 4.9) which controls self-diffusion in silicon below about 1270 [K]. The counterpart of the vacancy mechanism is the interstitialcy (or *kick-out mechanism*) which dominates self-diffusion in silicon above about 1270 [K] and plays a prominent role in the diffusion of several substitutional solutes (such as boron or gallium for instance) (Frank and Gösele, 1984.). Notice that *self-diffusion* is precisely the simultaneous combination of these two mechanisms (cf Section 4.2.3). The general mechanisms of bulk diffusion in crystals should include the formation of, and migration to or from point-defects aggregates such as "clusters" and "voids". Since their formation occurs at low temperature, the preceding simple and isolated mechanisms can be considered as predominant near and above the solid-liquid solidification interface.

For this reason, it should be remarked that microdefect simulations should be performed by employing time-dependent models, since transient mechanisms play a key role in the crystal upper part, where microdefects are forming (cf Section 4.5).

Vacancy mechanism and vacancy diffusivity

J. Frenkel introduced the concept of lattice vacancy in the early 1940s, which progressively became accepted as one of the most important forms of thermally induced

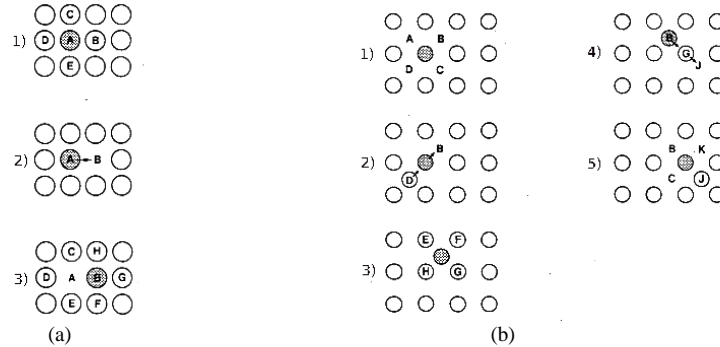


Figure 4.3: Successive jumps for the vacancy (a) and kick-out mechanisms (b). In the case of a tagged (tracer) atom (dashed point) these jumps are correlated; from Philibert, 1988.

equilibrium lattice defects in crystals (Glicksman, 2000). If a lattice site is not occupied, a nearest-neighbour atom (ie a lattice or a substitutional impurity atom) can jump onto this site, and the vacancy will appear on the site the atom has just vacated (Philibert, 1998). The vacancy itself diffuses by this *vacancy mechanism* to the opposite direction of the lattice atom (Figs. 4.3(a) and 4.2). Large-size dopants (such as antimony) in silicon diffuse predominantly via vacancies (Dornberger, 1998).

Lattice vacancies may be of thermal or stoichiometric origin (see Section 4.1.1). The interchange of a vacancy with one of its nearest-neighbour atoms requires local distortion of the lattice (see Fig. 4.4), the activation volume ΔV_V^m of which is a measure of the lattice dilation that accommodates the exchange between the diffuser and the vacancy. Note that activation volumes for vacancy-atom interchanges are typically several percents of the atomic volume, in such a way that the distortion energy is large compared with the strain energy caused by interstitial motion of light atoms (Glicksman, 2000). On the other hand, a *Helmoltz free energy* ΔF_V^m is required for reaching the activated state from the ground state, in such a way that the *Gibbs free energy of activation* reads (for a system at constant pressure P) $\Delta G_V^m = P\Delta V_V^m + \Delta F_V^m$ (Philibert, 1998). In a crystal of a pure element, the vacancy can jump toward any of its nearest-neighbour at any time; its successive jumps are indeed independent of each other, in such a way that $p_V=1$ and hence Eq. (4.2.1) reads as $D_V = g_V \omega_V$, where g_V is a factor taking into account the lattice constant, the fine geometry of the lattice structure and atomistic details of the diffusion process (Frank and Gösele, 1984) and where $\omega_V = \nu_V \exp(-\Delta G_V^m/k_b T)$ with ν_V , the *Debye frequency*. More refined models provide an additional activation entropic term taking into account the difference between the entropies of vibration of the ground- and activated states (Philibert, 1998).

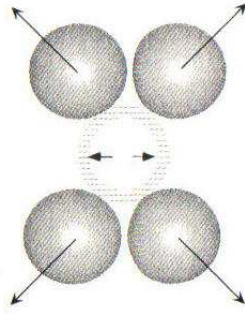


Figure 4.4: Local lattice distortion and activation volumes for vacancy-atom interchanges; from Glicksman (2000).

Kick-out mechanism and interstitial diffusivity

If an atom jumps from interstitial to interstitial site, this interstitial point-defect is said to diffuse by the direct interstitial mechanism (labeled “4” in Fig. 4.2) (Philibert, 1998). If the atom may, as pictured in the “5” th mechanism of Fig. 4.2, jump either to a substitutional or an interstitial position, the atom diffuses by a *kick-out mechanism*. Contrarily to the vacancy, this lattice defect is not well localised, but spreads out among a number of align atoms (cf Fig. 4.2) (Glicksman, 2000). The interchange quasi-chemical reaction involving self-interstitials (or a foreign atom such as Au in a silicon for instance, cf Frank and Gösele (1984) reads as



where A_s and A_i denote the self- (or foreign-) interstitial in substitutional and interstitial position, respectively. From left to right and right to left, reaction Eq. 4.2.6 corresponds to the filled and to the dashed arrow of mechanism “5” on Fig. 4.2, respectively. Notice that the real situation is somewhat more complex than what the drawing of Fig. 4.2 suggests because the jumps of the two atoms are not necessarily collinear (Philibert, 1988). The activation energy ΔG_I^m for an interstitial is higher than for a vacancy since it requires the same energy as for vacancy migration (by Eq. (4.1.2)) plus an additional amount accounting for the interstitial to “kick-out” a lattice atom by the kick-out reaction (4.2.6). In a crystal of a pure element, the probability for a self-interstitial with enough free energy to kick-out one of its neighbours is $p_I=1$, while $\omega_I = \nu_I \exp(-\Delta G_I^m/k_b T)$ with the Debye frequency ν_I .

Non-dimensional expression of point-defects diffusivities

Let the temperature-dependent migration (or activation) enthalpies and entropies be given by the linear expressions $H_{I,V}^m = H_{I,V}^{m0} + H_{I,V}^{m1}T$ and $S_{I,V}^m = k_b (S_{I,V}^{m0} + S_{I,V}^{m1}T)$, respectively. Define the effective enthalpies and entropies as

$$\begin{aligned}\bar{H}_{I,V}^m &= H_{I,V}^{m0} + k_b S_{I,V}^{m1} T_m^2, \\ \bar{S}_{I,V}^m &= S_{I,V}^{m1} T_m,\end{aligned}$$

in such a way that in a non-dimensional form, these diffusivities write as

$$D_{I,V}^m = D_{I,V}^{m0} \exp \left[-\frac{\bar{H}_{I,V}^m}{k_b T_m} \left(\frac{T_m}{T} - 1 \right) \right], \quad (4.2.7)$$

where the different parameters are given in a comparison table in Section 4.4 compiled with data from the crystal-growth literature.

Coupled dissociative mechanism

The typical coupled mechanism for self- or foreign- diffusion in silicon is the so-called *dissociative mechanism* involving substitutional, interstitial and vacant lattice sites according to the law



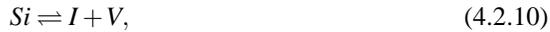
which in the case of self-diffusion in silicon is nothing else than the Frenkel reaction Eq. (4.1.2).

Self-diffusion

Self-diffusion means the diffusion of an Si self-atom in a silicon lattice both by the kick-out mechanism



and by the Frenkel reaction



which shows that supersaturation of self-interstitials cannot be maintained without the undersaturation of vacancies, and vice-versa. If the Frenkel reaction were instantaneous (which is not the case, even at high temperature, in view of the presence of

a barrier against self-interstitial–vacancy recombination and a high activation barrier against the spontaneous formation of Frenkel pairs in the bulk (Frank and Gösele, 1984), reaction Eq. (4.2.10) would maintain the local equilibrium:

$$C_I C_V = C_I^{eq} C_V^{eq}. \quad (4.2.11)$$

Note that high recombination rates, leading Eq. (4.2.11) to be very approximately satisfied, are enhanced by the presence of dislocations and micro-defects. Moreover, in experiments involving high dislocation densities, kick-out and Frenkel reactions can hardly be distinguished (Frank and Gösele, 1984). By incorrect custom the diffusion of an isotope Si^* , usually, but not necessarily radioactive, is referred to as self-diffusion (Philibert, 1988). In this case however, the probabilities p_V^* or p_I^* for vacancy- or interstitial-assisted diffusion to occur are equal to the probability that Eqs. (4.2.6) or (4.2.8) take place, respectively, and hence that Si^* finds a vacancy or an interstitial as neighbour, in such a way that $p_V^* = \exp(-\Delta G_V^f)/(k_b T)$ and $p_I^* = \exp(-\Delta G_I^f)/(k_b T)$. Therefore the tracer self-diffusion coefficient under thermal equilibrium writes as

$$D^T = \sum_{K=I,V} f_K g_K v_K \exp(-\Delta G_K^{SD}/k_b T) = \sum_{K=I,V} f_K D_K C_K^{eq}, \quad (4.2.12)$$

where $\Delta G_K^{SD} = \Delta G_K^f + \Delta G_K^m$ while f_K with $K = I, V$ denotes the correlation factors, allowing for the fact that successive vacancy or interstitial jumps are not independent (cf Fig. 4.2.3), noting in passing that correlation factors for interstitials are slightly more intricate to compute than for vacancies (Philibert, 1988). Following Frank and Gösele (1984), Bracht et al. (1995), and Lerner and Stolwijk (2005), by carefully analysing available data for diffusion of foreign atoms in silicon, it is possible to separate the contributions $D_V C_V^{eq}$ and $D_I C_I^{eq}$ but not to split the factors of $D_K C_K^{eq}$ (Frank and Gösele, 1984).

This remark will appear as crucial in Section 4.7.2, where a new material data set with higher equilibrium concentrations and lower diffusivities will be confronted to the classical values used in the crystal growth community.

4.2.4 The physics of thermo-diffusion

In Section 4.2.2 the Fick's law of diffusion was introduced as a postulate, while the drift terms were added without justifying the nature of the driving forces. Since diffusion is by nature an irreversible process, it is the Thermodynamics of Irreversible Processes that should provide a complete and general approach to the problem (Philibert, 1988; Degroot and Masur, 1984). Let us here analyse the case of the diffusion of vacancies and self-interstitials in a pure silicon crystal. The rate of entropy creation in this case writes as $\sigma = J_q X_q + J_I X_I + J_V X_V$, where $J_{I,V}$ are the interstitial and vacancy

fluxes [$\text{m}^{-2}\text{s}^{-1}$] (expressed in a frame of reference moving with an average atomic velocity (Philibert, 1988)), verifying, by Frenkel reaction, the relation $J_I + J_V = 0$. The term J_q denotes the heat flux while $X_{I,V}$ and X_q are the thermodynamic forces associated to the interstitial, vacancy and heat fluxes. It results that, for a vacancy-assisted diffusion of interstitials, $\sigma = J_q X_q + J_I (X_I - X_V)$ and hence that the fluxes are written in terms of the assumed linear Onsager relations (cf eg Degroot and Masur (1984)) as

$$J_I = V^{-1} (L_{II} (X_I - X_V) + L_{Iq} X_q) \quad (4.2.13)$$

$$J_V = V^{-1} (L_{VI} (X_I - X_V) + L_{Vq} X_q) \quad (4.2.14)$$

$$J_q = V^{-1} (L_{qI} (X_I - X_V) + L_{qq} X_q), \quad (4.2.15)$$

where L_{AB} are called the ‘‘phenomenological coefficients’’, whose diagonal terms have the meaning of defect mobility and thermal conductivity, while the off-diagonal terms describe interaction phenomena such as thermomigration (Philibert, 1988) and V here denotes the volume of the crystal (not to be confused with the same symbol used to denote vacancies). Moreover, the forces are classically written as

$$X_{I,V} = -\nabla \frac{\mu_{I,V}}{T} = -\frac{\nabla_T \mu_{I,V}}{T} - h_{I,V} \nabla \frac{1}{T} \quad (4.2.16)$$

$$X_q = \nabla \frac{1}{T}, \quad (4.2.17)$$

where $h_{I,V} = -\frac{(\partial \mu_{I,V} / \partial T)_T - \mu_{I,V}}{T^2}$, and with the chemical potentials ²

$$\mu_{Si,I,V} = \mu_{Si,I,V}^0 + k_b T \log N_{Si,I,V},$$

where n_V represents the number of vacancies contained in the crystal, while the total number of atoms is $n = n_{Si} + n_I + n_V$ with n_{Si} , the number of lattice atoms, and $n_{I,V}$ the number of interstitial and vacancies, respectively. Moreover $N_{Si,I,V}$ will denote the density $\frac{n_{Si,I,V}}{n}$. Let us now briefly analyse the case of thermo diffusion of interstitials by the vacancy mechanism. Therefore we introduce the chemical potential of lattice atoms, denoted as μ_{Si} with $N_{Si} \simeq 1$ and consider a region of oversaturation of interstitials, in such a way that μ_{Si}^0 and μ_I^0 can be assumed as independent of the concentration and hence such that $\nabla_T \mu_{Si} \simeq \nabla_T \mu_{Si}^0 = \nabla_T \mu_I^0 = 0$, while

$$\nabla_T \mu_I = \frac{k_b T}{N_I} \nabla_T N_I. \quad (4.2.18)$$

On the other hand, if the density of vacancy sources and sinks is high enough, that is, under the assumption of instantaneous equilibrium, it results that

$$\mu_V = 0 = \nabla_T \mu_V. \quad (4.2.19)$$

²The chemical potential of a thermodynamic system is the amount by which the Gibbs free-energy of the system would change if an additional particle were introduced, with temperature and pressure held fixed, i.e. $\mu_V := \frac{\partial G}{\partial n_V} |_{T,p}$.

Then, for a vacancy-assisted diffusion of interstitials, and from the linear assumption (Philibert, 1984) that

$$L_{Iq} = L_{II}Q_I^* \quad \text{and} \quad L_{Vq} = L_{VV}Q_V^*, \quad (4.2.20)$$

where the “heats of transport” $Q_{I,V}^*$ are introduced, ie, the contribution of the heat flux to the I- and V fluxes, respectively, it results from Eqs. (4.2.16)-(4.2.20) that

$$\begin{aligned} J_I &= \frac{1}{V} (L_{II} (X_I - X_V) + L_{Iq} X_q) = \frac{1}{V} \left(-\frac{1}{T} \nabla_T (\mu_I - \mu_V) L_{II} + \nabla \frac{1}{T} (L_{Iq} - h_I + h_V) \right) \\ &= \frac{L_{II}}{V} \left(-\frac{k_b}{n_I} \nabla_T n_I + \nabla \frac{1}{T} (Q_I^* - h_I + h_V) \right). \end{aligned}$$

It can be shown (Philibert, 1984) that the diffusion coefficients write as

$$L_{II} = \frac{n_I}{k_b} D_I \quad \text{and} \quad L_{VV} = \frac{n_V}{k_b} D_V,$$

in such a way that

$$J_I = -D_I \nabla_T C_I + C_I D_I Q_I^{**} \nabla \frac{1}{T}, \quad (4.2.21)$$

where the *reduced heat of transport* Q_I^{**} for interstitials has been defined.

For the diffusion of vacancies, the roles are inverted with respect to the previous analysis, in the sense that now self-interstitial and lattice atoms in thermodynamic equilibrium are associated with for (oversaturated) vacancy diffusion. The vacancy flux writes as

$$J_V = \frac{L_{VV}}{V} \left(-\frac{k_b}{n_V} \nabla_T n_V + \nabla \frac{1}{T} (Q_V^* - \mu_V + \mu_I) \right),$$

and hence

$$J_V = -D_V \nabla_T C_V + C_V D_V Q_V^{**} \nabla \frac{1}{T}. \quad (4.2.22)$$

Following (Philibert, 1984) very little is known either about the theoretical or about the experimental values of the reduced heats of transport $Q_{I,V}^{**}$.

Although in the crystal growth literature (cf eg Sinno et al. (1998), Ebe (1999), Voronkov and Falster (2002)) controversial values and signs are used for $Q_{I,V}^{**}$, it is however generally accepted that, in absolute value, the reduced heats of transport should not exceed the formation enthalpies. Most often these quantities are neglected in point-defect models.

4.3 Model equations and asymptotic analysis

Since the equilibrium concentrations, point-defect diffusivities and recombination rates depend on temperature, the simulation model has two aspects. A first key issue relates to the thermal modelling of the crystal, including the effect of melt convection in the liquid phase and radiation in overall the furnace, as briefly recalled in Section 4.3.1. On the other hand, the model equations for point-defects transport, diffusion and recombination follow the discussion of Sections 4.1 and 4.2 and will be given in Section 4.3.1, while time-dependent simulations will be performed and discussed in Section 4.5. Let us recall that, as the concentrations of intrinsic point-defects are lower than $10^{-6}/m^3$, the equilibrium concentrations, diffusivities and recombination rates can be assumed as independent of concentration. Therefore, any cross effects are neglected, and point-defect and thermal simulations can be decoupled, in such a way that C_I^{eq} , C_V^{eq} and K_{IV} are calculated (cf Tables 4.2 & 4.3) by using the temperature distributions obtained from the thermal simulations (Dornberger, 1998). Moreover, let us remark that thermodiffusion of intrinsic point-defects has been neglected in the thermal model, but is not a priori negligible in the point-defect model, as shown in Section 4.7.

4.3.1 Thermal and point-defect models

A key role is played by the thermal modelling of the crystal growth process, developed by N. Van den Bogaert and F. Dupret (1997) and further discussed by Dornberger (1998). Using the FEMAG simulation software, fully time-dependent numerical simulations have been performed in order to predict the global heat transfer in the furnace, the solid-liquid interface shape, and the resulting distribution of self-interstitials and vacancies in the crystal. All the system transients have been accurately taken into account including the effects of crystal and crucible vertical motion, of the heat capacity of the furnace constituents, of the solidification front thermal inertia, and of the inherently time-dependent defect governing laws. In order to accelerate the simulation computing time, the effect of the melt flow on the heat transfer has been modelled by means of an equivalent thermal conductivity, which is devoted to sum up in a simplified way the contributions of (i) heat convection, (ii) convective heat mixing, and (iii) heat diffusion (cf Section 4.6). More accurate results could be obtained by using a detailed turbulent flow model provided good model tuning be performed. Global time-dependent simulations have been performed to calculate the heat transfer on this basis. However only the results obtained inside the crystal are shown on Fig. 4.5. The following parameters were used:

- Pull rate: 0.53 mm/min

- Crystal diameter: 150 mm (6")
- Melt equivalent thermal conductivity: 110 W/mK.

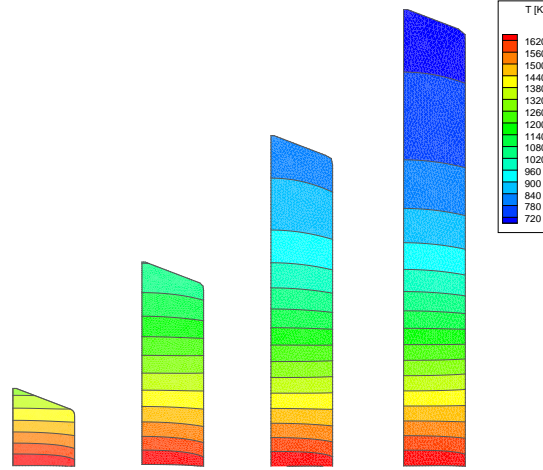


Figure 4.5: Temperature field in the crystal at several growth stages.

On the other hand, a system of *transport-diffusion-reaction* PDE's (henceforth called the *Sinno-Dornberger model* for point-defect simulation) has been shown to be adapted for our purpose. Details for the construction of this model have been discussed in Sections 4.1 and 4.2. The model writes as

$$\frac{DC_I}{Dt} = \nabla \cdot \left(D_I \nabla C_I + \frac{Q_I^{**} D_I}{k_b T^2} C_I \nabla T \right) - K_{IV} (C_I C_V - C_I^{eq} C_V^{eq}), \quad (4.3.1)$$

$$\frac{DC_V}{Dt} = \nabla \cdot \left(D_V \nabla C_V + \frac{Q_V^{**} D_V}{k_b T^2} C_V \nabla T \right) - K_{IV} (C_I C_V - C_I^{eq} C_V^{eq}) \quad (4.3.2)$$

where subscripts I and V indicate self-interstitials or vacancies, respectively, while C_I^{eq} and C_V^{eq} denote the corresponding equilibrium concentrations. Let us recall that the kinetic coefficient K_{IV} associated with the Frenkel recombination mechanism writes as

$$K_{IV} = K_{I,V}^m \frac{D_I + D_V}{D_I^m + D_V^m} \exp \left[-\frac{\bar{H}^r}{k_b T_m} \left(\frac{T_m}{T} - 1 \right) \right], \quad (4.3.3)$$

the Fickian diffusivities as

$$D_{I,V} = D_{I,V}^m \exp \left[-\frac{\bar{H}_{I,V}^m}{k_b T_m} \left(\frac{T_m}{T} - 1 \right) \right], \quad (4.3.4)$$

and the equilibrium concentrations (where referring to the general expression of Section 4.1.1, the entropic term has here been dropped) as

$$C_{I,V}^{eq} = C_{I,V}^m \exp \left[-\frac{\bar{H}_{I,V}^f}{k_b T_m} \left(\frac{T_m}{T} - 1 \right) \right]. \quad (4.3.5)$$

Moreover, symbols ∇ and

$$\frac{D}{DT} = \frac{\partial}{\partial t} + V \frac{\partial}{\partial z}$$

denote the gradient and material derivation operators (with z indicating the vertical direction), and k_b the Boltzmann constant ($k_b = 8.61 \cdot 10^{-5}$ [eV/K]), while $Q_{I,V}^{**}$ stands for the reduced heats of transport associated with interstitial or vacancy thermo-diffusion (or thermal drift) whose precise meaning has been discussed in Section 4.7. The boundary conditions are of two kinds. Along the solidification interface, equilibrium concentrations are imposed, while the concentration normal fluxes are set to zero along the crystal wall (equilibrium concentrations should normally be imposed in this latter case in order to account for the Schottky defect generation mechanism; however this will generate unacceptably thin and sharp concentration boundary layers along the crystal wall, and hence this effect is here neglected without significant loss of accuracy in the remaining domain). To facilitate model comparisons, it is of the utmost importance to use unambiguous expressions of the coefficients $C_{I,V}^{eq}$, D_{iv} , and K_{IV} as a function of temperature. This is the role of the material data compilation of Tables 4.2 & 4.3.

4.3.2 Matched asymptotic analysis

The following sections aim at rewriting the model equations in a non-dimensional form in order to determine by means of matched asymptotic analysis (cf eg Bender & Orzac) three regions in the crystal, each of which being affected by particular PD evolution mechanisms. The original idea for this development arise from the work of Voronkov (1982).

To this end, Eqs. (4.3.1) & (4.3.2) will be analysed in a 1D semi-infinite simplified geometry ($0 \leq z < \infty$) and under the quasi-steady assumption. Therefore we set

$$\frac{D}{Dt} = V \frac{\partial}{\partial z}, \quad (4.3.6)$$

while from the 1D assumption,

$$\nabla = \partial_z. \quad (4.3.7)$$

Non dimensional variables and numbers

Define the variables

$$\Delta := C_I - C_V \quad (4.3.8)$$

$$\Pi := C_I C_V > 0 \quad (4.3.9)$$

$$\Pi^{eq} := C_I^{eq} C_V^{eq} > 0 \quad (4.3.10)$$

and the constant

$$\Pi_m^{eq} := C_I^m C_V^m > 0, \quad (4.3.11)$$

and introduce the dimensionless variables

$$C'_{I,V} := \frac{C_{I,V}}{\Pi_m^{eq1/2}} > 0 \quad (4.3.12)$$

$$C'^{eq}_{I,V} := \frac{C^{eq}_{I,V}}{\Pi_m^{eq1/2}} > 0 \quad (4.3.13)$$

$$\Delta' := C'_I - C'_V \quad (4.3.14)$$

$$\Pi' := C'_I C'_V > 0, \quad (4.3.15)$$

in such a way that

$$C'_I = \Delta'/2 + (\Delta'^2/4 + \Pi')^{1/2} \quad (4.3.16)$$

$$C'_V = -\Delta'/2 + (\Delta'^2/4 + \Pi')^{1/2} \quad (4.3.17)$$

$$C'_I + C'_V = (\Delta'^2 + 4\Pi')^{1/2}. \quad (4.3.18)$$

In view of the forthcoming developments, introduce also the two dimensionless variables

$$\xi := \frac{-\Delta}{2\Pi_m^{eq1/2}} \quad \text{and} \quad (4.3.19)$$

$$\tau := \frac{\bar{H}_I^f + \bar{H}_V^f}{k_b T_m} \left(\frac{T_m}{T} - 1 \right), \quad (4.3.20)$$

in such a way that

$$C'^{eq}_{I,V} = C'^m_{I,V} e^{-\tau/2} \quad (4.3.21)$$

$$\Pi^{eq} = \Pi_m^{eq} e^{-\tau} > 0. \quad (4.3.22)$$

It will be firstly assumed that $\tau \in [0; \infty[$, while this hypothesis will be discussed at a later stage. Moreover, $D_{I,V} = D_{I,V}^m e^{-P_{I,V}\tau}$, while the following definitions introduce

non-dimensional material numbers³:

$$p_{I,V} := \frac{\overline{H}_{I,V}^m}{\overline{H}_I^f + \overline{H}_V^f} > 0, \quad (4.3.23)$$

$$p^r := \frac{\overline{H}^r}{\overline{H}_I^f + \overline{H}_V^f} \quad \text{here assumed } > 0, \quad (4.3.24)$$

$$q_{I,V} := \frac{-Q_{I,V}^{**}}{\overline{H}_I^f + \overline{H}_V^f} = \hat{r}_{I,V} p_{I,V}, \quad (4.3.25)$$

$$d_{I,V} := \frac{D_{I,V}^m}{D_I^m + D_V^m} > 0, \quad \text{with } d_I + d_V = 1. \quad (4.3.26)$$

Moreover, G denotes the norm of the axial temperature gradient at the interface, with

Refs	I, V	$p_{I,V}$	p^r
Sinno et al. (1998)	I	0.121	$0 < p^r < 1$
Sinno et al. (1998)	V	0.059	
Kulkarni et al. (2004)	I	0.112	$0 < p^r < 1$
Kulkarni et al. (2004)	V	0.05	

Table 4.1: Non-dimensional coefficients.

$$\gamma(z) := \frac{d(1/T)}{dz} \quad (4.3.27)$$

where $\gamma(0) = G/T_m^2 > 0$, while $\tilde{\gamma}(\tau)$ is defined from the relation

$$\gamma(z) = -\frac{1}{T^2} \frac{dT}{dz} = \tilde{\gamma}(\tau) \frac{G}{T_m^2}, \quad (4.3.28)$$

and is assumed to be regular, bounded between 2 positive constants, and such that $\lim_{\tau \rightarrow 0} \tilde{\gamma} = \tilde{\gamma}_0$, while its asymptotic behaviour for $z \rightarrow \infty$ will be discussed later.

The characteristic distance L is introduced as

$$L := \frac{k_b T_m}{\overline{H}_I^f + \overline{H}_V^f} \frac{T_m}{G}, \quad (4.3.29)$$

which using the the current SD model parameter, is estimated as being of the order 1 [cm]. It can be observed on Fig.4.5 that the “effective” characteristic length is about 5

³The value of p^r can be negative together with \overline{H}^r at melting temperature if a second-degree expression of the recombination rate of the form Eq. (4.1.4) is assumed instead of Eq. (4.3.3). However the higher-order terms will force the average exponent in Eq. (4.3.3) to become negative in the range of about 200K-400K below the melting temperature. This is why, to simplify the analysis without losing any significant effect, it is here assumed that p^r is positive while the higher-order terms are set to zero.

[cm]. Moreover, it results that

$$\frac{\partial}{\partial z} = \frac{\tilde{\gamma}(\tau)}{L} \frac{\partial}{\partial \tau}. \quad (4.3.30)$$

Finally, since $\frac{1}{T} - \frac{1}{T_m} = \frac{G}{T_m^2} z$, let us note that the physical meaning of L can be understood by observing that

$$L^{-1} = -\frac{d \log(C_I^{eq} C_V^{eq})}{dz}. \quad (4.3.31)$$

4.3.3 Non dimensional equations

Transport term. From Eqs. (4.3.1)-(4.3.2), (4.3.6), (4.3.22), and (4.3.30), this term writes as

$$V \partial_z C_{I,V} = \frac{V \tilde{\gamma}}{L} \Pi_m^{eq1/2} \partial_\tau C'_{I,V}$$

Self-diffusion term. From Eqs. (4.3.1)-(4.3.2), (4.3.7), (4.3.22), (4.3.23), (4.3.26), and (4.3.30) this term writes as

$$\partial_z (D_{I,V} \partial_z C_{I,V}) = \frac{\tilde{\gamma}}{L^2} \Pi_m^{eq1/2} d_{I,V} (D_I^m + D_V^m) \partial_\tau [\tilde{\gamma} e^{-p_{I,V} \tau} \partial_\tau C'_{I,V}]$$

Thermo-diffusion term. From Eqs. (4.3.1)-(4.3.2), (4.3.7), (4.3.22), (4.3.23), (4.3.26), (4.3.25) and (4.3.30) this term writes as

$$\begin{aligned} \partial_z \frac{Q_I^{**} D_{I,V} C_{I,V} \nabla T}{k_b T^2} &= \frac{\tilde{\gamma}}{L} \frac{G}{k_b T_m^2} q_{I,V} (\bar{H}_I^f + \bar{H}_V^f) \\ &\quad \cdot d_{I,V} (D_I^m + D_V^m) \Pi_m^{eq1/2} \partial_\tau [\tilde{\gamma} \exp(-p_{I,V} \tau) C'_{I,V}] \end{aligned}$$

Recombination term. From Eqs. (4.3.1)-(4.3.2), (4.3.26), (4.3.22), (4.3.24) and (4.3.30) this term writes as

$$\begin{aligned} -K_{IV}^m \frac{D_I + D_V}{D_I^m + D_V^m} \exp(-p^r \tau) (C_I C_V - C_I^{eq} C_V^{eq}) &= -K_{IV}^m \\ (d_I e^{-p_{I,V} \tau} + d_V e^{-p_V \tau}) \Pi_m^{eq} e^{-p^r \tau} (C_I' C_V' - e^{-\tau}). \end{aligned}$$

After simplification by $\frac{\tilde{\gamma}}{L} \Pi_m^{eq1/2}$ and division by $\frac{D_I^m + D_V^m}{L}$, with use of Eq. (4.3.29) and after introduction of the previous non-dimensional parameters, key dimensionless numbers are defined as follows:

The thermal Peclet number represents the ratio of transport over diffusion of I or V, as measured in $1/T$ scale, and writes as

$$Pe_T := \frac{V}{G} \frac{1}{2(D_I^m + D_V^m)} \frac{k_b T_m^2}{\bar{H}_{IV}} = \frac{VL}{D_I^m + D_V^m}, \quad (4.3.32)$$

where $\bar{H}_{IV} := \frac{\bar{H}_I^f + \bar{H}_V^f}{2}$. With the current parameters, Pe is estimated as being $O(1)$.

The Damkohler number represents the ratio of recombination over diffusion effects, and writes as

$$Da := \frac{K_{IV}^m L^2 \Pi_m^{eq1/2}}{D_I^m + D_V^m}. \quad (4.3.33)$$

With the current parameters, it is estimated as being of the order $O(1000)$.

Finally, the complete non-dimensional equations write as follows.

Non dimensional equations. The complete non dimensional equations write as

$$\begin{aligned} Pe_T \partial_\tau C'_{I,V} &= d_{I,V} \partial_\tau [\tilde{\gamma} e^{-p_{I,V} \tau} (\partial_\tau C'_{I,V} + q_{I,V} C'_{I,V})] \\ &- \frac{Da}{\tilde{\gamma}} (d_I e^{-p_I \tau} + d_V e^{-p_V \tau}) e^{-p^r \tau} (C'_I C'_V - e^{-\tau}). \end{aligned} \quad (4.3.34)$$

It is also interesting for the forthcoming analysis to express the evolution equations in terms of Δ' and Π' .

General Δ' equation. Without any limiting assumption on the recombination rate, Eq. (4.3.34) provides by a simple subtraction of the I and V equations, the so-called Δ' -equation:

$$\begin{aligned} Pe_T \partial_\tau \Delta' &= d_I \partial_\tau \tilde{\gamma} e^{-p_I \tau} [\partial_\tau C'_I + q_I C'_I] \\ &- d_V \partial_\tau \tilde{\gamma} e^{-p_V \tau} [\partial_\tau C'_V + q_V C'_V], \end{aligned} \quad (4.3.35)$$

where the concentrations C'_I, C'_V are given in terms of Δ' and Π' by means of Eqs. (4.3.16) & (4.3.17).

General Π' equation. Multiplying the I equation by C'_V and the V equation by C'_I , the summation of the two resulting equations provides the so-called Π' -equation:

$$\begin{aligned} Pe_T \partial_\tau \Pi' &= d_I C'_V \partial_\tau \tilde{\gamma} e^{-p_I \tau} [\partial_\tau C'_I + q_I C'_I] + d_V C'_I \partial_\tau \tilde{\gamma} e^{-p_V \tau} \\ &\cdot [\partial_\tau C'_V + q_V C'_V] - \frac{Da}{\tilde{\gamma}} (d_I e^{-p_I \tau} + d_V e^{-p_V \tau}) \\ &\cdot e^{-p' \tau} (\Pi' - e^{-\tau}) (C'_I + C'_V), \end{aligned} \quad (4.3.36)$$

where the concentrations are given in terms of Δ' and Π' by means of Eqs. (4.3.16)-(4.3.18).

Boundary conditions. Since the problem is 1D, the melting interface boundary conditions write as:

$$C'_{I,V}(\tau = 0) = C'^m_{I,V} \quad (4.3.37)$$

In theory, since Eqs. (4.3.34) or Eqs. (4.3.35)-(4.3.36) are both of the second-order, an additional pair of boundary conditions should be given at the other extremity of the 1D domain. However, as an infinite domain is assumed, infinite limits of $C'_{I,V}$ for $\tau \rightarrow \infty$ might be considered, as associated with non-physical but mathematically constant defect distributions. To avoid these situations, it is simply imposed that

$$\lim_{\tau \rightarrow \infty} C'_{I,V} \quad (4.3.38)$$

exists, while the value of the limits will be discussed in the following section.

4.3.4 Alternative temperature gradient assumptions.

Write

$$G = \frac{T_m - T_\infty}{z_0}, \quad (4.3.39)$$

in Eq. (4.3.28) in such a way that

$$\tilde{\gamma} := -\frac{T_m^2 z_0}{T^2 (T_m - T_\infty)} \frac{dT}{dz}. \quad (4.3.40)$$

Bounded and decreasing temperature field. Consider, as an example, the following temperature distribution

$$T = T_\infty + 2 \frac{T_m - T_\infty}{\frac{z}{z_0} + 1},$$

which satisfies Eq. (4.3.39) and exhibits a horizontal asymptote when $z \rightarrow \infty$. From Eq. (4.3.20), it results that

$$\frac{z}{z_0} = \frac{\tau T_m}{K(T_m - T_\infty) - \tau T_\infty},$$

with $K = \frac{\bar{H}_I^f + \bar{H}_V^f}{k_b T_m}$. The general formula

$$\tau = K \frac{T_m - T}{T}. \quad (4.3.41)$$

defines

$$\tau_{max} = \frac{K(T_m - T_\infty)}{T_\infty} \quad (4.3.42)$$

in such a way that

$$\tilde{\gamma} = \left(1 - \frac{\tau}{\tau_{max}}\right)^2,$$

exhibits a second-order zero $\tau = \tau_{max}$.

Radiative flux. Consider a simplified radiative flux outside the crystal without diffusion, i.e.

$$\frac{dT}{dz} = -A(T^4 - T_\infty^4),$$

such that, from Eq. (4.3.27),

$$\gamma = A\left(T^2 - \frac{T_\infty^4}{T^2}\right)$$

which by Eq. (4.3.41) rewrites as

$$\tilde{\gamma} = A \left(\left(\frac{T_m}{\tau/K + 1} \right)^2 - \frac{T_\infty^4}{T_m^2} (\tau/K + 1)^2 \right),$$

and, by Eq. (4.3.42), is normalised as

$$\tilde{\gamma} = \frac{\left(\frac{\tau_{max}/K + 1}{\tau/K + 1} \right)^2 - \left(\frac{\tau/K + 1}{\tau_{max}/K + 1} \right)^2}{\left(\tau_{max}/K + 1 \right)^2 - \left(\frac{1}{\tau_{max}/K + 1} \right)^2},$$

which exhibits a first-order zero at $\tau = \tau_{max}$. The related problem is quite complex without bringing up additional interesting features. To obtain some relevant information, the simpler expression:

$$\tilde{\gamma} = 1 - \frac{\tau}{\tau_{max}} \quad (4.3.43)$$

will be investigated.

4.3.5 Outer solution

The *outer equations* (Sinno et al., 1998) for vacancy and interstitial convection, diffusion and recombination is considered in a region described by the variable τ comprised between two transition values where the lower bound is vanishing as $Da \rightarrow \infty$, while the upper bound tends to infinity as $Da \rightarrow \infty$. Using a superscript “(o)” to indicate outer variables, the expansion

$$C'_{I,V}(\tau) = C'_{I,V;0}{}^{(o)}(\tau) + \varepsilon C'_{I,V;1}{}^{(o)}(\tau) + o_\tau(\varepsilon) \quad (4.3.44)$$

$$\Delta'(\tau) = \Delta_0{}^{(o)}(\tau) + \varepsilon \Delta_1{}^{(o)}(\tau) + o_\tau(\varepsilon) \quad (4.3.45)$$

$$\Pi'(\tau) = \Delta_0{}^{(o)}(\tau) + \varepsilon \Pi_1{}^{(o)}(\tau) + o_\tau(\varepsilon) \quad (4.3.46)$$

is assumed to hold for given τ , where $\varepsilon = Da^{-\beta}$ with $\beta > 0$ has to be determined. Introducing this decomposition in Eqs. (4.3.35) and (4.3.36), it results, at order 0, that the outer equations reduce, by dividing Eq. (4.3.36) by Da and passing to the limit $Da \rightarrow \infty$, to the following pair of equations:

$$\begin{aligned} Pe_T \partial_\tau \Delta_0{}^{(o)} &= d_I \partial_\tau \tilde{\gamma} e^{-p_I \tau} \left[\partial_\tau C'_{I0}{}^{(o)} + q_I C'_{I0}{}^{(o)} \right] \\ &\quad - d_V \partial_\tau \tilde{\gamma} e^{-p_V \tau} \left[\partial_\tau C'_{V0}{}^{(o)} + q_V C'_{V0}{}^{(o)} \right], \end{aligned} \quad (4.3.47)$$

$$\Pi_0{}^{(o)} = e^{-\tau}. \quad (4.3.48)$$

The limit conditions are

$$C'_{I,V;0}{}^{(o)}(\tau=0) = C'_{I,V}{}^m \quad (4.3.49)$$

$$\Delta_0{}^{(o)}(\tau=0) = \Delta_m := C_I^m - C_V^m \quad (4.3.50)$$

while the limit $\lim_{\tau \rightarrow \infty} \Delta_0{}^{(o)}(\tau)$ is assumed to exist and will be called $\Delta_0'^\infty$. Eq. (4.3.47) is integrated as:

Outer equation at order 0.

$$\begin{aligned} \frac{Pe_T}{\tilde{\gamma}} \left(\Delta_0{}^{(o)} - \Delta_0'^\infty \right) &= d_I e^{-p_I \tau} \left[\partial_\tau C'_{I0}{}^{(o)} + q_I C'_{I0}{}^{(o)} \right] \\ &\quad - d_V e^{-p_V \tau} \left[\partial_\tau C'_{V0}{}^{(o)} + q_V C'_{V0}{}^{(o)} \right]. \end{aligned} \quad (4.3.51)$$

$$\Pi_0{}^{(o)} = e^{-\tau}, \quad (4.3.52)$$

with

$$C'_{I,V;0}{}^{(o)} = \pm \Delta_0{}^{(o)} / 2 + (\Delta_0{}^{(o)} / 4 + e^{-\tau})^{1/2}. \quad (4.3.53)$$

4.3.6 Inner solution

The inner region is described by the variable τ'' corresponding to small values of τ . In fact, τ'' is defined from τ as the re-scaled variable:

$$\tau'' := Da^\beta \tau = \varepsilon^{-1} \tau, \quad (4.3.54)$$

in such a way that

$$\partial_\tau = \varepsilon^{-1} \partial_{\tau''}. \quad (4.3.55)$$

Moreover, using a superscript “(i)” to indicate inner variables, the following expansions are assumed, for fixed τ'' and variable $\varepsilon := Da^{-\beta}$:

$$C'_{I,V}(\varepsilon \tau'') = C'^{(i)}_{I,V;0}(\tau'') + \varepsilon C'^{(o)}_{I,V;1}(\tau'') + o_{\tau''}(\varepsilon) \quad (4.3.56)$$

$$\Delta'(\varepsilon \tau'') = \Delta_0^{(i)}(\tau'') + \varepsilon \Delta_1^{(i)}(\tau'') + o_{\tau''}(\varepsilon) \quad (4.3.57)$$

$$\Pi'(\varepsilon \tau'') = \Pi_0^{(i)}(\tau'') + \varepsilon \Pi_1^{(i)}(\tau'') + o_{\tau''}(\varepsilon), \quad (4.3.58)$$

where

$$\begin{aligned} \Pi_0^{(i)} &= C'_{I0}{}^{(i)} C'_{V0}{}^{(i)} \\ \Pi_1^{(i)} &= C'_{I0}{}^{(i)} C'_{V1}{}^{(i)} + C'_{I1}{}^{(i)} C'_{V0}{}^{(i)}, \end{aligned}$$

while

$$\tilde{\gamma} = \tilde{\gamma}_0 + \varepsilon \tau'' \tilde{\gamma}'_0 + o(\tau''). \quad (4.3.59)$$

where $\tilde{\gamma}'_0$ is the derivative of $\tilde{\gamma}$ w.r.t. τ at $\tau = 0$.

Inner $C'_{I,V}$ equations at order 0. The inner $C'_{I,V}$ equations rewrite as

$$\begin{aligned} \frac{Pe_T}{\varepsilon} \partial_{\tau''} C'_{I,V} &= d_{I,V} \partial_{\tau''} \tilde{\gamma} e^{-\varepsilon p_{I,V} \tau''} [\varepsilon^{-2} \partial_{\tau''} C'_{I,V} + q_{I,V} \varepsilon^{-1} C'_{I,V}] \\ &- \frac{1}{\varepsilon^\beta \tilde{\gamma}} \left(d_I e^{-\varepsilon p_I \tau''} + d_V e^{-\varepsilon p_V \tau''} \right) e^{-(1+p') \varepsilon \tau''} \left(\Pi' - e^{-\varepsilon \tau''} \right), \end{aligned} \quad (4.3.60)$$

Inner Δ' and Π' equations at order 0. The inner Δ' equation rewrites as

$$\begin{aligned} \frac{Pe_T}{\varepsilon} \partial_{\tau''} \Delta' &= d_I \partial_{\tau''} \tilde{\gamma} e^{-\varepsilon p_I \tau''} [\varepsilon^{-2} \partial_{\tau''} C'_I + q_I \varepsilon^{-1} C'_I] \\ &- d_V \partial_{\tau''} \tilde{\gamma} e^{-\varepsilon p_V \tau''} [\varepsilon^{-2} \partial_{\tau''} C'_V + q_V \varepsilon^{-1} C'_V], \end{aligned} \quad (4.3.61)$$

while the Π' equation rewrites as

$$\begin{aligned} \frac{Pe_T}{\varepsilon} \partial_{\tau''} \Pi' &= d_I C'_I \partial_{\tau''} e^{-\varepsilon p_I \tau''} [\varepsilon^{-2} \partial_{\tau''} C'_I + q_I \varepsilon^{-1} C'_I] \\ &+ d_V C'_I \partial_{\tau''} e^{-\varepsilon p_V \tau''} [\varepsilon^{-2} \partial_{\tau''} C'_I + q_V \varepsilon^{-1} C'_I] \\ &- \frac{1}{\varepsilon^\beta \tilde{\gamma}} \left(d_I e^{-\varepsilon p_I \tau''} + d_V e^{-\varepsilon p_V \tau''} \right) \\ &\cdot e^{-(1+p')\varepsilon \tau''} \left(\Pi' - e^{-\varepsilon \tau''} \right) (C'_I + C'_V). \end{aligned} \quad (4.3.62)$$

Inserting Eqs. (4.3.57)-(4.3.59) in Eqs. (4.3.61) & (4.3.62), multiplying by ε^β and passing to the limit $Da \rightarrow \infty$, the principle of least degenerescence shows β to be equal to 2, resulting in equations at order 0 writing as

$$\begin{aligned} d_I \partial_{\tau''}^2 C'_{I0}{}^{(i)} - d_V \partial_{\tau''}^2 C'_{V0}{}^{(i)} &= 0 \\ d_I C'_{V0}{}^{(i)} \partial_{\tau''}^2 C'_{I0}{}^{(i)} + d_V C'_I \partial_{\tau''}^2 C'_{V0}{}^{(i)} &= \tilde{\gamma}_0^{-2} (\Pi_0^{(i)} - 1) (C'_{I0}{}^{(i)} + C'_{V0}{}^{(i)}). \end{aligned}$$

This system rewrites as

$$\begin{bmatrix} \partial_{\tau''}^2 C'_{I0}{}^{(i)} \\ \partial_{\tau''}^2 C'_{V0}{}^{(i)} \end{bmatrix} = \begin{bmatrix} \frac{1}{d_I} \\ \frac{1}{d_V} \end{bmatrix} \tilde{\gamma}_0^{-2} (\Pi_0^{(i)} - 1). \quad (4.3.63)$$

Matching. Matching is imposed at some τ , for example $\tau = \varepsilon^{1/2}$ and hence $\tau'' = \varepsilon^{-1/2}$ (since the matching location must be large w.r.t. ε while small w.r.t. 1)

$$C'_{I,V;0}{}^{(i)}(\tau'' = 0) = C'_{I,V}{}^m, \quad (4.3.64)$$

$$\lim_{\tau'' \rightarrow \infty} C'_{I,V;0}{}^{(i)}(\tau'') = \lim_{\tau \rightarrow 0} C'_{I,V;0}{}^{(o)}(\tau) = C'_{I,V}{}^m. \quad (4.3.65)$$

Inner solution at order 0. From Eqs. (4.3.21), (4.3.49) and (4.3.63)-(4.3.65) the inner solution at order 0 writes as

$$C'_{I,V;0}{}^{(i)} = C'_{I,V}{}^m = C'_{I,V}{}^{eq} e^{\varepsilon \tau''/2} = C'_{I,V}{}^{eq} + o_{\tau''}(1) (\varepsilon \rightarrow 0) \quad (4.3.66)$$

for all values of τ'' .

It result from this analysis that inner solution in fact does not exist, since the above defined region is simply an “expanded solid-liquid interface” where a boundary condition is imposed.

4.3.7 Far-field solution

Since the temperature distribution in the far-field is not precisely defined, several variants of this problem are developed. The three attempts for the three assumptions on the temperature field will be here tested, with the superscript “(ff;i)” meaning far field solution, *i*th attempt.

First attempt.

The *far-field region* is described by the variable τ' corresponding to large values compared to $\tau \in [0, \infty[$.

Far-field variable. Let us define

$$\tau' := \tau - \alpha \ln Da. \quad (4.3.67)$$

Assumption on the temperature gradient. It is here assumed that

$$\lim_{\tau \rightarrow \infty} \tilde{\gamma} = \tilde{\gamma}_\infty, \quad (4.3.68)$$

where $\tilde{\gamma}_\infty$ is a positive constant.

The recombination term of Eq. (4.3.36) now writes as

$$- \frac{Da^{1-\alpha p^r}}{\tilde{\gamma}} \left(d_I Da^{-\alpha p_I} e^{-p_I \tau'} + d_V Da^{-\alpha p_V} e^{-p_V \tau'} \right) e^{-p^r \tau'} \\ \left(\Pi' - Da^{-\alpha} e^{-\tau'} \right) (C'_I + C'_V),$$

while all others terms on the right-hand side of Eqs. (4.3.35) and (4.3.36) exhibit decreasing exponentials. In view of the *least degenerescence principle* the exponent $1 - \alpha(p^r - 1)$ should be set to a value such that recombination is not completely vanishing in the limit $Da \rightarrow \infty$ (or $\varepsilon \rightarrow 0$). Therefore, it results from Table 4.3.2 that for silicon if the S-D parameters are used together with a positive average p^r , $\alpha = (\min\{p_I, p_V\} + p^r)^{-1} = (p_V + p^r)^{-1}$ in such a way that, after dividing Eq. (4.3.35) and (4.3.36) by Da and passing to the limit $Da \rightarrow \infty$, the *far-field equations* write as

$$Pe_T \partial_{\tau'} \Delta_0^{(ff;1)} = 0 \quad (4.3.69)$$

$$Pe_T \partial_{\tau'} \Pi_0^{(ff;1)} = -\frac{2}{\tilde{\gamma}_\infty} d_V e^{-(p_V + p^r) \tau'} \Pi_0^{(ff;1)} \left(\frac{\Delta_0^{(ff;1)2}}{4} + \Pi_0^{(ff;1)} \right)^{1/2} \quad (4.3.70)$$

where superscript $(ff;1)$ indicates the first variant of the far-field solution. From Eq. (4.3.69) it results that

$$\Delta_0'^{(ff;1)} = K.$$

By Eq. (4.3.48), the boundary conditions for the far-field solution writes as

Matching.

$$\begin{aligned} K &= \lim_{\tau \rightarrow \infty} \Delta_0'^{(o)}(\tau) = \Delta_0'_{\infty} \\ \lim_{\tau' \rightarrow -\infty} \Pi_0'^{(ff;1)}(\tau') &= \lim_{\tau \rightarrow \infty} \Pi_0'^{(o)}(\tau) = 0. \end{aligned}$$

Far-field solution at order 0. Having in mind that $0 < p_V + p^r < 1$, the solution of Eq. (4.3.70) verifies, if $\Delta_0'_{\infty} \neq 0$ and $\Pi_0'^{(ff;1)} \neq 0$, the relation

$$\begin{aligned} & \frac{\frac{\Delta_0'_{\infty 2}}{2} + \Pi_0'^{(ff;1)} + |\Delta_0'_{\infty}| \left(\Pi_0'^{(ff;1)} + \frac{\Delta_0'_{\infty 2}}{4} \right)^{1/2}}{|\Pi_0'^{(ff;1)}|} \\ &= A_1 \exp \left(- \frac{|\Delta_0'_{\infty}|}{(p_V + p^r) Pe_T \tilde{\gamma}_{\infty}} \frac{dV}{e^{-(p_V + p^r)\tau'}} \right), \end{aligned} \quad (4.3.71)$$

where $A_1 > 0$ is an integration constant. For $\Delta_0'_{\infty} = 0$ and $\Pi_0'^{(ff;1)} \neq 0$, the solution of

$$Pe_T \partial_{\tau'} \Pi_0' = - \frac{2dV}{Pe_T \tilde{\gamma}_{\infty}} \Pi_0'^{3/2} e^{-(p_V + p^r)\tau'} \quad (4.3.72)$$

writes as

$$-2\Pi_0'^{(ff;1)-1/2} = A_2 + \frac{2dV}{Pe_T \tilde{\gamma}_{\infty} (p_V + p^r)} e^{-(p_V + p^r)\tau'}, \quad (4.3.73)$$

while $\Pi_0'^{(ff;1)} = 0$ is always a solution of Eq. (4.3.70). We remark that matching with the outer solution is achieved for $\tau' \rightarrow -\infty$ if the solution is simply $\Pi_0'^{(ff;1)} = 0$. By unicity, the far-field solution is found to be

$$\Delta_0'^{(ff;1)} = \Delta_0'_{\infty} = C_{I0}'^{(ff;1)} \quad \text{or} \quad -C_{V0}'^{(ff;1)} \quad (4.3.74)$$

$$\Pi_0'^{(ff;1)} = 0. \quad (4.3.75)$$

This solution, however, is not satisfactory from a practical viewpoint, as soon as the first-order is sought. The reason for this is absence of practical meaning for assumption Eq. (4.3.68), which involves that $T \rightarrow 0$ [K] when $z \rightarrow \infty$.

Note that Eq. (4.3.75) does not imply that the recombination is infinite, since as one species has been completely annihilated, recombination has no physical meaning in the far field.

Second attempt.

In this case, it is assumed that

$$\tilde{\gamma} = \left(1 - \frac{\tau}{\tau_{max}}\right)^2 = \frac{1}{\tau_{max}^2} \tau'^2 \varepsilon^{2\alpha}, \quad (4.3.76)$$

with $\tau \in [0, \tau_{max}[$ which results in a bounded temperature field in an unbounded domain.

Far-field variable.

$$\tau' := \frac{\tau - \tau_{max}}{\varepsilon^\alpha}, \quad (4.3.77)$$

where α is a positive parameter to be determined, and in such a way that

$$\partial_\tau = \varepsilon^{-\alpha} \partial_{\tau'}. \quad (4.3.78)$$

Far-field equations for Δ' . From Eq. (4.3.35) it follows that

$$\begin{aligned} Pe_T \partial_{\tau'} \Delta' &= \frac{d_I}{\tau_{max}^2} \partial_{\tau'} \tau'^2 e^{-p_I(\tau_{max} + \varepsilon^\alpha \tau')} [\varepsilon^\alpha \partial_{\tau'} C'_I + \varepsilon^{2\alpha} q_I C'_I] \\ &- \frac{d_V}{\tau_{max}^2} \partial_{\tau'} \tau'^2 e^{-p_V(\tau_{max} + \varepsilon^\alpha \tau')} [\varepsilon^\alpha \partial_{\tau'} C'_V + \varepsilon^{2\alpha} q_V C'_V], \end{aligned} \quad (4.3.79)$$

in such a way that, letting $\varepsilon \rightarrow 0$,

$$Pe_T \partial_{\tau'} \Delta_0^{(ff;2)} = 0. \quad (4.3.80)$$

Far-field equations for Π' . From Eq. (4.3.36), it follows that $\forall \alpha > 0$

$$\begin{aligned}
 & \varepsilon^{\alpha+2} P e_T \partial_{\tau'} \Pi' = \\
 & = \frac{d_I}{\tau_{max}^2} C'_V \partial_{\tau'} \tau'^2 e^{-p_I(\tau_{max} + \varepsilon^\alpha \tau')} \left[\varepsilon^{2(\alpha+1)} \partial_{\tau'} C'_I + \varepsilon^{3\alpha+2} q_I C'_I \right] \\
 & + \frac{d_V}{\tau_{max}^2} C'_I \partial_{\tau'} \tau'^2 e^{-p_V(\tau_{max} + \varepsilon^\alpha \tau')} \left[\varepsilon^{2(\alpha+1)} \partial_{\tau'} C'_V + \varepsilon^{3\alpha+2} q_V C'_V \right] \\
 & - \frac{\tau_{max}^2}{\tau'^2} \left(d_I e^{-p_I(\tau_{max} + \varepsilon^\alpha \tau')} + d_V e^{-p_V(\tau_{max} + \varepsilon^\alpha \tau')} \right) \\
 & \cdot e^{-p^r(\tau_{max} + \varepsilon^\alpha \tau')} \left(\Pi' - e^{-(\tau_{max} + \varepsilon^\alpha \tau')} \right) (C'_I + C'_V), \quad (4.3.81)
 \end{aligned}$$

in such a way that, letting $\varepsilon \rightarrow 0$,

$$\Pi_0'^{(ff;2)} = e^{-\tau_{max}}. \quad (4.3.82)$$

Matching. The boundary conditions write as:

$$\begin{aligned}
 K & = \Delta_0'^{(ff;2)} = \lim_{\tau \rightarrow \infty} \Delta_0'^{(o)}(\tau) = \Delta_0'^{\infty} \\
 \lim_{\tau' \rightarrow 0} \Pi_0'^{(ff;1)}(\tau') & = \lim_{\tau \rightarrow \tau_{max}} \Pi_0'^{(o)}(\tau) = e^{-\tau_{max}}.
 \end{aligned}$$

Far-field solution. Therefore the far-field concentrations are constants and write as:

$$C'_{I,V;0} = \pm \frac{|\Delta_0'^{\infty}|}{2} + \left(\frac{\Delta_0'^{\infty 2}}{4} + e^{-\tau_{max}} \right)^{1/2}. \quad (4.3.83)$$

Third attempt.

In this third case, it is assumed that

$$\tilde{\gamma} = 1 - \frac{\tau}{\tau_{max}} = -\frac{1}{\tau_{max}} \tau' \varepsilon^\alpha, \quad (4.3.84)$$

with $\tau \in [0, \tau_{max}[$, resulting again in a bounded temperature field in an unbounded domain.

Far-field variable.

$$\tau' := \frac{\tau - \tau_{max}}{\varepsilon^\alpha}, \quad (4.3.85)$$

where $\alpha > 0$ and in such a way that

$$\partial_\tau = \varepsilon^{-\alpha} \partial_{\tau'}. \quad (4.3.86)$$

Far-field equations for Δ' . From Eq. (4.3.35), it follows that

$$\begin{aligned} Pe_T \partial_{\tau'} \Delta' &= -\frac{d_I}{\tau_{max}} \partial_{\tau'} \tau' e^{-p_I(\tau_{max} + \varepsilon^\alpha \tau')} [\partial_{\tau'} C'_I + \varepsilon^\alpha q_I C'_I] \\ &+ \frac{d_V}{\tau_{max}} \partial_{\tau'} \tau' e^{-p_V(\tau_{max} + \varepsilon^\alpha \tau')} [\partial_{\tau'} C'_V + \varepsilon^\alpha q_V C'_V], \end{aligned} \quad (4.3.87)$$

in such a way that, letting $\varepsilon \rightarrow 0$,

$$\begin{aligned} Pe_T \partial_{\tau'} \Delta_0'^{(ff;3)} &= -\frac{d_I}{\tau_{max}} e^{-p_I \tau_{max}} \partial_{\tau'} \tau' \partial_{\tau'} C_{I0}'^{(ff;3)} \\ &+ \frac{d_V}{\tau_{max}} e^{-p_V \tau_{max}} \partial_{\tau'} \tau' \partial_{\tau'} C_{V0}'^{(ff;3)}, \end{aligned} \quad (4.3.88)$$

or, equivalently, that

$$\begin{aligned} Pe_T \left(\Delta_0'^{(ff;3)} - K \right) &= -\frac{d_I}{\tau_{max}} e^{-p_I \tau_{max}} \tau' \partial_{\tau'} C_{I0}'^{(ff;3)} \\ &+ \frac{d_V}{\tau_{max}} e^{-p_V \tau_{max}} \tau' \partial_{\tau'} C_{V0}'^{(ff;3)}, \end{aligned} \quad (4.3.89)$$

where K is an integration constant, noted $\Delta_0'^{\infty}$.

Far-field equations for Π' . From Eq. (4.3.36), it follows that

$$\begin{aligned} \varepsilon^2 Pe_T \partial_{\tau'} \Pi' &= -\frac{d_I}{\tau_{max}} C'_V \partial_{\tau'} \tau' e^{-p_I(\tau_{max} + \varepsilon^\alpha \tau')} [\varepsilon^2 \partial_{\tau'} C'_I + \varepsilon^{\alpha+2} q_I C'_I] \\ &- \frac{d_V}{\tau_{max}} C'_I \partial_{\tau'} \tau' e^{-p_V(\tau_{max} + \varepsilon^\alpha \tau')} [\varepsilon^2 \partial_{\tau'} C'_V + \varepsilon^{\alpha+2} q_V C'_V] \\ &+ \frac{\tau_{max}}{\tau'} \left(d_I e^{-p_I(\tau_{max} + \varepsilon^\alpha \tau')} + d_V e^{-p_V(\tau_{max} + \varepsilon^\alpha \tau')} \right) \\ &\cdot e^{-p'(\tau_{max} + \varepsilon^\alpha \tau')} \left(\Pi' - e^{-(\tau_{max} + \varepsilon^\alpha \tau')} \right) (C'_I + C'_V), \end{aligned} \quad (4.3.90)$$

in such a way that, letting $\varepsilon \rightarrow 0$,

$$\Pi_0'^{(ff;3)} = e^{-\tau_{max}}. \quad (4.3.91)$$

Far-field equations at order 0. The far-field equations write as

$$\begin{aligned} Pe_T \left(\Delta_0'^{(ff;3)} - \Delta_0'^{\infty} \right) &= \quad (4.3.92) \\ &- \frac{d_I}{\tau_{max}} e^{-p_I \tau_{max}} \tau' \partial_{\tau'} \left(\frac{\Delta_0'^{(ff;3)}}{2} + \left(\frac{\Delta_0'^{(ff;3)2}}{4} + e^{-\tau_{max}} \right)^{1/2} \right) \\ &+ \frac{d_V}{\tau_{max}} e^{-p_V \tau_{max}} \tau' \partial_{\tau'} \left(-\frac{\Delta_0'^{(ff;3)}}{2} + \left(\frac{\Delta_0'^{(ff;3)2}}{4} + e^{-\tau_{max}} \right)^{1/2} \right) \end{aligned}$$

$$\Pi_0^{(ff;3)} = e^{-\tau_{max}}. \quad (4.3.93)$$

whose solution must comply the following conditions.

Matching. The boundary conditions are:

$$\lim_{\tau' \rightarrow 0} \Delta_0^{(ff;3)} = \Delta_0^{\prime\infty} \quad (4.3.94)$$

$$\lim_{\tau' \rightarrow \infty} \partial_{\tau'} \Delta_0^{(ff;3)} = 0, \quad (4.3.95)$$

verifying

$$\begin{aligned} \Delta_0^{(ff;3)} &= \Delta_0^{\prime\infty} \\ \Pi_0^{(ff;3)} &= e^{-\tau_{max}}, \end{aligned} \quad (4.3.96)$$

with constant concentrations as in the second attempt (Eq. (4.3.79)).

Our conclusion is that far field is not correctly treated with the sole Damkohler number. In fact, it is not clear how the transition from the outer- to the far field region, where recombination has been damped together with diffusion, should depend on Da, which accounts for the ratio between recombination and diffusion mechanisms. However, appart from pointing this paradox, it has not been possible to propose an alternative approach. Moreover, even in a 1D simplified geometry, a correct analysis should include the treatment of the lateral boundary condition, where the mechanisms are 2D: radial diffusion, vertical transport and high recombination rate above the interface. The difficulty resides in the fact that the boundary layer (BL) get thinner while T decreases and all mechanisms get frozen. Moreover, transport is uniform in the whole crystal and the impact of the thick BL above the interface is transported in the crystal core. This issue, too, has not found a positive answer.

4.4 A compilation of material data from the literature

The values presented below are taken from the recent literature on defect prediction in silicon. As shown by Tables 4.2 & 4.3, they differ sometimes by several orders of magnitude and, at a first glance, seem to lead to contradictory conclusions. These discrepancies might be explained by several reasons, as for instance the choice of the experimental technique and set-up quality (as eg the oxydation enhanced diffusion studied by Wijaranakula (1993), while most of the others workers considered metal diffusion experiments), the progress made in experimental approaches in a period of

20 years, or the temperature range at which experiments have been realised. Let us insist on this last point, as experimental devices are not able to measure material values at melting temperatures and as the theoretical laws (as, eg, the Arrhenius temperature dependence) fail in the range of high temperature (ie, close to the melting point). However, the aim is not here to discuss all these possible reasons, but rather to highlight the many uncertainties in the material data nowadays. Therefore, in view of the comprehension of the global physics of point-defect formation and evolution in single crystal growth, according to the values of Tables 4.2 & 4.3 and referring to the physical description and the scaling analysis of previous sections, some undiscutable remarks can be made:

- The vacancy dominates the interstitial concentration at the solid-liquid interface, showing two extreme cases
 - following Kulkarni et al. (2002), $C_V^m \simeq C_I^m$, while
 - following Bracht et al. (1995), $C_V^m \gg C_I^m$.

The first case seems to rely on some underlying thermodynamic property, justifying the equality between the two inseparable species at the formation interface, while the second would rather mean that for some physical reason the formation of vacancies at the solid/liquid interface is by far much easier than the formation of interstitials. Anyhow, this point still remains an open question.

- The interstitial dominates the vacancy diffusivity at the solid-liquid interface, with an agreement on a magnitude for their ratio of about one order of magnitude, with the exceptions of Bracht & Stolwijk (1995) which proposes three order of magnitude, and of Wijaranakula (1993) which proposes a situation where they are almost equal with a slight domination of the vacancy diffusion.
- Interstitial dominate by one order of magnitude vacancy self-diffusion. The self-diffusion coefficient $C_{I,V}^m D_{I,V}^m$ are in very good agreement (except for Wijaranakula (1993)) as the experimental methods for estimating the sum $\bar{H}_{I,V}^f + \bar{H}_{I,V}^m$ and the product $C_{I,V}^{eq} D_{I,V}$ are much more accurate than for these quantities separately.
- There is relatively good agreement for interstitial formation enthalpies, contrary to the vacancy formation enthalpies, which, in comparison, are always smaller. This implies that equilibrium interstitial concentration decreases faster than equilibrium vacancy concentration.

Let us also mention some discutable facts:

- Although it is generally accepted that $\overline{H}_I^m > \overline{H}_V^m$ (Sinno et al., 1998; Kulkarni et al., 2002), and hence that interstitial diffusivity decrease faster than vacancy diffusivity, some authors proposed the reverse relation (Bracht et al. 1995; Falster et al., 2000; Zimmermann & Ryssel, 1992; Wijarankula, 1993).
- Because of a lack of research made for this purpose, there is no convincing data for the recombination coefficient $K_{I,V}^m$, the recombination enthalpy \overline{H}^r and entropy \overline{S}^r . However, it is believed that in most of the defect modeling work, $K_{I,V}^m$ is not an important parameter. A finite value for $K_{I,V}^m$ will be chosen to give a diffusion-limited situation.
- Nothing is known about thermo-diffusion and there is not even agreement on its sign, that is, whether a positive $Q_{I,V}^{**}$ will increase or decrease the global diffusion of point-defects (see further discussion at Section 4.7).

Refs.	I,V	$C_{I,V}^m$ m^{-3}	$D_{I,V}^m$ m^2s^{-1}	$\frac{C_{I,V}^m}{D_{I,V}^m}$	$K_{I,V}^m$ $m^{-3}s^{-1}$
Sinno et al. (1998)	I	$9.71 \cdot 10^{20}$	$3.79 \cdot 10^{-8}$	$3.68 \cdot 10^{13}$	$2.99 \cdot 10^{-22}$
Sinno et al. (1998)	V	$1.18 \cdot 10^{21}$	$4.29 \cdot 10^{-9}$	$5.06 \cdot 10^{12}$	
Kulkarni et al. (2002)	I	$6.56 \cdot 10^{20}$	$3.94 \cdot 10^{-8}$	$2.59 \cdot 10^{13}$	$2.07 \cdot 10^{-20}$
Kulkarni et al. (2002)	V	$8.07 \cdot 10^{20}$	$3.97 \cdot 10^{-9}$	$3.18 \cdot 10^{12}$	
Falster et al. (2000)	I	$8.3 \cdot 10^{20}$	$3.6 \cdot 10^{-8}$	$2.98 \cdot 10^{13}$	10^{-17}
Falster et al. (2000)	V	$1.08 \cdot 10^{21}$	$4 \cdot 10^{-9}$	$4.32 \cdot 10^{12}$	
Bracht et al. (1995)	I	$8.77 \cdot 10^{20}$	$2.56 \cdot 10^{-8}$	$2.28 \cdot 10^{13}$	—
Bracht et al. (1995)	V	$1.44 \cdot 10^{23}$	$1.23 \cdot 10^{-11}$	$1.81 \cdot 10^{12}$	
Lerner & Stolwijk (2005)	I	—	—	$1.37 \cdot 10^{13}$	—
Lerner & Stolwijk (2005)	V	$6.95 \cdot 10^{22}$	—	$2.58 \cdot 10^{12}$	
Zimmermann & Ryssel (1992)	I	$6.42 \cdot 10^{21}$	$3.33 \cdot 10^{-9}$	$2.14 \cdot 10^{13}$	$5.61 \cdot 10^{-20}$
Zimmermann & Ryssel (1992)	V	$6.08 \cdot 10^{21}$	$3.48 \cdot 10^{-10}$	$2.12 \cdot 10^{12}$	
Tan & Gösele (1985)	I	$3.37 \cdot 10^{23}$	$6.35 \cdot 10^{-11}$	$2.14 \cdot 10^{13}$	$8.97 \cdot 10^{-24}$
Tan & Gösele (1985)	V	$2.06 \cdot 10^{23}$	$1.03 \cdot 10^{-11}$	$2.12 \cdot 10^{12}$	
Wijarankula (1993)	I	$1.14 \cdot 10^{23}$	$9.06 \cdot 10^{-11}$	$1.08 \cdot 10^{13}$	—
Wijarankula (1993)	V	$1.83 \cdot 10^{23}$	$8.09 \cdot 10^{-11}$	$1.48 \cdot 10^{13}$	
Larsen et al. (2001)	I	$9.71 \cdot 10^{20}$	$3.79 \cdot 10^{-8}$	$3.68 \cdot 10^{13}$	$1.69 \cdot 10^{-20}$
Larsen et al. (2001)	V	$1.18 \cdot 10^{21}$	$4.29 \cdot 10^{-9}$	$5.06 \cdot 10^{12}$	

Table 4.2: Comparison table for material data (1).

Refs.	I,V	$\overline{H}_{I,V}^f$ eV	$\overline{H}_{I,V}^m$ eV	\overline{H}^f eV	$\overline{S}_{I,V}^f$ eV/K	\overline{S}^f eV/K
Sinno et al. (1998)	I	4.4	0.937	-1.19	6.48	-12.43
Sinno et al. (1998)	V	3.34	0.457		5.94	
Kulkarni et al. (2002)	I	4.0	0.9	-1.80	0	-12.43
Kulkarni et al. (2002)	V	4.0	0.4		0	
Falster et al. (2000)	I	4.8	0.25	-	0	-
Falster et al. (2000)	V	4.6	0.35		0	
Bracht et al. (1995)	I	3.18	1.77	-	0	-
Bracht et al. (1995)	V	2.0	1.8		0	
Lerner & Stolwijk (2005)	I	-	-	-	-	-
Lerner & Stolwijk (2005)	V	2.44	-		-	
Zimmermann & Ryssel (1992)	I	3.83	0.97	-	-	-
Zimmermann & Ryssel (1992)	V	1.16	2.83		-	
Tan & Gösele (1985)	I	4.4	0.4	-	-	-
Tan & Gösele (1985)	V	2.0	2		-	
Wijarankula (1993)	I	3.1	1.86	-	-	-
Wijarankula (1993)	V	1.56	2.84		-	
Larsen et al. (2001)	I	4.4	0.937	-	-	-
Larsen et al. (2001)	V	3.34	0.457		-	

Table 4.3: Comparison table for material data (2).

4.5 Comparison of time-dependent and quasi-steady predictions

Our simulations show that dynamic effects deeply influence the defect distribution in CZ Si crystals for two reasons. On the one hand, the interface deformation caused by any change of the operating conditions (pull rate, heater power...) and in particular the rapid change of interface shape experienced during shouldering directly affect the thermal gradient above the interface and the resulting interstitial and vacancy densities through the well-known V/G ratio (cf Section 4.6). On the other hand, since point-defects are transported while diffusing and reacting, the defect distribution inside the crystal is a picture of the past history of defect generation and cannot be correctly predicted by means of a quasi-steady model.

In the present section, various simulation results are detailed to compare time-dependent and quasi-steady predictions and to illustrate the system sensitivity to the above-mentioned dynamic effects. In addition, the influence of the material parameters governing point-defect diffusion and recombination are investigated. Defect calculations were carried out using the model developed by Sinno and Dornberger without thermo-

diffusion effects. Various numerical experiments have demonstrated the high sensitivity of the predicted defect distribution to model parameters. Defect results are shown in Figs. 4.7 to 4.8, depicting the interstitial and vacancy distributions obtained together with their difference ($\Delta = C_I - C_V$) as resulting from quasi-steady (Figs. 4.6(a), 4.7(a), 4.8(a)) and time-dependent (Figs. 4.6(b), 4.7(b), 4.8(b)) defect simulations. A significant difference between quasi-steady and time-dependent results is observed from the crystal shoulder to about 1.5 to 2 crystal diameters from the shoulder. This difference is a consequence of a quickly varying heat transfer during and after shouldering, which directly affects defect formation during these stages. Subsequently the defect distribution in the top of the crystal is transported upwards without major changes when the crystal grows.

4.6 OSF-ring equilibrium of point-defects

Let us refer to E. Dornberger (1998) thesis for a complete discussion about the physical and computational aspects of this crucial phenomenon termed “OSF”-ring (Oxydation Stacking Fault) occurring in single crystal growth. Basically, the OSF-ring separates an interstitial- from a vacancy rich region and its location is of the utmost importance from a technological viewpoint. In fact, the location of the ring at the crystal rim and symmetry axis means a crystal filled with vacancies and interstitials only, respectively, whereas its location at the crystal half radius means two zones well separated by a ring of a certain radius such that in its interior no point-defects survive anymore. Moreover, it is observed that its location is only dependent on the ratio between V , the pulling rate, and G , the interface thermal gradient. In fact, the 1D asymptotic analysis, as presented in Section 4.3.2, is precisely aimed at the determination of V/G as a function of the material physical data (such as formation enthalpies etc.). We will propose a contribution to this question in Section 4.6.2 & 4.6.3.

- i. As equilibrium interstitial and vacancy concentrations decrease exponentially with temperature, recombination will be enhanced in regions where the temperature gradient is steep. Due to heat lost (predominantly by radiation), high temperature gradient are found near the solidification interface at the crystal external surface. Moreover, since recombination balances diffusion in this “inner region” (see Section 4.3.6), it results that

$$D_I - D_V = D_I^m - D_V^m + o(1)_{\tau''}(\varepsilon \rightarrow 0) > 0,$$

and hence interstitials are expected to be the dominating species near the external boundary, whereas vacancy domination is expected in the crystal centre.

- ii. Moreover, increasing the pulling rate will increase the relative effect of transport w.r.t. diffusion and hence create favorable conditions for vacancy domination. Moreover, the growth speed (ie the axial velocity of a material point w.r.t. the solidification front) is higher at the crystal center, since the interface is curved, creating a vacancy-rich region.

4.6.1 The Sinno-Dornberger model

Let us recall that all point-defect models can be written in the form of a pair of evolution equations,

$$DC_K/Dt = -\nabla \cdot \underline{J}_K - K_{IV}(C_I C_V - C_I^{eq} C_V^{eq}), \quad (4.6.1)$$

where subscript K stands for I or V to indicate self-interstitials or vacancies, respectively, C_K^{eq} denotes the corresponding equilibrium concentrations, K_{IV} is the kinetic coefficient associated with the Frenkel recombination mechanism, symbols ∇ and $D/DT = \partial/\partial t + V\partial/\partial z$ denote the gradient and material derivation operators (with z indicating the vertical direction), and \underline{J}_K stands for the interstitial or vacancy diffusion flux:

$$\underline{J}_K = -D_K \nabla C_K - (C_K D_K Q_K^{**}/k_b T^2) \nabla T, \quad (4.6.2)$$

with D_K , T , and k_b denoting the Fickian diffusion coefficients, absolute temperature, and Boltzmann constant ($8.61 \cdot 10^{-5} eV/K$), respectively, while Q_K^{**} stands for the so-called reduced heats of transport associated with interstitial or vacancy thermo-diffusion (or thermal drift as introduced in Section 4.7). Boundary conditions are of two kinds. Along the solidification interface, equilibrium concentrations are imposed, while the concentration normal fluxes are set to zero along the crystal wall (equilibrium concentrations should normally be imposed in this latter case in order to account for the Schottky defect generation mechanism; however this will generate unacceptably thin and sharp concentration boundary layers along the crystal wall, and hence this effect is here neglected without significant loss of accuracy in the remaining domain). To facilitate model comparisons, it is of the utmost importance to use an unambiguous expression of the coefficients C_K^{eq} , D_K , and K_{IV} as a function of temperature. Therefore, we write

$$C_K = C_K^m \exp \left[-\frac{\overline{H}_K^f}{k_b T_m} \left(\frac{T_m}{T} - 1 \right) + \overline{S}_K^f \left(1 - \frac{T}{T_m} \right) \left(\frac{T_m}{T} - 1 \right) \right], \quad (4.6.3)$$

$$D_K = D_K^m \exp \left[-\frac{\overline{H}_K^m}{k_b T_m} \left(\frac{T_m}{T} - 1 \right) \right], \quad (4.6.4)$$

$$K_{IV} = k_{IV;T_m} \frac{D_I + D_V}{D_I^m + D_V^m} \exp \left[-\frac{\overline{H}_K^r}{k_b T_m} \frac{T_m}{T} - 1 \right] + \overline{S}_K^r \left(1 - \frac{T}{T_m} \right) \left(\frac{T_m}{T} - 1 \right), \quad (4.6.5)$$

where \bar{H}_K^f , \bar{H}_K^m , and \bar{H}_K^r are effective formation, migration, or recombination enthalpies, \bar{S}_K^f and \bar{S}_K^r denote 2nd-order effective formation or recombination entropies, while C_K^m , D_K^m , and $k_{IV;T_m}$ stand for the values of C_K^{eq} , D_K , and K_{IV} at the melting temperature T_m (1685 [K]). Both entropic and enthalpic effects are taken into account in the definition of these coefficients. This approach is devoted to possibly provide 2nd-order expansions of C_K^{eq} and K_{IV} around T_m , in such a way that most available models can be exactly expressed. In particular, the S-D model writes as:

$$\begin{aligned} \bar{H}_I^f &= 4.4 \text{ eV}, & \bar{H}_V^f &= 3.34 \text{ eV}, \\ \bar{S}_I^f &= 6.48 \text{ eV}/k_b T_m, & \bar{S}_V^f &= 5.94 \text{ eV}/k_b T_m, \\ C_I^m &= 9.71 \cdot 10^{14} \text{ cm}^{-3}, & C_V^m &= 1.18 \cdot 10^{15} \text{ cm}^{-3}, \\ \bar{H}_I^m &= 0.937 \text{ eV}, & \bar{H}_V^m &= 0.457 \text{ eV}, \\ D_I^m &= 3.79 \cdot 10^{-4} \text{ cm}^2/\text{s}, & D_V^m &= 4.28 \cdot 10^{-5} \text{ cm}^2/\text{s}, \\ \bar{H}^r &= -1.194 \text{ eV}, & \bar{S}^r &= -12.43 \text{ eV}/k_b T_m, \\ Q_I^{**} &= 0, & Q_V^{**} &= 0. \end{aligned}$$

A key reason for the success of the S-D model is that it provides good estimates of the Oxygen Stacking Fault (OSF) ring location in Si crystals. The latter is generally assumed to be adjacent to the surface separating interstitial- and vacancy-rich regions (Tan and Gösele, 1985; von Ammon et al., 1995; Dornberger & von Ammon, 1996; Dornberger, 1998) and plays a major role to grow defect-free crystals (Falster et al., 2000; Voronkov & Falster, 2002). In fact, the good predictive quality of the S-D model can be explained by its agreement with the V/G criterion initially proposed by Voronkov (1982), which states that the $C_I = C_V$ surface is approximately located at the radial distance from the axis where the ratio of the pulling rate over the thermal gradient G (as measured just above the solidification front) has a critical value $(V/G)_{crit}$:

$$V/G = (V/G)_{crit}. \quad (4.6.6)$$

Estimations of $(V/G)_{crit}$ were provided by Dornberger and co-authors (von Ammon et al., 1995; Dornberger & von Ammon, 1996; Dornberger, 1998)) from a combination of experimental measurements and numerical simulations. As it was further explained by Sinno et al. (1998) by means of an asymptotic analysis of the behaviour of point-defects just after solidification, $(V/G)_{crit}$ can be linked to the point-defect governing parameters by the following relationship:

$$(V/G)_{crit} = \frac{C_I^m D_I^m (\bar{H}_I^f - Q_I^{**}) - C_V^m D_V^m (\bar{H}_V^f - Q_V^{**})}{k_b T_m^2 (C_V^m - C_I^m)}. \quad (4.6.7)$$

Variants of the S-D model have been proposed by Voronkov, Falster and co-authors (Voronkov & Falster, 2002; Falster et al., 2000), all respecting the V/G criterion with a slight modification of Eq. (4.6.7).

4.6.2 The Voronkov and Sinno simplified models

Voronkov formula. After showing how the type and concentration of the remaining defect (interstitials or vacancies) depend on the ratio of the pull rate V and the temperature gradient at the solidification interface G , Voronkov (1982) proposed in the beginning of the 80ies a criterion to determine the so-called *critical pull rate* at which the type of the dominating defect will change. In addition to the two basic assumptions of infinite recombination rate and equilibrium concentrations at the solidification front ($C_I = C_I^m$ and $C_V = C_V^m$), Voronkov also assumes that C_I and C_V are proportional to $e^{-z/L}$ and that D_I and D_V are constant. Then, by Eqs. (4.3.1)-(4.3.2),

$$V\Delta = D_I\partial_z C_I - D_V\partial_z C_V = -\frac{1}{L}(D_I C_I - D_V C_V),$$

it immediately follows (Voronkov, 1982) from Eq. (4.3.29) that

$$\left[\frac{V}{G}\right]_{VOR1}^{crit} = \frac{\bar{H}_{IV}}{k_b T_m^2} \frac{D_I C_{I0}^m - D_V C_{V0}^m}{C_{V0}^m - C_{I0}^m}. \quad (4.6.8)$$

A variant of this formula includes thermodiffusion and writes as (Voronkov & Falster, 2002)

$$\left[\frac{V}{G}\right]_{VOR2}^{crit} = \frac{D_I C_{I0}^m (\bar{H}_{IV} - Q_I^{**}) - D_V C_{V0}^m (\bar{H}_{IV} - Q_V^{**})}{k_b T_m^2 (C_{V0}^m - C_{I0}^m)}. \quad (4.6.9)$$

The authors here postulate that C_I and C_V are proportional to the square root of $C_I C_V = C_I^{eq} C_V^{eq}$.

Sinno-Dornberger formula. In this paper (Sinno et al, 1998), a 0-order matched asymptotic analysis is done for the inner and outer regions, but here, contrarily to Section 4.3.2 it is assumed that $\tilde{\gamma} = 1$, and it is postulated that C_I and C_V are proportional to $e^{-p'_I \tau}$ and $e^{-p'_V \tau}$, respectively, where the effective dimensionless enthalpies of formation for the actual concentrations profiles p'_I and p'_V are unknown in general and usually approximated by $\frac{\bar{H}_I^f}{\bar{H}_I^f + \bar{H}_V^f}$ and $\frac{\bar{H}_V^f}{\bar{H}_I^f + \bar{H}_V^f}$, in such a way that the resulting formula writes as

$$\left[\frac{V}{G}\right]_{SD}^{crit} = \frac{(\bar{H}_I^f - Q_I^{**}) D_I^m C_{I0}^m - (\bar{H}_V^f - Q_V^{**}) D_V^m C_{V0}^m}{k_b T_m^2 (C_{V0}^m - C_{I0}^m)}. \quad (4.6.10)$$

4.6.3 Computation of the V/G criterion

Referring to Section 4.3.2, the V/G criterion involves a vanishing value of Δ_0^∞ . Therefore by the preceding analysis the inner solution does not create a significant first-order correction of the outer solution, and neither does the far-field solution, which consists, up to the first-order, of frozen values of the interstitials and vacancies concentrations⁴. Eq. (4.3.51) will be rewritten in terms of the variable ξ , as given by Eq. (4.3.19) and by the relation

$$\begin{aligned} 2\frac{d}{d\tau}C_{I,V} &= \frac{d}{d\tau}\left(\pm\Delta + (\Delta^2 + 4\Pi)^{1/2}\right) \\ &= 2\Pi_{I_m}^{eq1/2}\left(\mp\xi + (\xi^2 + e^{-\tau})^{1/2}\right)\left(-\frac{1}{2}\mp(\xi^2 + e^{-\tau})^{-1/2}\frac{d\xi}{d\tau}\right). \end{aligned}$$

Therefore, Eq. (4.3.51) with $\Delta_0^\infty = 0$ is written as

$$\begin{aligned} \frac{4Pe_T}{\tilde{\gamma}}\xi &= d_I \exp(-p_I\tau)\left(-\xi + (\xi^2 + e^{-\tau})^{1/2}\right)\left(1 - 2q_I + \frac{2}{(\xi^2 + e^{-\tau})^{1/2}}\frac{d\xi}{d\tau}\right) \\ &\quad - d_V \exp(-p_V\tau)\left(\xi + (\xi^2 + e^{-\tau})^{1/2}\right)\left(1 - 2q_V - \frac{2}{(\xi^2 + e^{-\tau})^{1/2}}\frac{d\xi}{d\tau}\right). \end{aligned} \quad (4.6.11)$$

Exact value by means of a numerical integration of the V/G equation

With no restrictive assumption on the concentrations gradients at the solid-liquid interface (in fact only the mass action law Eq. (4.2.11) is satisfied above the interface), and in terms of the non-dimensional variable u defined as $\xi := \sinh u$, Eq. (4.6.11) re-writes as

$$\begin{aligned} 0 &= -\frac{C}{\tilde{\gamma}}\sinh u + d_I \exp(-p_I\tau)\exp(-u)\left(1 - 2q_I + 2\frac{du}{d\tau}\right) \\ &\quad - d_V \exp(-p_V\tau)\exp u\left(1 - 2q_V - 2\frac{du}{d\tau}\right), \end{aligned} \quad (4.6.12)$$

or, written as an ODE, as

$$\frac{du}{d\tau} = f(\tau, u; C), \quad (4.6.13)$$

⁴The first and second order analysis have been performed, but not reported in Section 4.3.2, since they did not bring any relevant information.

where

$$f(\tau, u; C) = \frac{\frac{C}{\gamma} \sinh u - (d_I \exp(-p_I \tau) \exp(-u)(1 - 2q_I) - d_V \exp(-p_V \tau) \exp u(1 - 2q_V))}{2(d_I \exp(-p_I \tau) \exp(-u) + d_V \exp(-p_V \tau) \exp u)}.$$

Since its denominator vanishes as $\tau \rightarrow 0$, while its numerator tends to $\frac{C}{\gamma} \sinh u$, Eq. (4.6.13) has no solution except $u=0$ for some critical value C_{crit} of C which turns out to determine the sign of $\frac{du}{d\tau}$. By a numerical resolution of this ODE with a relative error limited to 10^{-14} and values taken from the test model computed in Section 4.7.2, the following critical value estimate is found (let us recall that the V/G ratio is expressed in $[\text{cm}^2/\text{Kmin}]$):

$$1.281 \cdot 10^{-3} \leq \left[\frac{V}{G}\right]_{exact;TM}^{crit} \leq 1.282 \cdot 10^{-3}, \quad (4.6.14)$$

while using the values taken from Sinno and Dornberger model (as given in Tables 4.2 & 4.3 and recalled in Section 4.6.1) would rather give the estimate:

$$1.395 \cdot 10^{-3} \leq \left[\frac{V}{G}\right]_{exact;SD}^{crit} \leq 1.400 \cdot 10^{-3}. \quad (4.6.15)$$

Approximation formula for the V/G criterion

The slope of the solution at the origin writes as

$$p := \frac{du}{d\tau}(0) = \frac{C\xi_m + d_V \exp u_m(1 - 2q_V) - d_I \exp(-u_m)(1 - 2q_I)}{2(d_I \exp(-u_m) + d_V \exp u_m)}, \quad (4.6.16)$$

while the particular $\tau = \tau_{as}$ for which $u(\tau_{as}) = (d/d\tau)u(\tau_{as}) = 0$ reads

$$\tau_{as} = -\frac{2 \sinh^{-1} \xi_m (d_I \exp(-u_m) + d_V \exp u_m)}{C\xi_m + d_V \exp u_m(1 - 2q_V) - d_I \exp(-u_m)(1 - 2q_I)},$$

in such a way that $d_I \exp(-p_I \tau_{as})(1 - 2q_I) = d_V \exp(-p_V \tau_{as})(1 - 2q_V)$ and hence that $\ln \frac{d_I(1-2q_I)}{d_V(1-2q_V)} = (p_I - p_V) \tau_{as}$ and

$$C = \frac{2\Pi_m^{1/2} [d_V \exp u_m(1 - 2q_V) - d_I \exp(-u_m)(1 - 2q_I)]}{\Delta_m} + \frac{2\Pi_m^{1/2} \Lambda(p_I - p_V)}{\Delta_m \ln \frac{d_I(1-2q_I)}{d_V(1-2q_V)}},$$

where the subscript m indicates that $T = T_m$ and where $\Lambda := 2(d_I \exp(-\xi_m) + d_V \exp \xi_m) \sinh^{-1} \xi_m$. According to the data values tables, $\xi_m = 2.41 \cdot 10^{-2} \ll 1$ for the test

model and $\xi_m = 9.76 \cdot 10^{-2} \ll 1$ for the Sinno-Dornberger model in such a way that $u_m \simeq \sinh^{-1} \xi_m$ and Λ will hence be approximated by ξ_m and $2\xi_m$, respectively. Therefore, the approximate formula brought by our scaling analysis writes as

$$\left[\frac{V}{G}\right]_{approx}^{crit} = \frac{\bar{H}_{IV}^f (D_V^m \exp \xi_m (1 - 2q_V) - D_I^m \exp(-\xi_m)(1 - 2q_I))}{2k_b T_m^2 \xi_m} + \varepsilon_m$$

where the correction term ε_m writes as

$$\varepsilon_m = \frac{\Lambda(p_I - p_V) \bar{H}_{IV}^f (D_I^m + D_V^m)}{\xi_m \ln \frac{d_I(1-2q_I)}{d_V(1-2q_V)} k_b T_m^2}.$$

According to the data values table, we find the approximate value

$$\left[\frac{V}{G}\right]_{approx;TM}^{crit} = 1.3 \cdot 10^{-3} + 1.69 \cdot 10^{-4} = 1.469 \cdot 10^{-3},$$

for the test model and

$$\left[\frac{V}{G}\right]_{approx;SD}^{crit} = 1.4 \cdot 10^{-3} - 2.16 \cdot 10^{-4} = 1.184 \cdot 10^{-3}$$

for the Sinno-Dornberger model. We recall that the "semi-experimental" (the temperature gradient is given by simulations) critical value reads as (Dornberger, 1998; Sinno et al., 1998)

$$\left[\frac{V}{G}\right]_{pseudo-exp}^{crit} = 1.34 \cdot 10^{-3} \text{ (cm}^2/\text{Kmin)},$$

while, according to an "improved formula" of Sinno et al. (1998),

$$\left[\frac{V}{G}\right]_{SD}^{crit} = \frac{C_I^m D_I^m \bar{H}_I^f - C_V^m D_V^m \bar{H}_V^f}{k_b T_m^2 (C_V^m - C_I^m)}.$$

the related theoretical value reads $\left[\frac{V}{G}\right]_{SD}^{crit} = 1.38 \cdot 10^{-3}$.

4.7 The influence of thermo-diffusion

4.7.1 Discussion and modification of the S-D model

A major drawback of the S-D model and its variants comes from the strong discrepancy between the model diffusion coefficients and their experimental counterparts as

proposed in the literature by Stolwijk, Bracht, and other authors (Lerner and Solwijk, 2005; Bracht et al., 1995; Zimmermann & Ryssel, 1992; Tan & Gösele, 1985). In fact these values are between one and two orders of magnitude higher than in the S-D model. Therefore a major objective should be to reconcile both approaches. To achieve this goal, let us first remark that the S-D model assumes 0 values for the reduced heats of transport Q_K^{**} ($K = I, V$) as a consequence of complete lack of experimental data for these material parameters. However it is clear that thermo-diffusion can significantly affect the point-defect evolution. Indeed, putting Q_K^{**} in the form

$$Q_K^{**} = r_K \overline{H}_K^f, \quad (4.7.1)$$

where r_K stands for positive or negative dimensionless coefficients whose absolute value is normally strictly lower than 1 for physical reasons (Philibert, 1988; Schall, 1983), Fig. 4.10 shows how modifying Q_I^{**} through r_I will affect the S-D model predictions. Starting from this model, the influence of Q_V^{**} shows to be much lower since $C_V^m D_V^m$ is one order of magnitude lower than $C_I^m D_I^m$ in Eq. (4.6.7).

4.7.2 An attempt to reconcile experimental defect diffusion coefficients with the V/G criterion

Now the following path has been followed to test the effect of new diffusion and equilibrium concentration coefficients for the modelling of defect evolution in Si crystals:

- With $r_I = 1$ and $r_V = -1$ the numerator of Eq. (4.6.7) reaches its highest value without requiring any change of the experimentally well-known self-diffusion coefficients $C_I^m D_I^m$ and $C_V^m D_V^m$ (Bracht et al., 1995).
- The coefficient \overline{H}_I^m is taken from Sinno et al. (1998), while \overline{H}_I^f is adapted to agree with the maximal experimental value of $\overline{H}_I^f + \overline{H}_I^m$ (Bracht et al., 1995).
- The coefficient C_I^m is selected as the maximal experimental value proposed by Bracht et al. (1995).
- The coefficient C_V^m is adapted to keep the right-hand side of Eq. (4.6.7) equal to the effective value provided by the S-D model ($(V/G)_{crit} = 1.71 \cdot 10^{-3} \frac{cm^2}{min}$).
- The coefficient \overline{H}_V^f is adapted to agree with the experimental values of Lerner and Stolwijk (2005) for C_V^{eq} .
- All the other parameters of the S-D model are kept unchanged.

Accordingly the test-model writes as follows:

$$\begin{array}{ll}
 \overline{H}_I^f = 4.283 \text{ eV}, & \overline{H}_V^f = 1.57 \text{ eV}, \\
 \overline{S}_I^f = 0, & \overline{S}_V^f = 0, \\
 C_I^m = 9.52 \cdot 10^{15} \text{ cm}^{-3}, & C_V^m = 9.99 \cdot 10^{15} \text{ cm}^{-3}, \\
 \overline{H}_I^m = 0.937 \text{ eV}, & \overline{H}_V^m = 2.23 \text{ eV}, \\
 D_I^m = 3.92 \cdot 10^{-5} \text{ cm}^2/\text{s}, & D_V^m = 5.06 \cdot 10^{-6} \text{ cm}^2/\text{s}, \\
 \overline{H}^r = -1.194 \text{ eV}, & \overline{S}^r = -12.43 \text{ eV}/k_b T_m, \\
 Q_I^{**} = 4.283 \text{ eV}, & Q_V^{**} = -1.57 \text{ eV}.
 \end{array}$$

Typical results are depicted in Fig. 4.11. Comparison between the $C_I - C_V$ predictions obtained from the test-model and the S-D model shows that, although the OSF ring is nearly located at the same radial position for both models as expected, the test-model exhibits a much stronger interstitial concentration gradient near the crystal wall and a much more complex transient behaviour during and after conical growth and shouldering. Further numerical experiments are currently carried out in order to investigate and improve the model behaviour.

4.8 Conclusive remarks

Much work remains necessary to determine the complete set of material parameters governing the formation, diffusion and transport of point-defects in Si growth. For the particular model here tested, extreme (and hence normally non-physical (Philibert, 1988; Ebe, 1999; Schaal, 1983; Sinno et al., 1998) values have been selected for the reduced heats of transport in order to highlight their possibly non-negligible role. More realistic coefficients should be considered to achieve the construction of a definite model. Nevertheless the present study shows that the contradiction between the high experimental point-defect diffusion coefficients available in the literature (Lerner & Stolwijk, 2005; Bracht et al. 1995; Zimmermann & Ryssel, 1992; Tan & Gösele, 1985; Wijaranakula, 1983), on the one hand, and the key and unquestionable V/G criterion (Voronkov, 1982; Dornberger & von Ammon, 1996; Dornberger, 1998; Sinno et al., 1998, 2000; Voronkov & Falster, 2002), on the other hand, can be removed or at least strongly alleviated. It should also be observed that performing accurate time-dependent heat transfer simulations opens the door to analyzing the defect distribution at the crystal extremities, as governed by the complex transients acting in the beginning or the end of the growth process, and hence can provide a very accurate model validation tool (see Figs. 4.8(a)-4.11).

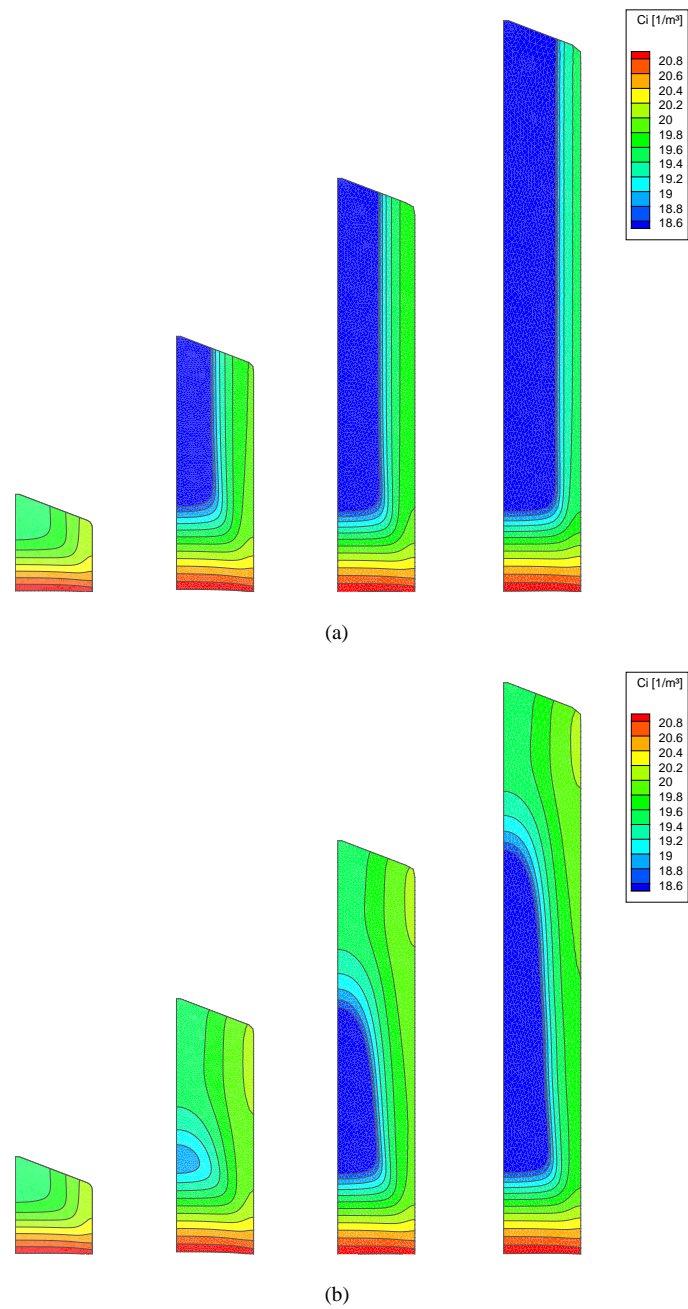
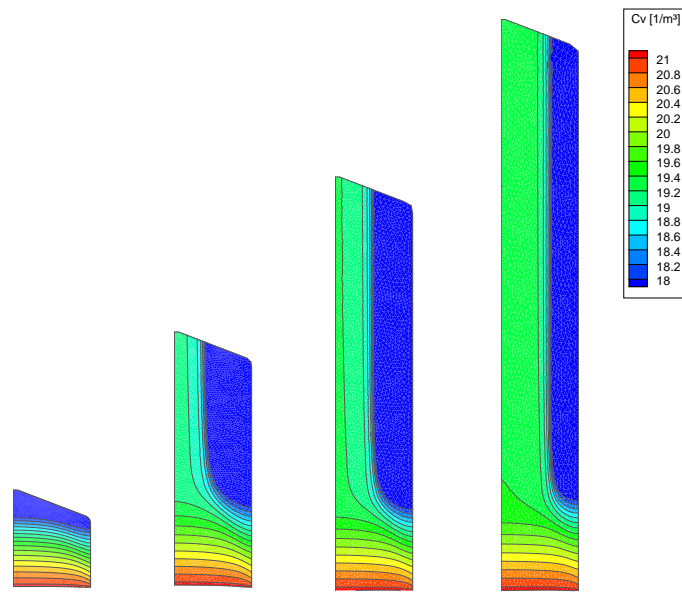
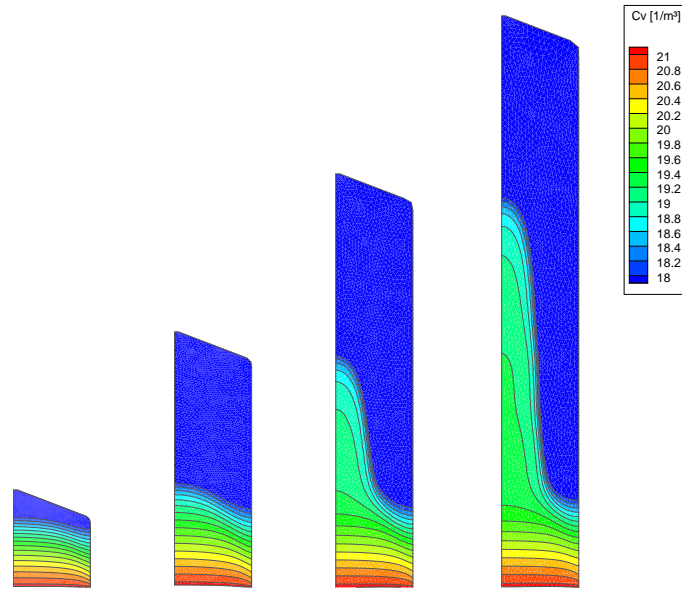


Figure 4.6: Predicted interstitial distribution with quasi-steady (a) and time-dependent (b) defect simulations.

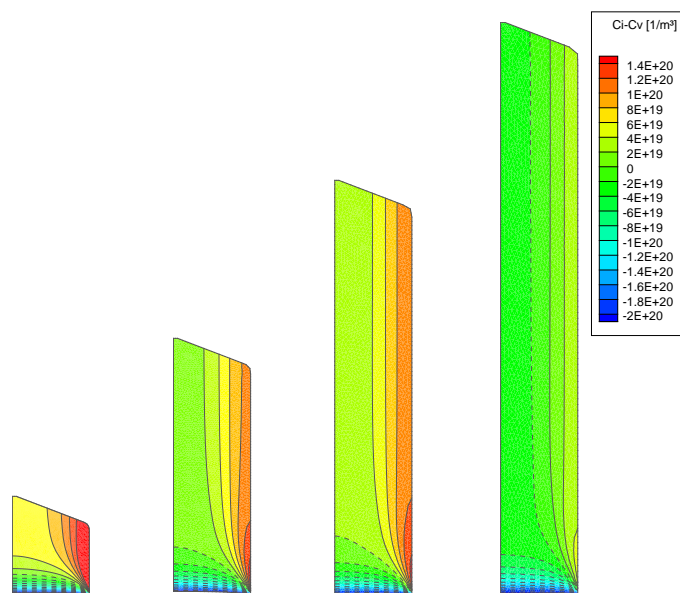


(a)

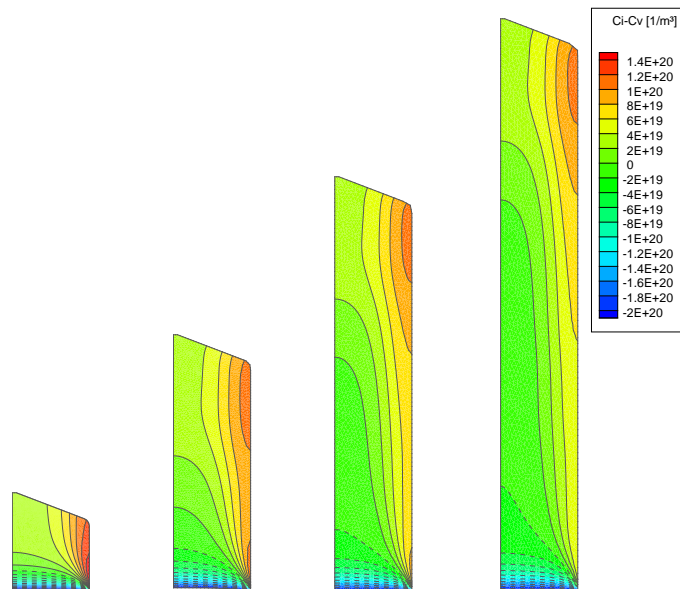


(b)

Figure 4.7: Predicted vacancy distribution with quasi-steady (a) and time-dependent (b) defect simulations.



(a)



(b)

Figure 4.8: Predicted defect difference ($C_I - C_V$) distribution with quasi-steady (a) and time-dependent (b) defect simulations.

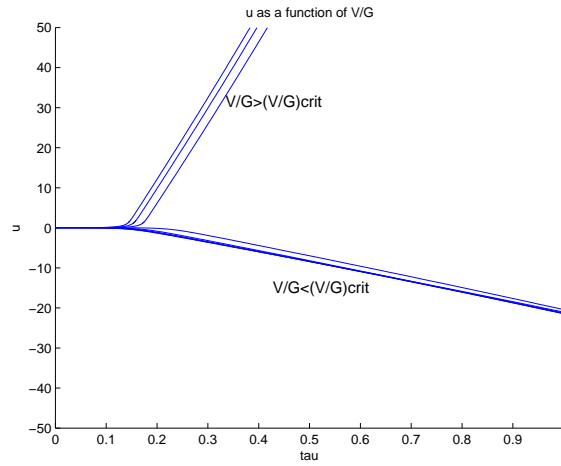


Figure 4.9:

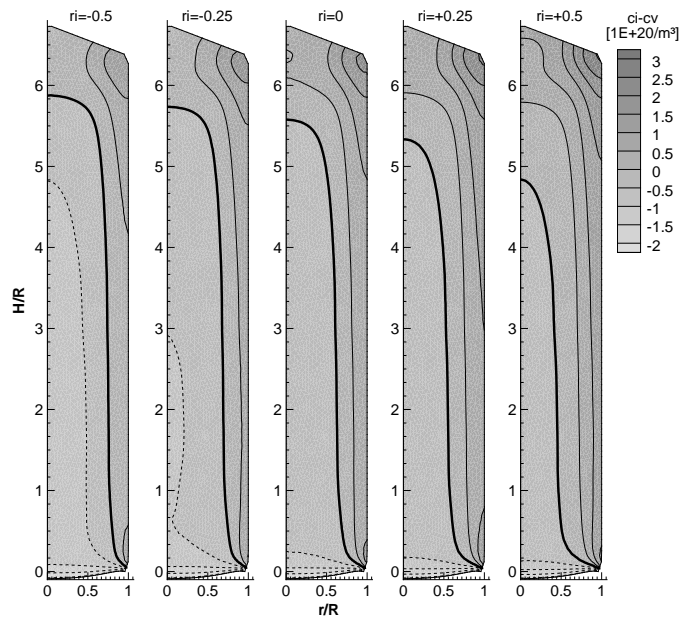


Figure 4.10: Influence of the reduced heat of transport $Q_i^{*} = r_i \bar{H}_i^f$ on the $C_I - C_V$ distribution. All the other material parameters are the same as in the S-D model. The $C_I - C_V = 0$ isoline is in bold. Same growth conditions as in Fig. 4.8(a).

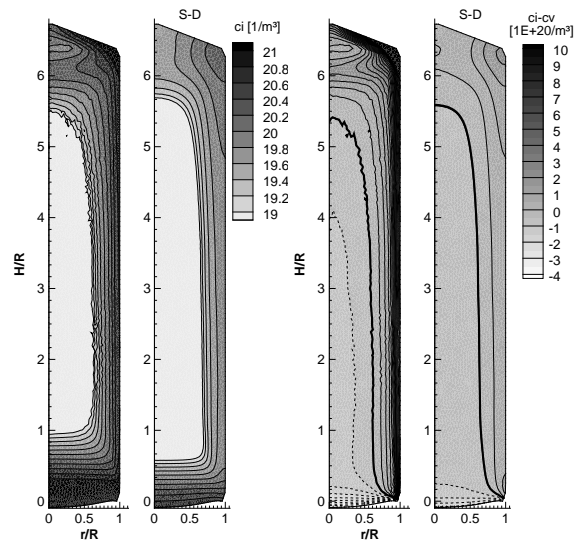


Figure 4.11: Comparison of the test- and S-D model predictions. Distributions of C_I (left) of $C_I - C_V$ (right) under the same growth conditions as in Fig. 4.8(a). The $C_I - C_V = 0$ isoline is in bold. At the height $H=2R$ the OSF ring location differs in the two solutions by 1 mm.

Part IV

Conclusions

The original scope of this thesis was the obtention of a complete defect model for semiconductor single crystals, with a view to providing a detailed picture of the growth of silicon and germanium crystals, for instance. In the crystal growth community, it is known for more than 40 years that silicon can be grown nearly without dislocations. In particular, if the growth speed is high enough, the process will rise to vacancy-rich crystals where the dominating defect is formed by micro-voids. However, since in comparison interstitial-rich crystals are of higher quality, but require to be grown slower, there is a fundamental interest for dislocation models because interstitial-rich conditions are known to cause the formation of dislocation loops in most of the crystal. On the other hand, considering materials such as III-V compounds, halides, and in particular gallium arsenide and indium phosphide, which exhibit very undesirable and resistant dislocations, there is a major need for the development of a complete defect model that could be applied to a large variety of single-crystals.

By complete model it is here intended a model describing the laws governing the creation, transport, diffusion and transformation of the different point defect species into each other. These defect species are basically of four kinds: (i) intrinsic point-defects including interstitials and vacancies, (ii) extrinsic point-defects including dopants and impurities, (iii) micro-voids, and (iv) dislocations loops or lines. Let us emphasise that all the mechanisms governing these defects are strongly coupled with the temperature evolution in the crystal, as illustrated for instance by the exponential Arrhenius-type laws governing several types of material coefficients, or by the existence of a thermal contribution to self-diffusion. As a first key application, let us recall that, nowadays, so-called “perfect silicon” is sought, in the sense of an ultra-pure, defect-free crystal. To this end, the growth is performed by keeping the OSF-ring inside the crystal, forming an annulus which, since there is equilibrium between interstitials and vacancies in this zone, is therefore free of defects, while away from the ring the point-defect densities remain low.

This thesis has provided several contributions to the the field of perfect silicon growth. Firstly, a time-dependent point-defect model, that is, a coupled system of equations governing the transport-diffusion-recombination of interstitials and vacancies, and relying on a thermal model of the crystal solid and liquid phases has been developed. This defect module is now part of the FEMAG software for crystal growth simulation and is used by several research groups and customers around the world (Taiwan, Japan, Korea, Germany, Czech Republic, USA...). In the meantime, a model for microvoids has been developed by the FEMAG team, as an extension of the previous model and including nucleation and growth of vacancy agglomerate. Let us remark that practical implementation of this additional model will not suffer from the difficulties encountered for the PD model, since nucleation occurs at a lower temperature and the material data should be easier to determine. In fact, the second contribution of this thesis in the field of PD modelling has been to point out the present lack of knowledge in the determination of silicon point-defect material parameters, especially at high temperature, and to discuss the unclear role of thermo-diffusion which, when considered as a non-negligible effect, facilitates the obtention of a material data set

differing from the conventional one by 1 or 2 orders of magnitude but agreeing much better with experimental measurements. Finally, our last contribution has been to point out that the conventional asymptotic analysis of the simplified 1D point-defect model is not complete, for several reasons, including the treatment of the far-field and the crystal lateral boundary layer. A correct far-field analysis is surely needed for the microdefect model, while the determination of an improved lateral boundary condition is also needed (originally for accounting for thermo-diffusion, but also to provide particular conditions for inner, outer and far-field zones in the growing crystal when a 2D analysis is performed). Moreover, an improved asymptotic analysis should probably include more than the sole Damkohler non-dimensional number, and the related crucial V/G formula, as devoted to determine the OSF-ring location as a function of the pulling rate, should accordingly be refined.

Our contribution to the field of dislocation modelling has been restricted to the static, geometric analysis of 2D and 3D dislocations, and has consisted in revisiting and restating a theory which emerged in the 50ies and whose major contributor is in our opinion Ekkehart Kröner. In fact, we have developed a 2D theory, and accordingly a 3D extension, to analyse dislocated single crystals at the meso-scale by combining a distributional approach with multivalued kinematic fields. The distributions are basically concentrated along the defect lines, which in turn form the branching lines of the multivalued fields. As a consequence of this analysis, a basic theorem relating the incompatibility tensor (as derived from the deformation field) to the Frank and Burgers vectors of the defect line has been established. This theory provides a framework for the homogenisation of the medium properties from meso- to macro-scale. In particular the macroscopic dislocation density is defined without stipulating an a-priori distortion decomposition into elastic and plastic parts (which does not exist, actually). The classical relationship between Bravais distortion and dislocation densities, instead of being a definition, now appears as a result taking its origin from the meso-scale analysis. Moreover, the 3D extension has provided new formulas for non-rectilinear defect lines, which remain to be homogenised from meso- to macroscale.

It is very surprising to observe that this geometric analysis has many conceptual links to other fields of physics. Let us here as an example mention the analogy between the presence of defects in an otherwise perfect lattice (creating curvature by the presence of point-defects and torsion by the presence of dislocations and disclinations) and the gravitation of massive bodies in the universe. As a second example the following analogy between elastostatics in the presence of defects and magnetostatics has been pointed out by Kröner (1981):

magnetostatics	elastostatics
$\text{div} \underline{\underline{B}} = 0$	$\text{div} \underline{\underline{\sigma}} = 0$
$\text{rot} \underline{\underline{H}} = \underline{\underline{j}}$	$\text{inc} \underline{\underline{\mathcal{E}}} = \underline{\underline{\eta}}$
$\underline{\underline{B}} = \underline{\underline{\mu}} \cdot \underline{\underline{H}}$	$\underline{\underline{\sigma}} = \underline{\underline{c}} : \underline{\underline{\mathcal{E}}}$
$\mathcal{E}^{magn.} = \frac{1}{2} \underline{\underline{B}} \cdot \underline{\underline{H}}$	$\mathcal{E}^{elast.} = \frac{1}{2} \underline{\underline{\sigma}} : \underline{\underline{\mathcal{E}}}$,

where $\underline{\underline{B}}$ and $\underline{\underline{H}}$ are the magnetic induction and field, respectively, while $\underline{\underline{\mu}}$ and $\underline{\underline{c}}$ are the magnetic permeability and elastic tensor, respectively. Let us emphasise that, although the same kind of conservation laws and gauge structure properties are observed in magneto- and elastostatics, the latter exhibits tensor of a higher tensorial order, and hence a much higher number of independent variables. In this respect, some authors (cf eg Kleinert (1989)) propose a theory of dislocations relating to the theories of vortex lines, using for instance the Ginsburgh & Landau model.

Let us now raise the question of the number of unknown fields in a global defect model (in the absence of disclinations), and verify that such a system can be closed by choosing appropriate constitutive laws. Let us recall that the Christoffel symbols, whose various combinations define torsion and curvature, and hence the dislocation, disclination, intrinsic and extrinsic point-defect densities, exhibit 27 independent components, which are all function of position and time. On the other hand, a closed PD model involves 2 defect densities. Moreover, a dislocation model will involve 6 unknown strain (or stress) components and 9 dislocation density components. Finally the temperature field is the last unknown. The PD model is closed as explained in Section 4 by 2 coupled evolution equations. The dislocation problem, in turn, shows 3 zero divergence conditions for the stress and the dislocation density, and 3 (differentially independent) incompatibility conditions (i.e. the “ $\text{inc} \mathcal{E} = \text{curl} \kappa$ ” relations), to which a constitutive law for the skew-symmetric part of the dislocation density might be added, in order to provide 15 equations. The energy equation provides the last equation. Therefore the system is apparently closed.

In a near future a first version of such a global model will be constructed and tested, but the lack of experimental data for the material parameters will remain the hardest obstacle for the obtention of a complete and indisputable model.

References

- Alexander, H., Haasen, P., 1968.** Dislocations and plastic flow in the diamond structure. *Solid State Phys.* 22, 27-158.
- Alexander, H., 1986.** Dislocations in solids. Ed. F. R. N. Nabarro, Vol. 7. North-Holland, Amsterdam.
- Almgren, F. J., 1986.** Deformations and multiple-valued functions. *P. Symp. Pure Math.* 44, 29-130.
- Ambrosio, L., Fusco, N., Palara, D., 2000.** Functions of bounded variation and free discontinuity problems. *Oxford Mathematical Monographs*, Oxford.
- Anthony, K. H., 1970.** Die Theorie der Disklinationen. *Arch. Rational Mech. Anal.* 39, 1, 43-88.
- Anthony, K. H., 1970.** Die Reduktion von nichteuklidischen geometrischen Objekten in eine euklidische Form und physikalische Deutung der Reduktion durch Eigenspannungszustände in Kristallen. *Arch. Rational Mech. Anal.* 37, 3, 161-180.
- Ariza, M. P., Ortiz, M., 2005.** Discrete crystal elasticity and discrete dislocations in crystals. *Arch. Rational Mech. Anal.* 178, 2, 149-226.
- Bender, C. M., Orszag, S. A., 1978.** *Advanced Mathematical Methods for Scientists and Engineers.* McGraw-Hill Book Company, New York.
- Bilby, B. A., 1960.** Continuous distribution of dislocations. *Solid Mechanics*, Eds. N. Sneddon and R. Hillin Progress, Vol. 1. North-Holland, Amsterdam.
- Bracht, H., Stolwijk, N. A., Mehrer, H., 1995.** Properties of intrinsic point defects in silicon determined by zinc diffusion experiments under nonequilibrium conditions, *Phys. Rev. B* 52, 16542-16560.

- Brezis, H., 1983.** Analyse fonctionnelle. Masson Editeur, Paris.
- Burgers, J. M., 1939.** Some considerations on the field of stress connected with dislocations in a regular crystal lattice. Proc. K. Ned. Akad. 42, 293-324.
- Cartan, E.** Sur une generalisation de la notion de courbure de Riemann et les espaces a torsion. C. R. Acad. Sci. Paris, 174:593.
- Cermelli, P., Gurtin, M. E., 2001.** On the characterization of geometrically necessary dislocations in finite plasticity. J. Mech. Phys. Solids 49, 1539-1568.
- Conti, S., DeSimone, A., Dolzmann, G., Müller, S., Otto, F., 2002** Multiscale modeling of materials—the role of analysis. In Trends in Nonlinear Analysis, M. Kirkilionis, S. Krömker, R. Rannacher und F. Tomi, eds., Springer-Verlag, Heidelberg, 375-408.
- Cosserat, E. and F., 1909.** Théorie des corps déformables. Hermann, Paris.
- Davini, C., 1986.** A proposal for a continuum theory of defective crystals. Arch. Rational Mech. Anal. 96, 4, 295-317.
- de Groot, S. R., Masur, P., 1984.** Non-equilibrium thermodynamics. Dover publications.
- Doghri, I., 2000.** Mechanics of deformable solids. Linear, Nonlinear, Analytical and computational aspects. Springer-Verlag, Berlin.
- Dornberger, E., von Ammon, W., 1996.** The dependence of ring-like distributed stacking faults on the axial temperature gradient of growing Czochralski silicon crystals, J. Electrochem. Soc., 143, 1648-1653.
- Dornberger, E., 1998.** Prediction of the OSF ring dynamics and grown-in voids in Czochralski silicon crystals, Ph.D. Thesis, Université catholique de Louvain, Belgium.
- Dubrovin, B. A., Fomenko, A. T., Novikov, S. P., 1992.** Modern geometry - methods and applications, Part 1 (2nd edn.). Springer-Verlag, New-York.
- Dupret, F., Nicodème, P., Ryckmans, Y., Wouters, P., Crochet, M. J., 1990.** Global modelling of heat transfer in crystal-growth furnaces. Int. J. Heat Mass Transfer, 33, 849-871.
- Dupret, F., Van den Bogaert, N., 1994.** Modelling Bridgman and Czochralski growth. In Handbook of Crystal Growth, Vol. 2B, Ch. 15, Elsevier, Neth., 875-1010.
- Ebe, T., 1999** Factors determining the saturation of point defects in growing silicon crystals. J. Crystal Growth, 203, 387-399.

- Eshelby, J. D., Frank, F. C., Nabarro, F. R. N., 1951.** The equilibrium linear arrays of dislocations. *Phil. Mag.* 42, 351-364.
- Eshelby, J. D., 1956.** The continuum theory of lattice defect. *Solid State Physics*, Eds. F. Seitz and D. Turnbull, Vol. 3. Academic Press, New-York.
- Eshelby, J. D., 1966.** A simple derivation of the elastic field of an edge dislocation. *Brit. J. Appl. Phys.* 17, 1131-1135.
- Estrada, R., Kanwal, R. P., 1989.** Regularization, pseudofunction, and Hadamard finite part. *J. Math. Anal. Appl.* 141, 195-207.
- Evans, L. C., Gariépy, R., 1992.** Measure theory and fine properties of functions. CRC Press, New York.
- Falster, R., Voronkov, V., 2000.** The engineering of intrinsic point defects in silicon wafers and crystals. *Mater. Sci. Eng. B* 73, 87.
- Falster, R., Voronkov, V., Quast, F., 2000.** On the properties of the intrinsic point defects in silicon: a perspective from crystal growth and wafer Processing. *Phys. Stat. Sol. (b)* 222, 219-244.
- Föll, H., Kolbesen, B., 1976.** Agglomerate von Zwischengitteratomen (Swirl-Defekte) in Silizium-ihre Bedeutung für Grundlagenforschung und Technologie. *Jahrbuch der Akademie der Wissenschaft in Göttingen* 27.
- Forest, S., van der Giessen E., Kubin, L., 2001.** Scale transitions: from atomistics to continuum plasticity. *Journal de Physique IV*, Vol. 11, Proceedings of the 5th European Mechanics of Materials Conference, Delft.
- Frank, F. C., 1958.** Liquid crystals: On the theory of liquid crystals, *Disc. Faraday Soc.*, 25, 19-28.
- Frank, W., Gösele, U., Mehrer, H., Seeger, A., 1984.** Diffusion in silicon and germanium. In *Diffusion in crystalline solids*, Ed. G. Murch and S. Nowick. Academic press, inc.
- Glicksman, M. E., 2000.** Diffusion in solids-Field theory, solid-state principles, and applications. John Wiley & sons, inc, New York.
- Gurtin, M. E., 2002.** A gradient theory of single-crystals viscoplasticity that accounts for geometrically necessary dislocations. *J. Mech. Phys. Solids* 50, 5-32.
- Harrison, J., Norton, A., 1991.** Geometric integration on fractal curves in the plane. *Indiana Univ. Math. J.*, 40 No. 2, 567-594.
- Harrison, J., Norton, A., 1992.** The Gauss-Green theorem for fractal boundaries. *Duke Math. J.* 67, 3, 575-588.

- Harrison, J., 1999.** Flux across nonsmooth boundaries and fractal Gauss/Green/Stokes' theorems. *J. Phys. A: Math. Gen.* 32, 5317-5327.
- Head, A. K., Howison, S. D., Ockendon, J. R., Tighe, S. P., 1993.** An equilibrium theory of dislocation continua. *Siam Rev.* 35, 4, 580-609.
- Jordan, A. S., Von Neida, A. R., Caruso, R., 2000.** The theory and practise of dislocation reduction in *GaAs* and *InP*. *J. of Cryst. Growth* 218, 555-573.
- Kleinert, H., 1989.** Gauge fields in condensed matter, Vol.1. World Scientific Publishing, Singapore.
- Knopp, K., 1996.** Theory of functions, Part 1&2. Dover Publications, New York.
- Kondo, K., 1952.** On the geometrical and physical foundations of the theory of yielding (in Proc. 2nd Japan Nat. Congr. Applied Mechanics). Tokyo.
- Kondo, K., 1955.** Non-Riemannian geometry of the imperfect crystal from a macroscopic viewpoint (in Memoirs of the unifying study of basic problems in engineering sciences by means of eometry, Vol.1, Division D)
- Kondo, K., 1962.** Non-Riemannian geometry of imperfect crystals from a macroscopic viewpoint (in RAAG Memoirs of the unifying study of basic problems in engineering and physical science by means of geometry, ed. K. Kondo, Vol. 3). Tokyo.
- Koslowski, M., Cuitino, A. M., Ortiz, M., 2002.** A phase field theory of dislocation dynamics, strain hardening and hysteresis in ductile single crystal. *J. Mech. Phys. Solids* 50, 2597-2635.
- Kratochvil, J., Dillon, O.W., 1969.** Thermodynamics of elastic-plastic materials as a theory with internal variables. *J. Appl. Phys.* 40, 8, 3207-3218.
- Kröner, E., 1955.** Die Spannungsfunktionen der dreidimensionalen anisotropen Elastizitätstheorie. *Z. Physik* 140.
- Kröner, E., 1980.** Continuum theory of defects. *Physiques des défauts, Les Houches session XXXV, Course 3*, ed. R. Balian.
- Kröner, E., 1990.** The differential geometry of elementary point and line defects in Bravais crystals. *Int. J. Theor. Phys.* 29, 11, 1219-1237.
- Kröner, E., 1992.** The internal mechanical state of solids with defects. *Int. J. Solids and Structures* 29, 14/15, 1849-1257.
- Kröner, E., 2001.** Benefits and shortcomings of the continuous theory of dislocations. *Int. J. Solids Struc.* 38, 1115-1134.

- Kubin, L. P., Canova, G., 1992.** The modelling of dislocation patterns. *Scripta Metallurgica et Materialia*. Vol. 27, no. 8, 957-962.
- Kulkarni, M., Voronkov, V., Falster, R., 2004.** Quantification of Defect Dynamics in Unsteady-State and Steady-State Czochralski Growth of Monocrystalline Silicon. *J. Electrochem. Soc.* 151 (10), G663.
- Larsen, T. L., Jensen, L., Lüdge, A., Riemann, H., Lemke, H., 2001.** Numerical simulation of point defect transport in floating-zone silicon single crystal growth. *J. Crystal Growth*, 230, 300-304.
- Lelong-Ferrand, J., 1963.** *Géométrie Différentielle*, Masson et Cie, Paris.
- Lerner, L., Stolwijk, N. A., 2005.** Vacancy concentrations in silicon determined by the diffusion of iridium into dilicon wafers. *Appl. Phys. Lett.*, 74, 011901-1-011901-3.
- Maroudas, D., Brown, R. A., 1991.** On the prediction of dislocation formation in semiconductor crystals grown from the melt: analysis of the Haasen model for plastic deformation dynamics. *J. of Cryst. Growth* 108.
- Mattila, P., 1995.** *Geometry of sets and measures in Euclidean spaces-Fractals and rectifiability*. Cambridge studies in advanced mathematics, Cambridge, 1995.
- Mawhin, J., 1992.** *Analyse: fondements, techniques, evolutions*. De Boek Université, Louvain-la-Neuve.
- Mura, T., 1987.** *Micromechanics of defects in solids* (2nd edn.). Kluwer Academic Publishers, Boston.
- Nabarro, F. R. N., 1967.** *Theory of dislocations*, Clarendon press, Oxford.
- Nicola, L., Bower, A. F., Kim, K.S., Needleman, A., Van der Giessen, E., 2006.** Surface versus bulk nucleation of dislocations during contact. *J. Mech. Phys. Solids* (preprint).
- Nye, J. F., 1953.** . Some geometrical relations in dislocated crystals. *Acta Metall.* 1, 153-162.
- Philibert, J., 1988.** *Atom movements, diffusion and mass transport in solids*. Monographies de physique, les éditions de physique, les Ulis, France.
- Remmert, R., 1996.** From Riemann surfaces to Riemann spaces. Proceedings of the colloquium to the memory of Jean Dieudonné, Nice, France, January 1996, Société Mathématique de France, Sémin. Congr. 3.
- Rodney, D., 2004.** Molecular dynamics simulation of screw dislocations interacting with interstitial frank loops in a model FCC crystal. *Acta mater.* Vol. 52, no 3, 607-614.

- Rodney, D., Le Bouar, Y., Finel, A., 2003.** Phase field methods and dislocations. *Acta mater.* Vol. 51, no 1, 17-30.
- Schaal, B., 1983.** Ph.D. Thesis, University of Stuttgart, Germany.
- Schouten, J. A., 1954.** Ricci-Calculus (2nd edn.). Springer Verlag, Berlin.
- Schwartz, L., 1957.** Théorie des distributions. Hermann, Paris.
- Schwartz, K. W., 1999.** Simulation of dislocations on mesoscopic scale. I. Methods and examples. *J. Appl. Phys.* Vol 85, no 1, 108-119. Paris.
- Senkader, S., Jurkschat, K., Wilshaw, P. R., Falster, R. J., 2000.** A study of oxygen dislocation interactions in CZ-Si, *Mater. Sci. Eng. B* 73, 111-115.
- Shewmon, P., 1989.** Diffusion in solids 2nd ed. The minerals, metals & material society.
- Sinno, T. Brown, R. A., Dornberger, E., von Ammon, W., 1998.** Point defect dynamics and the Oxidation-Induced Stacking-Fault ring in Czochralski-grown silicon crystals. *J. Electrochem. Soc.*, 145 (1), 302.
- Sinno, T., Dornberger, E., Brown, R. A., von Ammon, W., Dupret, F., 2000.** Defect engineering of Czochralski single-crystal silicon. *Materials Science and Engineering: R Reports*, 28, 149, 1-50.
- Sokolnikoff, I. S., 1946.** Mathematical theory of elasticity. Mc Graw-Hill, New-York.
- Tan, T. Y., Gösele, U., 1985.** Point defects, diffusion processes, and swirl defect formation in silicon. *Appl. Phys. A*, 37, 1-17.
- Taylor, G. I., 1934.** The mechanism of plastic deformation of crystals I-II, *Proc. Royal Soc. A.*, Vol. 145, No. 855; 362-387.
- Thom, R., 1980.** Concepts in the theory of ordered media. *Physiques des défauts, Les Houches session XXXV, Course 6*, ed. R. Balian.
- Unzicker, A., 2000.** What can physics learn from Continuum Mechanics? eprint arXiv:gr-qc/0011064.
- Van den Bogaert, N., Dupret, F., 1997.** Dynamic global simulation of the Czochralski process: I. Principles of the method; II. Analysis of the growth of a Ge crystal. *J. Cryst. Growth* 171, 65-76; 77-93.
- Volterra, V., 1907.** Sur l'équilibre des corps élastiques multiplement connexes. *Ann. Sci. École Norm. Sup.* 3, 24, 401-517.

- von Ammon, W., Dornberger, E., Oelkrug, H., Weidner, H., 1995.** The dependence of bulk defects on the axial temperature gradient of silicon crystals during Czochralski growth. *J. Crystal Growth*, 151, 273-277.
- Voronkov, V. V., 1982.** The mechanism of swirl defects formation in silicon. *J. Crystal Growth*, 59, 625-643.
- Voronkov, V. V., Falster, R., 2002.** Intrinsic Point Defects and Impurities in Silicon Crystal Growth. *J. Electrochem. Soc.*, 149 (3), G167-G174.
- Voronkov, V. V., Falster, R., 2003.** Grown-in Microdefects in Silicon as a Guide to the Properties of Point Defects. *Future Fab Intl.* Vol. 15.
- Whitney, H., 1935.** A function not constant on a connected set of critical points. *Duke Math. J.* 1, no. 4, 514-517.
- Wijaranakula, W., 1993.** A real-time simulation of point defect reactions near the solid and melt interface of a 200mm diameter Czochralski silicon crystal. *J. Electrochem. Soc.*, 140 (11), 3306-3316.
- Willem, M., 1995.** *Analyse harmonique réelle*, Hermann, Paris.
- Zimmermann, H., Ryssel, H., 1992.** Gold and platinum diffusion: the key to the understanding of intrinsic point defect behavior in silicon. *Appl. Phys. A* 55, 121-134.

